# A DIRECT-WRITE THREE-DIMENSIONAL BIOASSEMBLY TOOL FOR REGENERATIVE MEDICINE

by
Cynthia Miller Smith

---

A Dissertation Submitted to the Faculty of the

GRADUATE INTERDISCIPLINARY PROGRAM IN BIOMEDICAL ENGINEERING

In Partial Fulfillment of the Requirements
For the Degree of

Doctor of Philosophy

In the Graduate College

THE UNIVERSITY OF ARIZONA

2 0 0 5

FINAL EXAMINING COMMITTEE APPROVAL FORM

As members of the Dissertation Committee, we certify that we have read the dissertation prepared by Cynthia M. Smith

entitled A Direct-Write Three-Dimensional BioAssembly Tool for Regenerative Medicine

and recommend that it be accepted as fulfilling the dissertation requirement for the Degree of Doctor of Philosophy

_____ Date: November 1, 2005
Stuart K. Williams

_____ Date: November 1, 2005
Jennifer K. Barton

_____ Date: November 1, 2005
James B. Hoying

_____ Date: November 1, 2005
Ronald M. Lynch

_____ Date: November 1, 2005
William L. Warren

Final approval and acceptance of this dissertation is contingent upon the candidate's submission of the final copies of the dissertation to the Graduate College.

I hereby certify that I have read this dissertation prepared under my direction and recommend that it be accepted as fulfilling the dissertation requirement.

_____ Date: November 1, 2005
Dissertation Director: Stuart K. Williams

# STATEMENT BY AUTHOR

This dissertation has been submitted in partial fulfillment of requirements for an advanced degree at The University of Arizona and is deposited in the University Library to be made available to borrowers under rules of the Library.

Brief quotations from this dissertation are allowable without special permission, provided that accurate acknowledgment of source is made. Requests for permission for extended quotation from or reproduction of this manuscript in whole or in part may be granted by the head of the major department or the Dean of the Graduate College when in his or her judgment the proposed use of the material is in the interests of scholarship. In all other instances, however, permission must be obtained from the author.

SIGNED: Cynthia M. Smith

# ACKNOWLEDGEMENTS

I would like to thank my husband, Cole, for his endless support, understanding, and encouragement. Your help and comments helped me push through to do all of the work that needed to be done. I would also like to thank my daughter, Katie, for putting up with daycare, babysitters, and a constantly changing environment while I finished up this degree. You were a real trooper!

I would like to thank my parents for their encouragement and prayers. Thank you for spending so much time watching after Katie and proof reading! Your help made this all possible!

I would like to thank Charlotte Todd, Lori Taylor, and Debbi Howard for taking care of me. Thanks for making sure that I was on top of things. You made sure that deadlines were met, abstracts and papers were submitted, conference trips were quickly reimbursed, and that I was signed up for the proper coursework. You all have helped make the Biomedical Engineering Program a wonderful program!

I would like to thank my fellow graduate students (Kristen O'Halloran, Trevor Cardinal, Samatha Powis, Mark Schwartz, Edward Parkin, and Kevin Greer to name a few) for making the lab environment so much fun. Thanks for all of your help and encouragement! It was great sharing some of the same experiences with you! And, your advice and camaraderie helped make some of those rough days not only bearable but also comical!

I would like to thank Leigh Kleinert, Vangie Patula, Alice Stone, Faith Rice, and Helen Chen for their endless support and for helping me make sure I didn't do anything potentially harmful to Katie when I was pregnant. You all went above and beyond the call of duty.

I would like to thank my Dissertation Committee Jennifer Barton, Bill Warren, Ron Lynch, Jay Hoying, and Stuart Williams for their patience, feedback, encouragement, and direction.

I would like to give a special thanks to my mentor, Dr. Stuart Williams. Thank you for your patience and understanding in all of the ups and downs that come with completing this degree. Sometimes it felt like those down moments were going to swallow me whole! Thank you for your encouragement at just the right moments and for providing me with so many interesting and unique opportunities.

# DEDICATION

To my husband, Cole
And our daughter, Katie

You made this journey more fun and interesting!

TABLE OF CONTENTS

TABLE OF CONTENTS-continued

# LIST OF ILLUSTRATIONS

LIST OF ILLUSTRATIONS-continued

LIST OF ILLUSTRATIONS-continued

# LIST OF TABLES

# ABSTRACT

Tissue loss and end-stage organ failure caused by disease or injury are two of the most costly problems encountered in modern medicine. To combat these problems, a relatively new field, called tissue engineering, has emerged. This field combines the medical and engineering fields in hopes of establishing an effective method to restore, maintain, or improve damaged tissue. In order to best replace the diseased tissue, many approaches to fabricating new tissue have focused on trying to replicate native tissue. The overall hypothesis of this dissertation is that a direct-write, BioAssembly Tool (BAT) can be utilized to fabricate viable constructs of cells and matrix that have a specified spatial organization and are truly three-dimensional (3D). The results of the studies within this dissertation demonstrate that the BAT can generate viable, spatially organized constructs comprised of cells and matrix by carefully controlling the environmental parameters of the system. A joint hypothesis associated with this dissertation is that 3D microscopy and image processing techniques can be combined to generate accurate representative stacks of images of the tissue within 3D, tissue engineered constructs. The results of the studies examining this hypothesis demonstrate that by taking into account the attenuation with depth in the imaged construct as well as by looking at the intensity and gradient of each voxel, accurate and reproducible thresholding can be achieved. Furthermore, this tool can be utilized to aid in the characterization of 3D tissue engineered constructs. Based on these studies, 3D microscopy and image processing shows promise in accurately representing the cellular volume within a tissue. More importantly, 3D, direct-write technology, specifically the BioAssembly Tool, could be used in the fabrication of viable,

spatially organized constructs that can then be implanted into a patient to provide healthy tissue in the place of diseased or damaged tissue.

# 1. INTRODUCTION

Two of the most detrimental and costly issues in modern medicine are tissue loss and end-stage organ failure caused by disease or injury. Three main surgical approaches have been used to remedy these problems: whole organ transplantation, surgical reconstruction, and replacement with a mechanical device such as a prosthesis or dialysis machine. While these techniques have caused substantial improvements in health care, none of these approaches is perfect. Organ transplantation is severely limited by donor shortages, which worsen each year. Also, patients who have undergone an organ transplant must be on life-long immunosuppression. Surgical reconstruction, which involves replacing a diseased tissue with healthy tissue, can result in long-term problems. And, mechanical devices are not able to perform the full physiological function of the replaced tissue. Plus, they are limited to adult patients, since the metal devices cannot expand and grow with an immature patient. (Langer & Vacanti, 1993; Shieh & Vacanti, 2005)

In order to overcome these limitations, a new field called tissue engineering (TE) emerged. TE is an interdisciplinary field that utilizes the practices of engineering and sciences with the primary goal of developing biological alternatives that are capable of restoring, maintaining, or improving tissue function (Langer & Vacanti, 1993). The term "tissue engineering" was first coined in 1987 at a National Science Foundation meeting. Since that time, this field of research has greatly expanded and made an impact on industry. As more is learned about molecular and cell biology, TE promises to bring about a new generation of tissue and organ implants. And, it is estimated that by the year

2020, TE has the potential to be a $20 billion industry. It has been hypothesized that the success of TE is contingent upon it closely imitating nature (Lanza, et al., 2000). Some key observations have been made in the quest to better imitate natural tissue, namely that most tissues undergo remodeling; under favorable in vitro conditions, cells tend to assemble into the appropriate structures; and by providing a template, cells can be directed to organize into a specific architecture (Langer & Vacanti, 1993).

## TISSUE ENGINEERING TECHNIQUES

Various methods have been employed to generate TE constructs to repair or replace damaged tissue. While the majority of techniques use both cells and matrices, some use cells alone or matrices alone (Vacanti & Langer, 1999). Three main TE approaches have been developed: 1) using tissue-inducing substances, 2) using isolated cells or cell substitutes, and 3) placing cells on or within matrices (Langer & Vacanti, 1993).

The first method, which uses tissue-inducing substances, requires a procedure for the purification and large-scale production of the desired signal molecules as well as a method to deliver those molecules to the desired tissue (Langer & Vacanti, 1993). This method has been employed for therapeutic angiogenesis. Because new blood vessels can sprout from preexisting ones, it is believed that new blood vessels can be supplied to ischemic tissue by injecting proteins that induce vessel formation (Cao, et al., 2005; Post, et al., 2001). There has been experimental and clinical success demonstrating the benefits of therapeutic angiogenesis in both perfusion and function of the target organs (Post, et al., 2001). Using tissue-inducing substances has also had promising results in

treating hormone deficiencies resulting from diseases such as Type I diabetes, Alzheimer's disease, Parkinson's disease, and hemophilia (Aebischer, et al., 1991; Colton, 1995; Desai, et al., 2004).

This technique does not always use just an injectable protein. In some cases, the substance used is actually a polymeric capsule containing living cells. The first such human trial was attempted in 1994 to relieve pain in a patient by implanting a capsule containing calf cells capable of secreting a myriad of painkillers. The exciting results demonstrated that the cells could survive and release their analgesics for months. This success has spurred on an emergence of new treatments known as encapsulated-cell, immunoisolation, or biohybrid therapy (Lysaght & Aebischer, 1999).

Another TE technique to repair damaged or diseased tissue is to use isolated cells. In this approach, the cells are injected into the determined tissue location. This has the advantage that the patient does not have to undergo surgery; and it has the added benefit that the cells can be manipulated prior to injection. However, these cells may fail to perform the desired behaviors and there may be immunological rejection (Langer & Vacanti, 1993). This approach has been used to try to reverse the effects of some neurodegenerative diseases (Lindvall, et al., 2004). Substantial reversal of some of the incapacitating symptoms of Parkinson's in humans has been achieved by injecting normal fetal dopamine-producing cells into the brain (Lindvall, et al., 1990).

This technique has also been used to repair ischemic tissue by injecting cells associated with blood vessels. In one study, human umbilical cord blood mononuclear progenitor cells (HUCBC) were injected into a heart that had undergone acute myocardial

infarction, caused by left anterior descending coronary artery ligation. This study demonstrated that transplanting HUCBC to the site of myocardial infarction greatly reduced the infarct, resulting in a significant improvement in ventricular function (Henning, et al., 2004).

The most commonly used TE method is to seed cells onto a scaffold and implant the construct into the diseased or damaged tissue (Lavik & Langer, 2004). The scaffolds that are used may be comprised of natural materials or synthetic polymers (Langer & Vacanti, 1993). This method often uses random seeding of cells ex vivo, using the scaffold itself to provide an architectural guideline for the organization of the cells (Boudreau, et al., 1995; Langer & Vacanti, 1993; Shieh & Vacanti, 2005; Vacanti & Langer, 1999).

One application of this approach evaluated angiogenic patches containing a 3D human dermal fibroblast culture in a cardiac patch (Dermagraft®) (Kellar, et al., 2001). This study demonstrated that when the patch was administered to an infracted heart, angiogenesis was stimulated and the tissue was repaired. Other studies have examined sodding endothelial cells (EC) onto the lumenal surface of vascular grafts. This was done in hopes of helping prevent restenosis and thrombosis of the grafts (Ahlswede & Williams, 1994; Jarrell, et al., 1991). When the sodded grafts were implanted in a dog model, it was observed that the cellular lining remained stable for at least one year and the sodded grafts had a statistically significant improvement over nonsodded grafts (Williams, et al., 1994).

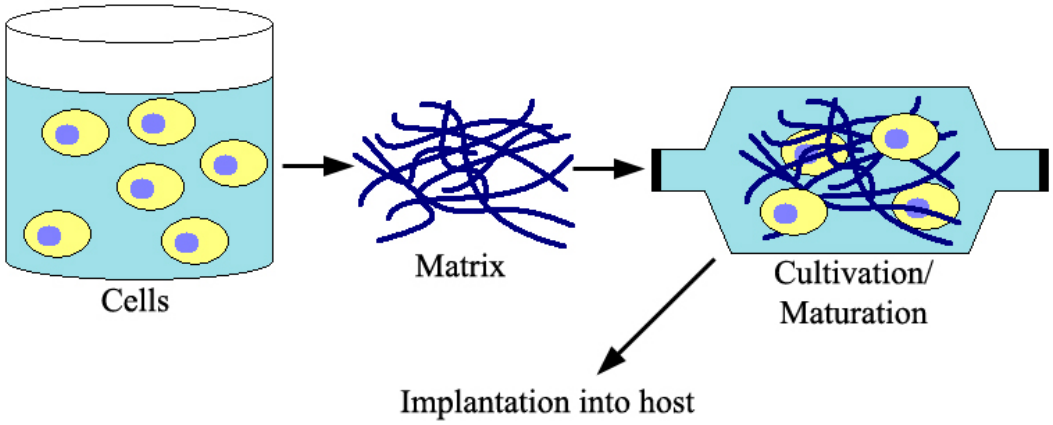


FIGURE 1.1, Steps in the Tissue Engineering Process

Cells are selected for the specific TE construct. These cells may be autologous, allogenic, or xenogenic. Next, a matrix of synthetic or natural material is selected. The cells are combined with the matrix in some fashion and then cultured. This culture may be static, stirred, or under dynamic flow. Once the construct is ready, it is implanted into the host (Langer & Vacanti, 1999).

Numerous studies have investigated implanting matrices containing vascular cells in order to supply a vasculature to a host. Nör, et al. (Nör, et al., 2001), embedded EC, the cells that line the interior of blood vessels, in a poly-L-lactic acid sponge. When these sponges were implanted dorsal subcutaneously, they formed into a vasculature, inosculated with the host vasculature, and carried blood throughout the construct. However, after 28 days while there were patent vessels within the sponges, a significant number of the implanted cells had died. Shepherd, et al. (Shepherd, et al., 2004), used intact microvessel fragments embedded in a collagen gel. This work demonstrated that when the vascularized gels were implanted dorsal subcutaneously, the vessels inosculated with the host vasculature and carried blood throughout the construct. An exciting result seen in this study was that after 28 days, many of the implanted cells were still viable. As this is the most common TE approach, the rest of the work in this dissertation will focus on using both cells and scaffold when creating a TE construct. A schematic representation of this technique can be found in Figure 1.1.

## SELECTING CELLS

When it comes to building a TE construct, the cell type chosen, as well as the source from which they are obtained, have a critical impact on the success of the construct (Lavik & Langer, 2004). A first consideration is the source from which the cells will be obtained. In order to avoid rejection, autologous cells, or cells from the host itself, may be used. However, these cells may not always be available. In that case, allogenic cells, cells from another member of the host's species, may be used. When the cells are only needed for chemical support, as in the forms of TE that use tissue-inducing

substances or cells alone, xenogenic cells may be used. However, when xenogenic cells are used, they must be encapsulated in order to protect them from the host's immune response (Lavik & Langer, 2004). Taking into account the availability of cells and immune response the cells will invoke, allogenic cells are often favored (Langer & Vacanti, 1999).

Once it is determined from where the cells will be obtained, a second consideration is the type of cell to use. In general, the cells that will be used in a TE construct will first need to be cultured. This allows the cells to proliferate such that there are enough cells available for use in the construct. For some tissue applications, primary cells may not be an option. This could be because the cells are not accessible or because they do not have the proliferative capacity to be feasible for TE. Thus, multipotent stem cells and progenitors have been examined (Lavik & Langer, 2004).

Embryonic stem cells (ESC) have the potential to differentiate into a wide array of cell types. However, using these cells brings up many ethical issues, and researchers are not yet able to differentiate the ESC such that they can be used for specific organs. Thus, progenitor cells have become a popular cell source in TE. These cells are not fully established and have the potential to differentiate into several different cell types (Langer & Vacanti, 1999).

## Selecting Scaffold Material

The overall goal of TE is to combine material with the appropriate cells such that a new, functional tissue is formed. Thus, the material that is used has a huge impact on the utility of the construct itself. Many different types of materials have been used,

including ceramics, metals, natural materials, and synthetic polymers (Lavik & Langer, 2004). Because they are found in the extracellular matrix (ECM) of native tissue, natural materials are a common choice for the scaffolding of TE constructs (Lavik & Langer, 2004).

Some of the natural materials that have been used are collagen (Freyman, et al., 2001), Matrigel™ (Guest, et al., 1997), and alginate (Murayama, et al., 2002). As collagen makes up 25% of the total protein mass of mammals, this ECM has been used extensively in TE applications. A typical collagen molecule has a helical structure comprised of three intertwined protein chains. While there are at least 15 different types of collagen, type I collagen is the most commonly used in biomedical applications. This form of collagen is a "rope-forming" collagen that can be found almost everywhere in the body (Alberts, et al., 1994).

Collagen is a viable choice in TE applications because it can be resorbed into the body, it produces a minimal immune response even between different species, it is non-toxic, and it promotes attachment and interaction with cells. In fact, it has been used in building vascular networks (Hoying, et al., 1996; Nicosia & Ottinetti, 1990b; Shepherd, et al., 2004), repairing nerve damage (Liu, et al., 1997), and generating bladder tissue (Atala, 2000). Also, collagen can be processed such that it can be used in numerous different forms, including sponges, gels, and sheets (Han, et al., 1999). The most compelling reason to use collagen in TE applications is that cells grown on collagen behave similarly to the way that they do in vivo (Lavik & Langer, 2004). Thus, in trying to mimic natural tissue, collagen is a good scaffold to use.

There are some disadvantages to using collagen, including altering cell behavior, poor mechanical properties, or even shrinkage (Han, et al., 1999; Vaissiere, et al., 2000). Fortunately, collagen can easily be manipulated by combining it with other natural or synthetic polymers. Also, because cells readily interact with collagen, they may reorganize the collagen structure themselves. While this could be a disadvantage because the original architecture may be altered, it can also be seen as an advantage in that the cells could cause the construct to be more similar to natural tissue (Han, et al., 1999).

Matrigel™ is another natural material commonly used in TE applications. It is a solubilized basement membrane preparation extracted from mouse sarcoma, a tumor rich in ECM proteins. The primary components of Matrigel™ are laminin, collagen IV, and heparan sulfate proteoglycans (Kleinman, et al., 1982). Matrigel™ polymerizes at room temperature to form a nonporous hydrogel (Novikova, et al., 2003). Some of the biomedical applications in which it has been used include repairing spinal cord damage (Xu, et al., 1999) and building vascular networks (Nicosia & Ottinetti, 1990b; Senger, et al., 1997). However, a major disadvantage of using Matrigel™ is that it is derived from a sarcoma cell line. Thus, it is problematic to use it in its original form in human applications (Novikova, et al., 2003).

Alginate, another natural material commonly used in TE applications, is a polysaccharide obtained from brown seaweed. It is a biocompatible material that can be dissolved in water and cross-linked with a nontoxic divalent cation solution, such as calcium chloride. Thus, there is no need for cytotoxic organic solvents when preparing alginate for biological applications (Becker & Kipke, 2002). In some countries, alginate

is used in food and for dressing wounds (Glicklis, et al., 2000). This material has a flexible viscosity when in the liquid phase, has mechanical stability in the solid phase, and has nonadhesive properties (Becker, et al., 2001). It is useful in biomedical applications because it is biodegradable, has controllable porosity, and can be easily linked to other molecules (Chung, et al., 2002; Rowley & Mooney, 2002). Alginate has been used for a number of biomedical applications including cardiovascular (Dar, et al., 2002), liver (Glicklis, et al., 2000), nerve (Mosahebi, et al., 2001), cartilage (Marijnissen & Lafeber, 2003) tissues, and endovascular embolization (Becker & Kipke, 2002). Some disadvantages of using alginate are its mechanical weakness and poor cell adhesion (Chung, et al., 2002).

Natural materials have their benefits, however, there are also some limitations or concerns associated with their use. The main problems are that it is difficult to control their mechanical properties (Lee, et al., 2001) and they may induce a serious immune response or harbor microbes or viruses (Schmidt & Baier, 2000). While thorough characterization and screening of natural materials mitigates many of these issues, much research has been done on creating biocompatible, synthetic materials.

An advantage that synthetic polymers have over natural materials is that they can be engineered to have specific mechanical and chemical properties. They also avoid immunogenicity issues, however, they introduce biocompatibility problems. Synthetic biomaterials fall into essentially two categories: non-degradable and degradable (Lavik & Langer, 2004). Some of the non-degradable polymers include polytetrafluoroethylene (PTFE or Teflon®), which has been used in vascular grafts (Kellar, et al., 2002; Sayers,

et al., 1998) and high density polyethylene, which has been used in hip implants (Garellick, et al., 1999). Non-degradable polymers can be engineered with well-controlled properties; but their permanence in the body gives rise to concerns regarding scarring and inflammation (Fournier, et al., 2003).

Because of the limitations of non-degradable polymers, many researches have focused their efforts on developing degradable polymers that have all of the properties of non-degradable polymers with the ability to degrade into metabolizable components (Vert, et al., 1998). Poly lactic acid (PLA), polyglycolic acid (PGA), and their copolymer polylactic-*co*-glycolic acid (PLGA) degrade by hydrolysis to lactic and glycolic acids. These polymers have been used in numerous devices approved by the Food and Drug Administration (FDA) (Lavik & Langer, 2004; Mooney, et al., 1994). The degradation rate of these polymers can be tailored to be a few weeks to years by controlling the molecular weight, crystallinity, and ratio of glycolic to lactic acid sububnits. These polymers are useful in a number of drug delivery devices. However, since their degradation is bulk degradation rather than surface degradation they are not ideal for some drugs. Another limitation of this family of polymers is that they are rather brittle (Lavik & Langer, 2004).

Polyanhydrides can be used instead of polymers from the PLGA family, if surface, rather than bulk, degradation is desired (Dang, et al., 1996). This polymer family has been approved by the FDA and is used to deliver carmustine for chemotherapy (Lavik & Langer, 2004). To overcome the limited mechanical properties of the PLGA family, poly-4-hydroxybutyrate or polyhydroxyalkanoate could be used. These polymers

have excellent elastomeric properties and have been used in TE applications such as heart valves (Sodian, et al., 2002a). While these polymers have highly elastic behavior, they are difficult to chemically modify. Also, their range of degradation times is smaller than for traditional polyesters (Lavik & Langer, 2004).

Hydrogels are another family of synthetic polymers often used for biomedical applications. They have a high degree of biocompatibility, mechanical properties similar to soft tissue, and can be injected as a liquid that gels in situ (Anseth, et al., 2002). Hydrogels can be physically or chemically cross-linked, are either degradable or non-degradable, and are water-soluble.

### Spatial Organization of Tissue

When considering how to build a viable TE construct, one must consider not only the cells and scaffold to use, but also the characteristics of natural tissue. Tissue is a complex structure of multiple cell types and extracellular matrix within a dynamic 3D microenvironment. The architecture of tissue is organized through multimeric adhesion complexes. These interact with the cells of the tissue to regulate cytoskeletal organization and activate signaling cascades (Juliano, 2002; Yeaman, et al., 1999). Numerous biological functions, such as tissue development, organ formation, wound healing, and homeostasis, depend on the interaction of cells within a tissue (Edelman & Crossin, 1991; McDevitt, et al., 2002; Takeichi, 1995; Zahir & Weaver, 2004). The specific architecture of cells within a tissue provides cell-cell and cell-ECM cues that are important in directing these functions.

Cells interact with other cells in a tissue through specialized junctional molecules, including tight junctions, adherens junctions, and cell adhesion molecules (Zahir & Weaver, 2004). Thus the spatial organization of cells within a tissue is necessary for the preservation of vital cell-cell adhesion (Geiger & Ayalon, 1992; Larue, et al., 1996; Shibuya, et al., 1995) as well as cell phenotype (Ben Ze'ev, et al., 1988). Cells also interact with the ECM through adhesion receptors, the most common of which is the integrin. Originally, it was believed that the ECM was solely a support structure for tissue. However, in the mid to late 1960's, it was shown that the ECM provided more than just an architectural role in tissue (Hauschka & Konigsberg, 1966; Wessells & Cohen, 1968). These discoveries lead to the conclusion that the ECM plays a crucial role in embryonic inductions (Hay, 1977).

Previous discoveries about the ECM lead to the hypothesis that the ECM has sequences recognized by specific adhesion molecules found on the surfaces of cells, and by 1982, a theory of "dynamic reciprocity" was introduced. This theory states that by interacting with the cell receptors, the ECM has a definite effect on the cytoskeleton and nuclear matrix inside the cell. This interaction can cause a signaling cascade within the cell resulting in the expression of specific genes, which could, in turn, effect the ECM in various manners (Bissell, et al., 1982). It is now commonly known that cell-ECM interactions work directly to promote cell adhesion, migration, growth, differentiation, and apoptosis (Ingber, 1991). Thus, the ECM plays a critical role not only in the stability of tissue, but also in the formation of tissue (Page-McCaw, et al., 2003).

It is believed that the spatial organization of cells within their 3D environment has a huge impact on cell fate decisions, such as survival and apoptosis (Zahir & Weaver, 2004). Thus, when creating a TE construct, it is critical that one take into account the spatial organization of the cells within the construct as well as the scaffold material to be used.

## Three-Dimensional Imaging of Tissue

Tissue has often been examined using two-dimensional (2D) imaging techniques. In the past two decades, there have been enormous improvements in optical microscopy, including axially resolved microscopy techniques. These techniques, including confocal microscopy, have become commonly available in life sciences laboratories (Lin, et al., 2005a). Using these imaging modalities, a user can obtain a stack of 2D images such that each image is at the same relative location in the $x$, $y$ plane but is focused at a different depth within the sample (Shotton & White, 1989).

Initially, these imaging modalities were used for morphological analysis of the microscopic structure of tissue. More recently, these techniques have also been used for quantitative analysis such as measuring the structure of the tissue components and calculating the volume of those components. When confocal microscopy was examined for its effectiveness in finding blood vessels within a tissue sample, it was determined that it is capable of finding more vessels than light microscopy. It was thus concluded that confocal microscopy is a viable method for quantitative and qualitative analysis of angiogenesis (Guo, et al., 2001).

Some automated algorithms have been proposed in the literature to quantify the volume and structure of single cells. These algorithms work well when quantifying single cells and chromosomes, however they do not appear to be sufficient in quantifying structures with complex branching structures (Lin, et al., 2005a). One method to automatically detect cells within a stack of images selects a threshold for each image within the image stack. This method is based on the assumption that each image has a unimodal histogram. Before actually thresholding the images, this method modifies the images in the stack to account for the intensity attenuation that is seen with depth (Umesh Adiga, 2002; Umesh Adiga & Chaudhuri, 1999). Another method incorporates the edge information with the intensity information for pixels in the same ($x$, $y$) location within the image stack. This method appears to work well in segmenting images of biofilms where there is only one foreground object within a single ($x$, $y$) location (Xavier, et al., 2001).

Most quantitative analysis of more complex structures, such as microvessels and neuritis, has required user intervention, and this manual manipulation may introduce extra error to the quantification (Bucher, et al., 2000). Sometimes the images are manually segmented to perform volume rendering of the imaged objects (Bucher, et al., 2000). Deconvolution has been used to aid in removing out-of-focus pixels, however this method was used in conjunction with user intervention to examine the structure of the objects (Lenander & Holmgren, 1999). And, confocal microscopy has been used with tissue processing techniques in order to image deeper into a sample. However, this technique was also used with manual segmentation (Young, et al., 1998).

Three-dimensional tracing methods have been employed to identify tube-like structures including microvasculature and neuronal processes (Can, et al., 1999; Cohen, et al., 1994; He, et al., 2003). However, these methods are more appropriate for examining the architecture of the structure than for measuring the volume occupied by the structure. While this architectural information is useful, a more accurate method that automatically generates volume information about constructs would be useful in analyzing tissue engineered constructs.

### PATTERNING CELLS: MICROFABRICATION

In order to better mimic the spatial organization of cells in vivo, techniques to generate detailed, small-scale patterns of cells have been developed. Microfabrication and micropatterning are two of the names given to a broad range of techniques based on semi-conductor engineering. For biological applications, materials with cell-adhesive properties are patterned so that cells will adhere to the generated architecture. This patterning of cells has provided valuable information on fundamental cell biology and has also been used for some TE applications (Chen, et al., 1997; McDevitt, et al., 2002; Mrksich & Whitesides, 1996). Two types of microfabrication methods used in medicine are photolithography and soft lithography.

Photolithography, the most common microfabrication technique, has been extensively developed and used for many applications of patterning cells (Andersson & van den, 2004). It has been used to pattern cells on the surfaces of hard materials. In this method, materials are patterned using lift-off techniques. Once the pattern is generated, cells are seeded onto the construct by incubating the construct in a cellular solution.

Some examples of cell-adhesion materials that have been used are polylysine, fibronectin, collagen, and Matrigel™ (Andersson & van den, 2004).

When it comes to fabricating small-scale structures for biological applications, soft lithography has emerged as a more desirable microfabrication technique. It is capable of controlling the molecular structure of surfaces, patterning complex biological molecules, fabricating channels that can be used for microfluidics, and manipulating cells (Whitesides, et al., 2001). This method uses stamps or molds generated from elastomeric polymers, and can generate 10 to 100 μm sized patterns of proteins and ligands on surfaces, 50 to 500 μm sized culture chambers, and 10 to 100 μm sized laminar flows of culture media in capillaries (Mrksich, et al., 1996; Xia, et al., 1999). When it comes to creating biological features at least 50 μm wide, soft lithography is a rapid and inexpensive technique (Whitesides, et al., 2001).

Microcontact printing (μCP), a form of soft lithography, involves micromachining of an elastomeric polymer in order to stamp a pattern to which cells can easily adhere. μCP can easily generate features 1.0 μm in size, and recent efforts have generated features as small as 200 nm. Subsequent seeding of cells onto the patterned material has provided valuable information on the effects of shape-based constraints on cells (Chen, et al., 1997; McDevitt, et al., 2002; Mrksich & Whitesides, 1996) as well as control of neurite growth (Oliva, Jr., et al., 2003). While microfabrication techniques can generate small patterns and have provided valuable information about cells, they are limited to two dimensions (Mrksich & Whitesides, 1996).

## RAPID PROTOTYPING

Because tissue is 3D, 2D methods for patterning cells are of limited use in building TE constructs. One way to circumvent this problem is to use a 3D rapid prototyping (RP) method. Rapid Prototyping is the most common name that is given to the group of technologies used to create physical, 3D objects directly from computer-aided design (CAD) sources. These methods build a 3D object in a layer-by-layer fashion. Some other common names are freeform fabrication, solid freeform fabrication, and layer manufacturing.

These methods are known as additive technology, because they add more to the construct with each layer. Prior to the creation of this technology, the common applications used to create complex structures were subtractive fabrication methods such as milling or turning. The use of additive technologies has reduced the time to market in manufacturing and has made it easier to communicate product designs between users and engineers. The ease of use of this technology has resulted in it being used by a wide array of people, including surgeons, architects, tissue engineers, and artists. There are numerous RP techniques, the most common being stereolithography, fused deposition modeling, and three-dimensional printing.

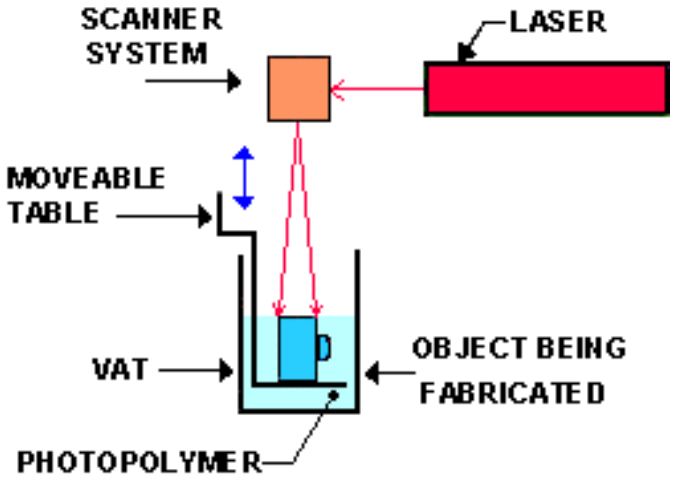




FIGURE 1.2, Schematic Representation of Stereolithography

Reprint with permission (Appendix E) from Castle Island, Co., http://home.att.net/~castleisland).

Stereolithography (SLA) is one of the most common types of RP. This method is based on selectively shining a laser beam onto the surface of a vat of liquid photopolymer. Just below the surface of the polymer is a moveable table. When the beam touches the liquid, that portion of the material quickly polymerizes becoming a solid. To build each layer of the construct, the laser beam moves across the surface of the polymer tracing the geometry of the cross-section of that layer. After each layer is completely traced and it has mostly solidified, the stage is lowered a small distance into the vat of liquid polymer. This allows the machine to polymerize another layer on top. As layers are built, each layer adheres to adjacent ones, creating a solid 3D object. A schematic illustration of SLA is seen in Figure 1.2.

If the construct being fabricated has undercuts or overhangs, these can be upheld by support structures. Once the manufacturing process is complete, these supports would be removed. When the final layer has been polymerized, the fabrication process is complete. The object is then removed from the vat, drained, and wiped off to remove excess material. Some, but not all, photopolymers require a final cure before they are completely stable. This further stabilizes the object by bathing it in light within an oven-like appliance called a Post-Curing Apparatus.

SLA has been considered to be the most accurate of the available RP technologies. Some limitations of working with this method are that it is very messy to use these photopolymers and most photopolymers require a post-curing step, which lengthens the time to obtain a final product. Thus, creating a photopolymer that is easier

and faster to work with is an ongoing research focus for those working with SLA machines.

Fused Deposition Modeling (FDM) is the second most widely used RP technology. In FDM, a plastic filament, approximately 1/16 inch in diameter, is unwound from a coil and goes through the nozzle. The nozzle is able to turn on and off a heating mechanism in order to selectively melt the plastic filament in its tip. This allows the machine to control the flow of a thin bead of liquid through the nozzle. This nozzle is able to move along the *x*-, *y*-, and *z*-axes in order to deposit the liquid plastic onto a scaffold. As each layer is built, the new layer of plastic bonds with the previous layer to form a solid construct. A schematic illustration of FDM is seen in Figure 1.3.

In order to have better control over the process, the entire machine is encased in an oven and held at a temperature just below the melting point of the plastic filament. This allows the system to only apply a moderate amount of additional thermal energy in order melt the plastic. Again, when there are overhangs or undercuts, support structures must be designed and included in the fabrication process. There are numerous materials that are usable with this method, including nylon-like polymers, machinable casting waxes, and investment casting waxes.

FDM is fast and not nearly as messy as SLA. It is able to rapidly fabricate objects on the order of a few cubic inches as well as objects that have tall, thin form-factors. However, with parts that have wide cross sections, this method is relatively slow; and, it is still not as accurate as SLA.

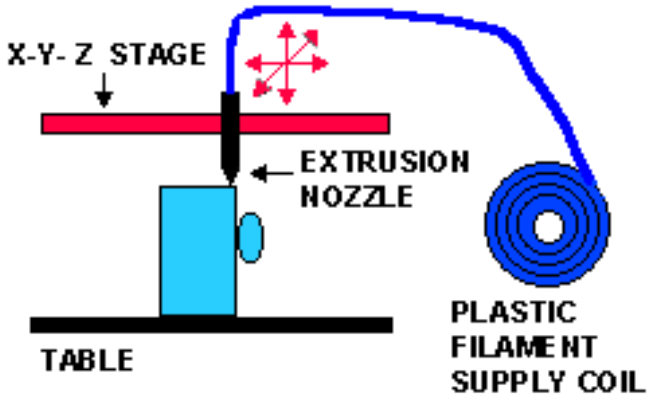




FIGURE 1.3, Schematic Representation of Fused Deposition Modeling

Reprint with permission (Appendix E) from Castle Island, Co., http://home.att.net/~castleisland).

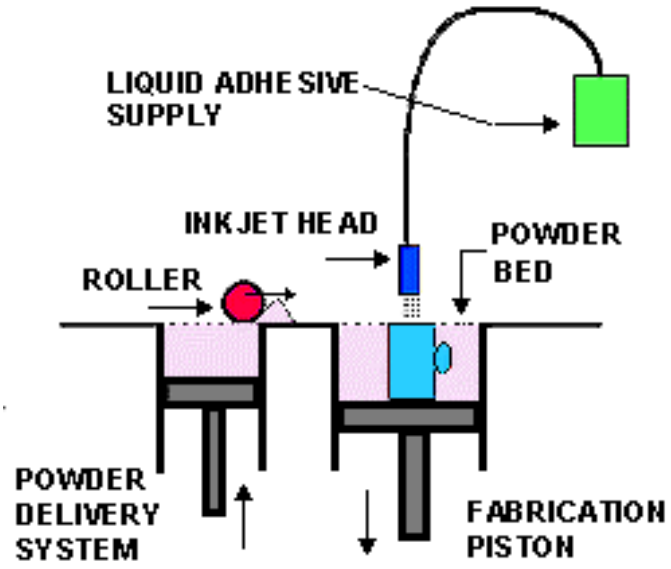




FIGURE 1.4, Schematic Representation of 3D Printing

Reprint with permission (Appendix E) from Castle Island, Co., http://home.att.net/~castleisland).

Three-Dimensional Printing (3DP) is a RP technology that was developed at MIT. This method is similar to SLS and FDM. The main difference is that an ink-jet head is used rather than a laser. A schematic illustration of 3DP is seen in Figure 1.4. This method works by running a print head over a bed of powder and selectively depositing liquid adhesive. The adhesive acts as a binder for the powder. After each layer is completed, the fabrication piston moves down, the powder delivery piston moves up, and the roller spreads and compresses more powder over the build cylinder. Once the object is completed, the extra powder is brushed away.

This technique had been licensed to numerous companies, including Soligen, Therics, ExtrudeHone, Specific Surface, and Z Corp. One nice feature of this method is that the powder bed acts as a support to overhangs in the construct, i.e., no external supports are necessary. The primary advantages of this method are low material costs and rapid fabrication. While it may be the fastest RP technique, it has limited resolution capabilities. Some other disadvantages of this method are the surface finish, part frailty, and lack of materials that can be used.

## BIOLOGICAL APPLICATIONS OF RAPID PROTOTYPING TECHNIQUES

SLA is the most common RP method used in biomedical applications, and it has been employed to build models of biological structures (Lermusiaux, et al., 2001; Pentecost, et al., 2001; Vanezi, et al., 2000; Yourtee, et al., 2000), bone substrate scaffolds (Cooke, et al., 2003), and heart valve scaffolds (Hoerstrup, et al., 2000; Sodian, et al., 1999; Sodian, et al., 2000a; Sodian, et al., 2002b). Other RP methods have also been used to create 3D, biomedical objects such as porous scaffolds (Zein, et al., 2002),

cranial implants (Gronet, et al., 2003), drug delivery devices (Leong, et al., 2001), models of pathologies (Berry, et al., 2002), scaffolds for cartilage repair (Sherwood, et al., 2002), metallic scaffolds for orthopedic applications (Curodeau, et al., 2000; Melican, et al., 2001), and oral dosage forms (Katstra, et al., 2000; Rowe, et al., 2000).

Most biomedical applications of RP methods have focused on creating TE scaffolds that are later invaded by cells either in vivo (Cooke, et al., 2003) or in vitro (Hoerstrup, et al., 2000; Sherwood, et al., 2002; Sodian, et al., 2000a). However, these methods use a random placement of cells. It has been proposed that using a RP technique to pattern not only the scaffold, but also the cells, will accelerate and improve tissue assembly (Mironov, et al., 2003). Based on this idea, there has been a recent emergence of various RP methods to not only lay down scaffold, but cells as well.

Optomec, Inc., has been developing a direct-write method to deposit biological materials into 3D, mesoscopic patterns. This method, trademarked as DWB™, uses an aerosol-based system to deposit cells into specific 2D patterns with a possible extension of directly writing cells onto a 3D, TE scaffold. This method is illustrated in Figure 1.5.

In this process, cells are first suspended in medium consisting of nutrients, antibiotics, and fungicides. This medium aids the cells by encapsulating them throughout the process. Applying carrier air to the cell suspension generates a stream of aerosolized particulate material. Co-flow gas is then used to sheath and guide the material to be deposited. The cell droplets are deposited onto a target substrate that is capable of moving along the *x*- and *y*-axes (Marquez, et al., 2002).

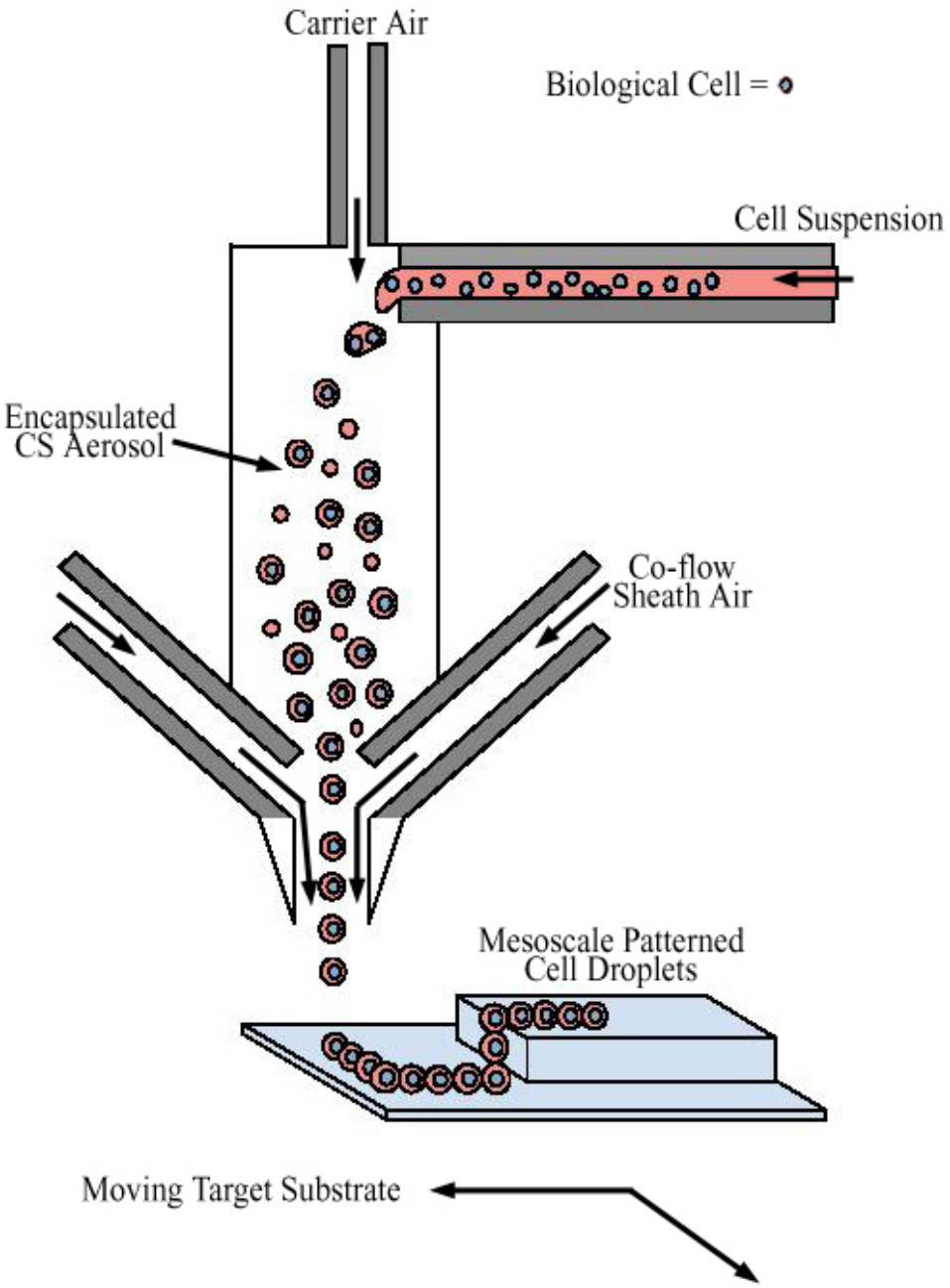


FIGURE 1.5, Schematic of the DWB™ Process to Deposit Cells

Reprint with permission (Appendix E) from the authors and Elsevier Ltd (Marquez, et al., 2002).

To show the utility of this system with biological materials, it has been used to deposit 3T3 mouse fibroblasts onto a 2D culture dish. The deposited drops of cells encapsulated in media were approximately 20μm in diameter. After deposition, the cells proliferated, forming a confluent monolayer after 72 hours. This demonstrated that the cells were, indeed, viable (Marquez, et al., 2002).

Further work is being performed to generate multi-cellular lines with a width less than 100μm. A critical element of this work is the rapid addition of growth medium. When this medium is not added, the cell membranes break down and the cells die. Two methods to protect against this problem have been wetting the target substrate prior to depositing the material and adding aerosolized media in the co-flow sheath air (Marquez, et al., 2002).

Thus far, the primary focus of this technology has been on generating 2D cellular layers, however, this system is capable of extruding multiple layers of cells. A unique feature of this system is that the deposition head is fixed and does not move along the *z*-axis. It could easily be designed to deposit complex 180° hemispherical scaffolds. This could be done by allowing the target substrate to rotate or by fixing the deposition head to a five-axis, wrist-like apparatus (Marquez, et al., 2002).

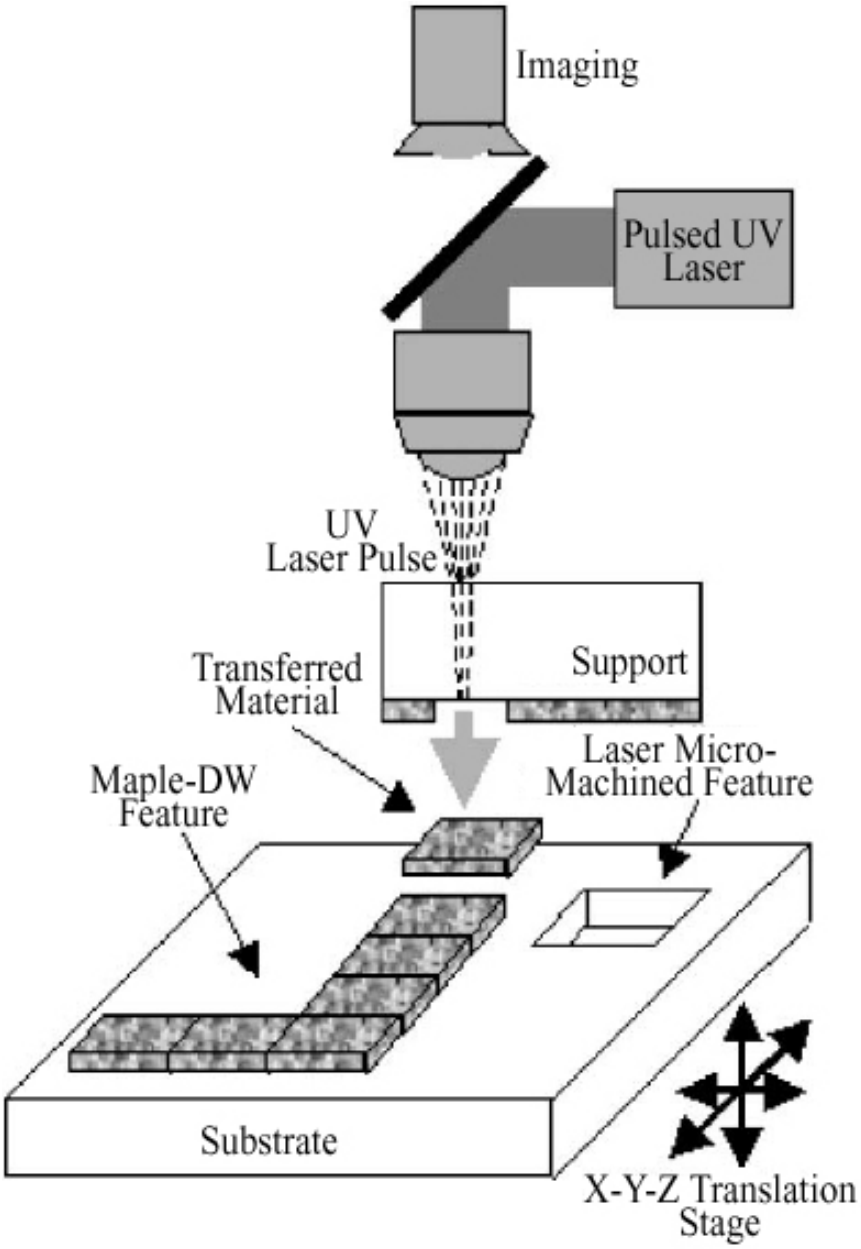


FIGURE 1.6, Schematic of the MAPLE-DW Machine

Reprint with permission (Appendix E) from the authors and Biomaterials (Ringeisen, et al., 2002a).

The Naval Research Labs have developed a direct-write system called Matrix Assisted Pulsed Laser Evaporation Direct-Write (MAPLE-DW) (Chrisey, et al., 2003; Ringeisen, et al., 2002a; Ringeisen, et al., 2002b; Ringeisen, et al., 2004). This laser forward transfer technique uses vaporization, or micro-explosions, to move material from the coating of a carrier support to the target scaffold. The goal for this system is that it be compact, rapid, highly automated, and capable of using almost any type of material to generate a construct with micro-resolution features. The main goal in fabricating this system is that the system has enough force to shape metals and oxides while also being gentle enough to transfer a cell without compromising its membrane. A schematic of the MAPLE-DW technique is illustrated in Figure 1.6.

This system focuses laser pulses onto a carrier support made of silica polymer and coated with a thin layer of material. As the pulse propagates through the support, the temperature at the material/support interface begins to increase. This generates a vapor that causes a small piece of the material to be propelled off of the support and onto the target substrate. This material can be laid down in a high-resolution pattern by scanning and modulating the laser.

Originally, MAPLE-DW was created to direct-write micron-scale, passive electronic devices. It has had success in fabricating high-performance electronic elements by laying down conductive, resistive, and dielectric inks (Chrisey, et al., 2003). It has also been shown to be capable of generating mesoscopic patterns of living cells and active proteins. Among the cells that have been viably patterned are E. coli bacteria, Chinese hamster ovaries, human osteoblasts, and mouse pluripotent cells. The proteins

that have been patterned are biotinylated bovine serum albumin (BSA) and anti-BSA (Ringeisen, et al., 2002a; Ringeisen, et al., 2002b; Ringeisen, et al., 2004). Using this technique, the Naval Research Labs have had success in depositing patterns of cells on a surface in an arbitrary pattern. Thus far, this work has only deposited cells into 2D patterns, but the goal is to move this technique into creating 3D tissues as well as high-density microarrays (Ringeisen, et al., 2002b).

Several groups have examined the use of ink-jet technology to create 2D and 3D constructs (Saunders, et al., 2004; Wilson, Jr. & Boland, 2003). It has been shown that this technology can be modified to print 2D constructs containing cells (Wilson, Jr. & Boland, 2003), and that it can be further modified to create multi-layer constructs by printing 600μm cell aggregates (Boland, et al., 2003). Some of the cell types that have been successfully printed include bovine aortic endothelial cells (Wilson, Jr. & Boland, 2003) and human fibroblasts (Saunders, et al., 2004). A joint group at Clemson University and the Medical University of South Carolina has done the most work with this technology. A description of their work follows.

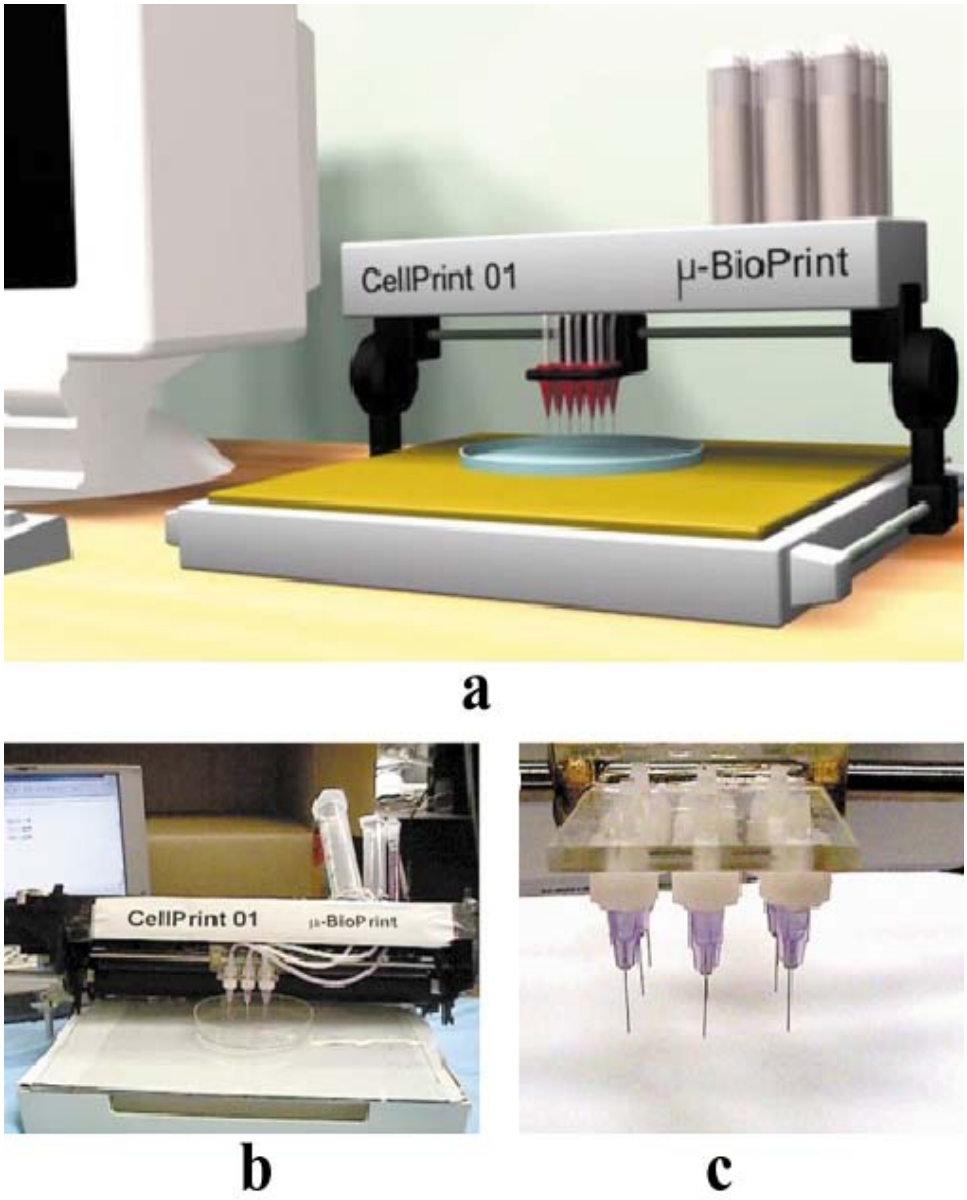


FIGURE 1.7, Modified Ink-Jet for Cell Printing

(a) Schematic of the HP 660C that was modified to be able to print proteins and cells. (b) Picture of the actual cell printer. (c) Close up image of the print heads attached to the cell printer. Reprint with permission (Appendix E) from the authors and Trends in Biotechnology (Mironov, et al., 2003).

Wilson and Boland demonstrated that an HP 550C ink-jet printer could be modified to enable it to print biological solutions such as proteins or cells. This printer can be seen in Figure 1.7. It has 9 print heads that can operate individually or simultaneously. Each print head is operated by a piezo pump and has tubing that connects it to a cell solution. To direct the printing of the cell solution, the user creates a text data file containing *x* and *y* locations as well as the print head to use. This file is then input into the computer controller and translated to information usable by the printer. The smallest *x* or *y* step that can be used is 50μm (Wilson, Jr. & Boland, 2003).

This system was originally designed to print 2D patterns. Their first attempts to print viable cells used bovine aortic endothelial cells (BAEC), which were printed onto Matrigel™ and collagen gels. The BAEC were suspended in media and printed using a 30 gauge needle. They observed that approximately 25% of the cells died and hypothesized that this was due to the evaporation of the media around the cells (Wilson, Jr. & Boland, 2003). It was further demonstrated that this system is capable of printing 3D constructs by printing collagen, a thermo-reversible polymer, and 600μm cell aggregates of BAEC. It was observed that when these aggregates are in close proximity in a collagen gel, they migrate toward each other and fuse together. This work demonstrates that ink-jet technology can be modified to print viable patterns of cells and matrix (Boland, et al., 2003).

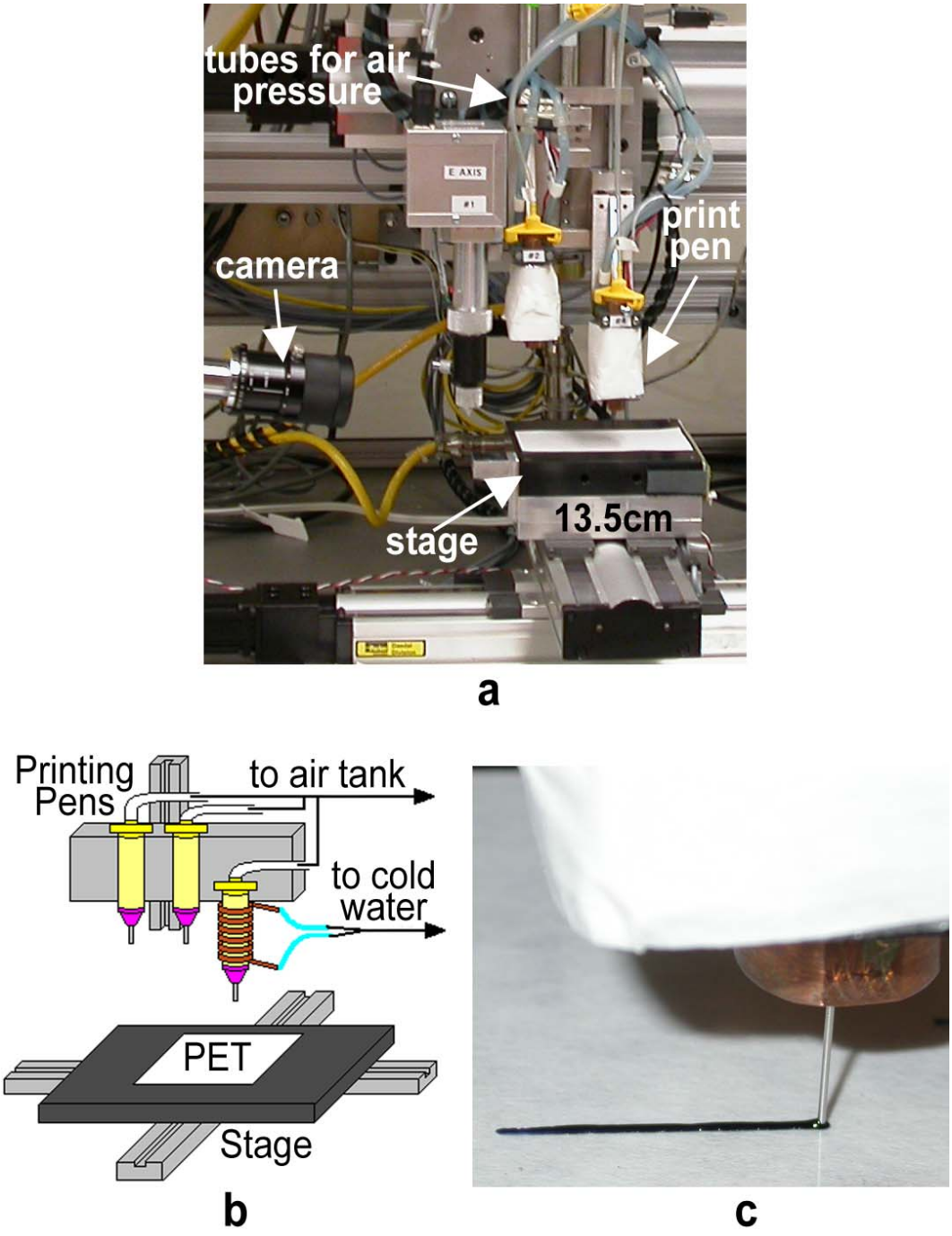


FIGURE 1.8, Images of the BAT

(a) Image of the actual BAT cabinet. (b) Schematic illustration of the printing components of the BAT. (c) Close up image of one of the pneumatic print pens extruding colored material.

## THE BIOASSEMBLY TOOL

The BAT is another RP system that has been designed to pattern both cells and matrix. Through funding from DARPA, Sciperio, Inc., worked with the University of Arizona to design and fabricate this 3D, direct-write system that is capable of depositing cells and matrix into viable, 3D constructs. Sciperio is a company that specializes in biotechnologies related to tissue engineering tools, vaccine-based innate and adaptive immunotherapy treatments, rare event cellular imaging, digital printing deposition technologies, RF wireless communications, and water purification technologies.

The BAT was designed as an upgradeable system accepting new units and functions to face upcoming tasks. To produce artificial constructs that would demonstrate properties of native tissue (microenvironment, 3D organization, and inter-cellular contact), techniques of digital printing and tissue engineering were combined. Pictures of the BAT can be seen in Figure 1.8. The BAT utilizes a computer-aided-design/computer-aided-manufacturing (CAD/CAM) approach to build 3D heterogeneous tissue models. It is a multi-head, through-nozzle deposition machine deemed to conformably deposit biomaterials, cells, and co-factors on various supporting surfaces to create surrogate tissues and tentative platforms for experiments in cell biology and tissue engineering. The device contains: an *xy* coordinate system with a stage; four *z*-traveling deposition heads; a combined water-jacket thermistor temperature controls for each deposition head; a water jacket temperature control for the stage; and a piezoelectric humidifier.

The process of deposition is controlled by specified software allowing flexible alteration of parameters such as 3D geometry of the deposition pathways, linear speed of

deposition, air pressure in the pneumatically actuated heads, and syringe plunger rate in the positive displacement head. The BAT features reproducibility of the *xyz* positioning of the extrusion nozzles with a resolution of better than 5μm. Reciprocal spatial calibration of the individual nozzles allows for the in-line replacement of one nozzle for another one with the same 5μm accuracy. The positive displacement deposition head allows for deposition rates of 12nl/sec up to 1ml/sec. The linear speed of the deposition for any of the pens can vary from 10μm/sec up to 50mm/sec.

The BioAssembly Tool, initially called the Biological Architecture Tool, was originally designed to construct 2D objects. However, it was quickly realized that this system could be used to fabricate 3D objects in a layer-by-layer fashion. Initial studies used a UV-polymerizable plastic paste comprised of a polypropylene fumarate (PPF) or polypropylene fumarate-co-ethylene glycol (PPF-PEG) base and 10 wt % dichloromethane, 0.5 wt % bis (2, 4, 6-trimethylbenzoyl) phenylphosphine oxide (BAPO), and 50-80 wt % sucrose filler. This paste was then polymerized using a TL003 Facial Sunlamp (Kachurin, et al., 2002).

The first 3D object that was fabricated was a model of the human external ear. A technique for scanning and digitizing a picture of a human ear was developed specifically for the BAT. In order to preserve the negative-angle elements, each layer was created using a raster-filling mode such that the raster direction was rotated 90° for every other layer. It took more than three hours to create a 19-layer construct that was approximately 15mm thick. While this experiment took a long time, it still showed promise in creating TE constructs (Kachurin, et al., 2002).

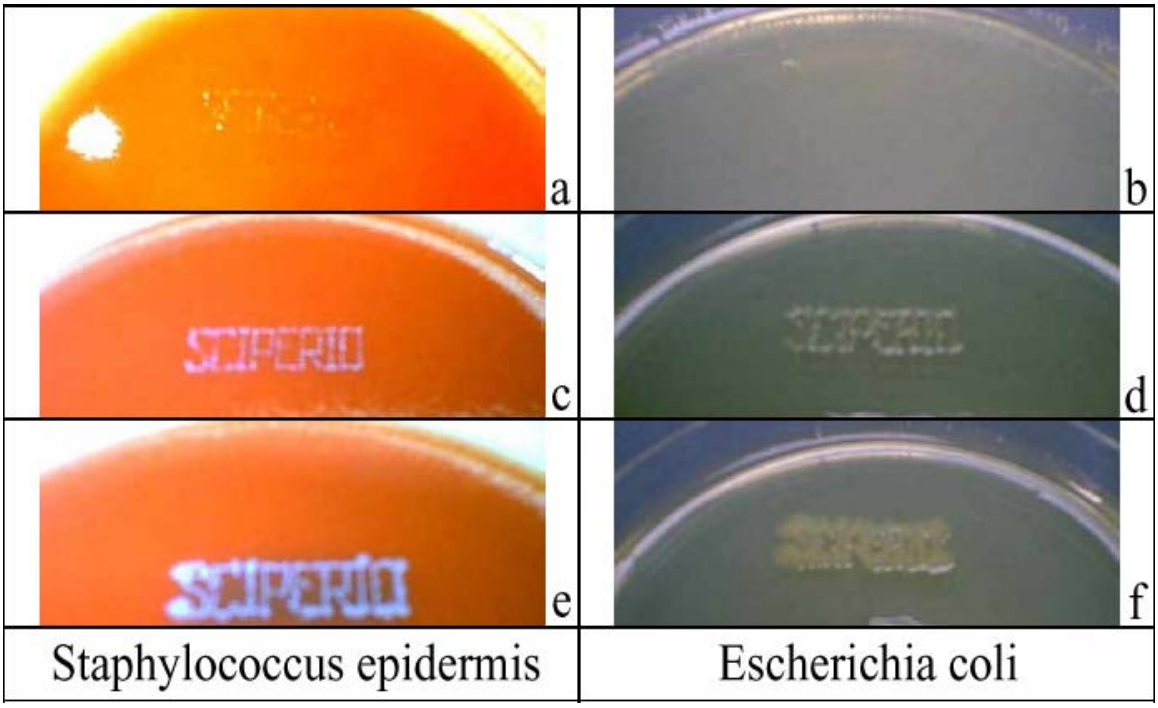


FIGURE 1.9, Patterned Bacteria

Laboratory safe staphylococcus epidermis (a, c, e) and escherichia coli (b, d, f) were extruded into a pattern of the company name “SCIPERIO”. Patterns were barely visible right after extrusion (a, b), but became readily apparent after 12 (c, d) and 36 hours (e, f) of incubation. Reprint with permission (Appendix E) from the authors and Trends in Biotechnology (Kachurin, et al., 2002).

The next step in examining the utility of the BAT in creating TE constructs was to demonstrate that it is capable of creating viable patterns of cells. To do this, non-hazardous laboratory brands of staphylococcus epidermis and escherichia coli were used. A 30μm inner diameter (ID) print head was used on a pneumatic print pen. The company name "SCIPERIO" was extruded into a petri disk. This pattern was easily seen soon after extrusion, and, after 12 and 36 hours it was clear that the bacteria had expanded within the pattern, exhibiting viability. Images of these patterns can bee seen in Figure 1.9 (Kachurin, et al., 2002).

The preliminary experiments using the BAT demonstrated that it is capable of creating 2D and 3D biological objects, including acellular scaffolds and cellular constructs. These experiments also demonstrated that computer-controlled dispensing systems have the ability to become integral parts of creating tissue engineered constructs (Kachurin, et al., 2002).

## RESEARCH PLANS

There are numerous organs and tissues that can be transplanted from one patient to another, including kidney, heart, liver, lung, pancreas, intestine, cornea, skin, bone, and bone marrow. The list of people waiting to receive a transplant in the United States is continually increasing; and for every 63 people who receive an organ transplant, another 16 people die waiting to receive a transplant. The increasing need for transplants is due to the shortage of available donor organs (US Dept of Health and Human Services, 2003).

As a way to make tissue available for transplantation, a relatively new field has emerged. Tissue engineering is a multidisciplinary field that utilizes expertise in medicine

and engineering to repair or replace damaged tissue. The driving hypothesis for this new field is that culturing cells in the appropriate 3D environment will allow the cells to organize into tissues and possibly organs (Langer & Vacanti, 1993).

Numerous methods have been employed to build viable, TE constructs. These include using cells alone, scaffold alone, or a combination or cells and scaffold. In the body, tissues and organs are a complex structure of both cells and matrix. Thus, the most commonly used TE approach has focused on using both cells and scaffold (Lavik & Langer, 2004). For the most part, this approach uses random seeding of cells ex vivo; however, the scaffold itself may provide an architectural guideline for the organization of the cells (Boudreau, et al., 1995; Langer & Vacanti, 1993; Shieh & Vacanti, 2005; Vacanti & Langer, 1999).

Because the spatial organization of both cells and ECM is important in natural tissue, it has been suggested that using a method to spatially organize both the cells and the scaffold would accelerate and improve tissue assembly (Mironov, et al., 2003). This would also aid the TE construct in performing more like native tissue. Thus, the field of TE has recently focused on patterning various cell types in a 3D construct (Andersson & van den, 2004).

Some RP systems have been developed with the ability to spatially organize both cells and matrix within a TE construct. These systems include an aerosol-based, direct-write system (Marquez, et al., 2002), a pulsed-laser, direct-write system (Ringeisen, et al., 2002a), and modified ink-jet printers (Saunders, et al., 2004; Wilson, Jr. & Boland, 2003). Each system has been shown to be capable of fabricating 2D mesoscopic patterns

of viable cells. Thus far, only the modified ink-jet printer has demonstrated the ability to generate viable, 3D constructs.

The work described within this dissertation focuses on utilizing a direct-write BioAssembly Tool to fabricate spatially organized, 3D constructs comprised of cells and matrix. To better characterize this system, three specific aims have been proposed. The overall driving hypothesis behind these aims is that a direct-write printing system designed for electronics is capable of fabricating viable constructs of cells and matrix that have a specified spatial organization and are truly 3D.

**Specific Aim #1**: Evaluate the ability of a 3D, direct-write BioAssembly Tool to generate viable, spatially-organized constructs by co-extruding cells suspended in matrix. **Hypothesis #1: Three-dimensional, direct-write technology can be used to generate viable constructs by co-extruding cells and matrix.** A 3D, direct-write BioAssembly Tool will be evaluated in its ability to create viable, spatially organized constructs comprised of collagen and bovine aortic endothelial cells. Printed constructs will be evaluated morphologically and histochemically.

**Specific Aim #2:** Develop an image processing algorithm to accurately determine the volume of cells within a 3D construct. **Hypothesis #2: An automated thresholding algorithm can be generated to accurately threshold stacks of confocal images.** A 3D collagen gel containing fluorescent microspheres will be generated by putting 0.25ml of the collagen solution into the well of a 48-well plate. Image stacks of the construct will be obtained using a confocal microscope. Algorithms to threshold the stacks will be

implemented and their accuracy will be accessed by comparing their volume measurements with the true volume of spheres. Once an accurate algorithm is determined, it will be tested on a tissue phantom containing microvessel fragments embedded in a collagen gel.

**Specific Aim #3:** Characterize the fabrication of spatially organized, 3D cellular constructs using a 3D, direct-write BioAssembly Tool. **Hypothesis #3a: The process of extruding cells through the BioAssembly Tool's pneumatic pens does not have an immediate effect on the viability of the extruded cells. Hypothesis #3b: Environmental parameters, such as humidity and stage heat, do have a direct impact on the viability of cells printed using the BioAssembly Tool.** Parameters associated with the BioAssembly Tool generating spatially organized collagen constructs will be examined for their effects on the viability of extruded cells. These parameters will include pen tip inner diameter, extrusion pressure, printing speed, cell concentration, and humidity. Three-dimensional collagen constructs will also be fabricated and measured for height and viability. Finally, cells will be layered within the 3D constructs to show that spatial organization is feasible even with 3D constructs.

# 2. A THREE-DIMENSIONAL BIOASSEMBLY TOOL FOR GENERATING VIABLE TISSUE ENGINEERED CONSTRUCTS

Portions of the chapter have been published in Tissue Engineering:

Smith, CM, AL Stone, RL Parkhill, RL Stewart, MW Simpkins, AM Kachurin, WL Warren, and SK Williams.

Three-Dimensional BioAssembly Tool for Generating Viable Tissue-Engineered Constructs. Tissue Engineering.

*Tissue Engineering.* 10 (9-10): 1566-1576, 2004.

## INTRODUCTION

The spatial organization of cells provides cell-cell adhesion cues that are important in directing numerous biological functions, such as embryonic tissue development, organ formation, and tissue regeneration instigated by wound healing (Edelman & Crossin, 1991; McDevitt, et al., 2002; Takeichi, 1995). This spatial organization is necessary for the preservation of vital cell-cell interactions (Geiger & Ayalon, 1992; Larue, et al., 1996; Shibuya, et al., 1995) as well as cell phenotype (Ben Ze'ev, et al., 1988). Due to the significance of these interactions, a considerable challenge in tissue engineering has been to control the spatial organization of cells. This is critical in tissues, such as nerves and blood vessels, where appropriate function depends on specialized architectures (Pardanaud, et al., 1989; Patel, et al., 1998; Risau, et al., 1988).

Techniques, such as soft lithography and photolithography, have been used to deposit biological materials into specific 2D geometries. Subsequent seeding of cells onto the patterned material has provided valuable information on the effects of shape-based constraints on cells (Chen, et al., 1997; McDevitt, et al., 2002; Mrksich & Whitesides, 1996) as well as control of neurite growth (Oliva, Jr., et al., 2003). However, tissue is 3D, thus 2D methods are of limited use in building tissue engineered constructs. One way to get around this problem is to use a 3D rapid prototyping method.

Rapid Prototyping refers to a group of technologies that build a physical, 3D object in a layer-by-layer fashion. Stereolithography, one of the most common types of RP, operates by selectively shining a laser beam into a vat of liquid photopolymer. This method has been employed in numerous biomedical applications such as building models of biological structures (Lermusiaux, et al., 2001; Pentecost, et al., 2001; Vanezi, et al., 2000; Yourtee, et al., 2000), bone substrate scaffolds (Cooke, et al., 2003), and heart valve scaffolds (Hoerstrup, et al., 2000; Sodian, et al., 1999; Sodian, et al., 2000a; Sodian, et al., 2002b). Other RP methods have also been used to create 3D objects for numerous biological applications, including porous scaffolds (Zein, et al., 2002), cranial implants (Gronet, et al., 2003), drug delivery devices (Leong, et al., 2001), models of pathologies (Berry, et al., 2002), scaffolds for cartilage repair (Sherwood, et al., 2002), metallic scaffolds for orthopedic applications (Curodeau, et al., 2000; Melican, et al., 2001), and oral dosage forms (Katstra, et al., 2000; Rowe, et al., 2000).

Most biological applications of RP methods have focused on creating TE scaffolds that are later invaded by cells either in vivo (Cooke, et al., 2003) or in vitro

(Hoerstrup, et al., 2000; Sherwood, et al., 2002; Sodian, et al., 2000a). These methods used random placement of cells. It has been proposed that using a RP technique to pattern not only the scaffold, but also the cells, will accelerate and improve tissue assembly (Mironov, et al., 2003). Based on this idea, there has been a recent emergence of various RP methods to not only lay down scaffold, but cells as well. Marquez, et al. (Marquez, et al., 2002), examined the used of an aerosol-based, direct-write system to deposit cells into specific 2D patterns with a possible extension of directly writing cells onto a 3D tissue-engineered scaffold. The Naval Research Labs have shown that a laser forward transfer technique can be used to generate 2D mesoscopic patterns of viable bacteria (Ringeisen, et al., 2002a) and mammalian cells (Ringeisen, et al., 2002b), with a goal of extending this research to 3D viable tissue. It has also been shown that ink-jet technology can be modified to print 2D constructs containing cells (Wilson, Jr. & Boland, 2003), and that it can be further modified to create multi-layer constructs by printing 600μm cell aggregates (Boland, et al., 2003).

It has previously been shown that a 3D, direct-write BioAssembly system can be used to create 3D scaffolds and that this technique can be extended to create patterned constructs containing living cells (Kachurin, et al., 2002). This system, designated the BioAssembly Tool, or BAT, is capable of using pneumatic or positive displacement pens to deposit material in a controlled 3D pattern. This study describes the utilization of the BAT to co-extrude cells and biomaterials into a 3D spatially organized, viable construct.

# MATERIALS AND METHODS

## Description of BioAssembly Tool

To produce artificial constructs that would demonstrate properties of native tissue (microenvironment, 3D organization, and inter-cellular contact) techniques of digital printing and tissue engineering were merged. The BioAssembly Tool utilizes a CAD/CAM approach to build 3D heterogeneous tissue models. The BAT is a multi-head, through-nozzle deposition machine deemed to conformably deposit biomaterials, cells, and co-factors on various supporting surfaces to create surrogate tissues and tentative platforms for experiments in cell biology and tissue engineering. The device contains: an *xy* coordinate system with a stage; a number of *z*-traveling deposition heads (currently up to 4), each of which is supplied with individual controlling video camera; a fiber optic light source to illuminate the deposition area and cure photopolymers in-line; individual ferroelectric temperature controls for each deposition head; a water jacket temperature control for the stage; and a piezoelectric humidifier.

## Mechanics of Depositing Materials

The process of deposition is controlled by specified software allowing flexible alteration of parameters such as 3D geometry of the deposition pathways, linear speed of deposition, air pressure in the pneumatically actuated heads, or syringe plunger rate in the positive displacement heads. The BAT features reproducibility of the *xyz* positioning of the extrusion nozzles with a resolution of better than 5μm. Reciprocal spatial calibration of the individual nozzles allows for the in-line replacement of one nozzle for another one

with the same 5μm accuracy. The positive displacement deposition heads allow for deposition rates of 12nl/sec up to 1ml/sec. The linear speed of the deposition for any of the pens can vary from 10μm/sec up to 50mm/sec.

The temperature stability of the deposition heads and the stage is 1°C within the range -10°C to 80°C. Recent versions of the BAT are encapsulated in positively pressurized and ventilated casings that meet BioHazard II safety requirements. Piezoelectric and optical sensors allow for conformable deposition on curved surfaces. The BAT has been designed as an upgradeable system accepting new units and functions to face upcoming tasks.

Pluronic F-127 Extrusion

A solution of 30% polyoxyethylene / polyoxypropylene was obtained by dissolving pluronic F-127 (PF-127; Sigma-Aldrich, St. Louis, MO) in water. This solution was then transferred to the reservoir of a 1ml positive displacement pen with a 350μm ID stainless steel capillary tip, where it was maintained at 2°C. A mock-up of a 2mm × 2mm × 1.5mm house was built with four walls and a two-sided roof. This was done in a layer-by layer fashion onto a standard 3-inch glass slide, which was fixed on the *xy* stage and maintained at 25°C. A syringe plunger rate of 2μm/sec and linear stage speed of 250μm/sec was used. The pen was raised 50μm between each layer.

Human Fibroblasts + PF-127 Extrusion

Human primary fibroblasts (Cambrex BioScience, Rockland MA) were grown to a confluent monolayer, trypsinized, and sedimented at 800G into a compact pellet. A

solution of 35% PF-127 was obtained by dissolving PF-127 (Sigma-Aldrich, St. Louis, MO) in fibroblast growth media (Cambrex Bio Science, Rockland, MA). This solution was then slowly mixed with the fibroblast pellet to a final concentration of 27%. The PF-127 + fibroblast solution was transferred to the reservoir of a 1ml positive displacement pen with a 450μm ID capillary tip where it was maintained at 2°C. The solution was then extruded in a spiral mode onto a polystyrene slide, which was fixed on the *xy* stage. The stage was maintained at 25°C by using a NESLAB water circulator. A tube was built with a diameter of 2.5mm and a height of 1.5mm. A positive displacement plunger speed of 1.5μm/sec was used with a linear speed of 200μm/sec. The pen was raised 100μm between each layer. After the deposition, the tubular construct was dissolved in phosphate buffered saline (PBS), and the fibroblasts were washed and sedimented in PBS. The fibroblasts were then subjected to a standard Trypan Blue penetration test to access viability.

Type I Collagen Extrusion

A solution of 3.0mg/ml collagen was prepared by mixing purified rat-tail Type I Collagen (BD Biosciences, Bedford, MA) with 4× DMEM. This solution was brought to a pH of 7.0-7.4 by the addition of 1M NaOH. Half a milliliter of the solution was then transferred to a 3ml pneumatic pen reservoir with a 25 gauge (250μm ID) or 33 gauge (90μm ID) tip (EFD, Inc., East Providence, RI) and maintained at 10°C. To determine the pen pressures needed to extrude continuous lines of type I collagen, both the 25 gauge and 33 gauge pen tips were used with pressure settings of 0.0-2.5psi. The collagen

solution was extruded onto the hydrophilic side of flat sheets of polyethylene terephthalate (PET or Mylar™; Bio-Rad Laboratories, Hercules, CA). Six sets of 5 lines were generated with a linear speed of 10mm/s and 20mm/s and a range of pressures, including 0, 0.5, 1, 1.5, 2, and 2.5psi. The constructs were stained for 5 minutes with Coomassie blue and then washed with DCF-PBS. The line widths for each construct were measured in 15 different locations. In order to show the ability of the BAT to generate complex geometries, single-layered linear to overlapping non-linear shapers were extruded onto the hydrophobic side of Mylar™. This was executed using the 33 gauge pen tip with a linear speed of 20mm/sec and a pen pressure setting of 1.7psi.

BAEC + Col I Solution Preparation

Bovine aortic endothelial cells (passages 2-9) were expanded in T75 culture flasks with warm culture medium of 10% heat inactivated fetal bovine serum (Gemini-Bio-Products, Inc., Carlsbad, CA) in Ham's F-12 (Invitrogen, Corp., Carlsbad, CA). After growing to a confluent monolayer, the cells were trypsinized and sedimented at 172G. The supernatant was removed and the cell pellet was suspended in 100µl of media with pen/strep and fungizone. The pellet was broken up by light pipetting and then put on ice. This solution was mixed with 3.0mg/ml type I collagen (method to create 3.0mg/ml collagen described above). Concentrations of 5-20 million BAEC/ml Col I were used. Prior to extrusion, the pneumatic syringe barrels, pen tips, and PET were ethylene oxide sterilized. These supplies were then cooled to -20°C to prevent early polymerization of the collagen. The BAEC + Col I solution was put into a 3ml pneumatic pen reservoir with

either a 25 gauge or 33 gauge tip (EFD, Inc., East Providence, RI) and maintained at 10°C.

BAEC + Col I Extrusion

The BAEC + Col I solution was extruded in a layer-by-layer fashion onto the hydrophilic side of Mylar™ (Bio-Rad Laboratories, Hercules, CA). For initial experiments, a 5-layered zigzag pattern was created with lines 11.5mm long and a distance between lines of 1.5mm (Figure 2.5c). For experiments constructing a physiological pattern, a 5-layered, continuous-extrusion pattern was created from the angiogram of a pig heart. The resulting pattern was less than 2mm × 1mm × 0.15mm. Table 2.1 contains information on linear speed, pressure, distance the pen was raised between each layer, amount of time that was waited before a layer was deposited on top of a previous layer, and amount of time the constructs were incubated prior to adding warm media. In order to prevent polymerization of the collagen within the pen, the pen was maintained at 10°C; and in order to speed up the process of polymerization a standard light was aimed at the construct to increase the temperature of the black stage. Each new layer was laid down on top of the previous layer after a specified waiting time (see Table 2.1), however new layers were extruded before previous layers had fully polymerized. After deposition, constructs were gently bathed in warm culture medium with pen/strep and fungizone and placed in a 37$^{o}$C incubator with 5% $CO_2$. After each session, the remaining solution was extruded into a 48 well tissue culture well plate as a positive control for cell viability.

| Pen Tip | Linear Speed | Air Pressure | Distance Between Layers | Wait Between Layers | Incubation Time |
|---|---|---|---|---|---|
| 33 g | 20 mm/s | 1.7 psi | 10 μm | 0 sec | 0 min |
| 25 g | 15 mm/s | 1.5 psi | 30 μm | 30 sec | 2 min |

TABLE 2.1, Parameters Used to Co-Extrude BAEC + Col I

Linear speed, pen pressure, amount the pen was raised between each layer, amount of time that was waited before a layer was deposited on top of a previous layer, and amount of time the constructs were incubated prior to adding warm media were all subject to change based on the pen tip used.

BAEC + Col I Imaging

Patterned constructs of BAEC + Col I were observed and imaged in vitro for up to 35 days using a Nikon Phase Contrast microscope at 4× and 10× magnification. Some BAEC + Col I constructs were incubated with Coomassie blue for 5 minutes and then rinsed twice with PBS in order to stain the cells.

Assessing Viability and Pattern Persistence

After 24 hours of incubation, constructs were imaged using phase microscopy in order to assess their viability. If cells were dark and round, they were counted as dead. If cells were bright and elongated, they were counted as alive. Using the two counts from multiple fields within multiple constructs, the relative viability was calculated as the total number of live cells divided by the total number of cells counted. After 1 hour and 24 hours of incubation, the total number of cells for a single line within a 1.2mm × 0.5mm field was counted. As a further test of viability as well as to examine proliferation, the total number of cells was calculated in constructs on days 0 and 1; this was done for 3-4 lines within 3 constructs. Using SigmaPlot, a paired student's T-test was utilized to examine the cell counts for the two time points. To examine the pattern persistence of the cultured constructs, line widths were calculated for 3-4 lines within 3 constructs. This was done for constructs in culture at days 0, 1, and 9. Using SigmaPlot, a paired student's T-test was utilized to examine the line widths between the three time points.

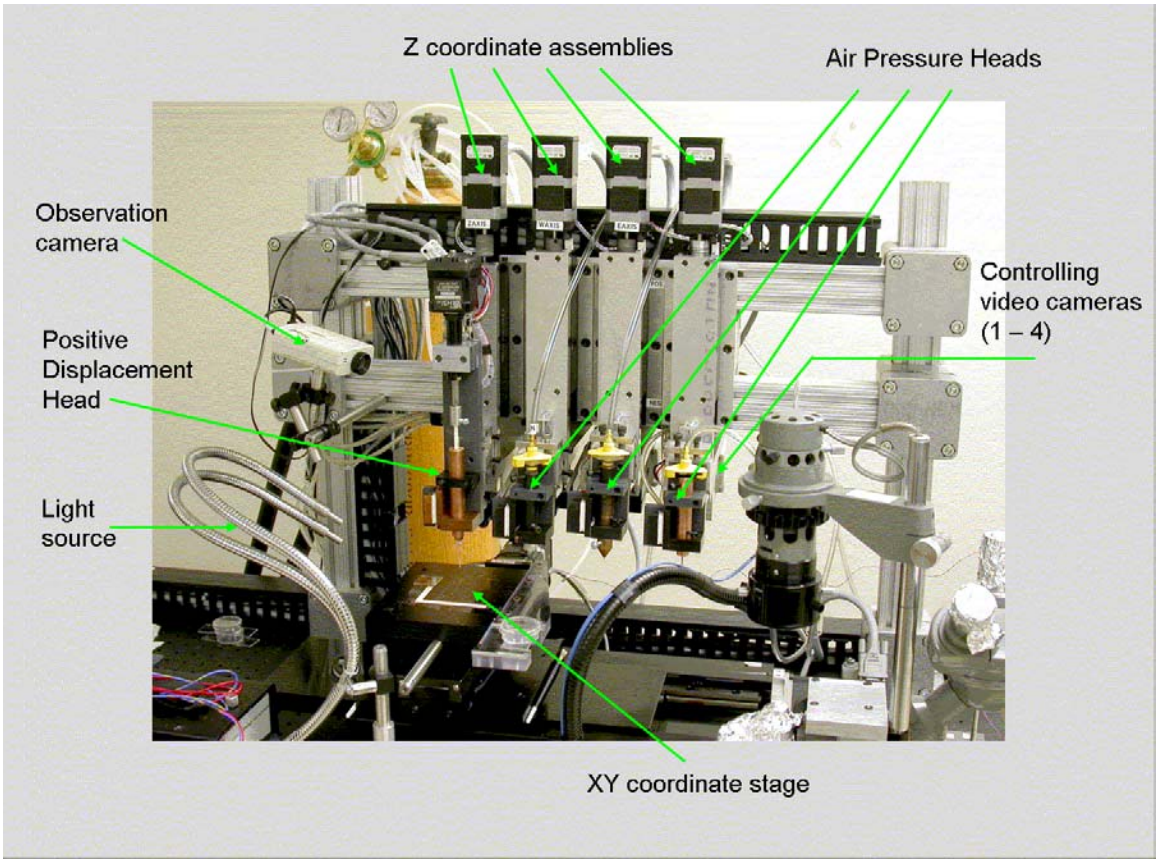


FIGURE 2.1, The 3D Direct Write BioAssembly Tool

Reprint with permission (Appendix E) from Tissue Engineering (Smith, et al., 2004).

# RESULTS

## BioAssembly Tool

The 3D, direct-write system, designated the BAT, is a three-axis machine capable of moving the stage and delivery pen in the *x*-, *y*-, and *z*-axes separately or simultaneously. This configuration provides the flexibility and control that enables the BAT to create complex 3D objects. The deposition mechanism of this system consists of four extrusion heads, or micro-dispense pens, with modular pen tips. There are two types of pens: a positive displacement pen and a pneumatic pen. Figure 2.1 illustrates the BAT and some of its components.

## Generating Complex 3D Structures

Text files, called scripts, are used to orchestrate the movement of the BAT. These scripts can be manually created by directly entering the movement commands, or they can be generated automatically by inputting a single image or a stack of images into a specially designed CAD program. The commands within a script control pen speed, air pressure, pen movement on the *z*-axis, and stage movement on the *x*- and *y*-axes. Because the BAT is a three-axis machine, it is capable of generating 3D linear and nonlinear patterns.

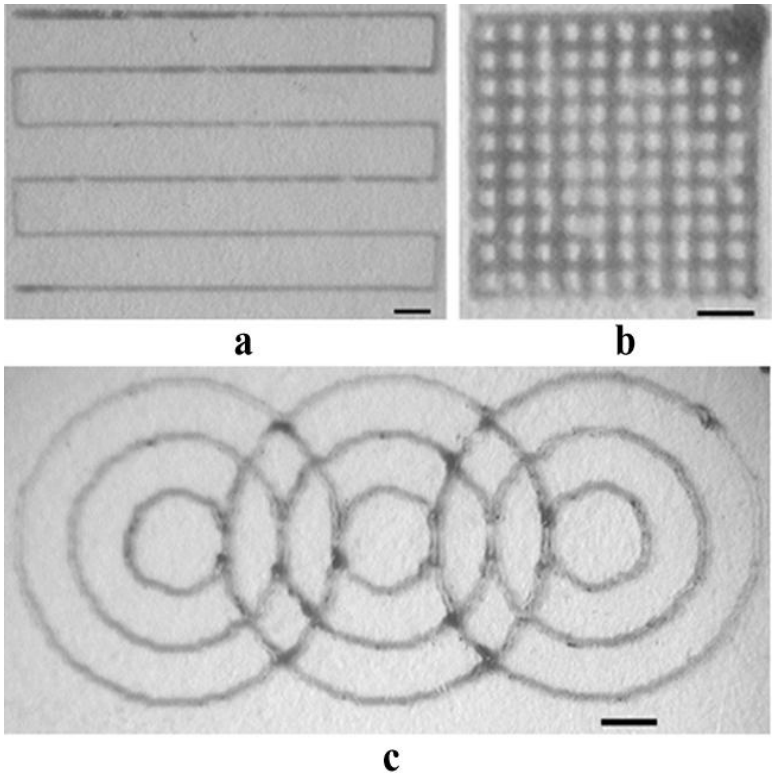


FIGURE 2.2, Linear and Nonlinear Patterns Generated with Collagen I Alone

Sample single-layered constructs of collagen alone, deposited in (a) zigzag, (b) overlapping grid, and (c) overlapping nonlinear patterns. Bar = 1mm. Reprint with permission (Appendix E) from Tissue Engineering (Smith, et al., 2004).

The pattern capabilities of the BAT were demonstrated by generating linear to overlapping nonlinear patterns comprised of collagen alone (Figure 2.2) as well as a 3D mockup of a house using PF-127 (Figure 2.3). Single layer collagen constructs were generated on the hydrophobic side of Mylar™ using a pneumatic pen with a 90μm ID pen tip. The width of the extruded lines was 90-110μm. The multi-layer house mockup was generated using a positive displacement pen with a 350μm ID pen tip; and the thickness of the walls was 350-400μm.

Constructing Fibroblast + PF-127 Tubes

In order to test the utility of the BAT in co-extruding cells and matrix, human primary fibroblasts were suspended in pluronic F-127 and extruded in a spiral mode onto a polystyrene slide (Figure 2.4). This was done using a positive displacement pen with a 450μm ID pen tip. The resulting structure had a wall thickness of 450-500μm. After deposition, the fibroblasts were then subjected to a standard Trypan Blue penetration test to access viability, which showed that the viability of the cells was approximately 60%.

Generating BAEC + Col I Constructs

Before extruding collagen containing cells, it was determined what pressure was required for both the 25 gauge and 33 gauge pens to print a continuous line of collagen. It was determined that the minimum pressure setting for the 25 gauge pen is 2.0psi and the minimum pressure setting for the 33 gauge pen is 2.5psi.

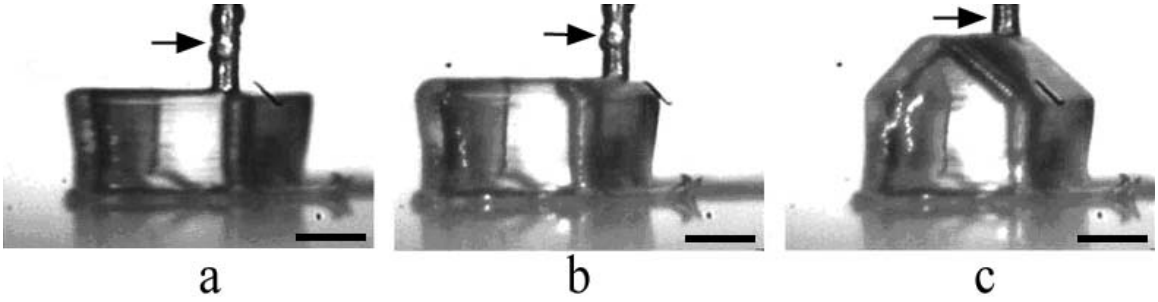


FIGURE 2.3, Mockup House Generated with 30% PF-127

Images of house mockup built in a layer-by-layer fashion, include (a) walls of house with no roof, (b) initial extrusion of 45° roof built with no support, and (c) final mockup of house including 2 walls and a 45° intact roof. Arrows point to the pen tip. Bar = 1mm. Reprint with permission (Appendix E) from Tissue Engineering (Smith, et al., 2004).

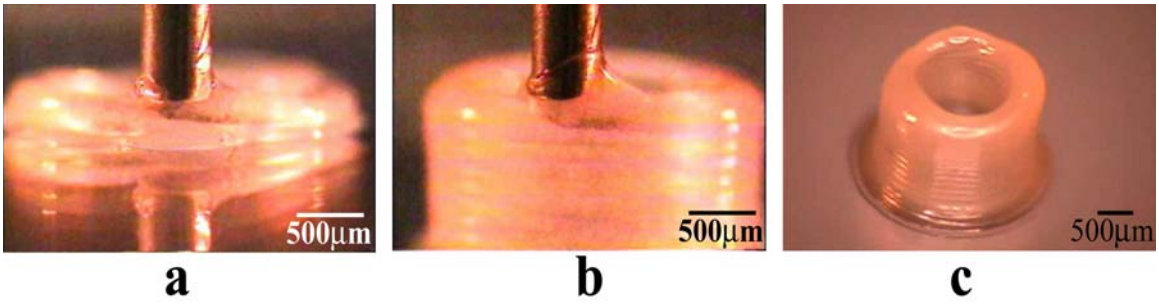


FIGURE 2.4, Human Fibroblast + PF-127 Tube

Images of tube built in a spiral, layer-by-layer fashion, include (a) first two layers of tube being built, (b) after multiple layers of the tube have been extruded, and (c) the final 15-layer fibroblast + PF-127 tube. Reprint with permission (Appendix E) from Tissue Engineering (Smith, et al., 2004).

To demonstrate that the BAT is capable of creating viable constructs containing other cells than fibroblasts, BAEC were suspended in a solution of collagen and extruded onto the hydrophilic side of Mylar™ using pneumatic pens with either a 25 or 33 gauge pen tip. The width of the lines was 2-3 times the width of the pen tip. When using a 250μm ID pen tip, the lines were approximately 700μm wide; and when using a 90μm ID pen tip, the lines were approximately 200μm wide. These lines were wider than the collagen alone constructs, because they have 5 layers instead of just 1 and they were deposited onto the hydrophilic side of PET rather than the hydrophobic side.

The BAEC + Col I lines appeared to have a consistent width as well as an even distribution of cells throughout the length of each line. As seen in figure 2.5a, the standard deviation of cell distribution in a 1.2mm × 0.5mm field of a single line was approximately 24%. Also the deviation of line widths in the constructs was approximately 9%, and when these constructs were maintained in culture, there was no significant difference in the line widths between days 0, 1, and 9 (Figure 2.5b).

If the media was added too vigorously or before the collagen fully polymerized, the middle of the line washed away resulting in a high concentration of cells on the edges of the deposited lines (Figure 2.5d). This was especially prevalent in constructs extruded using the larger, 25 gauge, pen tip. This was solved by waiting 30 seconds before printing a layer on top of another layer and by incubating the constructs for 2 minutes before adding media. If media was added greater than 2 minutes after printing, the viability of the constructs dropped to approximately 0%.

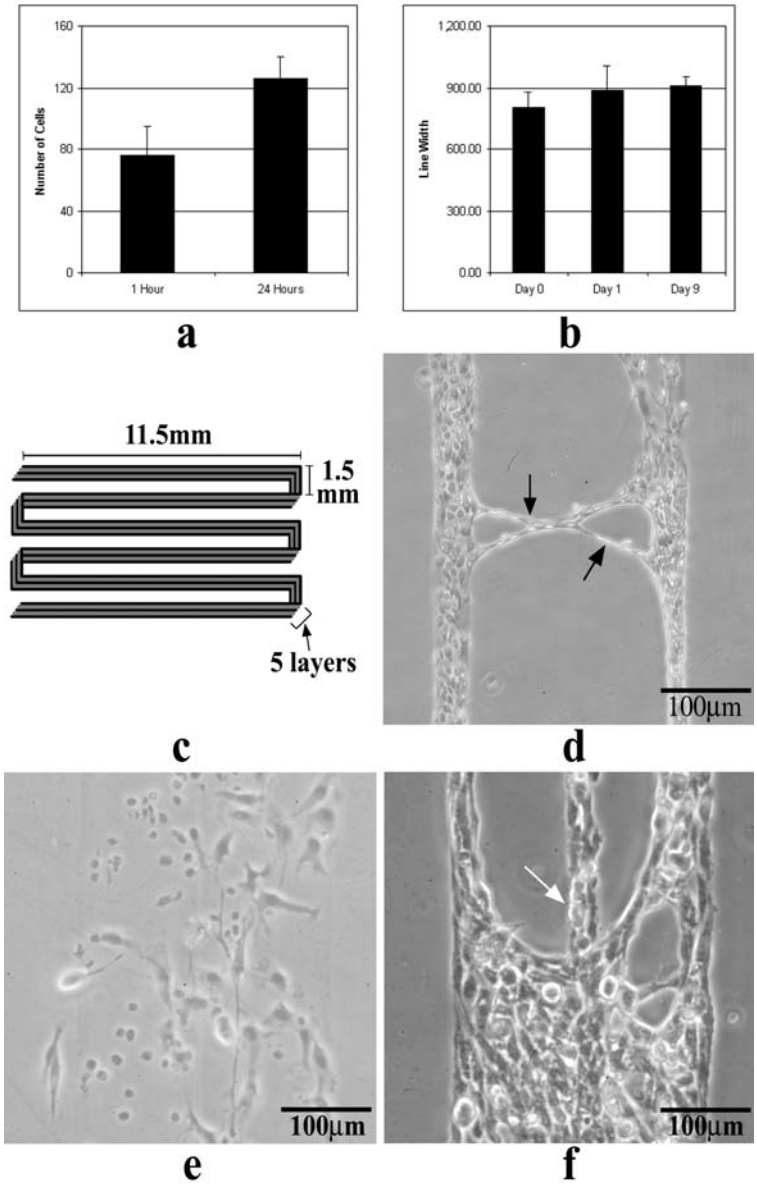


FIGURE 2.5, BAEC + Col I Zigzag Constructs Maintained in Culture

(a) Graph illustrating the increase in cell number between 1 hour and 24 hours in culture, $p = 0.0014$ (b) Graph illustrating the line widths of the constructs maintained in culture for 0, 1, and 9 days. (c) Schematic of the 5 layers that were deposited. (d) When media was added to the constructs too rapidly, the center of the line was washed away, as seen at day 2. Otherwise, the lines have a relatively even distribution of cells, as seen at days (e) 1 and (f) 35. Arrows point to a cord-like structure seen within constructs. Reprint with permission (Appendix E) from Tissue Engineering (Smith, et al., 2004).

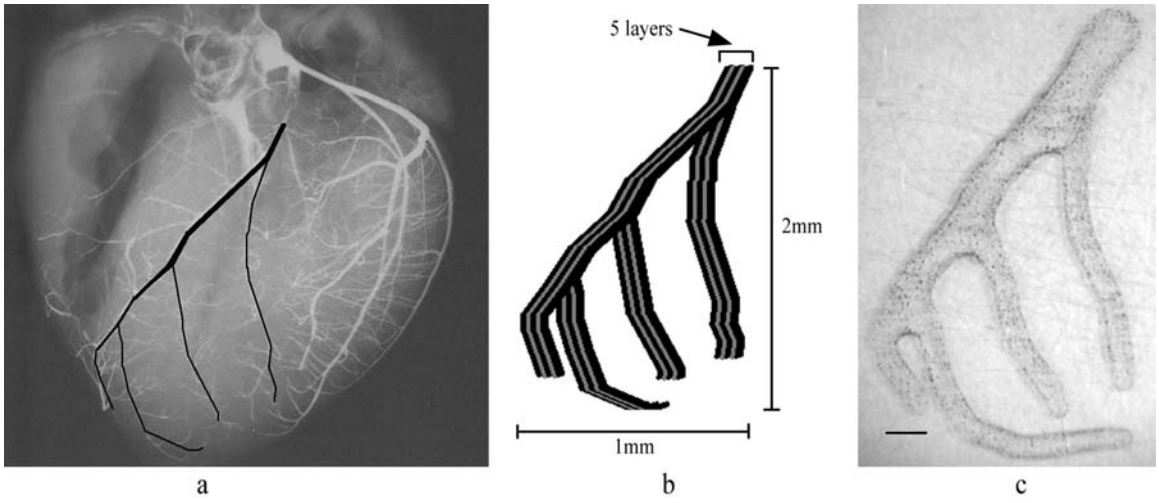


FIGURE 2.6, BAEC + Col I Constructs Generated Based on Anatomical Structure

(a) An angiogram of a pig heart was used to develop a script to direct the BAT to extrude five layers of solution in the pattern of the LAD and its four diagonals (black lines). (b) Schematic of the five layers that were printed. (c) Image of BAEC + Col I co-extruded using the angiogram script, as seen at day 0. Reprint with permission (Appendix E) from Tissue Engineering (Smith, et al., 2004).

After 24 hours of incubation, the cells began to elongate, demonstrating cell viability. By counting the number of elongated and round cells, the viability for the 33 gauge pen tip was calculated as 46% viable, while the viability for the 25 gauge pen tip was calculated as 86% viable. The vast majority of dead cells was seen at the edges of the generated lines, indicating that the wait period between extruding subsequent layers was not causing the constructs to dry out such that initial layers died. Viability was further assessed by examining the number of cells within a 1.2mm × 0.5mm field of a single line. As shown in figure 2.5a, between 1 hour and 24 hours, this number significantly increased by approximately 130%. This indicates both viability and proliferation. When maintained in culture for up to 35 days, the cells filled in the extruded pattern and as early as day 2, cord-like structures were observed within the constructs, implying that the cells recognized a 3D environment.

Physiological Pattern Deposition

To demonstrate the CAD/CAM capabilities of the BAT, a pattern was generated from a vascular tree structure observed in native tissue. The prototype structure used as a model in these studies was generated from an angiogram of the coronary vasculature of a pig heart. Figure 2.6a illustrates the angiogram of a heart with the left anterior descending (LAD) artery and four diagonal artery branches outlined in black. A 5-layered continual-extrusion script was generated from the outlined vessels (Figure 2.6b). In a layer-by-layer fashion, a construct of BAEC + Col I was fabricated with the same pattern as that found in the prototype. Figure 2.6c illustrates the construct 2 hours after extrusion, thus the cells have not yet begun to elongate and proliferate. As in the construction of the zigzag

pattern, each layer was built upon the previous layers while raising the pen tip 30μm between each layer. Results similar to those in the simpler constructs were observed in these more complicated constructs (not shown). Again, when maintained in culture for up to 35 days the results suggested proliferation, phenotypic differentiation, and pattern persistence.

## DISCUSSION

The primary focus of TE is to restore tissue and organ function loss caused by disease or injury. Because of the importance of spatial organization in directing biological function (Pardanaud, et al., 1989; Patel, et al., 1998; Risau, et al., 1988), a significant goal of TE is the controlled generation of 3D scaffolds. Numerous RP techniques have been employed in the creation of such scaffolds. Most applications involve acellular scaffolds followed by in vivo or in vitro cellular invasion (Park, et al., 1998; Sherwood, et al., 2002; Sodian, et al., 2000b). Recently there has been an emergence of RP systems capable of placing cells and scaffold into defined patterns (Boland, et al., 2003; Marquez, et al., 2002; Ringeisen, et al., 2002a; Ringeisen, et al., 2002b; Wilson, Jr. & Boland, 2003). It has been proposed that using such a technique will remove the cell invasion step and will thus accelerate and improve assembly of tissue (Mironov, et al., 2003). This study suggests using a 3D, direct-write system, such as the BAT, to create viable scaffolds by initially placing the cells in their desired location within the scaffold.

Other methods to lay down cells into defined 3D patterns have been investigated. One such method uses a modified ink-jet printer with an independently operated piezo

pump. Thus far, this method has been used to drop individual spheres of cells, called cell aggregates, onto 3D scaffolds (Boland, et al., 2003; Wilson, Jr. & Boland, 2003). Another method, MAPLE-DW, uses a laser to vaporize a matrix containing cells toward a scaffold (Ringeisen, et al., 2002a; Ringeisen, et al., 2002b). Yet another method deposits pneumatically or ultrasonically atomized cells encapsulated in growth media onto a substrate. This is done by generating a stream of aerosolized particulate material that is then sheathed by a co-flow gas, which deposits the particulate into a defined pattern.

The BAT is a three-axis system that can move along any of its axes separately or simultaneously. It has two mechanisms to extrude cells into a defined pattern: a positive displacement pen with variable plunger rates and a pneumatic pen with variable pressures. Thus, a key difference between the previously mentioned methods and the BAT is that the BAT, while capable of laying down individual dots of material, works by extruding a continuous segment of material similar to a log or rod. The other methods lay down single dots of material. These dots can be placed adjacent to previous dots such that they blend together to form a rod-like structure. The BAT is most similar to the modified ink-jet technology (Boland, et al., 2003; Wilson, Jr. & Boland, 2003) in that it utilizes modular syringe-like barrels and tips that can be separately sterilized. Also, the mixture that is extruded is combined prior to loading it into the system and each system has multiple pens such that multiple cellular solutions can be deposited during the same extrusion session.

Because of the BAT's ability to move along three axes simultaneously, this system is more flexible than systems constrained to raster scanning. This feature gives it

the ability to easily generate linear and nonlinear patterns. The directions for generating these patterns can be manually entered by a user or can be generated using a CAD program comprised of a single or multiple images (e.g., Magnetic Resonance or Computed Tomography images). Thus, the BAT can be used to generate multi-layered constructs based on true anatomical structure.

This chapter has demonstrated that a 3D, direct-write system, such as the BAT can be used to generate spatially organized constructs containing PF-127 plus fibroblasts as well as collagen plus BAEC. PF-127 is able to enhance stability of proteins loaded into the gel matrix with complete recovery of activity when dissolved in excess buffer (Barichello, et al., 1999; Stratton, et al., 1997) and has been used in biomedical applications, particularly as a drug delivery system for opthalmic (Desai & Blanchard, 1998; Desai & Blanchard, 2000; Edsman, et al., 1998), rectal (Miyazaki, et al., 1986), parenteral (Johnston, et al., 1992; Morikawa, et al., 1987; Pec, et al., 1992), and percutaneous (Miyazaki, et al., 1995) use. In this study, it was shown that the BAT could generate 3D structures of PF-127 and human fibroblasts and that after deposition, approximately 60% of the fibroblasts remained viable. Also, by building a mock-up of a house with a two-sided roof, it was demonstrated that a 45° angle could be generated without a supporting scaffold. Thus, this material could also be useful as a scaffold material when extruding less rigid type I collagen solutions.

In order to demonstrate that the BAT is capable of creating viable constructs containing cells other than fibroblasts, the system was used to co-extrude BAEC suspended in collagen. The in vitro findings indicated that when BAEC were extruded

with a 25 gauge tip they were 86% viable, and when they were extruded using a 33 gauge tip they were 46% viable. In fact, these findings also indicated proliferation and pattern persistence. Similarly, within the constructs, the formation of cord-like structures were observed, indicating phenotypic differentiation. These results correspond with previous work that stated when endothelial cells are cultured in type I collagen, they will undergo rapid proliferation (Madri & Williams, 1983), migration (Montesano, et al., 1983), and formation into cord-like structures (Iruela-Arispe, et al., 1991; Montesano, et al., 1983). Thus, this system could be used to study in vitro angiogenesis.

Nör, et al. (Nör, et al., 2001), showed that EC embedded in poly-L-lactic acid sponges implanted subcutaneously will differentiate into functional vessels that anastamose with the host vasculature. However, after 28 days, while there were blood vessels within the implant, most of the implanted cells had died. Other studies have shown that co-implantation of vascular endothelial cells and mesenchymal precursor cells have the ability to form a network of blood vessels that remain viable for up to one year (Koike, et al., 2004). Shepherd, et al. (Shepherd, et al., 2004), demonstrated that when microvessel fragments embedded in a collagen gel were implanted, the fragments would anastamose with the host vasculature and remain intact for at least 28 days. The BAT has the unique ability to extrude individual cells or possibly even microvessel fragments into specific architectures. In addition, because the BAT has multiple pens, it is capable of spatially organizing separate cellular solutions during a single deposition session. Based on these capabilities and previous studies, it is hypothezied that the BAT has the ability to

build TE constructs that are capable of inosculating with the host vasculature and remaining viable for a long period of time, e.g. up to 1 year.

Based on these results with PF-127, fibroblasts, collagen, and endothelial cells, it is believed this technique is capable of generating viable TE constructs by extruding various other cell types (e.g., neurons, osteoblasts, myocytes). Similarly, due to its ability to deposit multiple cell solutions during one extrusion session, the BAT can create 3D, multi-cellular constructs with spatial organization specific to each of the cell types being deposited. Because tissue is multi-cellular, a TE construct that more closely resembles native tissue could be generated. Thus, the BAT is a useful tool for generating TE constructs by laying down cells and matrix into specialized architectures.

# 3. ACCURATE VOLUMETRIC MEASUREMENTS OF VASCULATURE USING CONFOCAL MICROSCOPY AND IMAGE PROCESSING

## INTRODUCTION

Tissue is a complex structure of multiple cell types within a dynamic three-dimensional microenvironment. Numerous biological functions, such as tissue development, organ formation, wound healing, and homeostasis, depend on the interaction of cells within a tissue (Edelman & Crossin, 1991; McDevitt, et al., 2002; Takeichi, 1995; Zahir & Weaver, 2004). The specific architecture of cells within a tissue provides cell-cell and cell-extracellular matrix cues that are important in directing these functions (Geiger & Ayalon, 1992; Larue, et al., 1996; Shibuya, et al., 1995). The importance of this spatial organization is exemplified by the development and maturation of blood vessels through vasculogenesis, angiogenesis, and arteriogenesis (Pardanaud, et al., 1989; Risau, et al., 1988). Because cell and tissue survival is contingent upon proper blood flow, studying the structure and organization of blood vessels has been a prominent focus of research for several years (del Zoppo, 1994; del Zoppo & Mabuchi, 2003; Park, et al., 2003).

Various in vitro three-dimensional models have been created to study the formation and organization of blood vessels. These assays have examined using a single cell type, namely endothelial cells (Folkman & Haudenschild, 1980; Madri & Pratt, 1986; Nor, et al., 2001; Schechner, et al., 2000), or multiple cell types (Koike, et al., 2004; Nicosia, et al., 1982; Nicosia & Ottinetti, 1990; Shepherd, et al., 2004) to create an in

vitro environment similar to that with native vasculature. Other models use cultured, intact vessel segments that better recapitulate the angiogenesis process including sprouting of new vessels from the existing parent segments (Arthur, et al., 1998; Brown, et al., 1996; Hoying, et al., 1996; Nicosia, et al., 1982; Zhu, et al., 2000). In one example, implantation of the cultured fragments lead to the inosculation of construct vessels to the host circulation (Shepherd, et al., 2004).

Three-dimensional imaging has provided a wealth of information about tissue; however, it is primarily used for qualitative analysis or requires significant user intervention to obtain quantitative information. Recently, there has been an improvement in image analysis techniques that have resulted in automated routines to segment structures such as cell nuclei and genomic signals (Chawla, et al., 2004; Lin, et al., 2003; Lin, et al., 2005b). Three-dimensional tracing methods have been employed to identify tube-like structures including microvasculature and neuronal processes (Can, et al., 1999; Cohen, et al., 1994; He, et al., 2003). However, these methods are more appropriate for examining the architecture of the structure than for measuring the volume occupied by the structure.

The primary contribution of this chapter is the development of an accurate and efficient algorithm for automatically thresholding three-dimensional microvascular structures. First, a tissue phantom containing fluorescent microspheres was imaged using confocal microscopy. Various thresholding, or segmentation, algorithms found in the literature were examined for their effectiveness in accurately segmenting three-dimensional stacks of images. Next, new segmentation algorithms were generated and

examined. The parameters of these algorithms were determined by a specialized array of heuristic optimization techniques. Finally, the resulting segmentation algorithm was examined for its effectiveness with a new set of tissue phantoms as well as with microvascular constructs.

## MATERIALS AND METHODS

### Tissue Phantoms

Tissue phantoms were made by suspending 15μm fluorescent FocalCheck™ microspheres (Molecular Probes, Inc., Eugene, OR) in type I collagen gels. These spheres fluoresce throughout the whole sphere and the accuracy of their diameters is reported as ±3%, i.e., ±0.45μm. A solution of 3.0mg/ml collagen was prepared by mixing purified rat-tail type I collagen (BD Biosciences, Bedford, MA) with 4X DMEM. This solution was brought to a pH of 7.0-7.4 by the addition of 1M NaOH. The microspheres were suspended in the collagen at a concentration of 12,500 microspheres/ml. The microsphere/collagen suspensions were plated (0.25ml) into individual wells of a 48-well plate and incubated at 37°C for 15 minutes. To simulate cultured constructs, an equal volume of 10% fetal bovine serum (FBS) was added and constructs were maintained in culture up to 7 days. Constructs were fed every 3-4 days. On days 0 and 7, constructs were fixed for one hour in 2% paraformaldehyde in PBS. They were then rinsed three times in cold PBS and stored protected from light at 4°C in PBS. Because fluorescent spheres were used, there was no need for staining prior to imaging the constructs.

## Microvascular Constructs

Collagen I gels containing rat fat microvessel fragments (RFMF) were generated similar to the methods employed by Shepherd et al. (Shepherd, et al., 2004). Briefly, RFMFs were isolated from epididymal fat pads of retired breeder Sprague-Dawley rats. The harvested fat pads were finely minced and digested in 2mg/ml collagenase (Sigma-Aldrich, St. Louis, MO) plus 2mg/ml bovine serum albumin (BSA) in PBS. To obtain microvessel fragments, this solution was passed through a series of screens to remove large vessel pieces, tissue debris, and single cells. The microvessel fragments were suspended in 3mg/ml rat tail type I collagen at a concentration of 12,000-15,000 RFMF/ml. The preparation of this collagen is described above. The RFMF/collagen suspensions were plated (0.25ml) into individual wells of a 48-well plate and incubated at 37°C for 15 minutes. The constructs were then fed an equal volume of 10% FBS/DMEM and maintained in culture up to 10 days. Constructs were fed every 3-4 days.

## Staining Microvascular Constructs

On days 0, 3, 7, and 10 the microvascular constructs were rinsed in PBS and fixed for 1 hour in 2% paraformaldehyde in PBS. The constructs were then washed in cold PBS three times for 15 minutes each and placed in a blocking buffer (5% nonfat dry milk and 1.5% BSA in TBST buffer) overnight at 4°C. Constructs were incubated overnight with a FITC-conjugated anti-rat MHC primary antibody (eBioscience, San Diego, CA), diluted 1:50 in PBS. The constructs were washed again in cold PBS three times for 15 minutes each and stored protected from light at 4°C in PBS.

## Confocal Microscopy

Stacks of images were generated using a Biorad MRC-1024ES confocal microscope with a 488nm laser excitation and a 525-555nm emission filter. Each image stack was obtained using a 20x lens with a numerical aperture of 0.75, a working distance of 1mm, and an iris (or pinhole) setting of 1. The pixel size was $1.05 \times 1.05\mu m$. In order to simulate having cubic voxels, a $z$-step of $1.05\mu m$ was used; however, the thickness of each image in the stack, which is dependent upon the pinhole, laser wavelength, and numerical aperture of the lens, is defined as $2.48\mu m$. Each image in the stack was $512 \times 512$ pixels with each pixel taking on a value from 0 to 255. Stacks were obtained such that they followed all of the spheres or vessels throughout the whole image stack. This resulted in each stack of images containing a different total number of images, which was no greater than 125 images. For each stack of images, the gain and the offset parameters for the microscope were set such that the range of intensity values was fully utilized, i.e., it was ensured that within the stack there were a few voxels that would be assigned the minimum and maximum intensity values. For the purpose of these studies eight stacks of images were generated with four used as training data and four used as test data.

## Estimating True-Thresholded Microsphere Images

In order to determine the validity of volume estimates in the tissue phantom containing microspheres, each stack of images obtained for a microsphere gel was manually examined. The number of spheres within the image was counted as well as the center integer $(x, y, z)$-coordinate for each sphere. In other words, the center integer $(x, y)$-

coordinates as well as the center image were estimated for each sphere within the image stack by visual examination. After determining the centers of all of the spheres within the stack, a template was used to create black and white images that represent the optimally thresholded stack of images such that each sphere had *x*-, *y*-, and *z*-axis diameters of 15μm and a total volume of 1767$\mu m^3$. These "true-thresholded" images were generated using the sphere template seen in Figure 3.1, where the largest circle is a 15μm diameter circle found in the center image, and the smaller circles are found above and below that center image.

## Thresholding Stacks of Images

Stacks of images generated by the confocal microscope were thresholded to be binary images. These images were obtained by setting voxels that met a specified threshold to be white foreground voxels and voxels that did not meet the threshold to be black background voxels. Determining the threshold criteria is discussed in the next section.

## Estimating Accuracy of Thresholded Microsphere Images

Once microsphere images were thresholded, they were compared with the true-thresholded images in order to count the total number of correctly classified and misclassified voxels, including correctly labeled foreground voxels (True Positive), correctly labeled background voxels (True Negative), voxels labeled as foreground that should have been labeled as background (False Positive), and voxels labeled as

background that should have been labeled as foreground (False Negative). These values were then used to calculate the following:

$$\%\ True\ Volume = \frac{(Number\ of\ \ Foreground\ Voxels\ in\ True - Thresholded\ \ Stack)}{(Number\ of\ \ Foreground\ Voxels\ in\ Thresholded\ \ Stack)} \times 100$$

$$\%\ True\ Foreground = \frac{(True\ Positive)}{(True\ Positive) + (False\ Positive)} \times 100$$

$$\%\ True\ Background = \frac{(True\ Negative)}{(True\ Negative) + (False\ Negative)} \times 100$$

$$\%\ Foreground\ \ Found = \frac{(True\ Positive)}{(True\ Positive) + (False\ Negative)} \times 100$$

$$\%\ Background\ \ Found = \frac{(True\ Negative)}{(True\ Negative) + (False\ Positive)} \times 100$$

Connected Components Labeling

In order to determine the volume of individual objects within a thresholded image stack, a two-dimensional connected components labeling algorithm (Sonka, et al., 1998) was expanded to three dimensions. This three-dimensional algorithm examined the 26-connected neighborhood of the surrounding images, i.e., it examined the 9-connected neighborhoods above and below it as well as the 8-connected neighborhood of the indexed image. This algorithm was used to label each component with a different color to more easily follow each component through the stack. Also, this algorithm was used to calculate the volume of each component as well as the *x*-axis width, *y*-axis width, and *z*-axis height.

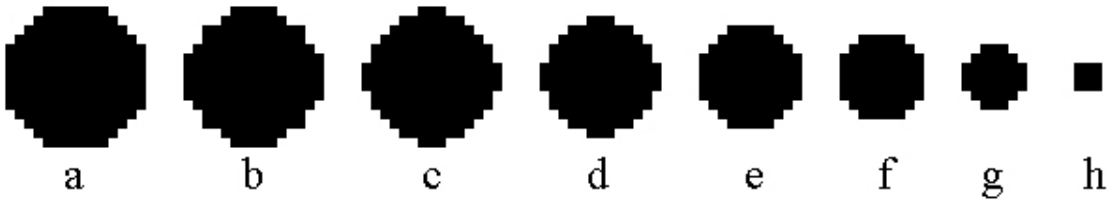


FIGURE 3.1, Sphere Template

The sphere template used to determine the optimally thresholded stack of images. The (a) center image in the stack, (b) a distance of one image above and below the center, (c) a distance of two from the center, (d) a distance of three from the center, (e) a distance of four from the center, (f) a distance of five from the center, (g) a distance of six from the center, and (h) a distance of seven from the center. Note that the template is based upon a sphere with a diameter of 15μm and an imaging resolution of 1.05μm × 1.05μm × 1.05μm.

### Three-Dimensional Averaging

After imaging microvascular constructs, the generated image stack was three dimensionally averaged. This averaging scheme looked at the 26-connected neighborhood of the surrounding images. Thus, each voxel was reassigned a value that was the average of 27 voxels.

## THRESHOLD SELECTION

### Examining Automated Thresholding Algorithms

First, various intensity and edge based thresholding algorithms from the literature (Kittler & Illingworth, 1986; Umesh Adiga & Chaudhuri, 1999; Umesh Adiga & Chaudhuri, 2001; Xavier, et al., 2001) were implemented. These methods were executed on the four stacks of images in the training data. The effectiveness of each algorithm was evaluated by comparing the images thresholded by each algorithm with the true-thresholded images. In particular, this comparison measured the total volume as well as the number of voxels correctly labeled. Additionally, we measured the number of false foreground, false background, true foreground, and true background voxels encountered by each method.

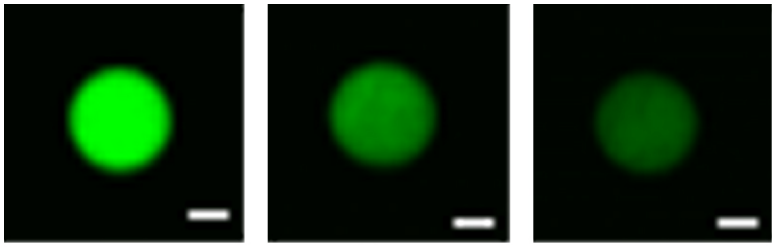

a b c

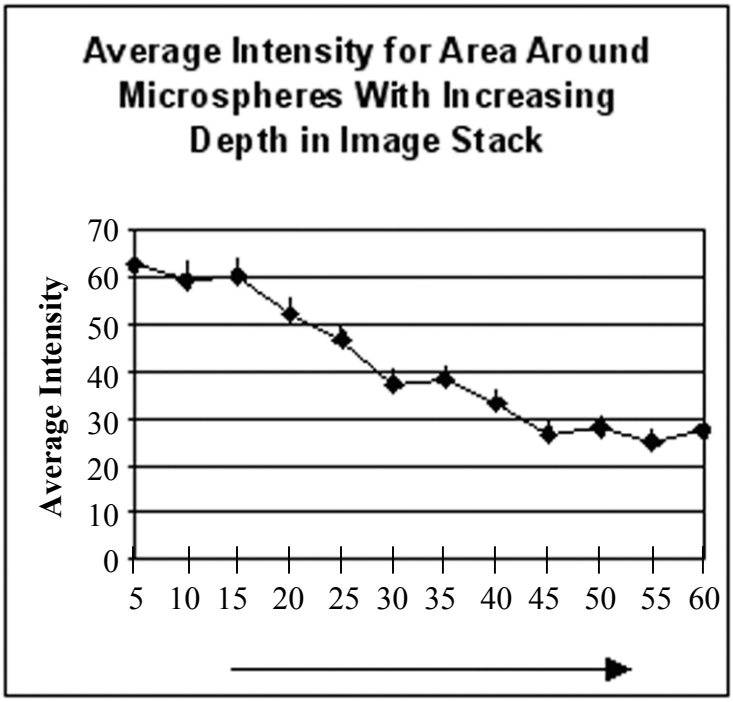


d

FIGURE 3.2, Average Intensity of Microspheres with Depth in Image Stack

Average intensity of microspheres decreases with depth in image stack. Visually, it is easy to see that microspheres deeper in the collagen gel have a smaller detected intensity. Representative microsphere centers found at depths (a) 10μm, (b) 26μm, and (c) 57μm are displayed in this figure. Bar = 5μm. (d) A graph displaying the average microsphere intensities for a 17μm × 17μm × 17μm cube around each sphere. The values shown are the average values for the four stacks of training data with error bars representing the standard deviations.

To improve the quality of the thresholded images, we turned our attention to proposing a suitable threshold scheme tailored to the scenario encountered in this paper. First, the average intensities of the spheres within each image stack were examined. As expected, images deeper in the stack were darker than images more shallow in the stack. In order to determine how much the attenuation affected the brightness of the images, the average intensity of a 17μm × 17μm × 17μm cube surrounding each sphere within the stack was calculated for the training data. The average intensity was then determined based on depth in the image stack. As seen in Figure 3.2, the average intensity for the spheres drops from 62 to 27 through approximately 60μm of the construct. Based on this attenuation, we believed that a global threshold for the entire stack would not yield accurate results for all of the images within the stack.

In order to determine a possible method for automatically thresholding a stack of images based on intensity, we examined the four stacks of images in the training data. Using these stacks, an intensity threshold for each image in the stack was determined by comparing the true-thresholded images with the corresponding confocal images. To accomplish this, this method simply examined candidate threshold values over each image and selected the one that minimized the combined total number of false positive and false negative values in each individual image. However, a reasonable (e.g., linear or exponential) equation could not be fit to these intensity threshold values, indicating that a threshold based on more than just intensity would result in fewer misclassifications than one based on intensity alone.

Thresholding Based on Gradient and Intensity Attenuation

The generated true-thresholded images were used in coordination with the original images to determine a threshold based on several attributes of each voxel. It was observed that in determining whether or not a voxel belongs to the foreground, it may be appropriate to examine not only the intensity and depth of the voxel, but also the rate at which the intensity changes varies with depth (i.e., its intensity gradient, or just "*z*-axis gradient"). For this study, the *z*-axis gradient of a voxel is defined as the difference in its current intensity and its intensity value at the next-highest depth, where the gradient of each voxel at the first image is zero. A Dual Thresholding Rule (DTR) was generated based on the intensity and gradient of each voxel, where each of these thresholds is determined as a function of the depth of the voxel. One implementation of the DTR assigns a voxel to the foreground if and only if the voxel had either an intensity value above some intensity threshold function or a *z*-axis gradient value above some gradient threshold function (called OR-acceptance). Alternatively, this rule can also be modified so that voxels are selected to be in the foreground if and only if both of these thresholds are met (called AND-acceptance).

As an initial guess for the shape of these threshold functions, a graph of the intensity and gradient was generated for three ($x$, $y$) locations for all values of $z$ within an image stack. These points were selected such that they corresponded to the ($x$, $y$) centers of three spheres at varying depths in the image stack. As with any fluorescent imaging modality, in confocal microscopy, there is exponential signal attenuation as a function of depth (Can, et al., 2003). Thus, when examining the intensity and gradient information

for the three ($x$, $y$) locations in order to fit threshold functions to these values, exponentially decaying functions were used. Based on these data, we determined the gradient and intensity functions that would yield a sphere height of approximately 15μm for each sphere by perturbing these functions such that for each ($x$, $y$) location there were approximately 15 voxels that had an intensity value on or above the intensity threshold curve and a $z$-axis gradient value on or above the gradient threshold curve. The general form of the gradient and intensity threshold functions was determined as follows:

$$f_t(z) = m_t e^{\frac{125-z}{125}} + b_t$$
$$f_g(z) = m_g e^{\frac{125-z}{125}} + b_g,$$

where $N$ is the total number of images in the stack, $z \in \{1, \ldots, N\}$ is the depth of the image, and $m_t$, $b_t$, $m_g$, and $b_g$ are scalar parameters that must be determined. Since the performance of this approach depends heavily on the quality of these parameter values, a detailed optimization scheme was developed for determining appropriate values of $m_t$, $b_t$, $m_g$, and $b_g$. The constant 125 that appears in these functions represents the (approximate) depth past which foreground structures become difficult to see in a confocal stack. (Varying values of this constant can be chosen, which in turn influence the selection of parameters $m_t$, $b_t$, $m_g$, and $b_g$, but without much effect on the behavior of this scheme.) Note that $N$ was not used in the equations, because these equations are based on the true depth in the stack irrespective of the total number of images in a given stack.

Optimizing Threshold Functions

We next employed optimization techniques to improve the parameters used for functions $f_t(z)$ and $f_g(z)$ under both OR- and AND-acceptance schemes. Additionally, we also considered replacing either or both of the threshold functions with affine functions of the form $az + d$ in lieu of an exponential threshold function. The most effective combination used OR-acceptance with exponential threshold functions for both intensity and gradient, and hence for the sake of brevity, we focus on this particular DTR implementation.

In order to determine appropriate values for the function parameters, we consulted a training data set, wherein the correct foreground/background status of each voxel is known *a priori*. One potential optimization problem would determine the parameter values that maximize the number of correctly classified voxels (equivalent to minimizing the number of misclassified voxels). Define an ordered set of the $M$ pixel positions within an image as $\{(x_i,y_i)\colon i=1, \ldots, M\}$. If there are $N$ image slices at various depths, $z$, in the data set, then we can index the voxel positions as $(i, z)$ for $i=1, \ldots, M$ and $z=1, \ldots, N$. Define $t_{iz}$ to be the intensity value of voxel $(i, z)$, and $g_{iz}$ to be the gradient value of voxel $(i, z)$, for $i = 1, \ldots, M$ and $z = 1, \ldots, N$. However, an optimization problem that minimizes misclassified voxels cannot be solved in this scenario within reasonable computational limitations, as any such algorithm to solve the problem would very likely require an exponential number of computations in general. (That is, the problem is *NP-hard* (Garey & Johnson, 1979), and no polynomial-time solution algorithm is known, or is believed to exist, for this problem.)

Instead, a three-phased heuristic is proposed to minimize the number of incorrectly classified voxels. In the first phase, we penalize for each foreground voxel ($i$, $z$) the minimum perturbation to $t_{iz}$ and $g_{iz}$ required for these values to meet or exceed their respective thresholds (i.e., $\max\{0, f_t(z) - t_{iz}\} + \max\{0, f_g(z) - g_{iz}\}$), and for each background voxel ($i$, $z$), the minimum perturbation to $t_{iz}$ and $g_{iz}$ required for these values to fall on or beneath their respective thresholds (i.e., $\max\{0, t_{iz} - f_t(z)\} + \max\{0, g_{iz} - f_g(z)\}$). This phase is achieved using linear programming models and algorithms (see Bazaraa, et al., 1990 for an exposition of linear programming). As opposed to an NP-hard problem, any linear program can be solved within reasonable (worst-case polynomial-time) computational limits. While this model does not accurately capture the same objective as the DTR optimization problem of minimizing false negative and false positive voxels, it provides a starting point for a reasonable set of parameter values. Define the following linear programming decision variables, where $F$ is defined as the set of voxels $(i, z) \in \{1, \ldots, M\} \times \{1, \ldots, N\}$ that are known to belong to the foreground, and $B$ is the set of voxels that belong to the background.

- $x_{tiz}$ represents the value $\max\{0, f_t(z) - t_{iz}\} \ \forall \ (i, z) \in F$
- $x_{giz}$ represents the value $\max\{0, f_g(z) - g_{iz}\} \ \forall \ (i, z) \in F$
- $y_{tiz}$ represents the value $\max\{0, t_{iz} - f_t(z)\} \ \forall \ (i, z) \in B$
- $y_{giz}$ represents the value $\max\{0, g_{iz} - f_g(z)\} \ \forall \ (i, z) \in B$

The following linear program is then formulated and solved.

Minimize $$\sum_{(i,z)\in F}\left(x_{tiz}+x_{giz}\right)+\sum_{(i,z)\in B}\left(y_{tiz}+y_{giz}\right) \quad (1)$$

subject to: $$x_{tiz} \geq \left(m_t e^{\frac{125-z}{125}}+b_t\right)-t_{iz} \qquad \forall(i,z)\in F \quad (2)$$

$$x_{giz} \geq \left(m_g e^{\frac{125-z}{125}}+b_g\right)-g_{iz} \qquad \forall(i,z)\in F \quad (3)$$

$$x_{tiz} \geq 0 \text{ and } x_{giz} \geq 0 \qquad \forall(i,z)\in F \quad (4)$$

$$y_{tiz} \geq t_{iz}-\left(m_t e^{\frac{125-z}{125}}+b_t\right) \qquad \forall(i,z)\in B \quad (5)$$

$$y_{giz} \geq g_{iz}-\left(m_g e^{\frac{125-z}{125}}+b_g\right) \qquad \forall(i,z)\in B \quad (6)$$

$$y_{tiz} \geq 0 \text{ and } y_{giz} \geq 0 \qquad \forall(i,z)\in B \quad (7)$$

$m_t$, $b_t$, $m_g$, $t_g$ unrestricted. (8)

Observe here that in order to enforce the relationship $x_{tiz} = \max\{0, f_t(z) - t_{iz}\}\ \forall(i, z) \in F$ (for example), it is stated that $x_{tiz}$ must be at least as large as both of those values. While this only enforces the relationship $x_{tiz} \geq \max\{0, f_t(z) - t_{iz}\}$, since we are minimizing $x_{tiz}$ (and since it will appear nowhere else in the model), the optimization process will force $x_{tiz}$ to be the lowest value possible and will hence equal to $\max\{0, f_t(z) - t_{iz}\}$ in the optimal solution to the linear program. This same observation holds for $x_{giz}\ \forall(i, z) \in F$, and for $y_{tiz}$ and $y_{giz}$, $\forall(i, z) \in B$.

A commercial software package, CPLEX 8.1, was used to optimally solve this linear programming problem. Each linear program requires on the order of $NM$ variables

and $M$ constraints. Since this can result in a very large linear programming model, the size of the model is reduced without sacrificing the optimality of the procedure by aggregating voxels belonging to the same image having the same intensity and gradient, and then penalizing their error proportionate to the number of aggregated voxels having these characteristics. That is, if $k$ voxels are described by the same depth, intensity, and gradient, we consider this as one voxel with a weight of $k$ in the objective function. Also, any voxel having an intensity less than 7 (on a scale from 0 to 255) is declared as a background voxel and eliminated this data from the optimization input file.

Now, in the second phase of this heuristic, suppose that a more appropriate penalty for foreground voxels $(i, z)$ is given by $\max\{0, \min\{f_t(z) - t_{iz}, f_g(z) - g_{iz}\}\} = \min\{\max\{0, f_t(z) - t_{iz}\}, \max\{0, f_g(z) - g_{iz}\}\}$, since only one of the threshold functions must be exceeded for the DTR to label this as a foreground voxel. While such a penalty cannot readily be represented by a (continuous) linear programming problem, we can use the solution to the first phase of our heuristic to anticipate whether $\max\{0, f_t(z) - t_{iz}\}$ or $\max\{0, f_g(z) - g_{iz}\}$ will be the minimum value at optimality, and penalize *only* the minimum of these terms. Hence, after determining the value of $y_{tiz}$ and $y_{giz}$ from the solution of the linear programming problem above, we remove the maximum of these terms from the objective function and resolve the linear program.

| | | % True Volume | %True Foreground | %True Background | %Foreground Found | %Background Found |
|---|---|---|---|---|---|---|
| **Kittler 2D** | **Ave** | 7,521.83 | 2.26 | 100.00 | 98.65 | 92.92 |
| | **Std Dev** | 6,129.91 | 1.33 | 0.00 | 0.59 | 3.54 |
| **Kittler 3D** | **Ave** | 14,564.06 | 1.57 | 100.00 | 99.05 | 82.36 |
| | **Std Dev** | 8,293.64 | 1.70 | 0.00 | 0.32 | 14.03 |
| **Umesh 2D** | **Ave** | 1,648.21 | 14.29 | 99.99 | 93.49 | 98.87 |
| | **Std Dev** | 2,108.61 | 9.57 | 0.00 | 0.97 | 0.92 |
| **Umesh 3D** | **Ave** | 62.77 | 96.14 | 99.93 | 47.26 | 100.00 |
| | **Std Dev** | 31.10 | 0.98 | 0.01 | 4.44 | 0.00 |
| **OTS** | **Ave** | 641.91 | 19.13 | 100.00 | 97.43 | 99.45 |
| | **Std Dev** | 268.56 | 1.80 | 0.00 | 0.73 | 0.13 |
| **Min Error** | **Ave** | 100.58 | 82.42 | 99.97 | 82.02 | 99.97 |
| | **Std Dev** | 17.43 | 7.70 | 0.01 | 5.79 | 0.02 |
| **DTR** | **Ave** | 87.83 | 84.54 | 99.97 | 82.45 | 99.97 |
| | **Std Dev** | 7.18 | 4.81 | 0.01 | 4.80 | 0.01 |

TABLE 3.1, Accuracy of Implemented Thresholding Algorithms on Training Data

Accuracy of implemented thresholding algorithms on four image stacks of training data. These equations to calculate these values are in the Materials and Methods section.

| Instance | Num Images | Num Voxels | Num Errors | Opt $m_t$ | Opt $b_t$ | Opt $m_g$ | Opt $b_g$ |
|---|---|---|---|---|---|---|---|
| **Stack 1** | 72 | $1.89 \times 10^7$ | 10, 047 | 61.97 | -69.41 | 23.43 | -27.71 |
| **Stack 2** | 64 | $1.68 \times 10^7$ | 9, 692 | 76.98 | -115.74 | 22.09 | -26.69 |
| **Stack 3** | 63 | $1.65 \times 10^7$ | 8, 461 | 59.31 | -76.66 | 23.40 | -30.62 |
| **Stack 4** | 62 | $1.63 \times 10^7$ | 7, 382 | 62.29 | -76.39 | 25.96 | -31.19 |

TABLE 3.2, Parameter Values and Error Results for the DTR on Training Data

Optimized parameter values and aggregate error results for the DTR on the four image stacks of training data. Observe that there is one moderate outlier for the DTR parameters (those recommended for Stack 2), and that the individual optimized parameters result in images containing very few misclassified voxels (roughly 0.05% misclassified per image stack).

The third phase of this algorithm operates as a local search heuristic from the starting point of $m_t$, $b_t$, $m_g$, and $b_g$ values obtained from the second phase of our algorithm. Holding three of these values as constants, we compute the perturbation required in the fourth parameter for each voxel to either swap from a false negative to a true negative or vice versa, or from a false positive to a true positive or vice versa. (This perturbation value will not exist if the voxel currently satisfies both thresholds.) We record the amount of the perturbation required and whether or not one more error or one fewer error would result from such a perturbation in a list of records. Then, this list is sorted in nondecreasing order of perturbations, and two $O(N)$ searches (starting from zero and increasing the perturbation, and starting from zero and decreasing the perturbation) are made to determine the perturbation amount that eliminates the most misclassified voxels. Following this search, we then rotate which parameter should be examined next (we chose the ordering $m_t$, $b_t$, $m_g$, $b_g$) while holding the other three parameters as constant values. This process continues until no improvement can be made by perturbing any single parameter value.

## RESULTS

### Exploring Thresholding Based on Intensity

Various thresholding algorithms based on intensity were found in the literature and examined. The classic Kittler method (Kittler & Illingworth, 1986), which assumes that an image has a bimodal intensity histogram, was implemented to find the best threshold for each image in the stack (Kittler 2D) as well as to find a global threshold for

the whole stack (Kittler 3D). Upon examining the microsphere images, it was noted that the vast majority of them do not have a bimodal intensity histogram. In fact, because there are few foreground voxels when compared with the number of background voxels, the foreground mode appears to be consumed by the background mode, giving the images unimodal histograms. An algorithm in the literature that uses a unimodal histogram model to find a threshold on the edge of the mode using the mean and standard deviation was implemented (Umesh Adiga & Chaudhuri, 1999; Umesh Adiga & Chaudhuri, 2001). As with the Kittler algorithm, this method was implemented to find the best threshold for each image in the stack (Umesh 2D) and for the whole stack (Umesh 3D). A third algorithm, called Objective Threshold Selection (OTS) (Xavier, et al., 2001), was implemented. This algorithm calculates a threshold for each ($x$, $y$)-location within an image stack based on edge and intensity information. Finally, the training data was thresholded by selecting an intensity threshold for each image in the stack such that the combined total number of false negative and false positive values was minimized (Min Error).

In order to determine whether or not our thresholding schemes were accurately determining the volume of the spheres, we devised a method to estimate what the true-thresholded images should look like. This method used the sphere template in Figure 3.1 to estimate which voxels should be marked as foreground and which ones should be marked as background. The thresholded images from our implemented algorithms were compared with these true-thresholded images to determine the estimated volume, percentage of foreground voxels, and the percentage of background voxels that were

found by each algorithm. Next, it was determined what percentage of the estimated foreground voxels was truly foreground and what percentage of the estimated background voxels was truly background. As can be seen in Table 3.1, most automated methods drastically overestimated the true volume of the image stacks. This resulted in a small percentage of true foreground voxels. The percentage of background voxels found for each method is relatively high, because there are many more background voxels in the images than there are foreground voxels.

Thresholding Based on Intensity and Depth Gradient

Although the Min Error thresholding method performed well, a smooth line could not be fit to the individual threshold values as a function of depth. This lead to the belief that a method based on intensity alone would not accurately threshold the image stacks. The OTS thresholding algorithm utilized edge as well as intensity information to select a single threshold for each ($x$, $y$)-location within the image stacks. As with other thresholding algorithms that were tested, this method overestimated the true volume of the foreground voxels, but it had fewer misclassified voxels. Based on this method, both the $z$-axis gradient and the intensity values were examined for some of the foreground voxels within the image stacks.

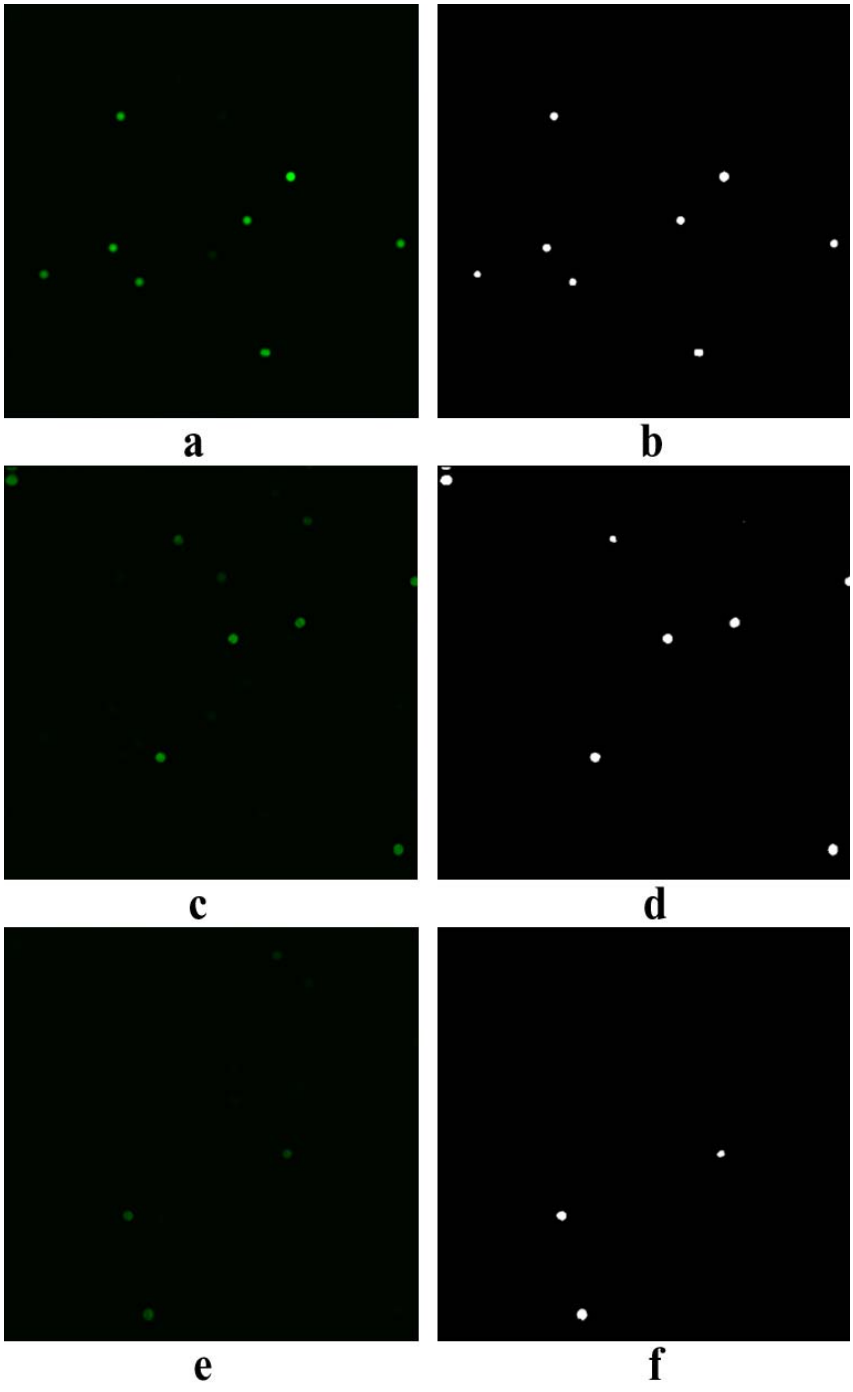


FIGURE 3.3, Sphere Images Before and After Thresholding Using the DTR

Representative sphere images at varying depths before (a, c, e) and after (b, d, f) thresholding using the optimized DTR algorithm. Images are taken at different depths within the image stack, including 6μm (a and b), 31μm (c and d), and 48μm (e and f).

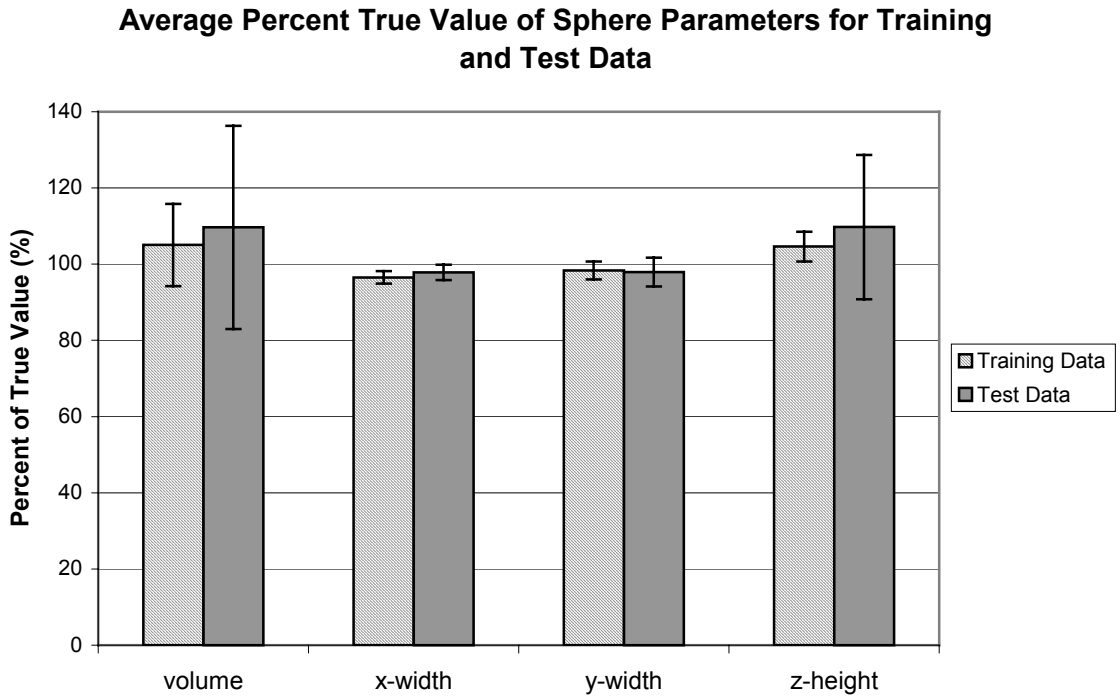


FIGURE 3.4, Graph Representing the Percent True Measurement of Total Volume

Graph representing the percent true measurement of total volume, *x*-axis width, *y*-axis width, and *z*-axis height of spheres after thresholding using the optimized DTR algorithm. The values shown are the average values for the four stacks of either training or test data with error bars representing +/- standard deviations.

The DTR parameter optimization scheme was executed on the four stacks of images in the training data. In practice, the first phase provides reasonable results, while the second phase makes only a modest improvement. The third phase reduces the total number of misclassified voxels by almost 20%. Table 3.2 displays the total number of images in each stack, the total number of voxels in the stack, the number of misclassified voxels (labeled "Num errors" in Table 3.2), and the optimized parameter values. Observe that the number of misclassified voxels is a small fraction of the total number of voxels, and that with the exception of Stack 2, the parameter values seem to be relatively consistent. Hence, the challenge is to find a single set of parameter values that is effective for all data sets by averaging the parameter values (and mitigating the outlier values). Based on our findings in Table 3.2, we initially proposed setting $m_t = 60$, $b_t = -75$, $m_g = 24$, and $b_g = -29$, and ran the phase three improvement scheme to adjust these values. Our adjusted final parameters are $m_t = 62$, $b_t = -74$, $m_g = 23.5$, and $b_g = -29$, and are effective for all training problem instances tested. Hence, there is evidence to suggest that these parameters are robust and extendable to more general settings.

Testing Optimized Threshold Values

Once the thresholding algorithm was optimized on the training data, it was run on another set of tissue phantoms and exhibited similar results. Figure 3.3 contains representative images that have been thresholded using the DTR algorithm. Figure 3.4 illustrates the average percent true value of the total volume, $x$-axis width, $y$-axis width, and $z$-axis height for thresholded spheres in both the training and test data. As can be seen in this figure, for both the training and test data, the $x$-axis and $y$-axis widths were close

to 100% of the actual width of the sphere (15μm). In general, these values were slightly underestimated. The *z*-axis height showed more variability in both the test and training data. The DTR algorithm overestimated the *z*-axis height slightly more on the test data than on the training data, and it produced a higher standard deviation on the training data than on the test data. However, on average the sphere height calculated by the DTR was below 110% of the true sphere height. While the overestimation of the *z*-axis height led to an overestimation of the total volume of the spheres in both the test and training data, this overestimation was less than 10% on average.

Next, the DTR algorithm was used to threshold microvascular constructs that had been fluorescently labeled. The DTR thresholding scheme appeared to find all of the vessels within the stacks of images. We did see some areas where the vessel was disconnected due to a lower fluorescence in parts of the vessels. However, this may not be a source of error, rather it may indicate that this section of the vessel is thinner or is truly disconnected from the rest of the vessel. As can be seen in Figure 3.5, there are some areas where a user might manually threshold the stack such that the whole vessel is filled in even in the first (Figure 3.5 a,b) and last (Figure 3.5 e,f) images, which may lead to an overestimation of the true volume of the vessel. When the thresholding algorithm was executed on raw stacks of images, some background noise was seen likely due to the staining process. As can be seen in Figure 3.6, once the stacks of images were averaged using the three-dimensional averaging scheme (mentioned in the Materials and Methods section), this background noise was not apparent in the thresholded images.

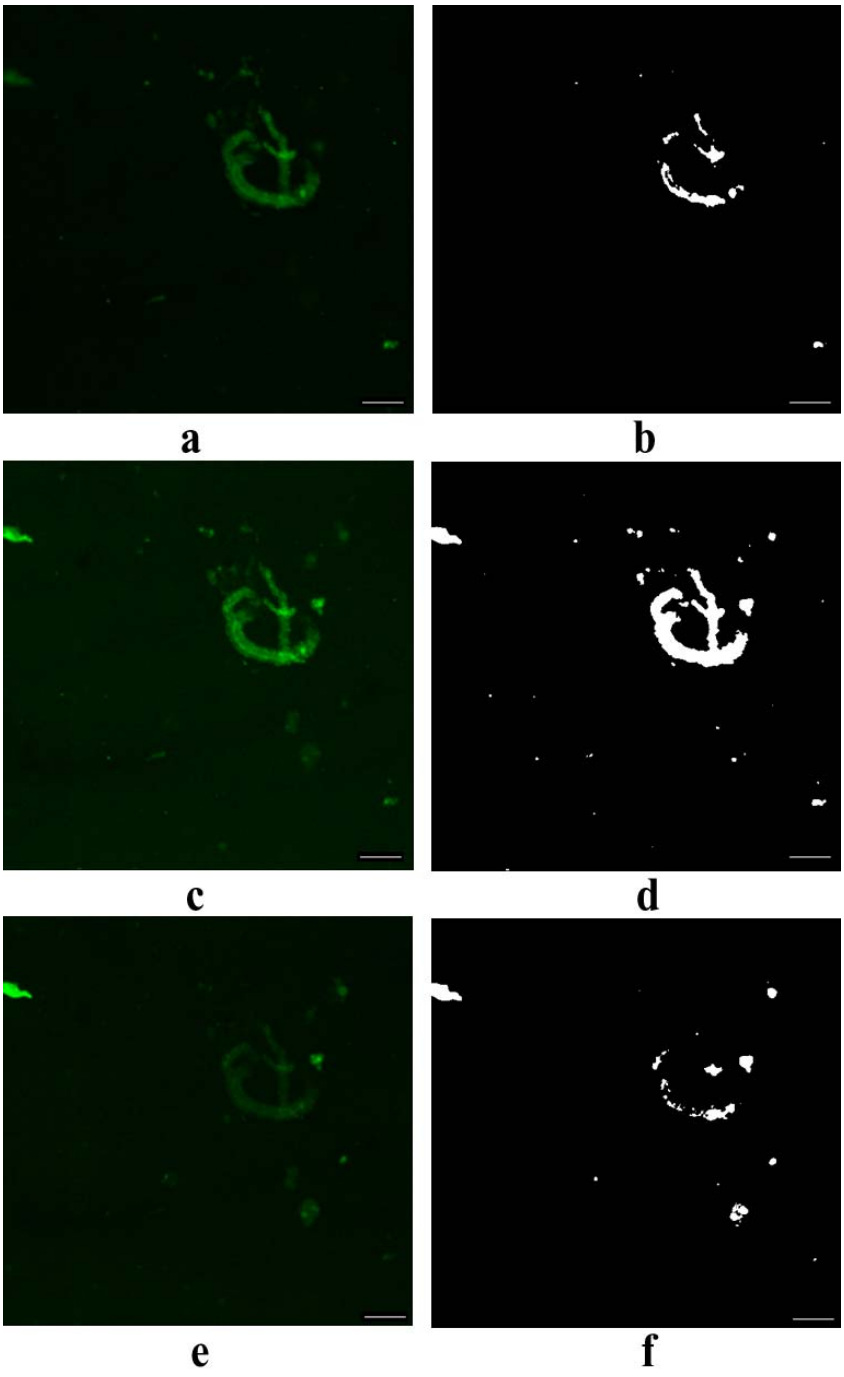


FIGURE 3.5, Microvascular Images Before and After Thresholding

Representative microvascular images at varying depths before (a, c, e) and after (b, d, f) thresholding using the optimized DTR algorithm. Bar = 50μm. Images are taken at different depths within the image stack, including 13μm (a and b), 33μm (c and d), and 44μm (e and f).

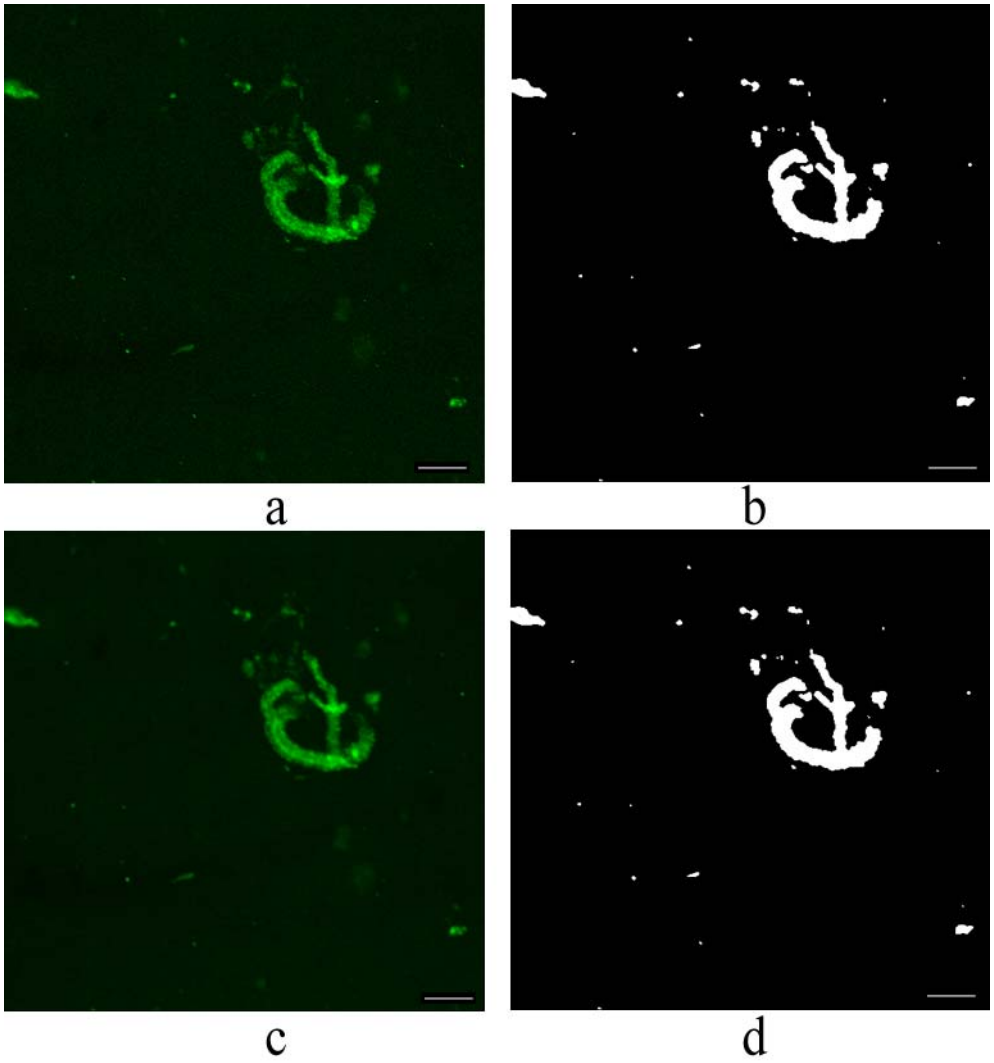


FIGURE 3.6, Vascular Images With and Without 3D Averaging

Representative images of microvasculature (a, b) without 3D averaging and (c, d) with 3D averaging. (b, d) Images were thresholded using the optimized DTR algorithm. When the image stacks were 3D averaged prior to thresholding, there was less noise seen in the background as can be seen in that there are fewer white dots in the background of (d) as compared with (b).

## Discussion and Conclusions

A dual intensity and *z*-axis gradient thresholding scheme was presented with the ability to accurately and automatically calculate the volume of fluorescently labeled tissue constructs. In the examples shown, it was demonstrated that when confocal microscopy is used to generate stacks of images containing microspheres, there is a definite attenuation of the detected fluorescence with increased depth in the image stack. Thus, a global thresholding scheme that selects one threshold for the whole stack of images was not able to accurately threshold the microsphere images.

Using a dual thresholding scheme and optimizing the parameters using training data, a set of equations was derived in order to threshold stacks of confocal images by examining both the intensity and *z*-axis gradient of each voxel within the image stack. When these equations were tested on another set of microsphere images, it yielded similar results with a total volume estimation of individual spheres under 110% of the true volume. As the true diameter of the spheres is reported as ±3%, and the volume of a sphere is $\frac{4}{3}\pi r^3$, a volume over estimation of as much as 9% may represent irregularities in the imaged spheres.

Similarly, when examining the stacks of microvascular images, it was found that the DTR algorithm detected vessels throughout the stack of images. When the microvascular data was averaged using a three-dimensional averaging scheme, the vessels were still easily detectable and there was less single-voxel background noise within the thresholded stacks of images. In a few stacks, there were some areas of

unevenness of fluorescence, which resulted in some breaks in the thresholded vessels. However, this may indicate thin or disconnected areas of the vessel rather than erroneous labeling. And, as fluorescent labels are improved and as new animal models with fluorescently tagged cells emerge, this may aid in reducing issues with uneven fluorescence.

The example constructs used in this paper contained a small volume of spheres or vessels, which resulted in stacks of images with far few foreground voxels than background voxels. Thus, the intensity histograms of the stacks of images were primarily unimodal. Bearing this in mind, it is not surprising that the thresholding scheme based on a bimodal histogram (Kittler & Illingworth, 1986) greatly overestimated the total volume of the microsphere images. However, the unimodal histogram thresholding scheme (Umesh Adiga & Chaudhuri, 1999; Umesh Adiga & Chaudhuri, 2001) also overestimated the total volume of the microsphere images. This is likely due to the fact that the example constructs had so small a volume of foreground voxels that the foreground voxels did not have a significant enough impact on the histogram. When a thresholding scheme that examined edge and intensity information (Xavier, et al., 2001) was employed, the overestimation was decreased even more; however, it still significantly overestimated the total volume.

Currently there are numerous methods to examine microvasculature using two-dimensional and three-dimensional imaging techniques. It has been noted that three-dimensional confocal microscopy is better able to detect vessels than two-dimensional light microscopy (Guo, et al., 2001). Confocal microscopy has been used to determine the

volume of blob-like structures including cells, DNA, and biofilms (Umesh Adiga & Chaudhuri, 1999; Umesh Adiga & Chaudhuri, 2001; Xavier, et al., 2001). It has also been used to determine the volume of tube-like structures, namely vessels and neurites. Many of these methods have used manual thresholding or significant user intervention (Bucher, et al., 2000; Crouch, 2000; Lenander & Holmgren, 1999; Young, et al., 1998). It has been noted that such manual manipulation may introduce extra error to the quantification (Bucher, et al., 2000). Automated methods have also been designed to trace and morphologically examine tube-like structures; however, they are not used to determine the volume of the structures (Can, et al., 1999; Cohen, et al., 1994; He, et al., 2003; Lin, et al., 2005a). Thus, some method for automated volume calculation is necessary.

Using an algorithm that examined both intensity and gradient yielded a more accurate volume calculation than any of the other methods that were examined. This Dual Thresholding Rule was capable of taking into account the intensity attenuation seen with depth in order to accurately estimate the volume of spheres throughout the image stack. Future research can also be conducted to explore marginal improvements in the optimization scheme by employing a hill-climbing mechanism in the third phase of our optimization scheme and/or simply randomly generating starting positions for this phase alone. However, since we only prescribe a general set of guidelines for the use of these parameters, a more promising study might examine the use of multiple thresholding rules, such as ensuring that the voxel forms part of a sufficiently-large connected component, in conjunction with rules that classify a voxel as part of the foreground if and only if some $k$ out of the $p$ individual threshold criteria are satisfied.

By examining both the intensity and *z*-axis gradient of each voxel, the total volume of the spheres within each stack of images was more closely estimated. In fact, even in the test data we overestimated the total volume of individual spheres by less than 10%, and there was not a significant change in the estimated volume of spheres at varying depths within the image stacks. Thus, using confocal microscopy combined with an intensity and *z*-axis gradient based thresholding scheme is a useful, automated way to obtain accurate and reproducible volume calculations for microvascular constructs.

# 4. CONTROLLING ENVIRONMENTAL PARAMETERS WITHIN THE BAT CABINET

## INTRODUCTION

Tissue Engineering is a relatively new field that combines expertise from both engineering and medicine to develop constructs that are capable of restoring, maintaining, or improving tissue function (Langer & Vacanti, 1993). A common belief in the TE community is that the success of this field is dependent upon the engineered tissue closely imitating natural tissue (Lanza, et al., 2000). When examining native tissue, it has been noted that the spatial organization of cells provides cell-cell adhesion cues that are especially important in tissues such as nerves and blood vessels (Pardanaud, et al., 1989; Patel, et al., 1998; Risau, et al., 1988). This spatial organization preserves vital cell-cell interactions (Geiger & Ayalon, 1992; Larue, et al., 1996; Shibuya, et al., 1995) as well as cell phenotype (Ben Ze'ev, et al., 1988). Also, it is believed that this spatial organization has a direct effect on the survival and apoptosis of cells (Zahir & Weaver, 2004). Thus, a significant focus in TE has been on fabricating spatially organized constructs.

Rapid Prototyping has been proposed as a viable method to fabricate spatially organized TE constructs. RP is a group of methods that are capable of building physical, 3D objects in a layer-by-layer fashion. These techniques have been used in numerous medical applications, including bone substrate scaffolds (Cooke, et al., 2003), heart valve scaffolds (Hoerstrup, et al., 2000; Sodian, et al., 1999; Sodian, et al., 2000a; Sodian, et al., 2002b), cranial implants (Gronet, et al., 2003), drug delivery devices (Leong, et al., 2001), and scaffolds for cartilage repair (Sherwood, et al., 2002). Most RP methods

spatially organize only the cells, however, it has been proposed that using a RP technique to pattern not only the scaffold, but also the cells, will accelerate and improve tissue assembly (Mironov, et al., 2003). Based on this idea, there has been a recent emergence of various RP methods to not only lay down scaffold, but cells as well (Boland, et al., 2003; Marquez, et al., 2002; Ringeisen, et al., 2002a; Ringeisen, et al., 2002b; Wilson, Jr. & Boland, 2003).

Using Rapid Prototyping technology to generate spatially organized TE constructs such that the technique is reproducible among different procedures requires that the mechanical and environmental properties of the system be carefully characterized. In chapter 2, it was shown that a direct-write, 3D BioAssembly Tool can be utilized to generate viable, spatially organized constructs. This chapter examines some of the mechanical properties associated with the BAT as well as some additional features that can be used to more tightly control the BAT environment. This chapter investigates the true applied pressure in the pneumatic pens, controlling the temperature of the deposition pens, controlling the humidity within the BAT cabinet, and heating the stage onto which the material is extruded.

## MATERIALS AND METHODS

### Measuring Pressure in the Pneumatic Pens

To measure the applied pressures for small pressure settings (0-6psi), a Mercury manometer was attached to the pneumatic print pens by Clay Adams™ polyethylene tubing (BD, Franklin Lakes, NJ). The applied pressure was measured through the pen

pressure supply nozzle by connecting the manometer directly to the nozzle and through a connected print pen with either a 25 gauge or 33 gauge pen tip. To measure the applied pressures for pressure settings up to 50psi, the pen pressure supply nozzle was attached directly to an Encore pressure gauge (Medi-Tech, Spencer, IN). For all measurements, BAT scripts were written to apply the desired pressure to the connected pen for 60 seconds. The applied pressure was measured as the steady state pressure. All measurements were obtained for both pens 2 and 4.

Cooling the Pneumatic Print Pens

Three methods were employed to cool the pneumatic print pens: 1) a thermoelectric cooler with a fan, 2) a cold-water circulator, and 3) a combined thermoelectric cooler and cold-water circulator. For the first method, a thermoelectric cooler was connected to a wire wound platinum RTD element (Omega Engineering, Inc., Stamford, CN). Both were then connected to an Omega CN9000A temperature-controlling device (Omega Engineering, Inc., Stamford, CN). For the second method, copper tubing was coiled around each pneumatic pen. The tubing was connected to an insulated cold-water circulator, Iceman Cold Therapy unit (Orthopedics, Inc., Vista, CA), which was packed into the cooler, followed by 2 liters of water. The combined method incorporated the thermoelectric cooling device with the cold-water circulator.

Monitoring the Temperature of the Pneumatic Pens

Approximately 1ml of water was put in a 3ml barrel with a 33 gauge tip. The 3ml barrel with 33 gauge tip was placed in the pen jacket and a thermometer was placed

inside the pen. Once the pen registered the temperature of the water at room temperature, the system was used to determine the effectiveness of each pen cooling method. The temperature of the print pen was monitored by keeping track of the temperature reported on the thermometer. This value was compared with the temperature reported by the CN9000A temperature-controlling device. For each pen cooling device, the temperature was recorded exactly once and assessed for reproducibility of measurements by evaluating the temperatures over time when using each pen cooling system while printing type I collagen.

Controlling Humidity

Two methods were examined for adding humidity to the BAT environment: 1) an evaporative humidifier and 2) an ultrasonic humidifier. The evaporative humidifier that was used was the Guardian 10 humidor (Vigilant, Inc., Dover, NH). This system had a 1 quart water reservoir capacity and was capable of humidifying 10 cubic feet. The ultrasonic humidifier that was used was a Holmes 2.8 Gallon Ultrasonic Humidifier (Holmes, El Paso, TX). This system had a 2.8 gallon water reservoir. As can be see in Figure 4.1, the humidifier was placed at an angle in the front right corner of the BAT cabinet, with its output port facing the stage.

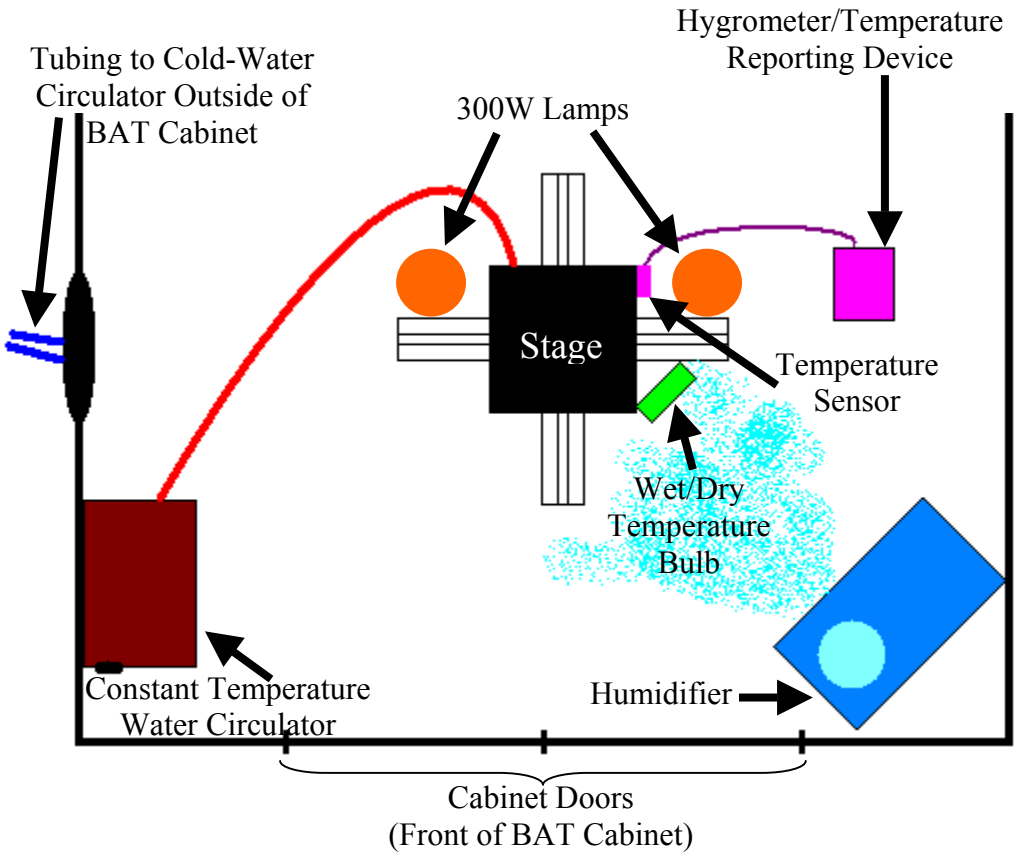


FIGURE 4.1, Top Down Schematic of BAT Cabinet

Schematic representation of the BAT cabinet showing the location of the constant temperature water circulator used to heat the stage, the humidifier used to add humidity to the cabinet, the wet/dry temperature bulb used to detect the true humidity, the temperature sensor attached to the stage to report the temperature of the stage, and, and the tubing that connects to the print pens and then goes outside of the BAT cabinet to the cold-water circulator.

## Measuring Humidity

In order to test the effectiveness of the humidifiers in creating a humid environment inside the cabinet, either system was placed inside the BAT cabinet with the output port facing the stage. The humidifier was turned on and the doors of the cabinet were closed and remained closed during measurements. The true humidity of the system was measured using a Wet/Dry Temperature bulb and this value was compared with the reported humidity from the Hygrometer/Temperature Sensor in the cabinet. The location of both sensors is illustrated in Figure 4.1. Because the BAT doors are opened and closed to prepare the system for printing and to remove the printed constructs for culture, the effects of opening the doors was examined with respect to its effect on the humidity within the cabinet. For each humidifier, the humidity was recorded exactly once and assessed for reproducibility of measurements by evaluating the humidity over time when using the system to add humidity to the BAT cabinet while printing type I collagen.

## Heating the Stage

Two methods were employed to heat the stage. First, two heat lamps with 300 Watt light bulbs were anchored on the scaffolding approximately 2.5 feet above the stage such that they shined directly onto the black stage. The two lamps were positioned such that the distance between them was approximately 12 inches. Second, a VWR constant temperature recirculating water bath (VWR Scientific, West Chester, PA) was used to heat the stage. The location of these devices can be seen in Figure 4.1. The temperature of the stage was monitored using two methods: 1) taping a thermometer onto the stage

and covering the tip with aluminum foil and 2) taping the sensor of the thermometer/hygrometer associated with the BAT to the back right side corner of the stage. For each stage heating device, the temperature was recorded exactly once and assessed for reproducibility of measurements by evaluating the temperatures over time when using each heating system while printing type I collagen.

## RESULTS

### Measuring Pressure in Pneumatic Pens

The pressure regulator that is connected to the BAT is a 100psi unit with an accuracy of 1% of full scale, i.e. ± 2psi. Currently, the BAT software has the maximum output of the regulator fixed to 50psi. The regulator uses a solenoid valve to control the pressure that is applied. When the BAT was first installed at the University of Arizona, the zero and span of the pressure regulator were calibrated to be within the tolerance. If there appears to be any problems with the pressure, the zero and span may need to be readjusted.

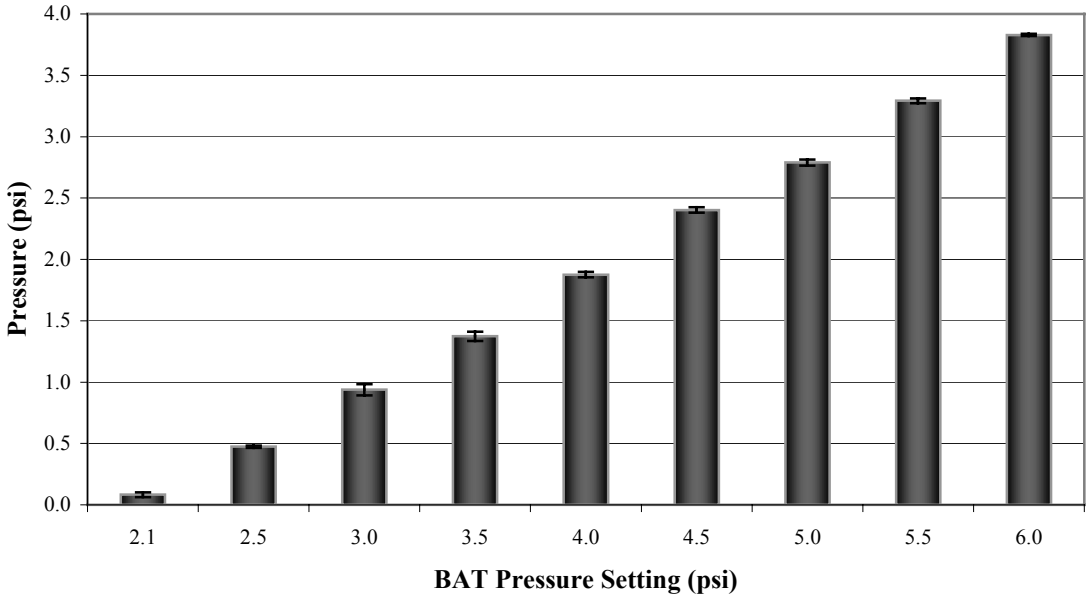


FIGURE 4.2, Measured Pressure for Low Pressure Settings

The displayed values are the average measured steady state pressures (psi) with error bars representing +/- standard deviation.

The connectors that are used to connect the tubing from the regulator to the BAT machinery (inside the black cabinet that contains the computer equipment associated with the BAT) had problems with leaking. And, when the pressure was too high (> 20psi), the tubing would get disconnected. In order to avoid this problem, the regulator on the air tank was set to a maximum the output pressure of 20psi. With this extra limitation in place, there were no further problems with the tubing being disconnected. And, since type I collagen was often the material extruded through the BAT, and this material needs an extrusion pressure setting of less than 2.5psi, this did not limit the printing capabilities.

The BAT pressure settings have a precision of 0.1psi. If a pressure setting with a smaller precision is entered in a BAT script, that number is rounded down to the smallest 0.1psi increment, i.e., if the pressure setting is 3.15, the applied pressure setting will be 3.1. Figure 4.2 displays the measured pressures for BAT pressure settings ranging from 2.1psi up to 6.0 psi. For pressure settings below 2.1psi, the true applied pressure could not be detected using the Mercury manometer. Based on these settings, an equation to estimate the pressure applied for any BAT pressure setting was calculated as follows: $(true\ pressure) = (BAT\ pressure) - 2.06$. This equation estimates that the BAT pressure setting is off by 2.06psi. The same pressure values were recorded with all pressure measurement methods, i.e., directly through the tubing, through the 25 gauge pen tip, and through the 33 gauge pen tip. Also, as the BAT pressure setting increased up to 20psi, the measured pressure followed the equation stated above. However, because the regulator on the air tank limits the pressure output to 20psi, the measured pressure for all pressure settings greater than 20psi were the same.

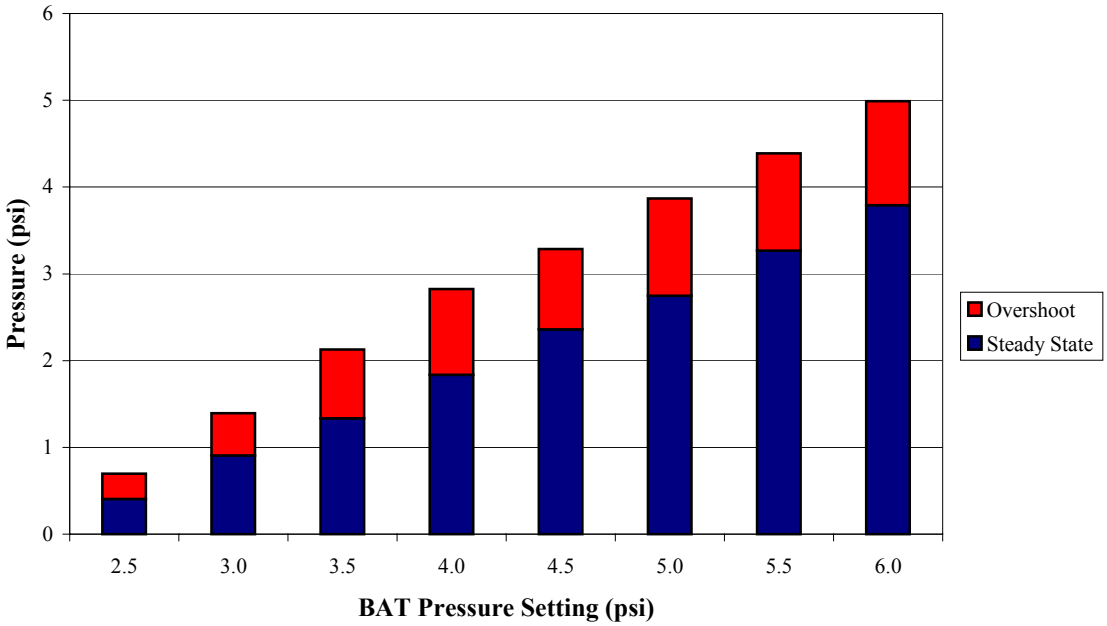


FIGURE 4.3, Overshoot Pressures Seen in Pneumatic Pens

When measuring the pressure directly or through a 25 gauge pen tip, there was a noticeable overshoot in the measured pressure before it leveled out at a lower steady state pressure. This graph shows representative maximum and steady state pressures.

Similar steady state pressures were detected for both the 25 gauge and 33 gauge tips as well as when the manometer was connected directly to the pen pressure supply nozzle; however, the measurements using the 33 gauge pen tip did exhibit a delay in reaching the steady state pressure. In fact, when using the 33 gauge pen tip, it took approximately 25 seconds to reach the steady state pressure when the BAT pressure setting was 6psi. As can be seen in Figure 4.3, when measuring the pressure directly or through a 25 gauge pen tip, there was a noticeable overshoot in the measured pressure which decreased to the steady state pressure within 1-2 seconds.

### Controlling Pneumatic Pen Temperature

Initially, the primary goal in controlling the temperature of the BAT's pneumatic pens was to keep the contents of the pens cold. This was due to the fact that the primary material being printed by the BAT was type I collagen, which polymerizes above 4°C. Multiple methods were examined for cooling the pneumatic print pens, including using a thermoelectric cooler with a fan attached, using a cold-water circulator, and using a combined thermoelectric cooler and cold-water circulator.

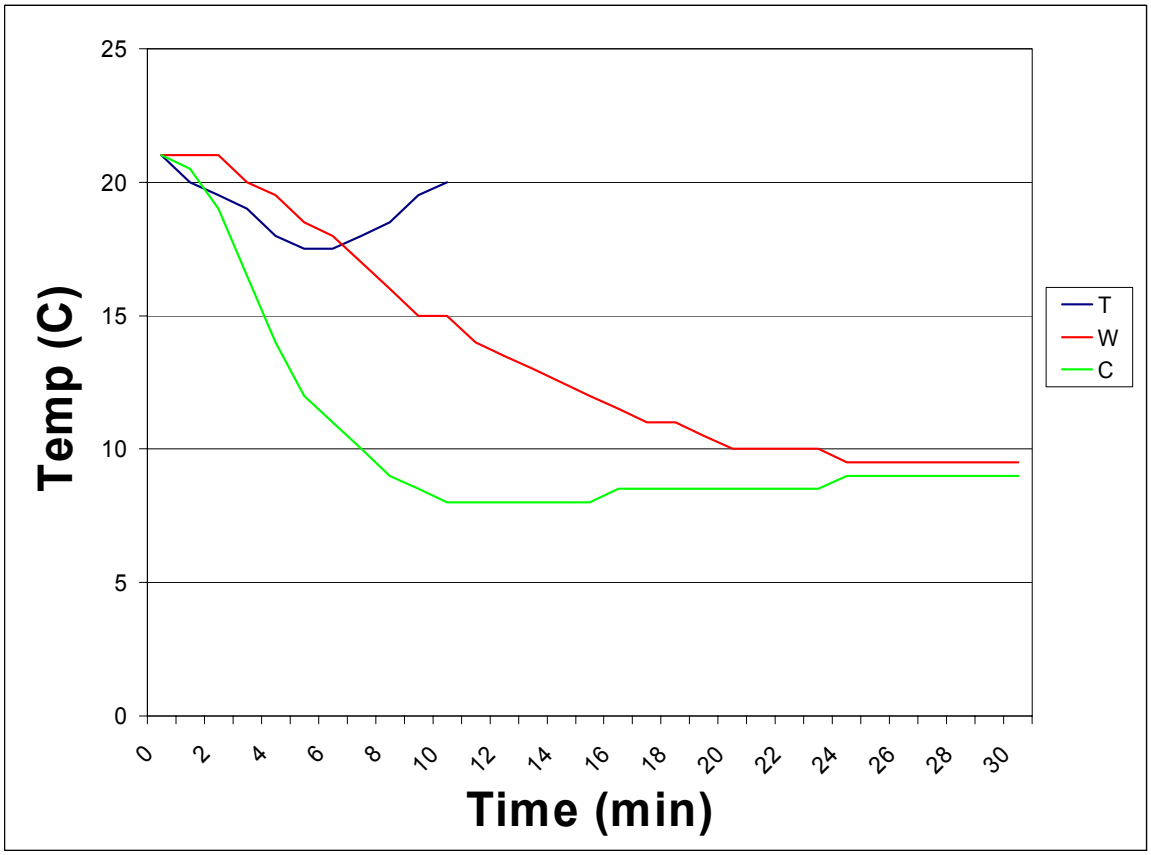


FIGURE 4.4, Pen Temperature Over 30 Minutes Using Cooling Devices

Pen temperature over 30 minutes as measured using a thermometer suspended in a 3ml pen barrel filled with water. Pen temperature was recorded once each when using a thermoelectric cooler set to 11°C (T), a cold-water circulator (W), and a combine thermoelectric cooler with a cold-water circulator set to 11°C.

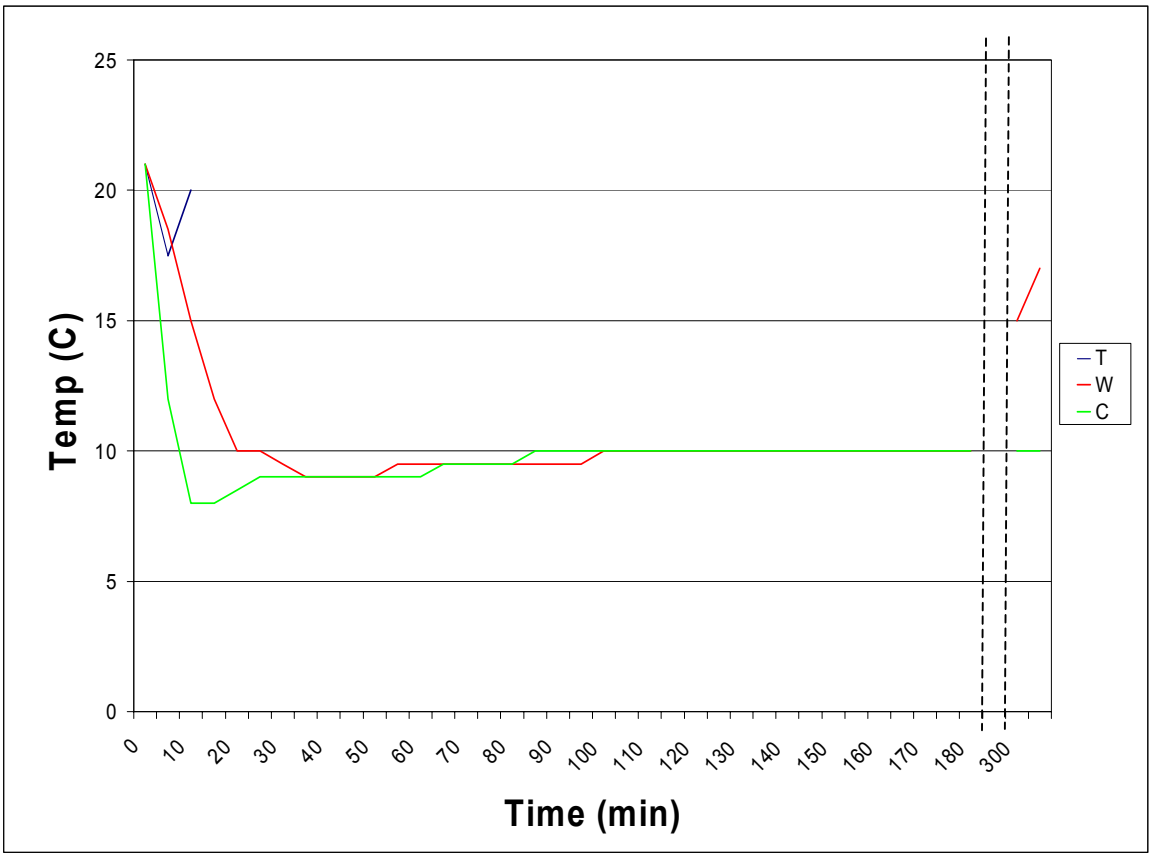


FIGURE 4.5, Pen Temperature over 6 Hours Using Cooling Devices

Pen temperature over 6 hours as measured using a thermometer suspended in a 3ml pen barrel filled with water. Pen temperature was recorded once each when using a thermoelectric cooler set to 11°C (T), a cold-water circulator (W), and a combine thermoelectric cooler with a cold-water circulator set to 11°C. Dashed lines in the graph represent a break in measuring the pen temperature.

The first method that was used to cool the print pens involved attaching a thermoelectric cooler with a fan to each of the print pens. This device was compact and had the added ability to heat the contents of the pen by simply reversing the current running through the thermoelectric cooler; however, it was soon realized that this device would not provide adequate cooling when printing with type I collagen. Often, the collagen would completely polymerize in the pen within 20 to 30 minutes of being placed in the print pen. Also, the wiring to the thermoelectric cooler was unstable, which became apparent, as the wires had to be soldered back onto the device numerous times. To examine its effectiveness at cooling the pens, the temperature-controlling device was set to maintain a temperature of 11°C. As can be seen in Figure 4.4, the temperature dropped approximately 5 degrees, however, within 10 minutes, it returned to close to the initial temperature.

In order to be able to print collagen for longer than 20-30 minutes, the thermoelectric cooler would be placed in the -80°C freezer. Once the temperature-controlling device reported that the temperature of the pen was 7°C, the print pen with the collagen solution was inserted into the thermoelectric cooling device. Using this method, approximately an hour would pass before the temperature-controlling device reported that the pen temperature was between 12 and 15°C. At that point, printing would be stopped, the collagen solution was put on ice, and the thermoelectric cooler was placed back in the -80°C freezer. Admittedly, this is not a reasonable procedure to follow with any frequency.

After determining that the thermoelectric cooler alone would not properly cool the pens such that collagen could be extruded over a long period of time (greater than one hour), a different method was employed to cool the print pens. This method used a cold-water circulating device to chill the contents of the pens. As can be seen in Figure 4.4, it took approximately 25 minutes to reach an equilibrium temperature within the print pen. This temperature was then maintained for close to 3 hours (Figure 4.5). When a small volume (<0.5ml) of collagen was in the print pen, that solution could remain in the cooling devise for 3-4 hours before it would polymerize such that it could no longer be extruded. And, because this method used a simple cold-water circulator, removing some of the excess water from the cooler and replacing it with ice could extend this time.

One of the main purposes of the BAT is to be able to extrude different types of solutions. Thus, in order to provide more flexibility in the types of materials that can be extruded through the BAT, a third pen-cooling mechanism was examined. This method combined the first two methods that were used, i.e., it combined the thermoelectric cooler with the cold-water circulator. Because the cold-water circulator maintained the pen temperature at 11°C, the temperature-controlling device was initially set to 11°C. As can be seen in Figures 4.4 and 4.5, it took approximately 8 minutes for the pen to reach a temperature of 8-9°C. This temperature gradually increased over time, but after 7 hours, the pen was still maintained around 11°C.

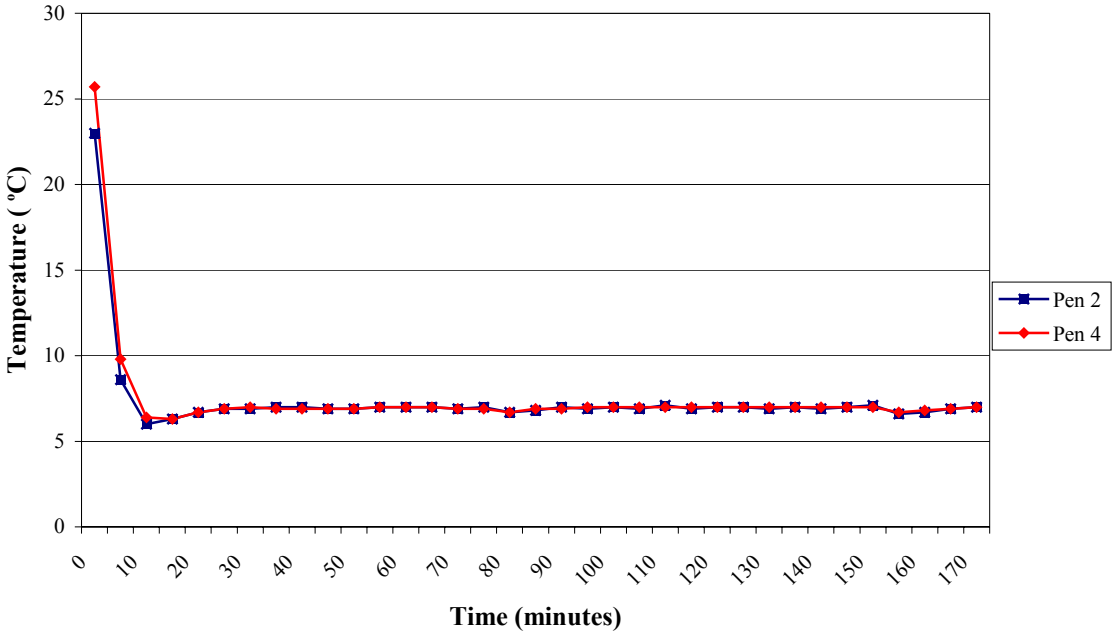


FIGURE 4.6, Pen Temperature for Two Pens Using Combined Cooling System

The pen temperatures were recorded during a single session.

This system provided more flexibility in printing the type I collagen, because it could be printed for at least 7 hours without needing to modify the cooling device, i.e., without having to put the cooling device in the freezer and without having to replenish ice to the cooler. This method also provides the benefit that the pen temperature can be regulated to either heat or cool the pen to a specified temperature. Thus, this method can be used for many different types of polymers, not just type I collagen.

Selecting the Pen Temperature

The primary objective for using the pen-cooling device was to allow for the printing of type I collagen without it polymerizing in the print pen. Using the cold-water circulator, the collagen could be maintained within the print pen for at least three hours without polymerization within the pen. However, this was only true when the print pen contained less than 0.5ml of solution. When, this volume was increased, there were often problems printing. The problems encountered were that the solution being extruded from the print pen appeared to have the consistency of water and dried out rapidly. When this occurred, the print pen was inspected and often, the collagen solution within the pen was solid.

Thus, in order to print with a larger volume of collagen in the print pen, a lower temperature was examined. Because collagen begins to polymerize above freezing, the combined thermoelectric cooler and cold-water circulator was used to maintain a pen temperature between 0-4°C. At 0°C, the contents of the pen froze and the collagen could not be extruded. When the contents were maintained at 4°C, the collagen that was

extruded from the pen was less viscous. Instead, the collagen flowed out onto the Mylar™ as if it were water. When a temperature setting of 7°C was used, the extruded collagen was viscous rather than watery; and more than 0.5ml of collagen could be placed in the print pen. Based on these results, it was decided that when printing type I collagen, the pen should be maintained at 7°C. Similar results were seen when cooling a single pen using a setting of 7°C or 11°C setting. As can be seen in Figure 4.6, the combined method is capable of cooling two pens to 7°C almost as quickly as it cooled one pen to 11°C (Figure 4.4).

Controlling Humidity

Most work detailing the use of 3D RP techniques to generate viable constructs have commented on the humidity of the environment being a key factor in maintaining the viability of the cells. This chapter looks at two methods for providing humidity within the BAT cabinet: evaporative humidification and ultrasonic humidification. Evaporative humidifiers put moisture in the air by using a fan to blow air through a moistened material, such as a filter. These humidifiers are not expected to disperse a substantial amount of minerals into the air. However, when they use standing water, they may allow for the growth of microorganisms. Ultrasonic humidifiers create a mist of water that is dispersed into the air. This is accomplished using ultrasonic sound vibrations. Because these humidifiers actually disperse the water into the air, they are more likely to transmit microorganisms and minerals into the air.

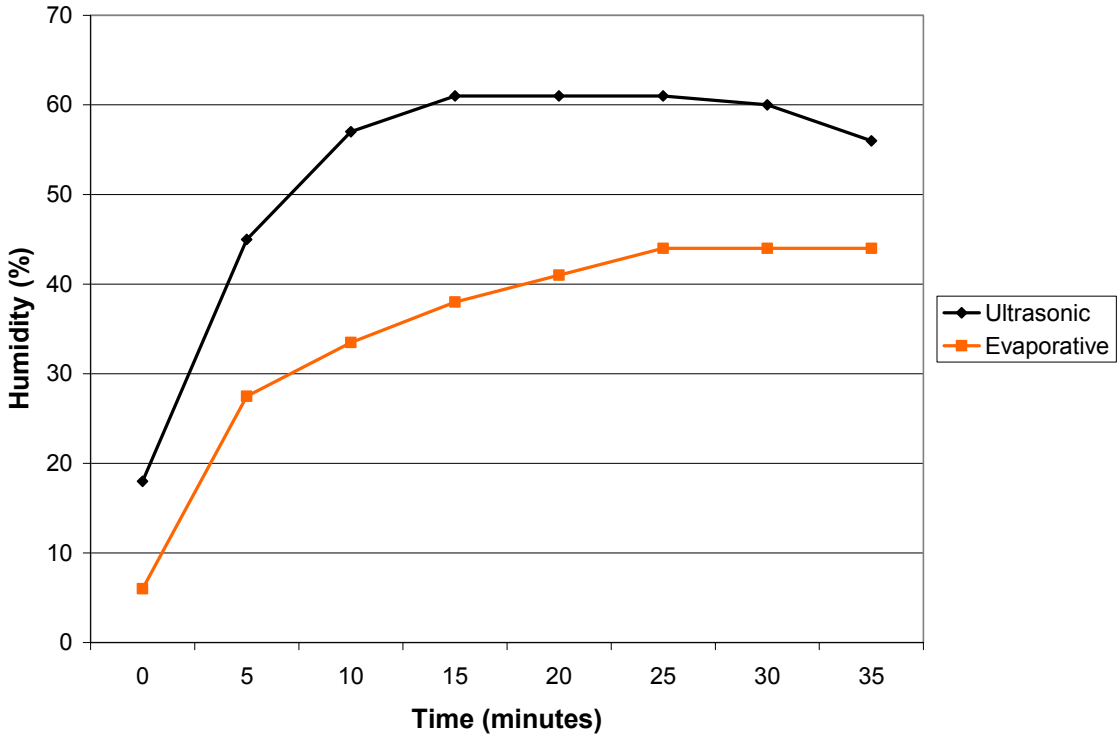


FIGURE 4.7, Adding Humidity to the BAT Cabinet

The true humidity was measured using a Wet/Dry temperature bulb when adding humidity to the BAT cabinet using the ultrasonic humidifier on its lowest setting and the evaporative humidifier on its highest setting. These values were recorded during a single session, i.e., only one measurement was taken.

Because evaporative humidifiers are less likely to disperse both minerals and microorganisms into the air, this type of humidifier was investigated first. As can be seen in Figure 4.7, when the evaporative humidifier was used inside the BAT cabinet on its highest setting, a steady state humidity of 50% was obtained within 30 minutes. Because the doors to the BAT cabinet are opened and closed in order to prepare the system for printing and to remove the printed constructs for culture, the effects of opening the doors were examined with respect to the effect on the humidity within the cabinet. When the doors were open for 30 seconds, the humidity dropped to approximately 40%. It then took almost 15 minutes to return to the steady state humidity of 50%.

An ultrasonic humidifier was also used to provide humidity to the BAT cabinet. As can be seen in Figure 4.7, when the ultrasonic was used inside the BAT cabinet on its lowest setting, this humidifier added as much if not more humidity to the cabinet as did the evaporative humidifier. When the humidifier was turned up to disperse more water particulates, the humidity within the cabinet reached 100%. Thus, this system for adding humidity to the cabinet allows the user to control a larger humidity range.

To test the effectiveness of each humidification method when the BAT is in use, the BAT cabinet doors were opened and closed during the humidification process. Using the evaporative humidifier, the humidity dropped 10% when the cabinet doors were opened and it took 15 minutes to return to the steady state humidity. Because the ultrasonic humidifier adds humidity to the cabinet more rapidly than the evaporative humidifier, opening the cabinet doors did not have as big an impact as that seen with the evaporative humidifier.

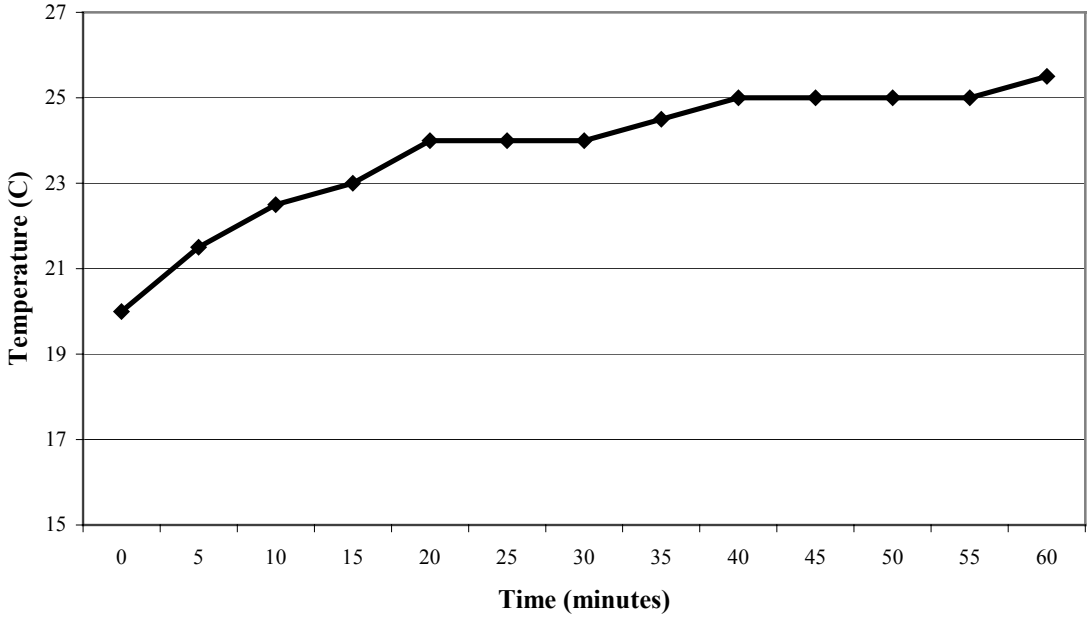


FIGURE 4.8, Stage Temperature Using Heat Lamps

The temperature of the stage was measured during a single session, i.e., only one measurement was taken

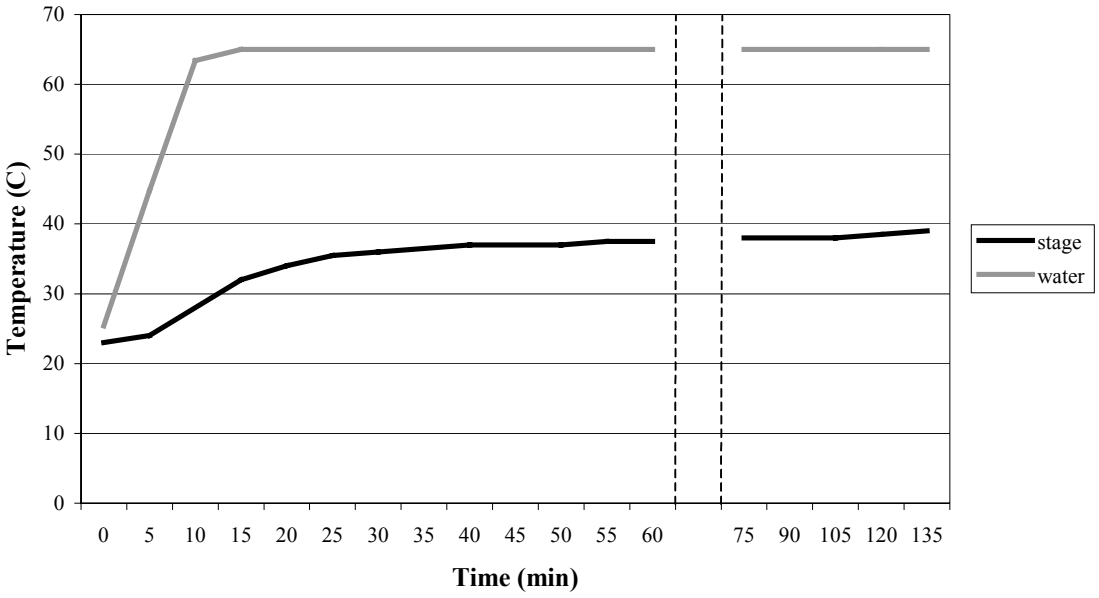


FIGURE 4.9, Stage Temperature Using a Water Circulator Set to 67°C

Both the temperatures of the stage and of the circulating water were recorded during a single session, i.e., only one measurement was taken.

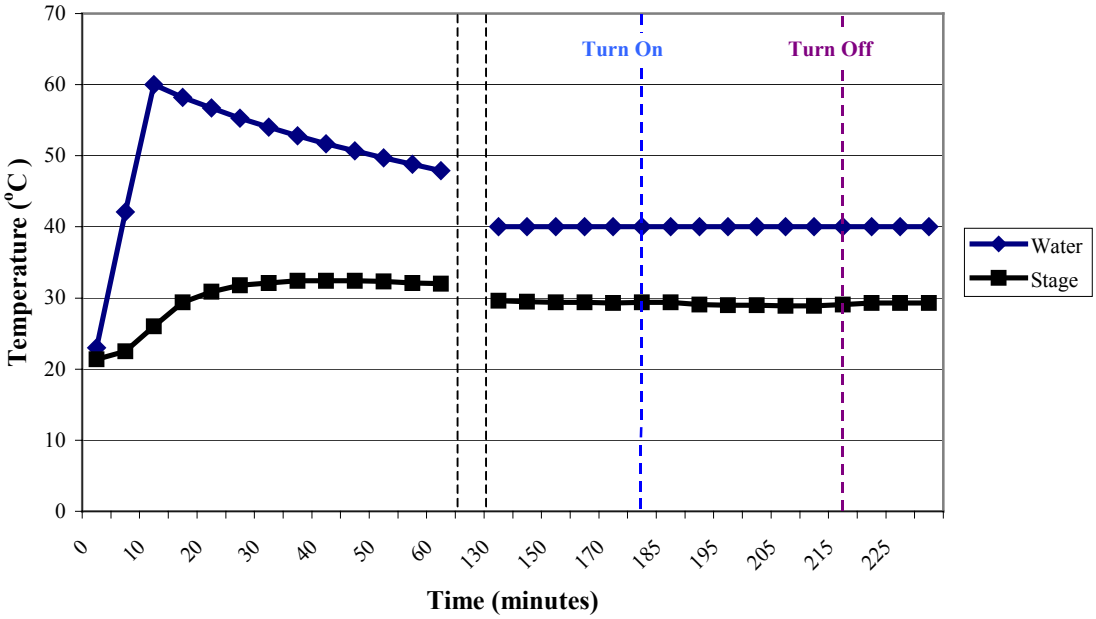


FIGURE 4.10, Stage Temperature Using Water Circulator Set to 60°C Then 40°C

Stage and water temperature using a constant temperature water circulator to heat the stage. Once the stage had reached a steady state temperature, the ultrasonic humidifier was turned on for 30 minutes in order to assess the effects of added humidity on the temperature of the stage. Both the temperature of the stage and of the circulating water were recorded during a single session, i.e., only one measurement was taken.

Heating the Stage

One of the first materials that was extruded through the print pens was type I collagen. Initially, there were problems with some of the collagen washing away when media was added to the constructs. It was believed that this was because the collagen had not fully polymerized; however, if the media was added too late, the viability of the printed cells greatly decreased. Because this material polymerizes with increased temperature, two methods to heat the stage were examined: 1) shining two 300-Watt heat lamps onto the stage and 2) using a constant temperature water circulator.

The first method that was examined used two heat lamps shining onto the stage. Because the stage is black, it was expected that this method would be capable of significantly raising the temperature of the stage. Also, this method was desirable because it did not introduce the potential for water leaks or flooding within the BAT cabinet. As can be seen in Figure 4.8, it took an hour to raise the temperature of the stage approximately 6 degrees.

Because shining the heat lamps onto the stage took a long time to moderately increase the temperature of the stage, a second stage warming method was examined. This method used a constant temperature water circulator. Initially, the desire was to raise the temperature of the stage to a physiological temperature of 37°C. It was determined that in order to obtain this temperature, the water circulator needed to be set to 65°C. Figure 4.9 illustrates the temperature of the water in the circulator as well as the temperature of the stage when the water circulator was set to 65°C. This method was able

to warm the stage to 37°C, approximately 15 degrees higher than the starting temperature, in less than 30 minutes. The temperature of the stage did stay close to 37°C; however, over time, the temperature did drift higher. This was concerning, because as the temperature increases above 37°C, the cells are more likely to die and the collagen is more likely to dry out.

To ensure that the printed cells were not overheated, the stage was maintained at 29-31°C. This temperature range is able to warm the collagen to aid in speeding up its polymerization, without getting close to the temperature at which the cells will die. In order to rapidly reach this range, the water circulator was set to circulate water at 60°C for 10 minutes and then changed to maintain a water temperature of 40°C. Figure 4.10 illustrates the stage and water temperatures over time using this method.

To determine whether or not adding humidity to the system would significantly decrease the temperature of the stage, the ultrasonic humidifier was turned on to its lowest setting and the doors of the BAT cabinet were closed. As can be seen in Figure 4.10, there was no decrease in the temperature of the water that was being circulated and there was only a slight (<1°C) decrease in the temperature of the stage. Also, once the humidifier was turned off, the stage temperature returned to its original steady state temperature in less than 5 minutes.

## DISCUSSION

The same pressure values were recorded with both pressure measurement methods and the same steady state pressures were detected for both the 25 and 33 gauge

tips as well as when the manometer was connected directly to the pen pressure supply. Based on these measurements, it was concluded that the actual pressure that is applied to the pneumatic pens is approximately 2psi less than the setting that is used in the scripts that direct the movements of the BAT. Based on the measured values, the following equation can be used to estimate the applied pressure when given the BAT pressure setting: $(true\ pressure) = (BAT\ pressure) - 2.06$. Because the compressed air tank is regulated to a maximum of 20 psi, this equation is only valid for BAT pressure settings up to 20 psi.

A difference was noted between the applied pressures when measuring pressure through the 33 gauge pen tip verses pressure directly through the pen's connector or through a 25 gauge pen tip. When using the 33 gauge pen tip to measure the applied pressure, there was a noticeable delay before the steady state pressure was reached; and when the pressure was measured directly through the connector or through the 25 gauge pen tip, there was a noticeable over shoot before the steady state was reached. This is probably due to the fact that there is a much higher resistance seen through the 33 gauge pen tip than through the connector itself or even through a 25 gauge pen tip.

Because the BAT software regulates the pressure to be less than 50psi and because the regulator on the air tank supply further limits the system to 20psi, it could be argued that a pressure regulator with a smaller output pressure should be used with the BAT. This would provide better precision in the small range pressure, which is what is currently being used. In the future, more viscous materials may be used, and the current regulator allows for the extrusion of materials as viscous as peanut butter or toothpaste.

However, before attempting to print materials that require an extrusion pressure greater than 20psi, the connectors on the tubing inside the BAT's black box need to be adjusted or replaced such that when this pressure is applied, the tubing does not disconnect from its connectors.

Three different methods were examined to cool the contents of the pneumatic print pens, including using a thermoelectric cooler with a fan attached, using a cold-water circulator, and using a combined thermoelectric cooler and cold-water circulator. Using a thermoelectric cooler alone has the benefit that it is compact and capable of either heating or cooling the pen. However, this device was not able to provide sufficient cooling capabilities to the BAT when printing type I collagen. Using a cold-water circulator to keep the contents of the pens cool, the contents of the pen were maintained at 11°C for at least 3 hours, and this time could easily extended by adding more ice to the system. One limitation of this device is that does not have a wide range of temperatures it can maintain. To add more control to the system, a constant temperature water circulator was connected to the device creating a combined thermoelectric cooler and water circulator. This system has the flexibility to heat or cool the pens to a specified temperature. This demonstrated that the combined method could cool a single pen to 7°C or 11°C for at least 7 hours, and that it could also cool 2 pens to 7°C for that long as well.

It is believed that in order to use RP techniques to generate viable constructs, the environment in which the cells are extruded must be humid (Boland, et al., 2003; Mironov, et al., 2003). Thus, two different methods to provide humidity within the BAT cabinet were explored, namely evaporative humidification and ultrasonic humidification.

Evaporative humidifiers have the advantage that they generally do not disperse a substantial amount of minerals into the air. In contrast, ultrasonic humidifiers do disperse the water into the air and are thus more likely to transmit more microorganisms and minerals into the air. This study found that the ultrasonic humidifier is capable of increasing the humidity within the BAT cabinet more quickly and to a higher percent humidity. Using an evaporative humidifier built for a larger area could improve the capabilities of using such a humidifier. This system is also not as effected by the opening and closing of the BAT cabinet doors as was evidenced by the fact that the humidity in cabinet did not decrease as rapidly as it did when an evaporative humidifier was used.

One problem encountered when using the ultrasonic humidifier is that it sometimes stops producing a mist of water. This occurred when testing its effectiveness. Thus, a drop is seen in the humidity reported in Figure 4.7. When this happens, the humidifier generally does not run properly for a few hours. Lifting the water tank and dropping it back down on the base a few times remedied the problem. The systems that were tested for adding humidity to the BAT cabinet are inexpensive humidifiers used in cigar cabinets and houses. Thus, in order to add humidity to the cabinet that is reliable and easily adjustable (without having frequently to open the cabinet doors to increase or decrease the output), it is recommended that a professional grade humidifier be purchased for the BAT cabinet.

To aid in the polymerization of type I collagen, which polymerizes more rapidly with increased temperature, methods to heat the stage were explored. When the heat lamps were used, it took an hour to increase the temperature of the stage almost 6°C.

Using a constant temperature water circulator caused the temperature of the stage to more rapidly increase. When humidity was added to the BAT cabinet, a slight decrease in stage temperature was witnessed. However, once the humidifier was turned off, the stage returned to its steady state temperature within 5 minutes.

Based on the results seen in this study, it was concluded that a combined water circulator and thermoelectric cooler with a temperature-controlling device should be used to cool the contents of the extrusion reservoirs. This method was more efficient and flexible than using a thermoelectric cooler or water circulator alone when it came to cooling the reservoirs. It was also concluded that a professional grade humidifier be purchased for the BAT cabinet. The tests in this chapter demonstrated that the ultrasonic humidifier provides a higher humidity to the BAT cabinet, and it is thus more likely to have an impact on maintaining the viability of extruded cells. However, as this system does add water particulates to the air, it is recommended that purified, distilled water be used in the system. If contaminations are witnessed in the generated constructs, it would be wise to sterilize the whole humidifier in case microorganisms had begun growing within the humidifier itself. Also based on these results, it was concluded that a constant temperature water circulator should be used to maintain the temperature of the stage onto which cells are extruded.

# 5. UTILIZING A DIRECT-WRITE BIOASSEMBLY TOOL TO FABRICATE VIABLE THREE-DIMENSIONAL CONSTRUCTS WITH A DEFINED ARCHITECTURE

## INTRODUCTION

Tissue engineering is an interdisciplinary field that utilizes the practices of engineering and science with the primary goal of developing biological alternatives that are capable of restoring, maintaining, or improving tissue function (Langer & Vacanti, 1993). As the spatial organization of tissue is vital in directing biological functions (Pardanaud, et al., 1989; Patel, et al., 1998; Risau, et al., 1988), the field of TE has focused on generating 3D scaffolds with a controlled architecture. In fact, it has been proposed that in order to best develop these biological alternatives, these constructs must closely imitate nature (Lanza, et al., 2000). Rapid Prototyping techniques, which lay down material in a layer-by-layer fashion, have been utilized to fabricate 3D spatially organized constructs. A majority of these methods build acellular scaffolds that are later seeded with cells through either in vitro or in vivo cellular invasion (Park, et al., 1998; Sherwood, et al., 2002; Sodian, et al., 2000b).

There has recently been an emergence of RP technologies to spatially organize both cells and matrix into viable constructs that can potentially be used to replace or repair damaged tissue (Boland, et al., 2003; Marquez, et al., 2002; Ringeisen, et al., 2002a; Ringeisen, et al., 2002b; Wilson, Jr. & Boland, 2003). It has been proposed that using such a method will accelerate and improve the assembly of tissue by removing the

need for a cell invasion step (Mironov, et al., 2003). In chapter 2, it was demonstrated that a direct-write, 3D BioAssembly Tool is capable of generating viable, spatially organized constructs by coextruding cells and matrix (Kachurin, et al., 2002; Smith, et al., 2004). Other laboratories have investigated using an aerosol-based direct-write system (Marquez, et al., 2002), a laser forward transfer technique (Ringeisen, et al., 2002a; Ringeisen, et al., 2002b), or a modified ink-jet printer (Boland, et al., 2003; Wilson, Jr. & Boland, 2003) to fabricate viable 2D and 3D constructs.

A key difference between the BAT and other RP methods used to pattern cells and matrix is that this system works by laying down individual dots or by extruding a continuous segment of the cell/matrix solution. Most other methods lay down a single dot of material; this dot may then meld together with an adjacent dot in order to form a continuous segment. The BAT, like modified ink-jet technology (Boland, et al., 2003; Wilson, Jr. & Boland, 2003), has modular extrusion barrels and tips and has multiple pens such that more than one cellular or acellular solution can be patterned during the same printing session.

In this chapter, the use of a direct-write, 3D BioAssembly Tool is characterized for its ability to generate spatially organized viable constructs. This instrument is highly versatile in that it is capable of generating 2D or 3D constructs comprised of multiple separate cellular suspensions. This chapter is focused on characterizing some of the environmental factors that have a direct impact on the viability of generated constructs. This work also focuses on using the BAT to spatially organize 2 separate solutions of collagen within 2D and 3D constructs.

## MATERIALS AND METHODS

### Measuring Viscosity of Collagen

A solution of 3.0mg/ml collagen was prepared as previously described (Smith, et al., 2004). Briefly, purified rat-tail type I collagen (BD Biosciences, Bedford, MA) was mixed with 4× DMEM and brought to a pH of 7.0-7.4 by the addition of 1M NaOH. A Gilmont Falling Ball Viscometer (Gilmont Instruments, Barrington, IL) was used to measure the viscosity of the collagen solution. A #5 stainless steel ball with a density of 8.35g/cm$^3$ and a viscometer constant value of 3.3 was used. Five times, the amount of time required for the ball to drop from one marked location to another was recorded. This value was averaged and then plugged into the viscometer equation of $\mu = K(p_f - p) * t$, where $\mu$ is the viscosity, $K$ is the viscometer constant, $p_f$ is the density of the ball, $p$ is the density of the collagen, and $t$ is the time it took the ball to drop from one marked location to the other. In order to calculate the viscosity of the collagen, the density needed to be determined. To discount the amount of collagen that clings to the pipet tip when it is pulled up, the weight of the pipet tip was measured and then the weight of 0.25ml of collagen was weighed while it was still in the pipet tip. The weight of the collagen was calculated as the weight of the pipet tip and collagen minus the weight of the pipet tip alone. Three measurements were taken and this value was averaged. The average weight was divided by 0.25ml to give the density in grams per milliliter.

## Description of the BioAssembly Tool

The BAT has been previously described in more detail (Smith, et al., 2004). Briefly, the BAT is a three-axis printing machine capable of moving the stage and delivery pen in the *x*-, *y*-, and *z*-axes separately or simultaneously. This configuration provides the flexibility and control that enables the BAT to create complex 3D objects. Commands to direct the movement of the BAT are put into text files called scripts. The printing mechanism of this system consists of 4 print heads, or micro-dispense pens, one of which is a combined positive displacement and pneumatic pen that utilizes ceramic pen tips of varying sizes. The 3 other pens that were used in this study are pneumatic syringes with printing tips chosen based on the viscosity and size of particulates (e.g., cells) in the material being extruded. The pressure regulator used to control the pressure applied to the pneumatic pens is a 100psi unit with an accuracy of 1% of full scale, i.e. ± 2psi. The pressures measured through the pens have been consistently 2psi less than the BAT pressure setting, i.e., an extrusion pressure setting of 5psi applies an actual pressure of 3psi to the print pen.

## Characterizing Lines

A solution of 3.0mg/ml collagen was, put into a 3ml pneumatic pen reservoir with a 25 gauge (250μm ID) or 33 gauge (90μm ID) tip (EFD, Inc., East Providence, RI), and maintained at 7°C. Lines of collagen were extruded onto the hydrophilic side of Mylar™ (Bio-Rad Laboratories, Hercules, CA) with various pressure settings and speeds. Extrusion pressure settings of 2 (or 2.5 for the 33 gauge pen tip), 4, 6, 10, and 20psi were

used. Lines were generated using the previously mentioned pressure settings at a linear pen speed of 10mm/s and 20mm/s. When using the 20mm/s speed, lines were generated with 4 different settings: no applied stage heat or humidity, cabinet humidity maintained above 65%, stage heat maintained between 29-31°C, and both stage heat and humidity. A script to print 10mm lines was used to extrude 5 lines for each group. After extrusion, the lines were stained with Coomassie Blue for 1 minute and then washed in DCF-PBS. The lines were imaged and measured using Scion Image (Scion Corporation, Frederick, MD). The line widths were measured in 10 distinct locations and the length of each line was measured. Special effort was made to measure the smallest and largest widths of each line. A student's T test was used to evaluate the line widths.

Preparing Cellular Type I Collagen Solutions

Rat microvascular cells (RMC) were isolated from the epididymal fat pads of male Fischer rats (Wagner & Matthews, 1975) and used between passages one to five. RMC + Collagen solutions were prepared according to previously published methods (Smith, et al., 2004) with modifications. Briefly, cells were expanded to confluence in culture flasks, trypsinized, and sedimented at 172G. Cell pellets were mixed with 3.0mg/ml type I collagen to obtain a RMC + Collagen solution at a concentration of $10^5$, $10^6$, or $10^7$RMC/ml of collagen. This solution was then transferred to a 3ml pen reservoir with either a 25 gauge or 33 gauge tip and maintained at 7°C. Prior to extrusion, the pneumatic syringe barrels, pen tips, and Mylar™ were ethylene oxide sterilized.

Assessing Viability

To assess the viability of the printed constructs, a fluorescent-based live/dead assay (Molecular Probes, Inc., Eugene, OR) was used. A staining solution containing calcien AM and ethidium homodimer in DCF-PBS was prepared following the instructions included with the kit. The printed constructs were washed with DCF-PBS and then bathed in the staining solution for 30 minutes at room temperature, protected from light. The constructs were then washed 2 times for 15 minutes with DCF-PBS and imaged within 1 hour after staining using a Nikon epifluorescent microscope to image the live (Excitation: 488nm; Emission: 530nm) and dead (Excitation: 528-553nm; Emission: 580nm) cell fluorescence. A negative control of RMC + Collagen that had been fixed in 2% paraformaldehyde was also stained. The total number of cells was counted within 20 fields of view using a 20× objective, which consisted of a 0.127mm$^2$ area of the extruded construct. Cells were counted as live if they had a homogenous bright green staining throughout the cell, and cells with bright red staining were counted as dead. Percent viability was calculated as the number of live cells divided by the total number of cells counted. A student's T test was used to evaluate the viability measurements.

Examining Effects of Cell Concentration, Pressure, and Pen Tip on Viability

Cell concentration, extrusion pressure, and pen tip inner diameter were examined to determine their effects on the viability of printed cells. Three separate suspensions of RMC + Collagen were prepared as previously described at concentrations of $10^5$, $10^6$, and $10^7$cells/ml. These suspensions were placed in the barrels of pneumatic pens with a 25

gauge or 33 gauge pen tip and maintained at 7°C. The solutions were then extruded onto the hydrophilic side of Mylar™ using an extrusion pressure setting of 2 (or 2.5 for the 33 gauge pen tip), 4, 6, 10, and 20psi. After extruding the solution at the specified pressure, the construct was incubated at 37°C for 2 minutes and then bathed in warm culture media containing antibiotics. Soon after extrusion and after 3 days in culture, the constructs were assessed for viability as described above.

Examining the Effects of Stage Heat and Humidity on Viability

In order to examine the effects of humidity on the viability of extruded cells, a solution of $10^6$RMC/ml of collagen was placed in a pen reservoir with a 25 gauge pen tip and maintained at 7°C. A 10-layered 5mm × 5mm solid square construct was generated with a 1μm height separation between each layer. Constructs were generated on 2 separate days with the stage at room temperature or with the stage maintained at 29-31°C using a constant temperature water circulator (VWR Scientific, West Chester, PA). For all sets of constructs, 3 groups were generated, including using no humidifier, maintaining the humidity between 45-55% using an evaporative humidifier, and maintaining the humidity between 65-80% using an ultrasonic humidifier. Constructs were incubated at 37°C for 2 minutes after extrusion and then bathed in warm culture media containing antibiotics. On days 0 and 3, the viability of the printed constructs was assessed as described above.

Membrane Labeling Cells

Prior to printing, two separate suspensions of cells were fluorescently labeled using membrane intercalating dye PKH-26 or PKH-67. Methods for staining cells with PKH dyes have been previously described (Dailey, et al., 1991). Briefly, a loose cell pellet containing at least $2\times10^6$cells/ml was obtained. The pellet was then rinsed with 1ml of DCF-PBS and spun at 400G for 4 minutes. The supernatant was aspirated and the pellet was mixed with the membrane labeling solutions. After 3 minutes, the reaction was counteracted with an equal volume of 1% bovine serum albumin in DCF-PBS. After 1 minute, the cell solution was diluted with an equal volume of complete media. The cells were washed 4 times by suspending them in 10ml of complete media and centrifuging at 400G for 10 minutes. The cells were then seeded in a tissue culture flask with warm media and maintained in culture for 1 day prior to printing.

Spatially Organizing Separate Cellular Solutions

After membrane labeling two suspensions of cells, the BAT was examined for its ability to print two lines adjacent to each other without any overlap between the lines. Separate solutions of $10^6$RMC/ml of collagen were placed in 2 pen reservoirs with 25 gauge pen tips and maintained at 7°C. One pen contained cells labeled with PKH-26 and the other pen contained cells labeled with PKH-67. Two pneumatic print pens were calibrated manually and calibration data were recorded by software. Constructs containing 10 layers of adjacent lines were printed on Mylar™ simultaneously with a linear stage speed of 20mm/s and alternating the active pen between layers. During the

extrusion process, the stage temperature was maintained between 29-31°C and the humidity was maintained above 60% using an ultrasonic humidifier. The distance between adjacent lines was increased from 50 to 500μm in increments of 10μm. The completed constructs were immediately incubated at 37°C and 5% $CO_2$ for 2 minutes in a 6-well plate to promote polymerization of the collagen, then covered in culture media with antibiotics and returned to the incubator.

Measuring Separation in Adjacent Lines

After 2 days in culture, the constructs were fixed in 2% paraformaldehyde in PBS for 45 minutes and washed 2 times for 15 minutes in PBS. The constructs were imaged using a Nikon epifluorescent microscope with an excitation/emission setting of 488nm/530nm to detect PKH-67 labeled cells or 528-553nm/580nm to detect PKH-67 labeled cells. Image analysis was performed automatically using macros within the Metamorph Imaging System (Molecular Devices Corporation, Downingtown, PA). This analysis consisted of segregating each image into 15 bins, where each bin was 100 μm wide. The total number of red (PKH-26 labeled) and green (PKH-67 labeled) cells was counted within each bin. A distribution curve was calculated denoting the percentage of green and red cells within each bin. Next, a cell-mixing index denoting the total mixing of red and green cells within each bin was calculated. This value was calculated as the ratio of red and green cells as a function of position relative to the midpoint of total cell population, where 0 suggests no mixing and 1 suggests complete mixing.

| Layer | Lift Before Layer | Wait Before Layer |
|---|---|---|
| 2 | 15.0μm | 0 seconds |
| 3 | 10.0μm | 15 seconds |
| 4 | 3.0μm | 20 seconds |
| 5-6 | 2.0μm | 15 seconds |
| 7-10 | 1.5μm | 15 seconds |
| 11-14 | 1.5μm | 10 seconds |
| 15-17 | 1.0μm | 15 seconds |
| 18-31 | 1.0μm | 10 seconds |
| 32-104 | 0.5μm | 10 seconds |

TABLE 5.1, Lift and Wait Parameters Used to Generate 3D Squares

The amount that the pen was lifted and the time that elapsed before printing specified layers.

Generating 3D Collagen Constructs

A solution of $10^6$cells/ml of collagen was placed in a pen reservoir with a 25 gauge pen tip and maintained at 7°C. Collagen constructs comprised of 104 solid layers in the shape of a 7.5mm × 7.5mm square. An extrusion pressure setting of 2.25psi was used for the first layer, 2.15psi was used for the second layer, and 2psi was used for subsequent layers. During extrusion the stage was maintained between 29 to 31°C and the humidity within the BAT cabinet was kept above 65%. The amount that the pen was lifted as well as the time it waited before extruding a subsequent layer is detailed in Table 5.1. After the construct was fabricated, it was maintained at 37°C for 5 minutes and then bathed in warm culture media containing antibiotics. On 2 separate days, the RMC + Collagen solution was extruded into the pattern of the 3D square. Viability was assessed (as described above) after 3 days in culture.

Measuring the Height of 3D Collagen Constructs

To estimate the height of the printed constructs, 3D collagen constructs were generated as described above using yellow-green 15μm Fluospheres (Molecular Probes, Eugene, OR) suspended in type I collagen at a concentration of $1.6\times10^6$ spheres/ml. The heights of the Sphere + Collagen constructs were measured in 5 locations using both a Biorad MRC-1024ES confocal microscope with a 488nm laser excitation and 525-555nm emission filter and a Nikon fluorescent microscope with an excitation filter of 465-495nm and an emission filter of 530nm. For each measurement, the height of the construct was

estimated based on the bottom of the deepest and the top of the shallowest microsphere that was detected.

### Spatially Organizing 3D Collagen Constructs

The script that was used to generate 3D collagen constructs was modified to generate a 7.5mm × 7.5mm square using two pneumatic print pens instead of one. The same pressure settings, lifts, and waits were used. The script was modified such that it laid down 5 separate 20 layered sections resulting in a construct comprised of 20 layers of collagen alone, 20 layers of RMC + Collagen, 20 layers of collagen alone, 20 layers of RMC + Collagen, and 20 layers of collagen alone. During extrusion the stage was maintained between 29 to 31°C and the humidity within the BAT cabinet was kept above 65%. After the construct was fabricated, it was maintained at 37°C for 5 minutes and then bathed in warm culture media containing antibiotics. The viability of the constructs was assessed as described above. To measure the height of the resulting layers, fluorescent microspheres were used in place of RMC, and a confocal microscope was used to examine and measure the heights of the layers.

## RESULTS

### Measuring the Viscosity of Collagen

The viscosity of the collagen samples was calculated based on density. Because collagen is viscous and tends to cling to the pipet tip when aspirated, the collagen weight was determined by first weighing the pipet tip and then weighing the pipet tip with

collagen. Using this technique, the density of 3.0mg/ml collagen was calculated as 1.056g/ml. A Gilmont Falling Ball Viscometer was used to determine the viscosity of the collagen. This viscometer works by measuring the time needed for a ball of known density to fall a specific length. Once the time is known, the viscosity, $\mu$, is calculated as $\mu = K(p_f - p) * t$, where $K$ is the viscometer constant, $p_f$ is the density of the ball, $p$ is the density of the collagen, and $t$ is the time it took the ball to fall the specified length. The average time it took the ball to fall was 47.4 seconds (+/-). Using this value and the measured density, the viscosity of the collagen was calculated as 1.056g·s/ml.

Line Widths

The minimum pressure setting required to obtain a continuous line of collagen using a pneumatic print pen was measured as 2psi for a 25 gauge pen tip and 2.5psi for a 33 gauge pen tip. At this pressure setting, the BAT extrudes a uniform, continuous line. As can be seen in Figure 5.1, as the pressure increases, the line widths, and sometimes their lengths, increases. Also, with added pressure, the lines take on a less uniform and sometimes more blob-like shape.

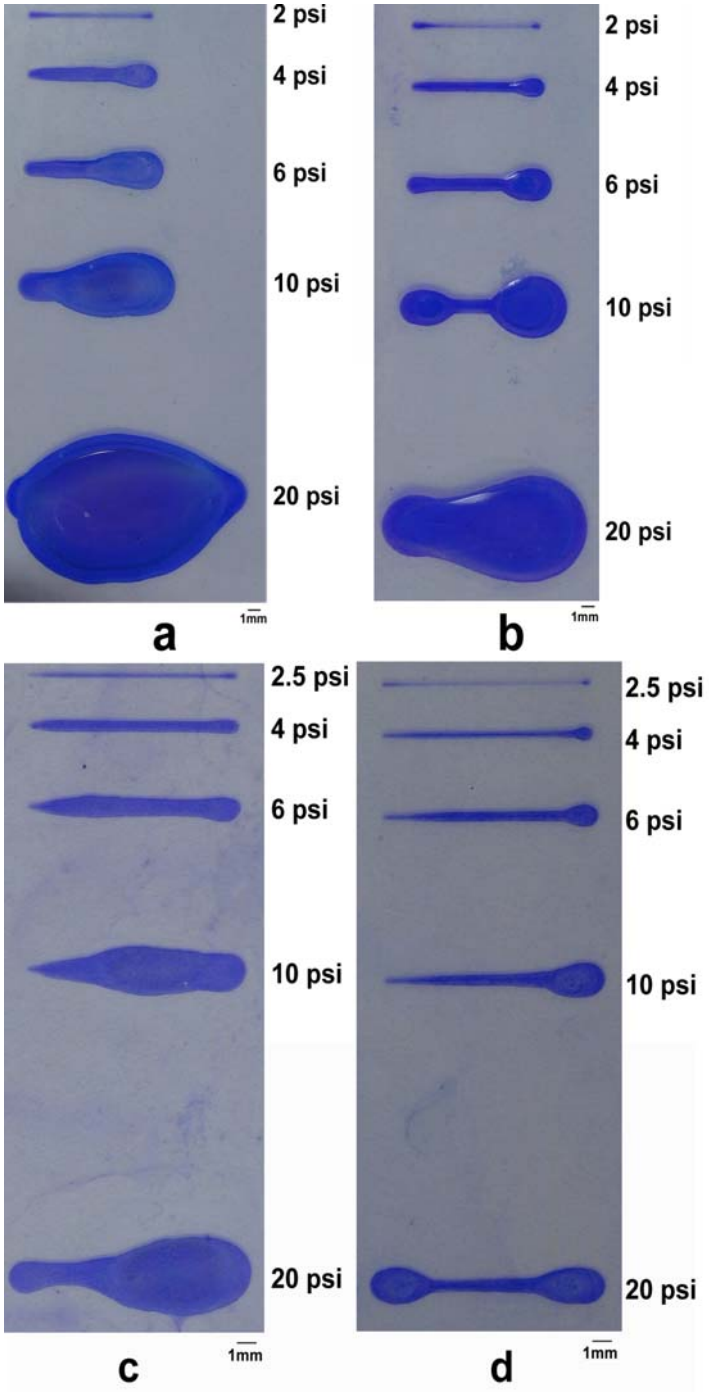


FIGURE 5.1, Representative Collagen Lines

Representative images of collagen alone lines printed using a 25 gauge (a,b) or 33 gauge (c,d) pen tip at a linear speed of 10mm/s (a,c) or 20mm/s (b,d) with BAT pressure settings ranging from 2-20psi.

| | | 2.5psi | 4psi | 6psi | 10psi | 20psi |
|---|---|---|---|---|---|---|
| **10mm/s** | Ave | 187.88 | 488.79 | 834.24 | 1323.64 | 1944.24 |
| | Std Dev | 15.58 | 72.71 | 156.90 | 257.49 | 315.32 |
| **20mm/s** | Ave | *152.12 | *363.03 | *534.85 | *733.03 | *1000.61 |
| | Std Dev | 10.95 | 46.31 | 53.51 | 70.10 | 99.71 |
| **Added Humidity** | Ave | †189.70 | †391.52 | †615.15 | †919.70 | †1206.97 |
| | Std Dev | 29.42 | 29.02 | 99.70 | 139.78 | 174.75 |
| **Stage Heat** | Ave | †157.27 | †382.42 | †590.00 | †844.24 | †1024.55 |
| | Std Dev | 22.10 | 90.26 | 90.26 | 147.25 | 163.55 |
| **Humidity + Stage Heat** | Ave | †162.12 | †413.64 | †610.61 | †867.58 | †1042.12 |
| | Std Dev | 24.34 | 57.30 | 93.87 | 124.67 | 162.91 |

TABLE 5.2, Average Line Widths for 33 Gauge Prints

These values represent the average line widths (μm) for each group of parameters as well as the standard deviations. * indicates a significant decrease in the line width as compared with the 10mm/s print and † indicates a significant increase in the line width as compared with the 20mm/s print ($p > 0.001$) with no added humidity or stage heat.

| | | 2psi | 4psi | 6psi | 10psi | 20psi |
|---|---|---|---|---|---|---|
| **10mm/s** | Ave | 476 | 984 | 1,801 | 3,761 | 9,636 |
| | Std Dev | 47 | 312 | 596 | 644 | 760 |
| **20mm/s** | Ave | 460 | 765 | 1,327 | 2,800 | *6,048 |
| | Std Dev | 37 | 152 | 171 | 239 | 425 |
| **Added Humidity** | Ave | 472 | 811 | 1,515 | 3,565 | †7,834 |
| | Std Dev | 27 | 153 | 210 | 275 | 955 |
| **Stage Heat** | Ave | 444 | 708 | 1,171 | 2,442 | †4,528 |
| | Std Dev | 43 | 162 | 207 | 806 | 699 |
| **Humidity + Stage Heat** | Ave | 488 | 958 | 1,439 | 2,578 | †4,984 |
| | Std Dev | 38 | 286 | 378 | 378 | 659 |

TABLE 5.3, Average Line Widths for 25 Gauge Prints

These values represent the average line widths (μm) for each group of parameters as well as the standard deviations. * indicates a significant decrease in the line width as compared with the 10mm/s print and † indicates a significant change in the line width as compared with the 20mm/s print ($p > 0.001$) with no added humidity or stage heat.

As can be seen in Table 5.2, when using a 33 gauge pen tip, the lines extruded at a linear speed of 20mm/s were always significantly thinner ($p > 0.001$) than those extruded using a linear speed of 10mm/s. Also, when using a 33 gauge pen tip, applying stage heat or humidity significantly increased the width of the extruded lines ($p > 0.001$) as compared with lines printed at the same linear speed and pressure with no added humidity or stage heat. Additionally, when a higher pressure was used to extrude the collagen, the line widths were always significantly wider ($p > 0.001$) than those extruded at the lower pressures. This held true even when environmental features such as stage heating and humidity were applied to the BAT cabinet.

As can be seen in Table 5.3, the widths of the lines generated using a 25 gauge pen tip were not as significantly affected by changing printing parameters. Even though, the lines generated using the same pressure settings with a different linear speed were on average smaller for the faster speeds, statistically, the only significant differences appeared for pressure settings of 10psi ($p > 0.01$) and 20psi ($p > 0.001$). Also, when printing using a 25 gauge pen tip and a linear speed of 20mm/s, the line widths decreased with stage heat was added and increased when humidity was added, but showed no change when both stage heat and humidity were used, as compared with lines printed at a linear speed of 20mm/s with no stage heat or humidity.

| | | $1\times10^5$ cells/ml | | $1\times10^6$ cells/ml | | $1\times10^7$ cells/ml | |
|---|---|---|---|---|---|---|---|
| | | **Day 0** | **Day 3** | **Day 0** | **Day 3** | **Day 0** | **Day 3** |
| **Pipet** | **Ave** | 97.07 | 96.30 | 94.57 | 96.14 | 93.39 | 70.77 |
| | **Std Dev** | 5.09 | 4.57 | 5.30 | 4.80 | 2.01 | 11.58 |
| **2.5psi** | **Ave** | 94.38 | 96.04 | 94.92 | 96.37 | 92.52 | 87.62 |
| | **Std Dev** | 8.20 | 6.65 | 3.91 | 2.91 | 2.60 | 4.69 |
| **4psi** | **Ave** | 93.91 | 94.93 | *90.47 | 95.83 | 94.58 | 88.47 |
| | **Std Dev** | 6.52 | 5.32 | 9.78 | 2.12 | 1.84 | 3.93 |
| **6psi** | **Ave** | 94.90 | 96.27 | 93.62 | *94.66 | 92.70 | 86.65 |
| | **Std Dev** | 7.18 | 5.65 | 4.32 | 3.77 | 3.25 | 4.24 |
| **10psi** | **Ave** | 94.86 | *93.61 | *89.39 | *94.02 | 93.60 | *76.84 |
| | **Std Dev** | 7.12 | 6.63 | 10.26 | 3.30 | 2.10 | 5.40 |
| **20psi** | **Ave** | 95.35 | *93.05 | *87.68 | *92.30 | 93.49 | *72.10 |
| | **Std Dev** | 5.76 | 6.97 | 7.22 | 5.71 | 1.99 | 9.92 |

TABLE 5.4, Average Viability of Cells Extruded Through 33 Gauge Pen Tip

Constructs were assessed for viability soon after extrusion (day 0) and after 3 days in culture. Average viability and standard deviation values are reported. * indicates a significant decrease in the viability as compared to the corresponding 2.5psi extrusion ($p > 0.001$).

| | | $1\times10^5$ cells/ml | | $1\times10^6$ cells/ml | | $1\times10^7$ cells/ml | |
|---|---|---|---|---|---|---|---|
| | | **Day 0** | **Day 3** | **Day 0** | **Day 3** | **Day 0** | **Day 3** |
| **Pipet** | **Ave** | 97.07 | 96.30 | 94.57 | 96.14 | 93.39 | 70.77 |
| | **Std Dev** | 5.09 | 4.57 | 5.30 | 4.80 | 2.01 | 11.58 |
| **2psi** | **Ave** | 95.60 | 94.20 | 94.43 | 95.81 | 93.86 | 78.62 |
| | **Std Dev** | 6.39 | 6.75 | 3.81 | 2.28 | 2.27 | 4.39 |
| **4psi** | **Ave** | 97.67 | 96.40 | 93.73 | *91.80 | 94.15 | 79.31 |
| | **Std Dev** | 4.25 | 4.43 | 3.52 | 4.11 | 2.87 | 4.61 |
| **6psi** | **Ave** | 96.76 | 95.59 | 94.68 | *93.49 | 94.08 | 79.61 |
| | **Std Dev** | 4.30 | 5.35 | 3.67 | 2.65 | 1.99 | 6.96 |
| **10psi** | **Ave** | 97.32 | 96.46 | 95.19 | *94.30 | 94.02 | *72.48 |
| | **Std Dev** | 4.07 | 4.24 | 3.10 | 3.69 | 2.77 | 5.76 |
| **20psi** | **Ave** | 95.90 | *90.71 | 96.63 | *88.62 | *92.26 | *62.82 |
| | **Std Dev** | 5.61 | 8.35 | 2.49 | 5.81 | 2.95 | 4.37 |

TABLE 5.5, Average Viability of Cells Extruded Through a 25 Gauge Pen Tip

Constructs were assessed for viability soon after extrusion (day 0) and after 3 days in culture. Average viability and standard deviation values are reported. * indicates a significant decrease in the viability as compared to the corresponding 2psi extrusion ($p > 0.001$).

Effects of Pressure, Pen Tip, and Concentration on Cell Viability

To determine whether or not the actual process of printing has an effect on the viability of the extruded cells, applied pressure, cell concentration, and inner diameter of the pen tip were varied. The average viability for the generated constructs can be found in Tables 5.4 and 5.5. As can be seen in these tables, for days 0 and 3, there was no significant decrease in the viability of cells extruded through the BAT at the lowest pressure setting (2psi for the 25 gauge tip and 2.5psi for the 33 gauge tip) as compared with the same concentration of cells that were pipetted. This indicates that the actual process of printing cells through the BAT at the lowest pressure settings does not have an adverse effect on the viability of the cells. When cells were extruded or pipetted at a concentration of $10^7$cells/ml, the viability of those cells significantly ($p > 0.001$) decreased after 3 days in culture (as compared with corresponding day 0 constructs). Most of the significant decreases in viability were seen after 3 days in culture, indicating that in general, the extrusion process itself does not cause the cells membranes to rupture.

For constructs generated with a 25 gauge pen tip and cultured for 3 days, there was a significant difference in the viability of cells extruded at a pressure setting of 20psi when compared with those extruded at a pressure setting of 2psi. Furthermore, for the 2 higher cellular concentrations, there was a significant difference in cells extruded at a pressure setting of 10psi. There were more significant differences seen in the viability of cells extruded through a 33 gauge pen tip and cultured for 3 days. For all concentrations, there was a significant decrease in the viability of cells extruded at pressure settings of 10 and 20psi when compared with those extruded at a pressure setting of 2.5psi. It was also

noted that when cells were extruded at a concentration of $10^7$cells/ml and maintained in culture for 3 days, the cells extruded through a 25 gauge pen tip had significantly lower viabilities than those extruded through a 33 gauge pen tip at the same pressure.

Effects of Stage Heat and Humidity on Viability

To assess the effects of humidity on the viability of printed constructs, a solution of RMC + Collagen was extruded onto the hydrophilic side of Mylar™ using no humidifier (N), an evaporative humidifier (E) to maintain the humidity between 45% to 55%, or an ultrasonic humidifier (U) to maintain the humidity between 65% to 80%. This was done with and without heating the stage on which the material was extruded. Figure 5.2 illustrates the average viability for the constructs immediately after extrusion (day 0) and after 3 days in culture. As can be seen in this figure, on both days 0 and 3, the viability of cells extruded with a heated stage and no added humidity was significantly ($p > 0.001$) lower than the viability of cells extruded onto a room temperature stage with no added humidity. When humidity was added to the BAT cabinet, the extruded cells had a significantly higher viability than cells extruded using the same settings (stage heat or no stage heat) without added humidity. This held true for both humidity levels, with the higher humidity level resulting in a higher viability immediately after extrusion.

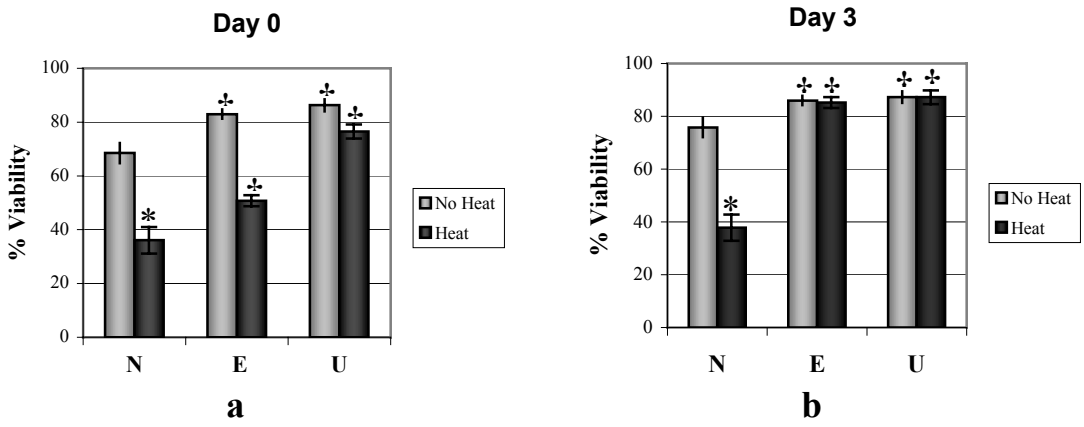


FIGURE 5.2, Average Viability With and Without Added Humidity.

The average viability of constructs generated with and without stage heat as well as with no humidity (N), with humidity maintained at 45 to 55% using an evaporative humidifier (E), and with humidity maintained at 65 to 80% using an ultrasonic humidifier (U) as seen (a) a few hours after extrusion and (b) after 3 days in culture. Error bars represent +/- standard deviation. * indicates a significant decrease in viability as compared to the corresponding "No Heat" value. † indicates a significant change in viability as compared with the corresponding "No Humidity" value. ($p > 0.001$)

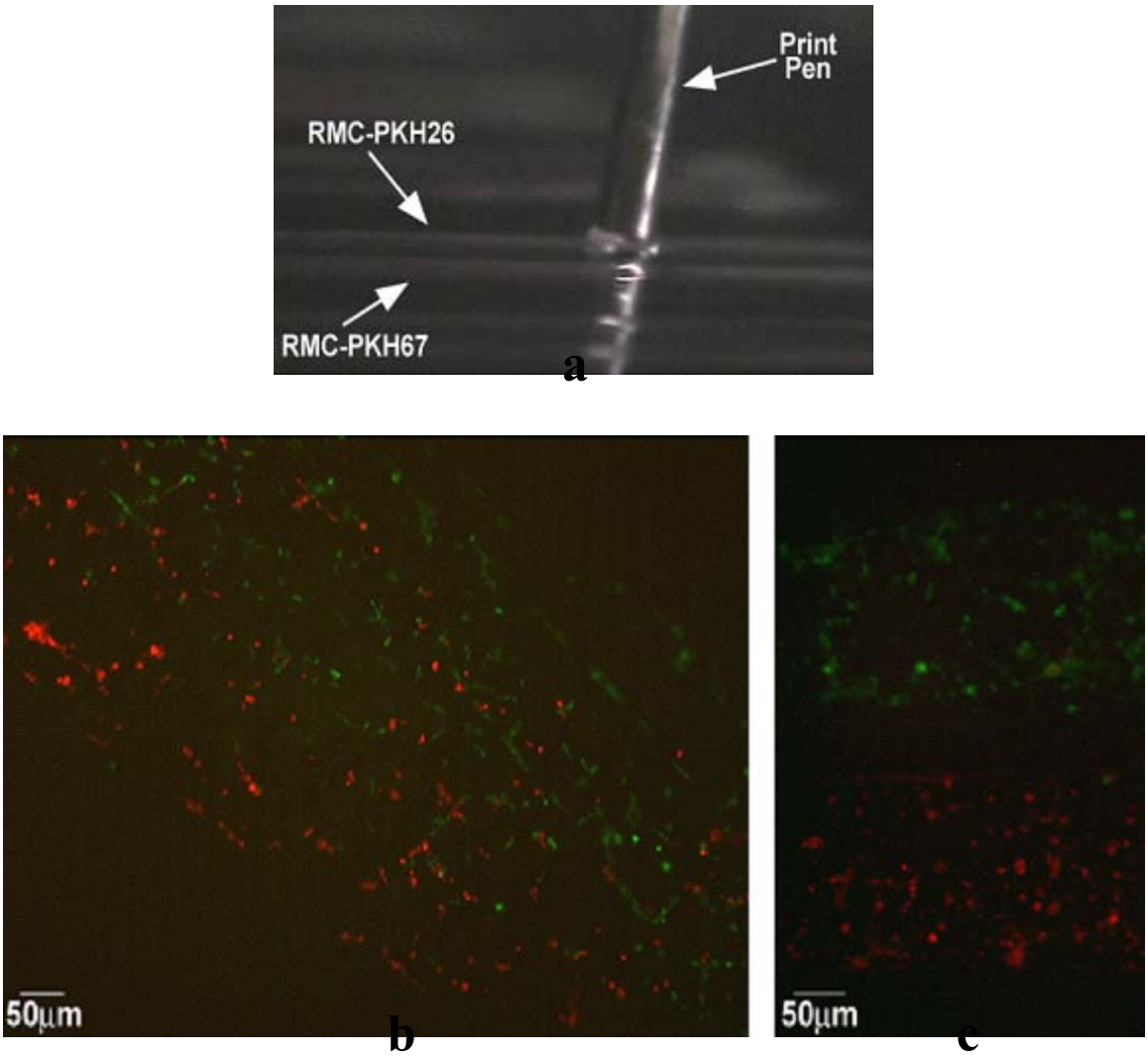


FIGURE 5.3, Adjacent Lines of Separate Cellular Solutions

(a) A print pen is actively extruding PKH-26 labeled cells adjacent to a line of PKH-67 labeled cells. When lines were printed too close to each other there was a considerable amount of (b) overlap; however, if the separation was sufficient, the lines (c) did not overlap.

## Spatially Organizing Separate Cellular Solutions

To determine how close adjacent lines of collagen could be printed without overlap, solutions of collagen were printed with membrane labeled RMCs. Representative images of the printed lines can be seen in Figure 5.3. A cell-mixing index was calculated to determine how much overlap existed between adjacent lines of separate solutions of RMC + Collagen. As expected, most lines printed with a separation of 400μm or less had a cell mixing index greater than 0, indicating that there was some overlap of the two lines. In order to have a complete separation of the two lines, they had to be printed with a separation of at least 550μm.

## Generating 3D Collagen Constructs

Three-dimensional Sphere + Collagen constructs were generated in a layer-by-layer fashion resulting in a 7.5mm × 7.5mm square with an average height of 128μm. A solution of RMC + Collagen was extruded in this fashion and assessed for viability at the edges and center of the generated square. As can be seen in Figure 5.4, there is no significant difference between the viability of cells in the middle of printed constructs as compared with cells in the pipetted constructs. However, there was a slight significant decrease ($p > 0.001$) of 10% in viability at the edges of the printed constructs, which is likely due to the collagen at the edge being thinner and more prone to drying out causing the cells to die.

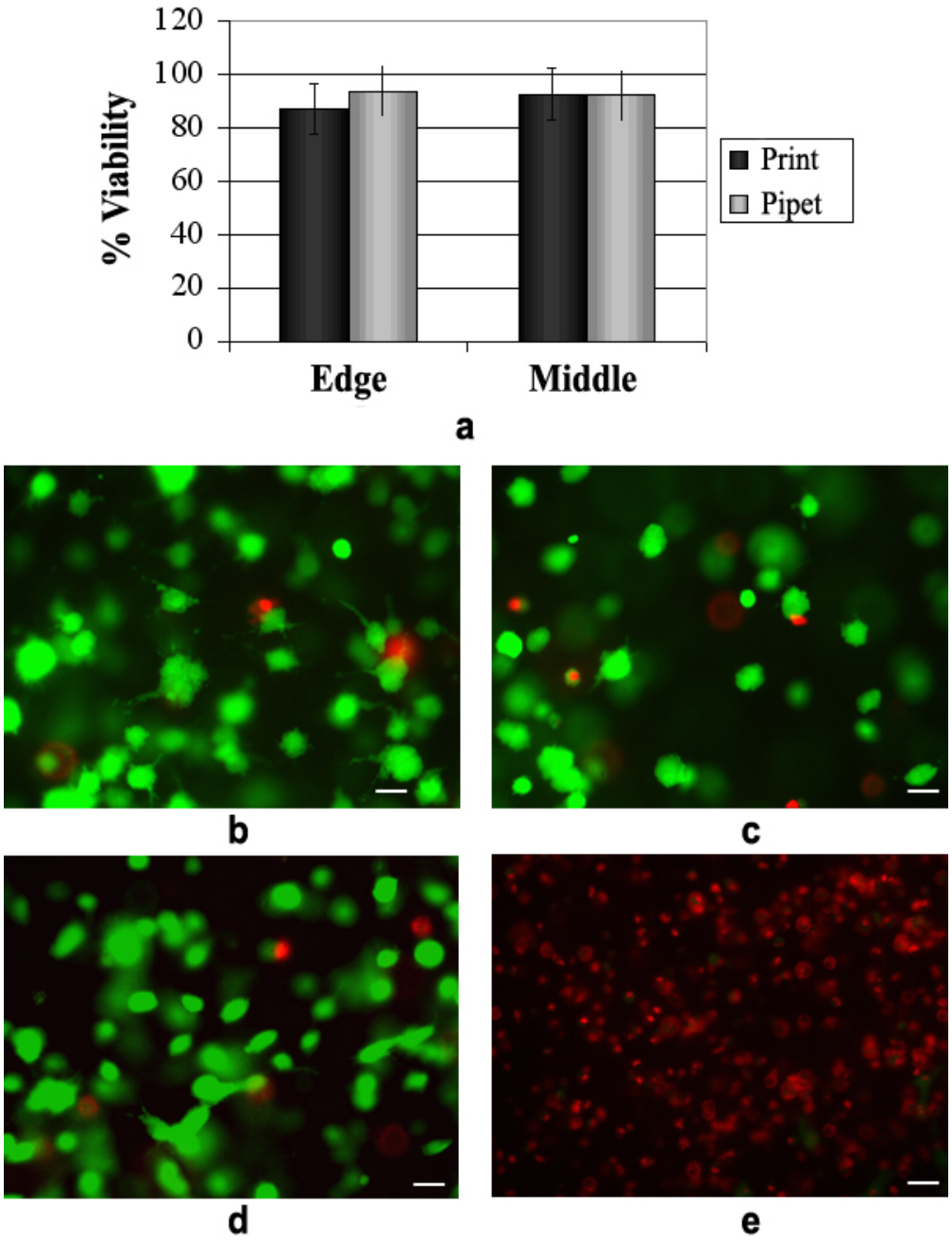


FIGURE 5.4, Viability of Printed and Pipetted 3D Collagen Constructs

(a) Chart showing the viability of cells found at the edge and middle of both pipetted and printed 3D constructs. Values reported are the average values with bars representing +/- standard deviation. Representative images of 3D constructs stained for viability as seen on day 3 (b) in the middle of a pipetted gel, (c) in the middle of a printed construct, (d) on the edge of a printed construct, and (e) in a control gel that had been fixed in paraformaldehyde. Bars = 30μm.

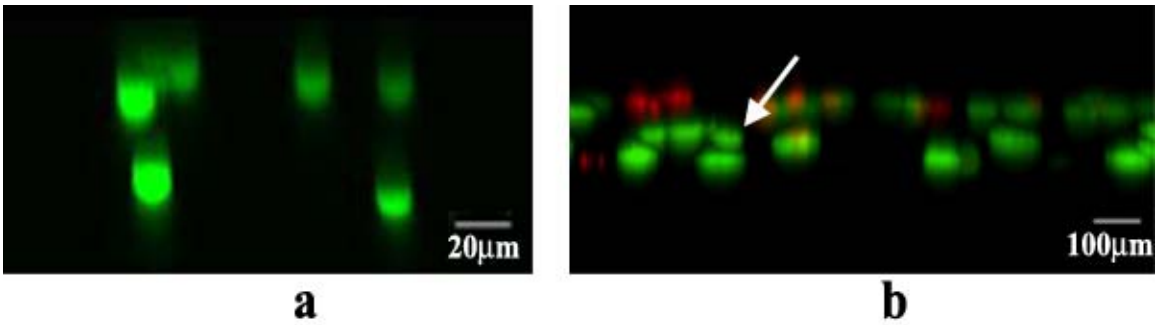


FIGURE 5.5, Segmented 3D Constructs

Projection images illustrating a 90-degree view of the sides of (a) microspheres and (b) RMCs in spatially organized, 3D constructs. The RMCs were stained with a fluorescent live/dead assay to show the viability of cells at day 3. Some separation is still apparent; however, cells have begun to migrate through the acellular collagen that separates the 2 cellular layers (denoted by an arrow).

### Spatially Organizing 3D Collagen Constructs

Using a script similar to the one used to build solid 3D collagen constructs, the BAT was able to generate 3D constructs containing 5 distinct layers consisting of 3 layers of collagen alone separated by 2 layers of Spheres + Collagen. Taking into account the diameter of the printed spheres (15μm), the sphere layers were determined to be approximately 30μm thick. The collagen alone layer between the two sphere layers was determined to be approximately 25μm thick. To assess the viability of these multi-layered constructs, RMC were printed in place of microspheres. The printed cells were found to have a similar viability as compared with pipetted cells (96%). And, as the cellular constructs were maintained in culture, the cells migrated through the acellular collagen layers such that by day 3, the layers were no longer distinguishable.

## DISCUSSION

Due to the importance of spatial organization in natural tissue (Pardanaud, et al., 1989; Patel, et al., 1998; Risau, et al., 1988), the field of TE has recently turned its focus toward using RP technology to generate spatially-organized 3D constructs by laying down both cells and matrix (Boland, et al., 2003; Marquez, et al., 2002; Ringeisen, et al., 2002a; Ringeisen, et al., 2002b; Wilson, Jr. & Boland, 2003). It is believed that this approach will accelerate and improve the assembly of TE constructs (Mironov, et al., 2003). It has previously been shown that a direct-write, 3D BioAssembly Tool can be used to generate viable spatially organized constructs (Smith, et al., 2004). This chapter

characterizes the effects of using such a system to coextrude cells and matrix with the primary focus on the viability of the printed cells.

When a pneumatic print pen with a 25 gauge or 33 gauge pen tip was used to extrude lines of type I collagen, the lines became increasingly less uniform as the extrusion pressure increased. As the collagen was being printed onto a hydrophilic surface, this increased flow caused the collagen to balloon out onto the scaffold surface. The linear speed used during the extrusion process had more of an impact on the smaller pen tip, as was evidenced by the fact that there was a significant decrease in line width when a 20mm/s speed was used rather than a 10mm/s speed. This difference was not seen when using a 25 gauge pen tip. Vozzi, et al. (Vozzi, et al., 2002), defined the relationship between the width ($a$) of extruded lines to the radius of the pen tip ($R_s$), viscosity of the solution ($\mu$), linear speed of the print pen ($v_o$), height of the extruded line ($h$), and applied pressure gradient ($dp/dz$) as follows:

$$a = \frac{\pi R_s^4}{8\mu v_o h}\frac{dp}{dz}$$

This equation agrees with the results that were reported in this study in that the line width decreased as the linear speed of the pen increased and the line width increased as the applied pressure increased.

Vozzi, et al., further expanded the equation to take into account the length of the tapered zone of the extruding pen ($h_z$) as well as the applied extrusion pressure ($P+P_{crit}$), where $P_{crit}$ is the critical pressure needed before the solution exits the pen tip:

$$a = \frac{\pi R_s^4}{8\mu v_o h}\frac{P + P_{crit}}{h_z}$$

The length of the tapered zone of the 25 gauge pen is significantly longer than that of the 33 gauge pen. Additionally, when the actual extrusion pressure was measured through the 33 gauge and 25 gauge pens, it was noted that the 25 gauge pens often exhibited a pressure overshoot before reaching the steady state pressure. These two traits likely lead to the fact that the change in linear speed did not significantly affect the widths of the 25 gauge prints.

When using the BAT to generate viable spatially organized patterns, cells were suspended in type I collagen at concentrations ranging from $10^5$ to $10^7$ cells/ml and extruded through pneumatic print pens with an inner diameter as small as 90μm. The viability was assessed using a fluorescent live/dead assay that labeled cells with intracellular esterase activity as "live" and cells with a compromised cell membrane as "dead". The results in this chapter indicate that even after 3 days in culture, there is no significant decrease in the viability of cells when they are extruded at the minimum pressure necessary to obtain a continuous line. This indicates that under typical conditions, using the BAT to print cells suspended in a solution as viscous as 3.0mg/ml type I collagen does not cause the cell membranes to rupture and it does not significantly alter the viability of the cells. The lower concentrations of cells ($10^5$ and $10^6$cells/ml) had a significantly higher viability than the highest concentration of cells ($10^7$cells/ml), which became more prominent after 3 days in culture. This suggests that while the cell membranes are still in tact soon after extrusion, if cells are printed at too high of a concentration, their viability will be significantly decreased.

When printing type I collagen, it was noticed that maintaining the stage temperature between 29°C to 31°C aided in the polymerization of the collagen, which aided in the maintenance of the printed pattern when media was added. However, when stage heat was added to the BAT environment, the viability of the printed cells was significantly decreased. When humidity level within the cabinet was maintained between 65% to 80%, the viability of the printed cells was significantly increased. And, after 3 days in culture, the cells printed with stage heat and added humidity had a similar viability to cells printed with no stage heat or added humidity. These results agree with other research which has suggested that humidity is a critical issue in generating viable constructs by simultaneously laying down cells and matrix (Wilson, Jr. & Boland, 2003).

It has been shown that the BAT is capable of extruding two separate solutions of collagen and cells in distinct lines. The ability to control the distance between two printed constructs has meaningful applications, such as performing cell migration studies in three dimensions using printed constructs containing cells and applicable molecules. These results demonstrated the ability of the BAT to generate separated lines of two different solutions of RMC + Collagen. In order to have a complete separation of the printed lines, they needed to be printed with a separation of at least 550μm; however, while these lines did not overlap, they also did not touch. Thus, if it is critical to have the lines touching, but not overlapping, a supporting matrix other than collagen may be necessary.

It has been demonstrated that the BAT is able to generate 3D constructs that are both viable and spatially organized. Solid squares containing fluorescent microspheres were fabricated with a height of 128μm. Solid squares of RMC + Collagen were also

fabricated and were shown to have the same viability in the center as RMC + Collagen constructs that were created by pipetting the solution into a well plate. There was a slight (10%) decrease in viability at the edges of the printed constructs, which is likely due to there being a smaller volume of material at the edges of the constructs. This leads to a more rapid drying out of the collagen and could lead to cell death.

When the Sphere + Collagen solution was printed in a multi-layered fashion, two distinct 30μm thick layers of spheres were detected with a dividing layer of 25μm thick collagen alone. When RMC + Collagen was laid down in this fashion, the cells demonstrated the same viability as those extruded into solid squares of RMC + Collagen. However, as these constructs were maintained in culture, the cells migrated through the acellular collagen such that it was difficult to find a separation between the adjacent layers.

This chapter characterizes the use of a direct-write 3D BioAssembly Tool to generate viable, spatially organized constructs comprised of type I collagen and microvascular cells. These results demonstrate that the process of printing cells at a concentration at or below $10^6$ cells/ml using the minimum pressure necessary to obtain a continuous line does not significantly alter the viability of the cells. Also, the addition of media aids in maintaining the viability of the extruded cells, especially if the stage is maintained above room temperature. These results also demonstrated that the BAT is capable of generating spatially organized 3D constructs comprised of type I collagen and microvascular cells, and that it is able to spatially organize the cells within the 3D

construct. Thus, the BAT is capable of generating viable, 3D constructs that can potentially be used in tissue engineering applications.

# 6. CONCLUSIONS AND DISCUSSION

Tissue Engineering is a multidisciplinary field that combines the practices of the medical and engineering fields to attempt to remedy two of the most costly issues in modern medicine, namely tissue loss and end-stage organ failure caused by disease or injury. The driving goal of this field is to develop a biological alternative that is capable of restoring, maintaining, or improving tissue function (Langer & Vacanti, 1993). Tissue engineers have focused on developing replacement tissue that closely imitates natural tissue (Lanza, et al., 2000).

The spatial organization of tissue provides cell-cell and cell-ECM cues that are critical to many biological functions, including tissue development, organ formation, wound healing, and homeostasis (Edelman & Crossin, 1991; McDevitt, et al., 2002; Takeichi, 1995; Zahir & Weaver, 2004). Because this spatial organization is vital to tissue structure and function, researchers have examined using rapid prototyping methodsto fabricate complex 3D TE constructs. Initially, this technology was used to build acellular scaffolds that were later randomly seeded with cells (Park, et al., 1998; Sherwood, et al., 2002; Sodian, et al., 2000b). However, it is believed that spatially organizing both the cells and supporting scaffold material will accelerate and improve the assembly of TE constructs (Mironov, et al., 2003). This has lead to a recent emergence of RP techniques to carefully control the patterning of both cells and matrix in 2D and 3D constructs (Boland, et al., 2003; Marquez, et al., 2002; Ringeisen, et al., 2002a; Ringeisen, et al., 2002b; Wilson, Jr. & Boland, 2003).

With the recent improvements of axially resolved optical systems, it has become fairly routine to use systems such as confocal laser scanning microscopy to obtain stacks of images of 3D tissue where each image in the stack is at the same relative location in the ($x$, $y$)-plane but focused at different depths within the sample (Shotton & White, 1989). Image processing techniques have been incorporated with confocal microscopy to obtain qualitative and quantitative information about complex, branching structures; however, most methods require user intervention to segment, or threshold, the images (Bucher, et al., 2000; Lenander & Holmgren, 1999; Young, et al., 1998). To automatically examine branching structures, 3D tracing routines have been developed (Can, et al., 1999; Cohen, et al., 1994; He, et al., 2003); however, these methods provide more structural than volumetric information.

The studies presented in this dissertation propose three specific aims that examine the use of a direct-write 3D BioAssembly Tool to fabricate viable constructs as well as the development of an automated method to accurately quantify volume information about 3D microscopic structures. The primary focus is on the use of the BAT to fabricate viable TE constructs with a specific architecture. A secondary focus is on developing an automated thresholding algorithm that can be used on confocal images to obtain accurate volumetric measurements of 3D structures within tissue. The following is a brief summary of the results found in this dissertation followed by possible future research directions.

## EXPERIMENTAL SUMMARY

The hypothesis from the first specific aim stated that 3D, direct-write technology is capable of generating viable constructs by laying down both cells and matrix. Data presented in Chapters 2 and 5 support this hypothesis. First, the BAT was described; this system was designed based on both digital printing and tissue engineering principles to be able to build 3D heterogeneous tissues. The BAT is a three-axis printing machine capable of moving a delivery pen along the *x*-, *y*-, and *z*-axes separately or simultaneously. The printing mechanism of this system consists of four print heads, or micro-dispense pens. One pen is a combined positive displacement and air pressure driven pen, and the three other pens are pneumatic syringe pens with printing tips chosen based on the viscosity and size of particulates in the material being extruded.

Because the BAT is a three-axis system, it is capable of generating 3D nonlinear patterns. The scripts used to direct the generation of these patterns can be created manually or by a CAD program. The patterning capabilities of the BAT were demonstrated using two different polymers: collagen and pluronic F-127. When using PF-127, the BAT was able to rapidly generate complex 3D constructs with 45° overhangs that did not need supporting scaffolding. Using the collagen, the BAT was able to generate complex linear to nonlinear patterns.

Next, the ability of the BAT to generate viable constructs was examined. Using the positive displacement pen, human fibroblasts suspended in PF-127 were deposited into the shape of a 3D cylinder using a pen tip with a 450μm ID. After extrusion, approximately 60% of the cells were viable. Using a pneumatic pen, bovine aortic

endothelial cells suspended in type I collagen were extruded into a multi-layered zigzag pattern using either a 33 gauge or 25 gauge pen tip. Cells extruded using a 33 gauge pen tip were 46% viable, while cells extruded through a 25 gauge pen tip were 86% viable. When these constructs were maintained in culture, they exhibited proliferation and pattern persistence.

The BAT was also shown to be capable of fabricating viable constructs patterned after architectures seen in natural tissue. A script was generated to print the pattern of the left anterior descending artery as seen in a pig heart. Using this script, BAEC suspended in collagen were successfully patterned in the shape of the LAD artery. The cells exhibited the same viability as those seen in the simpler zigzag pattern.

Because there exists a need for an accurate and automated method for segmenting 3D microscopic branching structures, a second hypothesis was developed and tested. This hypothesis proposed that an automated algorithm could be generated to accurately threshold stacks of confocal images. Chapter 3 combined confocal microscopy with image processing and optimization techniques to propose an automated algorithm to accurately obtain volumetric information about 3D tissue.

Thresholding algorithms found in the literature were implemented. These algorithms calculated thresholds based on a bimodal intensity histogram (Kittler & Illingworth, 1986), a unimodal intensity histogram (Umesh Adiga & Chaudhuri, 1999; Umesh Adiga & Chaudhuri, 2001), and edge and intensity information for each ($x$, $y$)-location within the image stack (Xavier, et al., 2001). These algorithms were tested for

their effectiveness at calculating the true volume of microspheres embedded in collagen gels, and it was found that each one greatly overestimated (>600%) the volume.

Due to the attenuation of the spheres with depth in the stack, it was also apparent that a global intensity threshold would not yield accurately thresholded images. Upon examining the stacks of microsphere images, it was observed that it might be appropriate to use the gradient information, or the rate at which a voxel is brightening or dimming in the stack, to threshold each voxel in the image stack. A dual thresholding rule was developed based on the depth, intensity, and *z*-axis gradient of each voxel with an OR-Rule implementation such that a voxel was assigned to the foreground if and only if the voxel has either an intensity value above the intensity threshold function or a gradient value above the gradient threshold function.

An initial prediction was made for the shape of the intensity and gradient thresholding functions. To account for the exponential signal attenuation seen in fluorescent microscopy (Can, et al., 2003), the general form of the *z*-axis gradient and intensity threshold functions were exponentially decaying functions of the following form:

$$f_t(z) = m_t e^{\frac{125-z}{125}} + b_t$$
$$f_g(z) = m_g e^{\frac{125-z}{125}} + b_g,$$

where $N$ is the total number of images in the stack, $z \in \{1, \ldots, N\}$ is the depth of the image, and $m_t$, $b_t$, $m_g$, and $b_g$ are scalar parameters that must be determined. Optimization techniques were employed to improve the parameters used for functions $f_t(z)$ and $f_g(z)$, and the adjusted final equations were:

$$f_t(z) = 62 \times e^{\frac{125-z}{125}} - 74$$

$$f_g(z) = 23.5 \times e^{\frac{125-z}{125}} - 29.$$

These values were effective for all training problem instances tested, indicating that these parameters are robust and extendable to more general settings.

Next, the thresholding algorithm was used on a new set of test data containing microspheres. For both the training and test data, the *x*-axis and *y*-axis widths were slightly lower than 100% of the actual width of the sphere (15μm); and on average, the *z*-axis height was below 110% of the true sphere height. The overestimation of sphere height led to a slight overestimation (<10%) of the total volume of the spheres in both the test and training data. As the sphere diameters had an accuracy of +/-3%, this overestimation may be a result of spheres that are slightly larger than expected. Also, as the *z*-axis resolution is greater than the *z*-step, these slight overestimations in the height of the spheres are expected.

When the thresholding algorithm was used on stacks of images of fluorescently labeled microvascular constructs, it was noted that averaging the voxels in the stacks of images prior to thresholding greatly reduced the amount of single voxel noise seen within the thresholded images. The algorithm found all of the vessels within the image stacks. Based on these results it was concluded that by using both the intensity and *z*-axis gradient, one can automatically and accurately determine volume information in stacks of images generated by a confocal microscope.

Initially, there was a significant amount of variability seen in the viability of the printed cells. Some days, most of the cells would be dead; and other days, most of the

cells would be alive. To make the process more consistent and reproducible, various parameters to control the environment within the BAT cabinet were examined. Chapter 4 examines the true pressure applied to the pneumatic print pens, methods to cool the pens, systems to provide humidity to the BAT cabinet, and methods to heat the stage on which the constructs are fabricated.

Based on measurements of the pressure applied to the pneumatic pens, it was concluded that the actual pressure applied to the pens is approximately 2psi less than the BAT pressure setting used. Thus, for a BAT pressure setting of 10psi, the true applied pressure is approximately 8psi. Also, while the pressure regulator on the compressed air tank is set to a maximum of 20psi, the applied pressure cannot be greater than 20psi. As this regulator also limits the applied pressure used by the BAT, it is recommended that the true applied pressure be examined whenever the air tank is moved or replaced.

Three methods to cool the pneumatic print pens were examined. A fan attached to a thermoelectric cooler did not sufficiently cool the contents of the print pens. Using a cold-water circulator, the pen temperature could be maintained at 11°C for up to 3 hours, which could easily be extended to a longer time by adding more ice to the system. To maintain the temperature of the pneumatic pens at a specific temperature and for a longer period of time, a cold-water circulator was combined with a thermoelectric cooler. Using this method, the temperature of the pens was maintained at 11°C for at least 7 hours, without needing to add extra ice. When printing type I collagen, it was determined that the pen temperature should be maintained around 7°C; and using the combined cold-

water and thermoelectric cooling device, two pneumatic pens could be maintained at 7°C for at least 7 hours.

It has been hypothesized that humidity is a key element needed in RP techniques that generate viable constructs by laying down both cells and matrix (Boland, et al., 2003; Mironov, et al., 2003). Thus, two methods to provide humidity to the BAT environment were examined. The ultrasonic humidifier was capable of increasing the humidity with the cabinet more rapidly and to a higher percent humidity than was the evaporative humidifier. Also, opening the cabinet doors has a smaller impact on the humidity provided by an ultrasonic humidifier. As some polymers polymerize more rapidly when heated, two methods to heat the stage were examined. It was determined that using a constant temperature water circulator provided the most flexibility and heating potential.

After characterizing methods to control the BAT environment, the next step was to determine the effects of those environmental parameters on the viability of cells printed by the BAT. Thus, a third aim and hypothesis was developed and tested. This aim characterized the fabrication of spatially organized constructs generated by the BAT. The driving hypothesis of this aim was that using the minimum pressure setting to extrude cells does not have an immediate effect on the viability of the extruded cells; however, the environmental parameters of the BAT cabinet have a direct impact on the viability of these cells. Chapter 5 examines the effects of the environmental parameters on the viability of extruded cells.

The results in this chapter demonstrated that extruding cells through the pneumatic pens at the lowest pressure required to obtain a continuous line does not

significantly alter the viability of the cells. It was also shown that adding humidity to the printing environment significantly increased the viability of printed cells, especially when stage heat was used. Also, maintaining the humidity at a high percentage (>65%) yielded the highest cell viability. The systems used to add humidity to the cabinet are inexpensive models designed for cigar cabinets or rooms in a house. And, since the ultrasonic humidifier was able to add the higher humidity level to the cabinet and it was the system that frequently stopped generating a mist of water, it is recommended that a professional grade humidifier be purchased for the BAT cabinet.

It was also demonstrated that the BAT is capable of extruding separate solutions into spatially organized constructs. When printing type I collagen lines with a 25 gauge pneumatic pen, it was determined that the separation between adjacent lines should be at least 550μm in order to keep the lines from overlapping. At this separation, the lines did not touch at all. Thus, if it is important for the 2 adjacent lines to touch but not overlap, it may be necessary to use a different supporting matrix or to lay down a thin, cell permeable wall of material between the two lines.

The BAT is capable of generating 3D collagen constructs that are both viable and spatially organized. Solid squares of collagen with a height of 128μm were fabricated, and the viability of the cells in the middle of the construct was similar to that of cells pipetted into a well plate (96%); however, cells on the edges of the printed construct had a slightly lower viability (86%). This decrease is likely due to collagen drying out near the edges of the printed constructs. It was also demonstrated that the BAT is able to generate 3D constructs with distinct layers such that the layers of cells have the same

viability as cells found in pipetted constructs. Though, after a few days in culture, the cells had migrated through the acellular collagen such that it was difficult to distinguish a separation between the layers. This corresponds with results found by other labs, where it was noted that when endothelial cells are seeded in type I collagen, the cells migrate through the collagen (Montesano, et al., 1983).

## DISCUSSION

In recent years, RP has become a popular application to use in generating 3D spatially organized constructs for TE. Such applications include building models of biological structures (Lermusiaux, et al., 2001; Pentecost, et al., 2001; Vanezi, et al., 2000; Yourtee, et al., 2000), bone substrate scaffolds (Cooke, et al., 2003), heart valve scaffolds (Hoerstrup, et al., 2000; Sodian, et al., 1999; Sodian, et al., 2000a; Sodian, et al., 2002b), porous scaffolds (Zein, et al., 2002), cranial implants (Gronet, et al., 2003), drug delivery devices (Leong, et al., 2001), models of pathologies (Berry, et al., 2002), cartilage repair scaffolds (Sherwood, et al., 2002), metallic orthopedic scaffolds (Curodeau, et al., 2000; Melican, et al., 2001), and oral dosage forms (Katstra, et al., 2000; Rowe, et al., 2000). Based on the idea that laying down both cells and matrix will accelerate and approve tissue assembly in such constructs (Mironov, et al., 2003), there has been a recent emergence in RP techniques to lay down the cells at the same time as the scaffolding.

Cell Deposition Systems

As all of these cell deposition systems are slightly different, one interesting avenue of future research is to examine the effects of each system on the viability of patterned cells. To examine the effects of each system, one must first understand how each method patterns the cells. One method to pattern both cells and matrx, DWB™ (Marquez, et al., 2002), generates 2D patterns of cells using an aerosol-based system. By suspending the cells in medium, the cells are encapsulated while they are being laid down. This method was used to generate viable cellular patterns, and it is hypothesized that it can easily be modified to fabricate 3D patterns by simply adding movement along the *z*-axis. As was shown in Chapter 5, the humidity of the environment has a definite impact on the viability of cells. Thus, using the DWB™ system to lay down cells encapsulated in only media is likely to produce patterns with a smaller viability than constructs comprised of cells encapsulated by a material that evaporates less rapidly. However, it is probable that the cells could be suspended in an encapsulating polymer, such as collagen. Similarly, it was demonstrated that pressure has an impact on cell viability, especially when a small ID extrusion pen or high pressure is used to deposit the cells. This raises the question of whether using an aerosolized system will have a more significant impact on the viability of the deposited cells than a system that uses pressure to push cells through a deposition pen.

Another system to deposit both cells and matrix, MAPLE-DW (Chrisey, et al., 2003; Ringeisen, et al., 2002a; Ringeisen, et al., 2002b; Ringeisen, et al., 2004), is a pulsed-laser direct-write system that uses vaporization to pattern material on a scaffold. A

laser is focused onto material containing the cells such that the temperature increases causing a small piece of material to be propelled onto the target scaffold. This system is similar to the BAT in that it was originally used to fabricate electronic elements by laying down conductive, resistive, and dielectric inks (Chrisey, et al., 2003). Because the pulse causes the temperature of the cellular material to increase, special care must be taken to ensure that the temperature of the cells does not get so hot that the cells die before they are even deposited. As with the last aerosol-based system, a question of whether using such force has more of an impact on the viability of the deposited cells than does a system that uses pressure to push cells through a deposition pen. Again, with small droplets being deposited onto a scaffold, it appears that humidity should be tightly controlled in such a system. Also, using such a system greatly limits the materials that can be deposited along with the cells. Materials that polymerize with increased temperature, e.g., type I collagen, would not be a viable scaffold material for such a method. It also appears materials that are polymerized with light would solidify before they were even deposited onto the target scaffold. This system has been shown to be capable of generating 2D patterns of viable cells; however, as with the DWB™ system, it has not yet been used to generate 3D constructs.

A system similar to the BAT uses ink-jet technologies to create 2D and 3D constructs (Saunders, et al., 2004; Wilson, Jr. & Boland, 2003). This system is similar in that it has multiple print pens that use air pressure to extrude material. One difference is that the modified ink-jet system allows for the use of multiple pens simultaneously. Thus, while two lines of material could be extruded at the same time, the proximity of the lines

to each other is limited by the position of the pens with respect to each other. Another difference is that the BAT has a positive displacement pen in addition to the pneumatic pens. One limiting factor with the ink-jet system is that the smallest *x* or *y* step that can be used is 50μm, while the BAT allows for much smaller steps. This greatly limits the complexity of the patterns that can be generated, and will become more limiting in the future, especially as technology develops such that smaller constructs can be fabricated while maintaining cellular viability. As a need arises, the current stepper motor could be replaced with a new one that uses a smaller step size. This system has been used to generate patterned 2D and 3D constructs. When BAEC were printed onto Matrigel™ and collagen gels using a 30 gauge needle, the cells exhibited a 75% viability. This corresponds with results in Chapter 2 that reported a viability of 86% for BAEC extruded through a 25 gauge pen and of 46% for BAEC extruded through a 33 gauge pen. This system was also used to deposit 600μm aggregates of BAEC into 3D constructs, which behaved similarly to the BAEC constructs described in Chapter 2.

The BioAssembly Tool

The BAT has two different deposition pens. Both have been shown to be capable of generating spatially organized patterns of viable cells. In Chapter 2 it was demonstrated that fibroblasts suspended in PF-127 that were extruded through the positive displacement pen have a viability of 60% soon after extrusion. It was also demonstrated that the viability of BAEC suspended in collagen was 86% when extruded through a 25 gauge pen tip and 46% when extruded through a 33 gauge pen tip. Finally,

in Chapter 5 it was demonstrated that there is no difference in the viability of RMC extruded into a blob-like structure using a 25 gauge or 33 gauge pen, when the cellular concentration is below $1\times10^6$ and the applied pressure is below 2psi. Based on these observations, and the fact that humidity plays such an important role in maintaining the viability of printed cells, it is believed that the lower viability that was initially seen in the BAEC extruded through a 33 gauge pen was due to the lines being thinner and drying out more rapidly.

The fibroblasts suspended in PF-127 were extruded with a larger pen tip (450μm), but had a smaller viability than the BAEC suspended in collagen and extruded through a 25 gauge pen tip. This raises the question as to whether this decrease in viability is inherent in the cell type, caused by the supporting medium, caused by the extrusion method, or caused by the environmental parameters that were maintained during extrusion. As fibroblasts are often the first cell type used when looking at cell deposition systems (Marquez, et al., 2002; Saunders, et al., 2004), it is unlikely that the cells themselves are less robust and viable than BAEC. PF-127 is used in a number of biomedical applications, including drug delivery systems for opthalmic (Desai & Blanchard, 1998; Desai & Blanchard, 2000; Edsman, et al., 1998), rectal (Miyazaki, et al., 1986), parenteral (Johnston, et al., 1992; Morikawa, et al., 1987; Pec, et al., 1992), and percutaneous (Miyazaki, et al., 1995) use. Thus, it should not have a significant impact on cell viability. This leads to the hypothesis that the actual method of depositing the cells had an impact on the viability of the cells. In order to test this hypothesis, it would be interesting to examine the viability of fibroblasts, BAEC, and RMC after they

are deposited into a blob-like structure by both the positive displacement pen and a pneumatic pen. To ensure that the supporting medium is not the cause of in the reduced viability, the viability of the cells should be examined when they are suspended in collagen and when they are suspended in PF-127.

As seen in Chapter 2, when PF-127 and the positive displacement pen were used, complex 3D constructs with a 45° overhang could be fabricated without using any supporting structures. It took 10 to 15 minutes to build the 2mm tall mock up of a house, whereas it took more than 30 minutes to build the 7.5mm × 7.5mm × 128μm square of collagen that was discussed in Chapter 5. While type I collagen has the benefit that it is a natural material and does not have a negative effect on the viability of cells, it is difficult to use in building complex 3D structures. Thus, it would be beneficial to examine other biologically compatible materials that could be used with the BAT. Of course, with the use of any new material, it should be examined for its effect on the viability of the cells before and after being extruded through the print pens.

Matrigel™ (Guest, et al., 1997) and alginate (Murayama, et al., 2002) are both natural materials that could be used with the system. Matrigel™ is similar to collagen in that it polymerizes at room temperature, and it probably provides no structural advantages over type I collagen. Some synthetic materials that could be used include PLA, PGA, and PLGA, which are currently used in numerous medical devices (Lavik & Langer, 2004; Mooney, et al., 1994); polyanhydrides, which exhibit surface biodegradation (Dang, et al., 1996); and hydrogels (Anseth, et al., 2002), which have mechanical properties similar to soft tissue.

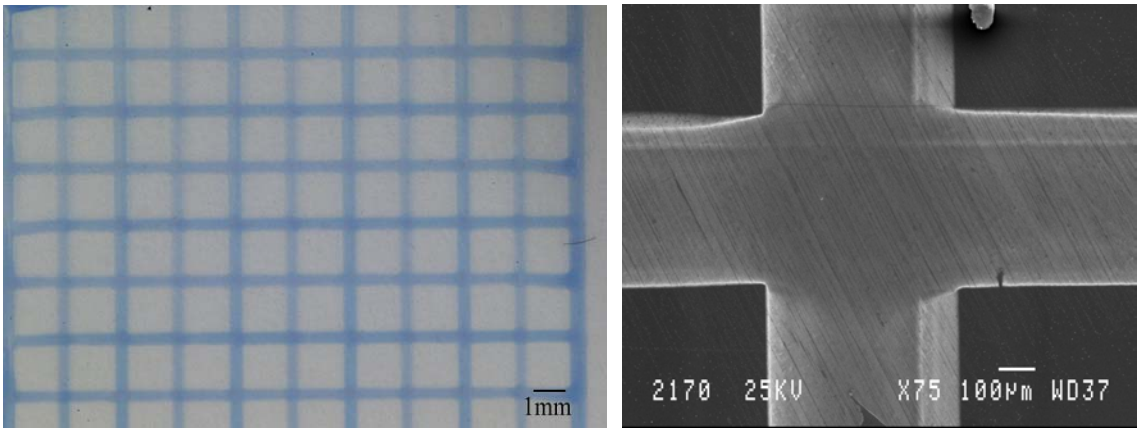


**a** **b**

FIGURE 6.1, Printed Alginate Grid

Representative images of an alginate grid printed using a pneumatic print pen as seen with a (a) digital camera and (b) SEM.

Alginate is used in many biological applications because one can easily control its porosity or link it to other molecules. As can be seen in Figure 6.1, some simple structures with alginate have been printed. These constructs were imaged using both a digital camera and a scanning electron microscope (SEM). A 5% alginate solution was prepared by mixing powdered alginate (Sigma-Aldrich, St. Louis, MO) with sterile milliQ water. To make the alginate easier to see, a blue stain was added to the solution. The alginate was laid down in a 20mm × 20mm grid and polymerized by laying a separate solution of 1% CaCl on top of the printed alginate. This created a stable construct that rapidly polymerized, leading to the belief that the material can be used to create complex 3D structures. As this alginate comes from a powder, the prepared alginate solution will need to be sterilized prior to using it with cells. As many polymers call for autoclaving in order to sterilize prepared solutions, it is believed that the alginate solution could also be autoclaved without severely affecting the structure of the polymer.

Similarly, it would be beneficial to examine the effects of the supporting base on the actual viability, size of generated features, and pattern persistence of the printed constructs. As seen in Chapter 2, when PF-127 was printed onto a glass slide, the width of the generated lines was 100 to 115% of the ID of the depositing pen tip; and when collagen was printed onto the hydrophilic side of Mylar™, the width of the generated lines was 200 to 300% of the ID of the depositing pen tip. When collagen was printed onto the hydrophobic side of Mylar™, the resulting line widths were much closer to the width of the ID of the depositing pen tip. Based on these results, it is clear that the supporting base has an impact on the size of the generated features.

To compare constructs printed on the hydrophilic and hydrophobic sides of Mylar™, solutions of BAEC + Collagen were printed in the pattern of the LAD artery in a pig angiogram (script described in Chapter 2) onto Mylar™. The lines printed on the hydrophobic side of the Mylar™ had a smaller width than those printed on the hydrophilic side. When printing on the hydrophilic side, there were some problems with nonintersecting lines bleeding together; this was not a problem when printing on the hydrophobic side. As can be seen in Figure 6.2, when the constructs were maintained in culture, the cells printed on the hydrophobic side proliferated and migrated outside of the printed pattern. This caused the generated pattern to break down and not be detectible by SEM (Figure 6.2b) or have a fuzzy appearance in phase microscopy (Figure 6.2d). In the areas where there was reduced viability (denoted by arrows), the printed pattern was maintained longer than in areas where there was high cell viability.

The base material used in most of these studies, Mylar™, is rigid and could potentially be abrasive if implanted in an area that experiences significant movement. Thus, when it comes time to examine pattern persistence and functionality of these constructs in vivo, it would be beneficial to examine different base materials. Some possible materials to consider are amnion or Dacron, as they have been used in cardiovascular TE (Hoch, et al., 1989; Jarrell, et al., 1986). Another possible approach would be to print a thicker or larger construct that can be a stand-alone construct, and hence would not need the Mylar™ or glass slide for stability. Once the construct has polymerized it could easily be removed from the base material.

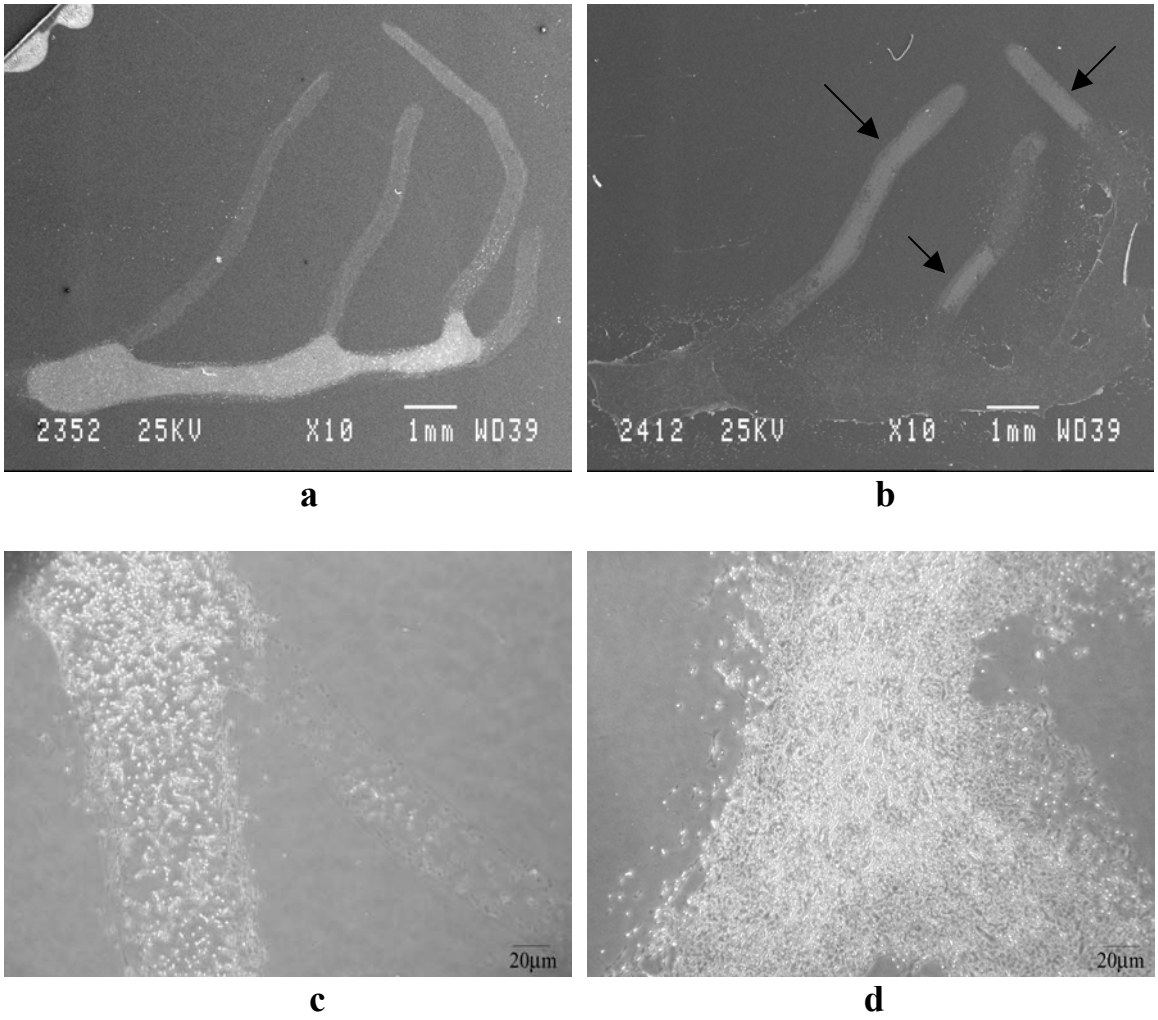


FIGURE 6.2, Images of BAEC Printed on Hydrophobic Side of Mylar™

BAEC printed using the angiogram script described in Chapter 2 as seen by SEM (a) soon after printing and (b) after 4 days in culture; and a close up of the trunk of the printed pattern as seen by phase microscopy after (c) 1 and (d) 4 days in culture. When BAEC + Collagen was printed on the hydrophobic side of Mylar™, the cells migrated out of the printed pattern, causing the pattern to break down and not be detectible by SEM. In the areas where there was reduced viability (denoted by arrows), the printed pattern was maintained longer than in areas where there was high cell viability.

Volumetric Measurements in Confocal Microscopy

Axially resolved microscopy systems, such as confocal laser scanning microscopy, have become commonly assessable to biological laboratories (Al Kofahi, et al., 2003). Segmentation of images generated by such microscopy systems is key for statistical evaluation of complex structures such as blood vessels and nerves. Algorithms to segment these complex image stacks fall into three main categories: 1) intensity-based segmentation, 2) line-filtering methods, and 3) manual or semiautomatic segmentation (Abdul-Karim, et al., 2003). As shown in Chapter 3, using only the intensity to threshold an image stack results in poor segmentation of the images with a lot of background noise. Line-filtering methods use a Gaussian cross-sectional vessel profile to threshold stacks of images (Frangi, et al., 1999; Sato, et al., 1998; Streekstra & van Pelt, 2002). These methods are time consuming and thus are difficult to scale with respect to image size. Manual or semiautomatic thresholding algorithms, which are the gold standard, involve labor-intensive manual tracing, counting, or visual inspection of the stacks of images (DeFouw, et al., 1989; Dellas, et al., 1997; Dellian, et al., 1996; Endrich, et al., 1979; Kirchner, et al., 1996; Li, et al., 1994).

In Chapter 3, it was demonstrated that an automated and accurate algorithm can be devised to segment stacks of confocal images by using the depth, intensity, and *z*-axis gradient information about each voxel. Based on the results seen in this chapter, the Dual Thresholding Rule algorithm can be used to obtain accurate volume information about blob-like structures as well as complex, branching vasculature. Similarly, it could be extended to examine numerous other structures, such as biofilms, chromosomes, and

neuronal forests. As the staining of the microvascular constructs was sometimes uneven, this algorithm could benefit from being combined with a tracing algorithm; however, this may not be necessary as fluorescent labels are improved and more animals are genetically altered such that particular cell types are tagged with a fluorescent label, e.g., the green fluorescent protein Tie-2 severe combined immunodeficient (SCID) Mouse.

Such thresholding methods could be use to provide accurate volumetric information about tissue, and can thus be used to provide valuable information about 3D constructs generated by cell deposition systems such as the BAT. Another potential use for the thresholded images is as input into these cell deposition systems. Currently, 3D images of parts of the body are typically obtained by magnetic resonance imaging or X-ray computed tomography in order to provide input into RP machines (Kachurin, et al., 2002). However, these imaging modalities do not provide microscopic information about physiological structures. Thus, obtaining accurately segmented images of the physiological structure of native tissue is not only valuable in providing volumetric information about the tissue, but also for generating scripts to direct the movement of RP systems.

## Future Research Directions

Since using a system such as the BAT to spatially organize both cells and matrix is a relatively new procedure, there is a wealth of future research directions that can be explored, including using different scaffolding materials to fabricate complex 3D constructs, observing the pattern persistence of constructs under in vivo conditions, and spatially organizing constructs that can perform specific functionality under in vivo

conditions. The following is a description of a proposed future research direction that would use the BAT to generate functional TE constructs, which are spatially patterned and contain a mature vasculature. Once a protocol is established, these constructs have many potential uses, including in vitro and in vivo models to study steps in the process of angiogenesis. This could lead to a better understanding of vessel assembly and the effects of various drugs or growth factors on angiogenesis or to a spatially organized ischemic repair device.

One major limitation to TE constructs is that they are constrained to approximately 2 cubic mm due to the need for nutrition, gas exchange, and elimination of waste (Folkman & Hochberg, 1973). It is believed that incorporation of a vascular network will improve the long-term function of the implanted construct (Kidd, et al., 2002). Most approaches to solving this problem have focused on inducing the host to vascularize the TE construct. This has been accomplished by incorporating pro-angiogenic factors, such as basic fibroblast growth factor (bFGF) and vascular endothelial growth factor (VEGF), into the TE construct. Some methods explored include coating the construct with bFGF or VEGF (Witzenbichler, et al., 1998), seeding the construct with cells that produce these factors (Kellar, et al., 2001), adding slow release microspheres to the host system (Lalan, et al., 2001), and using recombinant protein or gene transfer (Freedman & Isner, 2001). Another approach is to use porous polymers, such as expanded polytetrafluoroethylene (ePTFE) (Williams, et al., 1994), which allow for tissue integration. Other approaches have examined using cellular constructs to provide a vasculature to TE constructs. These methods have examined implanting EC

alone (Nör, et al., 2001; Schechner, et al., 2000), EC and mural cells (Koike, et al., 2004), or intact vessel fragments (Shepherd, et al., 2004). Nör, et al. (Nör, et al., 2001), showed that when EC are embedded in poly-L-lactic acid sponges and implanted subcutaneously, these cells will form into patent vessels that inosculate with the host vasculature. However, after 28 days, while there are still blood vessels within the implant, most of the implanted cells have died. Shepherd, et al. (Shepherd, et al., 2004), demonstrated that when microvessel fragments are implanted dorsal, subcutaneously, the fragments inosculate with the host vasculature. And, after 28 days, the implanted fragments were still within the implanted construct. Another study examined implanted constructs containing 10T1/2 cells and EC. These cells formed patent vessels that inosculated with the host vasculature, and the implanted cells remained viable and within the constructs for at least one year (Koike, et al., 2004). These works indicate the importance of mural cells in forming a mature and stable vasculature.

It has been shown that 10T1/2 cells, an undifferentiated mesenchymal cell line, differentiate toward a mural cell lineage when co-cultured with endothelial cells in vitro. This is demonstrated as an increase in smooth muscle cell markers such as alpha-smooth muscle cell actin (α-SMC actin) and myosin heavy chain (MHC) (Hirschi, et al., 1998; Hirschi, et al., 1999). Initial in vivo studies demonstrated that 10T1/2 cells have the ability to incorporate into the medial layer of developing vessels (Hirschi, et al., 1998). Furthermore, as mentioned above, when these cells were implanted with EC, the cells formed into a patent vasculature that remained intact for up to one year (Koike, et al., 2004). Further in vitro studies examined the effects of 10T1/2 cells on EC. These studies

concluded that 10T1/2 cells induce a tightening of endothelial cell-to-cell contacts. Specifically, there is an increase in the expression and localization of zonula occludens 1 (ZO-1), zonula occludens 2 (ZO-2), occludin, and Vascular Endothelial Cadherin (VE-Cadherin). These studies concluded that 10T1/2 cells aid in stabilizing endothelial cell-to-cell contacts (Kurzen, et al., 2002).

The most drastic change in expression and localization of endothelial cell-to-cell contact proteins in co-cultures of 10T1/2 cells and EC was seen in VE-Cadherin and ZO-1. VE-Cadherin is a cadherin found specifically in EC, and it is required for proper development of vasculature in the embryo as well as for angiogenesis in the adult (Carmeliet, et al., 1999; Vittet, et al., 1997). Similarly, VE-Cadherin is required for multiple EC functions such as tube formation, cell-to-cell adhesion, and survival (Breier, et al., 1996; Matsumura, et al., 1997). ZO-1 is a peripheral membrane protein. In EC, ZO-1 is found in association with tight and adherens junctions (Itoh, et al., 1997). Thus, if an increase in VE-Cadherin and ZO-1 expression is seen in EC, this indicates a possible stabilization of the endothelial cell-to-cell contacts.

As seen in Chapter 2, when BAEC were suspended in type I collagen and printed on Mylar™, tube-like structures (TLS) were observed as early as day 2 throughout the printed constructs. These structures were formed in two different ways: 1) in some areas, cells migrated within the printed pattern and formed TLS in shapes similar to spider webs, and 2) in other areas, cells assembled into TLS in the center of the printed line. Previous work has shown that when EC form into these elongated TLS, it is likely that these structures have actually formed a true lumen. Figure 6.3 illustrates the lumen (L)

seen when EC formed TLS on a basement membrane (bm) of collagen rich amnion as seen by transmission electron microscopy (TEM) (Madri & Williams, 1983). In Chapter 5, it was demonstrated that the BAT is capable of spatially organizing separate solutions into distinct layers in 2D and 3D constructs. This suggests that the BAT can generate spatially organized, viable constructs comprised of EC and muscle cells suspended in collagen.

As a first step toward fabricating a functional microvascular construct, the EC should be spatially organized adjacent to mural cells. In vitro experiments could be performed to evaluate the response of printed, microvascular endothelial cells and mural cells suspended in type I collagen. Immunohistochemical, morphological, and Real-Time PCR evaluations could be used to determine the relative maturity of the printed constructs as well as the interactions between the two cell types. The overall objective of this study would be to evaluate phenotypic differentiation of rat microvascular endothelial cells (RMVEC) when they are co-printed adjacent to smooth muscle-like 10T1/2 cells. Immunohistochemical analysis would be used to evaluate the proliferation of printed constructs at different time points in culture as well as the viability of the constructs following extrusion. The localization and expression of both VE-Cadherin and ZO-1 would be examined using immunohistochemical analysis and Real-Time PCR. Similarly, constructs should be stained with von Willebrand Factor (vWF), α-SMC actin, and MHC and examined morphologically.

As mentioned in Chapter 5, if the two cellular solutions are printed too close to each other, the lines will mix and intermingle. This intermingling causes the lines to no

longer be distinct and uni-cellular; however, if the lines are printed too far away from each other, they will never touch. As there is evidence that contact between the 10T1/2 cells and EC is important (Hirschi, et al., 1999), special care should be taken to ensure that the lines touch. One possible approach is to print one cell type and allow those lines to polymerize. Once the lines have polymerized, the construct could be returned to the BAT cabinet and the other cell type could be printed adjacent to the polymerized lines. Another approach is to allow the collagen to polymerize after each layer or cell type is printed. While this approach maximizes the resolution and accuracy of the printed pattern, it also exposes the cells to a longer time in the BAT cabinet, which could affect the viability of the cells. Because PKH dyes fade over time due to exposure to light or proliferation of the cells, another method to identify the cell types may be necessary. Constructs could be stained with vWF and MHC to identify the RMVEC and 10T1/2, respectively.

The second proposed step in fabricating a functional microcirculation would be to test the ability of the construct to form into a patent vasculature in vivo. In vivo experiments would be performed to evaluate the angiogenic response associated with spatially organized constructs containing endothelium and mural cells. Labeling of cells prior to implantation, as well as intra vital labeling could be used to determine the perfusion and pattern persistence of implanted constructs. In vitro experiments would also be performed alongside in vivo experiments to assess the maturity of the printed constructs.

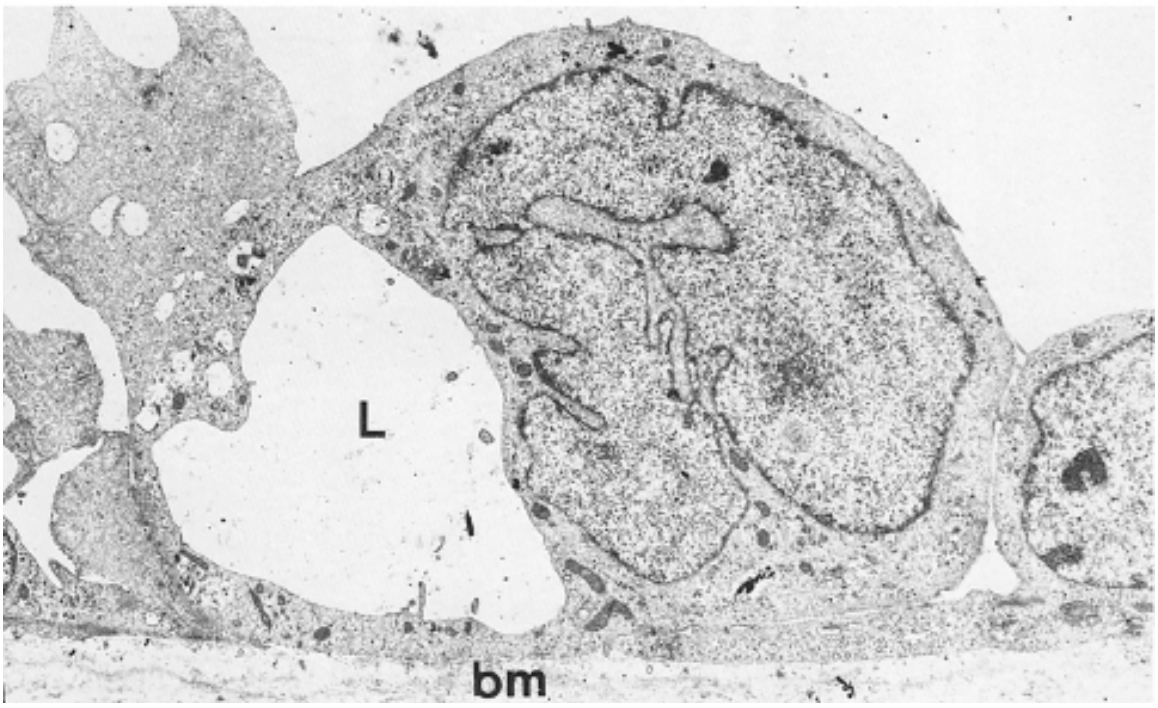


FIGURE 6.3, TEM of EC Forming a Lumen

The lumen (L) seen when EC formed TLS on a basement membrane (bm) of collagen rich amnion (Madri & Williams, 1983).

The overall objective of this study is to determine the in vivo reaction to a printed construct that contains both endothelial and mural cells. These experiments would use the BAT-printed TE constructs in a SCID mouse subcutaneous tissue transplantation model. Evaluations should include orthogonal polarization spectroscopy, intra vital labeling, immunohistochemical, and morphological measurements.

During the time in vivo, the collagen lines may shrink, making them undetectable in the explanted samples. A possible alternative approach to this problem is to print thicker lines. A similar approach is to create a thick scaffold of collagen alone and then print the cellular solution on top of the collagen. It has been shown in a previous study that when collagen alone is implanted, the collagen will remain acellular (Shepherd, et al., 2004). Thus, it is believed that while vascular cells can migrate through this medium, the printed cells may be able to maintain their printed pattern.

Another possible problem is that it may be difficult to print a small enough construct such that it can be implanted dorsal subcutaneously into mice. One alternative approach would be to implant the constructs into a larger animal, such as a rat. However, this removes the use of the SCID mouse model, which allows for the implantation of cells from other animals and species. Thus, either autologous cells or use Fischer 344 rat cells would need to be used. Both endothelial and mural cells could be isolated from the epidiymal fat pad of the rats (Wagner & Matthews, 1975).

## SUMMARY

The results presented in this study have demonstrated the ability of the BAT to fabricate spatially organized 2D and 3D biological constructs, including tissue scaffolds and cellular constructs. A method such as this could be used to fabricate next-generation tissue-based sensing devices (Corbisier, 1997; Pancrazio, et al., 1999; Patel, et al., 1998; Ptitsyn, et al., 1997; Ramanathan, et al., 1997), to build 3D cellular TE constructs (Heath, 2000; Patel, et al., 2000), or to selectively separate and differentially culture cells for a number of in vitro research applications (Pan, et al., 1999; Sattar, et al., 1999; Thomas, et al., 1999). Thus, it has the potential to become an integral part of many biological laboratories.

In closing, the current studies represent the use of a 3D BioAssembly Tool to generate viable spatially organized constructs as well the development of an accurate, automated algorithm for thresholding 3D data. The findings presented in this dissertation demonstrate that the BioAssembly Tool can be used to fabricate viable constructs that are both 3D and have a specific architecture. Also, these findings indicate that by using depth, intensity, and *z*-axis gradient information, one can accurately threshold stacks of confocal images without user intervention. The main points of this study demonstrate the following:

- The BAT is capable of generating viable constructs by coextruding cells + matrix.
- The BAT is capable of generating 3D constructs that are both viable and spatially organized.

- Extruding cells through the pneumatic pens at the lowest pressure required to obtain a continuous line does not significantly alter the viability of the cells.
- The BAT can use PF-127 to build 3D structures with an overhang of 45° without supporting scaffolding.
- By using the depth, intensity, and gradient information for each voxel, stacks of confocal images can be thresholded to obtain accurate volumetric information about 3D constructs.
- Providing humidity to the BAT environment is instrumental to maintaining the viability of extruded cells, especially when stage heat is used.
- The BAT is capable of laying down two separate solutions into 2D and 3D constructs with specific architectures.
- The primary limitations in building complex 3D constructs using the BAT are not mechanical limitations of the system itself, rather they are limitations imposed by the biological nature of the material being printed, for example:
    - Biocompatibility of the Supporting Matrix
    - Required Extrusion Pressure for the Selected Matrix
    - Permeability of Matrix to Cells and Nutrients

# APPENDIX A: GENERATING SCRIPTS FOR THE BAT

Scripts are used to direct the movement of the BAT. These scripts are essentially computer code. They are text files that contain instructions that the BAT can use to generate spatially designed constructs. Scripts can be manually created by directly entering the movement commands, or they can be generated automatically by inputting a single image or a stack of images into a specially designed CAD program. The commands within the script control pen speed, air pressure, pen movement on the *z*-axis, and stage movement on the *x*- and *y*-axes. The following is a description of how to manually or automatically create scripts to be used by the BAT.

## CREATING SCRIPTS MANUALLY

Scripts can be created manually by typing the BAT commands into a text file. A list of commands that can be put into the script can be found in Table A.1, and a sample script can be found in Figure A.1. Windows Notepad is a simple program to use to create the script. It automatically saves files with a ".txt" extension so that all programs know it is a text file. The first things that need to be put into the script are the pen to use and the linear speeds at which the stage should move. The command to tell the BAT what pen to use is "selectpen" followed by the pen number (1-4). This line is not necessary. If no pen is written into the script, the BAT will use the pen that is currently selected when the script is executed. The command to tell the BAT what speed to use when moving the stage is "movespeed" followed by a number. This number represents the speed in mm/s.

When the speed of the stage is too high, e.g., above 20mm/s, the stage will begin to shake when making sharp turns along any of the axes.

Once the pen and stage speed are entered, the information about the pattern to print can be entered. This includes pen pressures and *x*-, *y*-, and *z*-axis movement. It is a good idea to first enter the pressure to use in extruding the material from the pen. This is done using the command "setpressure" followed by a number that represents the BAT pressure in pounds per square inch (psi). Once the pressure is entered, stage and pen movement commands can be entered in order to generate the desired pattern. If the pattern being created is not continuous, i.e., it requires distinct areas that do not touch, then commands can be entered to set the pressure to 0, pull the pen up along the *z*-axis, move to the new location, move the pen back down along the *z*-axis to the stage, and set the pressure back to the desired extrusion pressure. If multiple layers are being extruded, the pen should be raised along the *z*-axis prior to printing subsequent layers in order to keep the pen from dragging through the previously extruded layer. And, once the script has finished creating the pattern, the pressure should be set back to 0 and the pen should be raised along the *z*-axis so that it is no longer touching the construct.

| Command | Description |
|---|---|
| `move X Y Z` | Relative move command along the *x*-, *y*-, *z*-axes (in mm) |
| `quad X Y Z P` | Relative move along *x*-, *y*-, *z*-axes (in mm) and absolute pump position (P) from 0.0 to 1.0 |
| `Moveabs X Y Z` | Absolute move along *x*-, *y*-, *z*-axes (in mm) from the script start position, which is defined as (0, 0, 0) |
| `Quadabs X Y Z P` | Absolute move along *x*-, *y*-, *z*-axes (in mm) from the script start position and pump position (P) from 0.0 to 1.0 |
| `movexyabs X Y` | Absolute move from script start position, only along *x*- and *y*-axes (in mm) |
| `setpressure R` | Sets the pressure (in psi) for the currently selected pen |
| `movespeed M` | Sets the speed (in mm/s) to use in moving the stage and pens |
| `pumpspeed S` | Sets the pump speed (in mm/s) to use in moving the pump in pen 1 |
| `movetocure C` | Moves to the specified cure state (C) from 1 to 4 |
| `returnfromcure` | Returns from the curing station |
| `wait W` | Specifies the amount of time (in seconds) to wait (W) |
| `leftlighton` | Turns on the left light |
| `Leftlightoff` | Turns off the left light |
| `rightlighton` | Turns on the right light |
| `rightlightoff` | Turns off the right light |
| `relay1on` | Turns on relay 1 |
| `relay1off` | Turns off relay 1 |
| `relay2on` | Turns on relay 2 |
| `relay2off` | Turns off relay 2 |
| `digitalon D` | Turns on digital line (D), which can take on values from 4-7 |
| `digitaloff D` | Turns off digital line (D), which can take on values from 4-7 |

TABLE A.1, Table of the Commands Used in BAT Scripts

X, Y, Z, P, R, M, S, and C are numbers that do not have to be integers and where C and D are integer numbers. Note that there are 2 available relay, or AC, lines and 4 available digital lines. There are available in case other electronics, such as a vacuum pump for the stage, need to be added to the system. The rows shaded in light gray refer to actions used with the pen 1, the positive displacement pen.

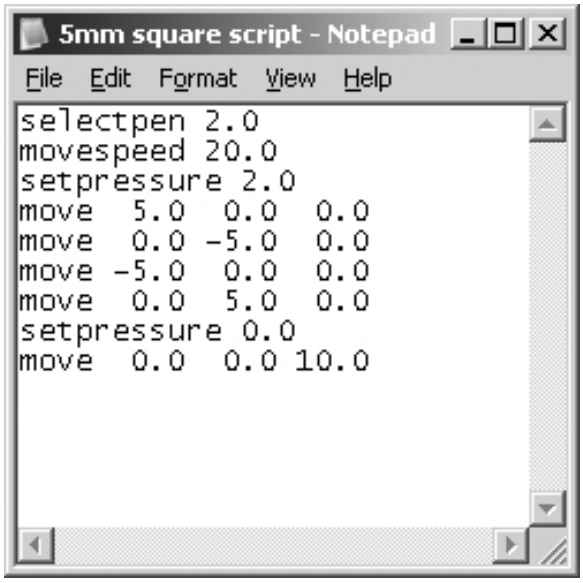


FIGURE A.1, Sample Manually Generated Script for the BAT

This script selects pen 2.0, which is a pneumatic pen. It also uses a linear stage speed of 20mm/s. The script then sets the pressure of pen 2.0 to be 2.0psi and creates a 5mm × 5mm square. It does this by moving right 5mm (along the *x*-axis), down 5mm (along the *y*-axis), left 5mnm, and back up 5mm. After creating the square, it sets the pressure of pen 2.0 to 0.0psi and raises the pen 10mm along the *z*-axis.

For the convenience of adding new equipment to the BAT, there are some relays and digital lines that can be controlled by the script. There are two relay lines which can be turned on and off by the commands relay1on (or relay2on) and relay1off (or relay2off). Currently, there is a vacuum attached to relay 1. This vacuum is attached to the stage to help hold the scaffold in place on the stage. To use, this vacuum, the phrase "relay1on" needs to be added to the top of the script, or a separate script to turn on this relay can be used. Currently, there are scripts to turn on and off the vacuum ("vacuumon.txt" and "vacuumoff.txt"). This relay will remain on until the relay off command is executed through a script, .i.e, you must run a script with the phrase "relay1off" in it. There are 4 digital lines that can be used. These can be turned on and off by entering the commands "digitalon D" and "digitalOff D" where D is the digital line (4, 5, 6, or 7) that the user wants to manipulate.

### CREATING SCRIPTS USING COMPUTER AIDED DESIGN

A special CAD program was written specifically for generating scripts for the BAT. This program is called "multicolpath". Figure A.2 (a) displays the interface of the program once it is opened. In the upper right corner are three rows of colored blocks. The top row shows what color pens will be displayed when showing paths on the screen. When the paths to be printed are displayed on the screen, the colors displayed represent the pen that will print that path. In order, red represents pen 1, green pen 2, blue pen 3, and pink pen 4. Thus, if a green path is displayed on the screen, it is clear that pen 2 is scripted to follow that path. The second, or middle, row of colors represents the colors that each pen will use in an image when converting that image to a script. This row is

selectable and represents five parameters: pen 1, pen 2, pen 3, pen 4, and global. Global is only selectable in conjunction with the Adjust Parameters Button, and will be discussed below. The third row displays the range of colors that the selected pen (in row 2) will use. This represents a range of colors whereas the color in row 2 represents the median color. This range is adjustable using the Adjust Parameters Button and will be discussed more in another section.

Multicolpath Buttons

The buttons that are displayed down the right side of the program are described in Figure A.2 (b). The first two buttons are the Change Layer Buttons. These buttons are used when generating multi-layered scripts. They scroll through the layers, where layer 0 is the first layer to be printed. The next button is the Open File Button. This button acts as a general-purpose open file button as it will allow the user to open either a bitmap file, a "project" file, or a "pen parameter" file. This is based upon the current mode of the program and will be discussed further in the descriptions below. The Save File Button saves either a "project" file or a "pen parameter" file.

The Filter Mode Button can be used to put the program into the "filter bitmap mode." This uses the currently selected colors for the pens, i.e., the colors in the row displayed in the top right corner of the program, and displays what pixels will be written and with what pens. When in this mode, if the Open File Button is clicked, it will allow the user to open a new bitmap and go into "bitmap mode." Clicking the Bitmap Mode Button displays the currently selected bitmap for the current layer. When in this mode, the Open File Button allows the user to open a new bitmap. Also, in this mode, the user

can right click on a location in the bitmap. This will use the color of the clicked on pixel as the median color of the currently selected pen (middle row of colors in the upper right corner of the interface).

The Generate Path Button generates paths for the pens based on their parameters. In this mode, the Open File Button can be used to open a "project file" and the Save File Button can be used to save a "project file." Once the path is generated, the Select Path Mode Button is activated. The Save Script Button generates a script file that can be used by the BAT.

The Select Path Mode Button lets the user select paths/vertices by clicking on them and dragging them around the screen. When this mode begins, the path with the vertex closest to the mouse is highlighted in white. If the left mouse button is clicked, that path is now selected and its individual vertices will be drawn as squares. The vertex closest to the mouse will be drawn a little brighter white. If the left mouse button is clicked again and held down, that vertex will be moved to the mouse position. Right clicking backs up in mode. The insert and delete keys are activated in this mode. When in the top most mode (an entire path is highlighted but all the vertices are not drawn as square yet) pressing the delete key will delete the highlighted path. When in the "vertex mode", the delete key will delete the closest vertex. The insert button will place a new vertex after the closest vertex at the mouse position. The Draw Path Mode Button allows the user to draw paths with the selected pen. Left clicking the mouse starts a path for that pen. Continued left mouse clicking extends the path. Right clicking the mouse ends the path.

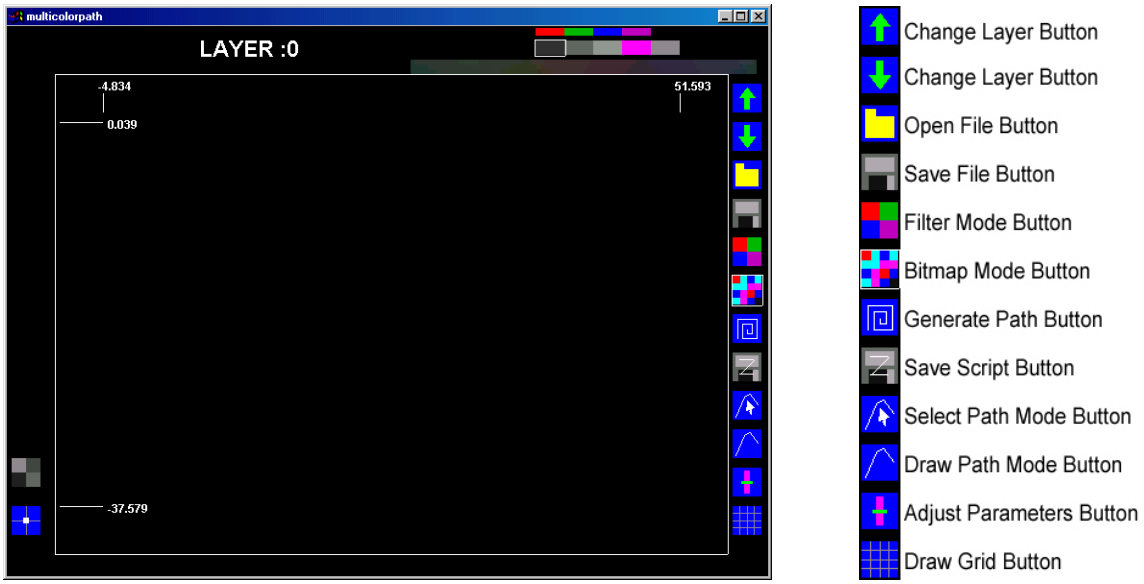


FIGURE A.2, Multicolpath Interface

(a) The Multicolpath program soon after is opened as well as (b) a list and description of the buttons that are on the right side of the program's interface.

The Adjust Parameters Button brings up a screen based on the currently selected pen. If the "global" pen is selected, the parameters that can be adjusted are global. The various screens that will appear based on the selected pen can be found in Figures A.3, A.4, and A.5. The following is a description of the parameters that can be adjusted for pen 1. On the left side of the screen are two graphs that represent the pump opening (top) and closing (bottom) sequence. The *x*-axis for both graphs is time and the *y*-axis is the position of the plunger from 0.0 (fully closed) to 1.0 (fully open). The graphs are point to point. These points can be dragged around. If the rightmost point of the top graph or the leftmost point of the bottom graph is dragged outside of the graph area, the graph time axis is rescaled. Clicking the delete key will remove the selected point, and clicking the insert key will add a point. The green vertical line represents the start of *x*-, *y*-, *z*-motion for the top graph, and the stop of *x*-, *y*-, *z*-motion for the bottom graph. On the right are several sliders and two buttons. The "redfilter, greenfilter, bluefilter" buttons control the median color for the pen displayed in the middle row of the upper right. These can vary from 0-255, just like RGB values. The filterangle and filtermag sliders control how much a color in the bitmap can vary from the RGB value in "angle" and magnitude in order to still be used in the generated script. This makes the RGB value into a 3D vector. Then, comparing any other RGB vector to it, there will be an angle difference and magnitude difference. The filtermag and filterangle sliders control the allowable differences. The bottom row of the upper right stuff shows the approximate current "range" of allowable colors. The user should be careful when adjusting the angle and magnitude, because these can be modified such that effectively every color will be used in generating the script.

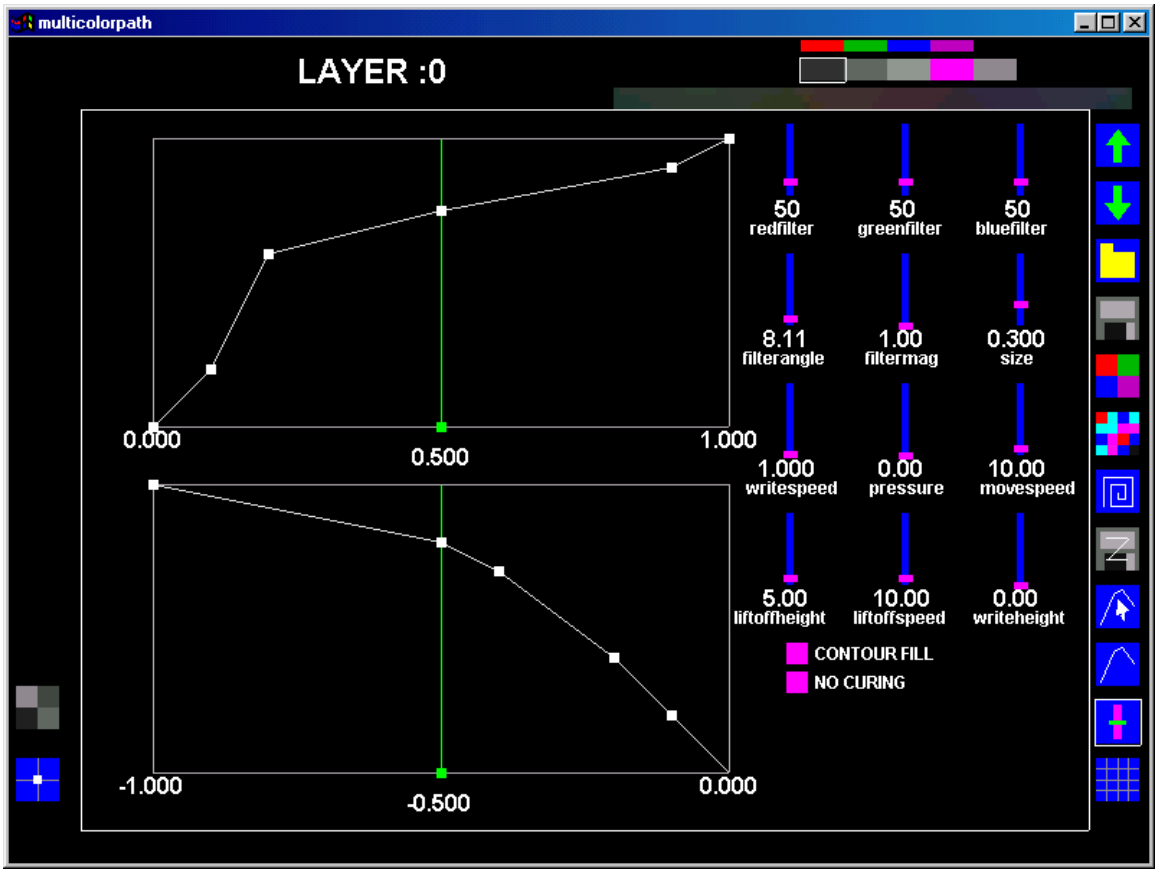


FIGURE A.3, Adjust Parameters Screen for Pen 1

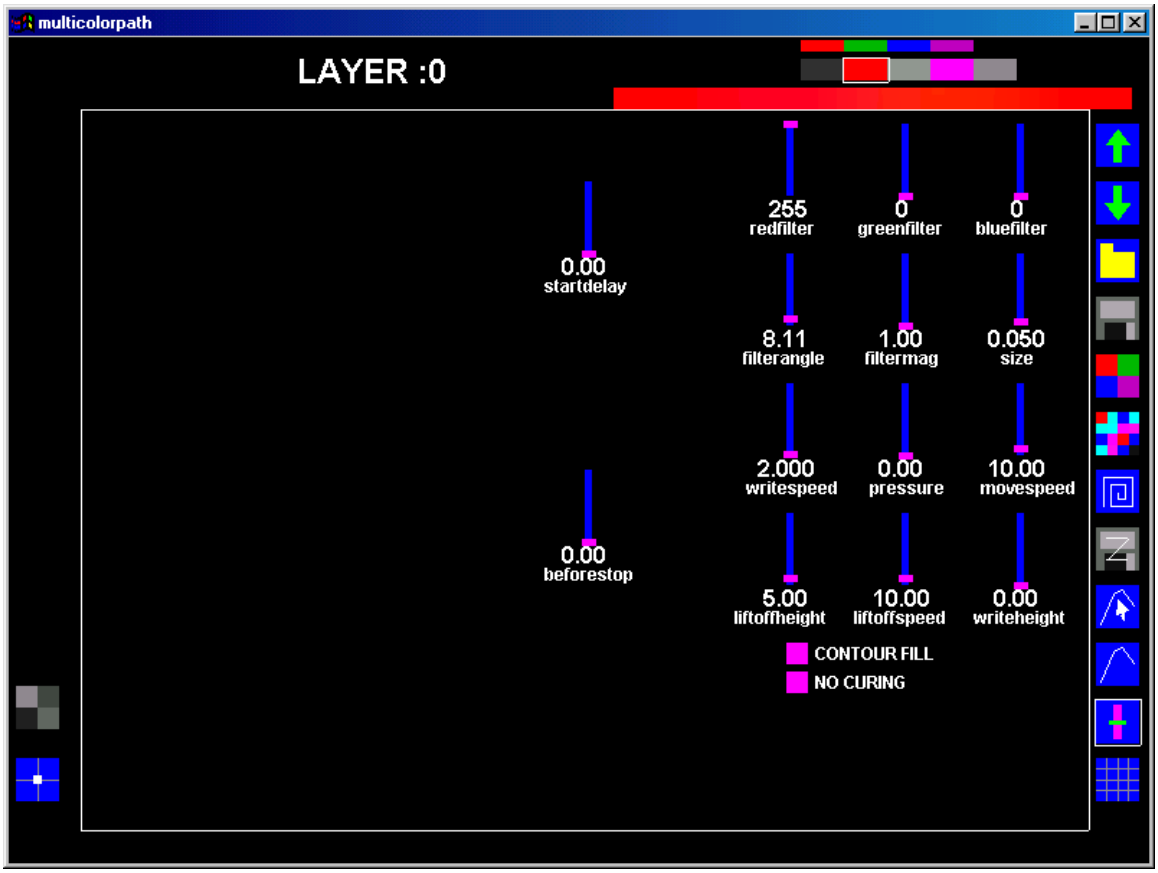


FIGURE A.4, Adjust Parameters Screen for Pens 2 to 4

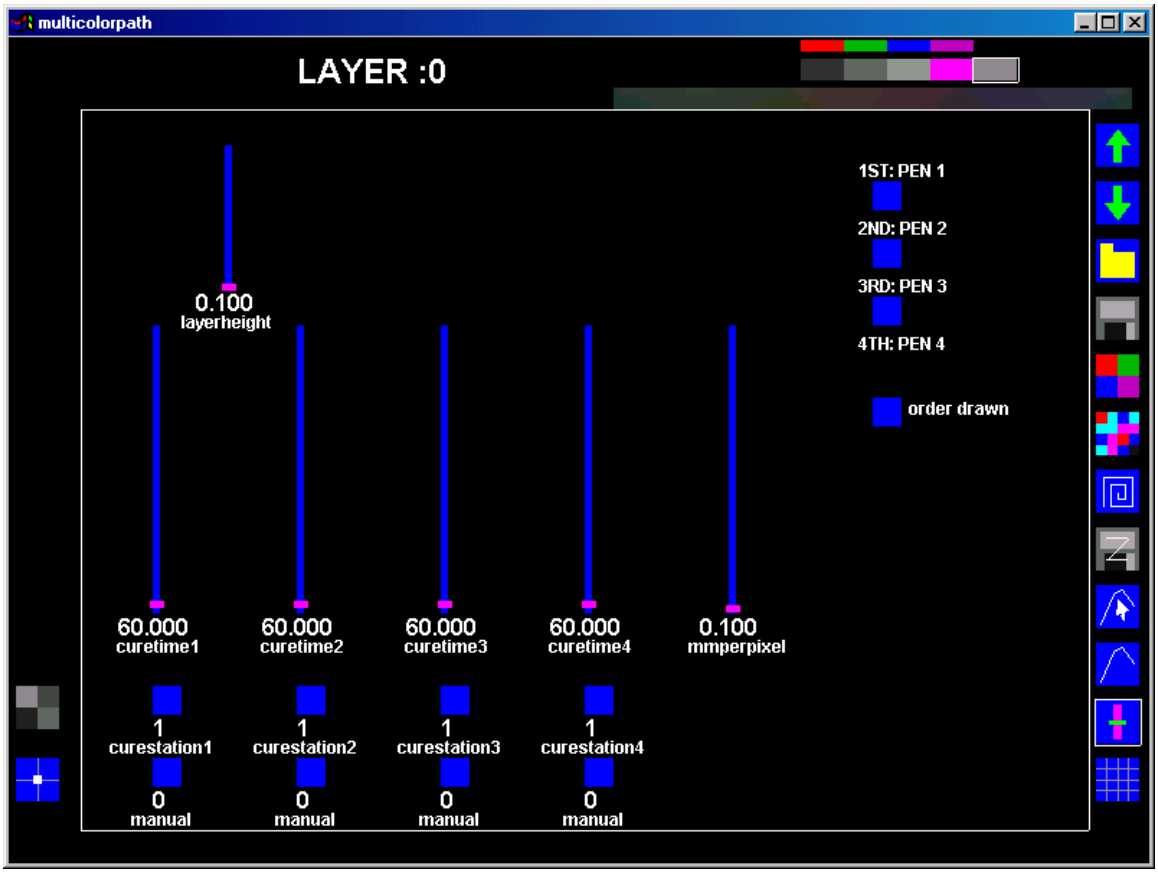


FIGURE A.5, Adjust Parameters Screen for Global Pen

The other sliders that apply to pen 1 are Size, Write Speed, Pressure, Move Speed, Lift Off Height, Lift Off Speed, and Write Height. The Size slider determines the spacing, in millimeters, between adjacent paths. The Write Speed slider indicates how fast, in mm/s, the pen should move when extruding material. The Pressure indicates the pressure, in psi, to apply to the pen. The Move Speed slider indicates how fast the pen should move, in mm/s, when not extruding material. The Lift Off Height slider indicates how high the pen should lift when it has finished writing a line. The Lift Off Speed indicates how fast, in mm/s, the pen should lift off the stage when done writing a line. The Write Height slider indicates how high above the current layer the pen should be when extruding a line.

The two buttons that apply to pen 1 are the Autofill Style Button and the Curve Style Button. The top button, the Autofill Style Button, selects what type of autofill the Generate Path Button (on the main multicolpath interface) will use in generating a path. The three options are contour, raster, and freehand. Contour is similar to keeping your hand along the wall of a shape and filling in that way. Raster fills in the object using a horizontal raster motion. Freehand only allows drawing using the Draw Path Mode Button for that pen. The bottom button, the Curve Style Button, selects what "curve style" to use for the selected pen. This will be discussed further later.

The following is a description of the parameters that can be adjusted for the pneumatic pens (2-4). For these pens, the sliders are similar to those used for pen 1, however, the two graphs are not used for these pens. There are also two more sliders available for these pens. The Start Delay slider indicates how long, in seconds, the system

will wait after applying pressure to the syringe pen before it will move have *x*-, *y*-, *z-axis* movement. This is used for slow reacting fluids. The Before Stop slider indicates how long, in seconds, before stopping *x*-, *y*-, *z*-axis movement the pressure is turned off to the syringe. Again, this is available for slow reacting fluids.

The following is a description of the parameters that can be adjusted if the global pen is selected. The set of parameters is different and is more global in nature. The Layer Height slider indicates the *z*-axis height of the layers, in millimeters. The Pen Order option, in the upper right, controls the order to use in generating the script. The lower button of this group selects either "order drawn" or "above order". If "order drawn" is selected, the paths are extruded in the order that they were drawn, and if "above order" is selected, the paths are extruded according to the order displayed in the group above it. The Curvetime1, 2, 3, 4 option indicates how long for curvestyle 1, 2, 3, 4 the material will remain in cure. The Curestation 1, 2, 3, 4 option indicates the cure station to use for that style. The Manual/relay1/relay2 option indicates whether or not a relay will be turned on automatically.

The Draw Grid Button, on the main multicolpath interface, toggles the drawing of a grid to aid in making paths. The size of this grid can be powers of 2. This is adjustable by small arrow buttons that appear in the lower right when the grid is active. There are two more buttons that appear in the lower left. The Ghost Bitmap Button displays the lowered intensity version of the currently selected bitmap behind the paths drawn when in "path mode". This allows the user to trace paths manually. The Snap to Grid Button snaps vertices to the grid when in Select Path Mode. Some keyboard commands that are

also available are the A/Z keys, which zoom in and out quickly, and the S/X keys, which zoom in and out slower. The image can also be moved using the arrow keys. And, there is a white box with an ×, which is drawn to show where the script will begin. It defaults to the upper left of a bitmap. It can be changed by positioning the mouse where desired on the screen and pressing the home key.

Example Using Multicolpath to Generate a Script

Multicolpath was run by double clicking on the program on the desktop of the BAT computer. Using the Open File Button, an image file, “hand blood vessels.bmp”, was opened. This file can be found in the “arizonamachine” directory on the desktop. Figure A.6 illustrates the screen after this bitmap was opened. Using the “S” and “X” keys, the image was zoomed in such that it filled most of the screen. Pen 2 was selected as the pen that will be used for generating a pattern. This was done by clicking on the green rectangle in the first row of colors in the upper right corner of the interface. Next, the mouse arrow was moved over the red blood vessels in the hand and the right mouse button was clicked. This selected red as the median color to use for generating a script for pen 2. This action changed the color on the second row of colors in the upper right corner of the interface. Next, the Adjust Parameters Button was clicked in order to set the parameters to use for printing with pen 2. In order to see the path that will be used, the Generate Path Button was clicked. Finally, the Save File Button was used to save the script to a text file that can now be used to generate the red blood vessels seen in the bitmap.

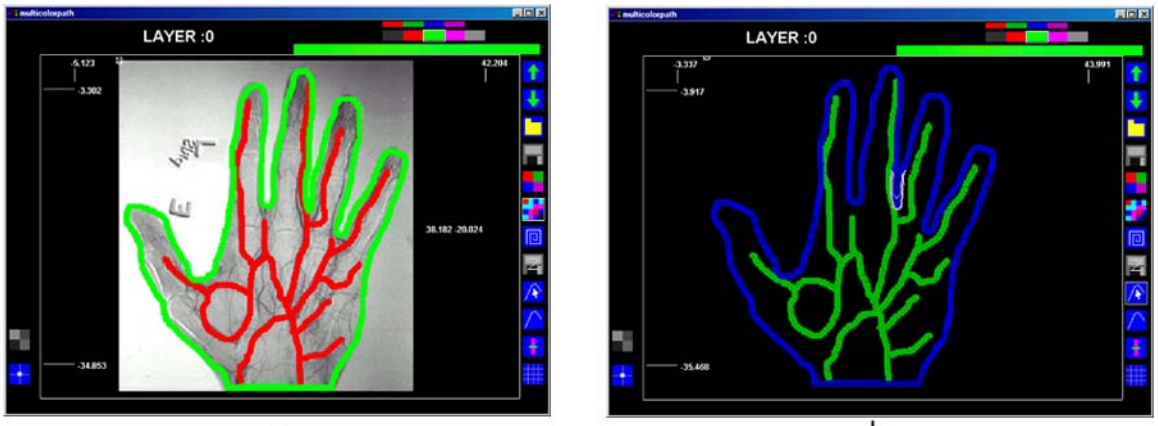


a b

FIGURE A.6, Multicolpath Screens with an Examle Image

The Multicolpath screens showing the path for the example image, “hand blood vessels.bmp”. The first image (a) displays the screen when red lines have been selected for pen 2 and green lines have been selected for pen 3. The second image (b) displays the generated paths for each pen, where green now represents the path for pen 2 and blue represents the path for pen 3.

# APPENDIX B: DETAILED METHODOLOGIES FOR PRINTING CELLS

## PREPARING THE BAT ENVIRONMENT FOR PRINTING

Before beginning to print, the environmental features of the BAT should be set up, including cooling the pneumatic pens, heating the stage, and adding humidity to the BAT cabinet. The following is a description of how to prepare the BAT cabinet before starting to print cells using the pneumatic print pens.

### Cooling the Pneumatic Pens

1. If the Iceman circulator is currently connected to the printer, disconnect it, remove the lid, and drain the water.
2. Fill the cooler with ice, add 2 liters of water, and put the lid back on the cooler.
3. Connect the 2 tubes of the Iceman cooler to the water circulating tubes on the printer.
4. To start circulating cold-water, plug the Iceman cooler into the electrical outlet. (Note: Before you plug it into the electrical outlet ensure that all of the water hoses are properly plugged in!)
5. Turn on the cooling panel on the front of the black BAT cabinet that is under the computer screen and video monitor.
6. There are 3 temperature controllers that can be turned on or off. The first one controls pen 2, the second one controls pen 3, and the third one controls pen 4. Ensure that only the desired units are turned on to cool the pen (s) to 7°C. The following are some notes on the temperature controllers:

a. Flipping the switches up on the temperature controllers will cause the TE units to heat the pens to the entered temperature. Flipping the switches down will cause them to cool the pens.
b. When the temperature controlling devices were put in place, the second one (associated with pen 3) had to be removed because it did not fit with the other two in place. Because of this, the second controller blinks “ERR”.
c. There were some problems with the sensors. Every now and again they report the wrong temperature. In one case the pen was super cooled such that frost developed on the outside of the pen and its contents were frozen. Monitor the pens to make sure they are reporting reasonable values.

7. When the pen jackets that are being used have reached 7°C, they are ready for the print pen containing collagen and cells to be inserted into the pen holder.

Heating the Stage

1. Ensure that there is water in the stage water circulating system.
2. Turn the system on, and set the temperature to 55°C.
3. Once the water circulator reports that its temperature is 55°C, turn the temperature down to 40°C.
4. When the stage temperature is between 29-31°C, the stage is ready for printing to commence.

Adding Humidity to the BAT Cabinet

1. Ensure that the ultrasonic humidifier is plugged into an electrical outlet.
2. Ensure that the ultrasonic humidifier has water in its reservoir. If it is low on water, fill it with sterile milliQ water.
3. Turn the ultrasonic humidifier to its lowest setting and close the doors of the BAT cabinet.
4. Once the hygrometer in the BAT cabinet reads at least 35% humidity, the system is ready to print cells.

## PREPARING THE CELLULAR COLLAGEN SOLUTION

### Making 3.0 mg/ml Type I Collagen Solution

Depending on the stock of collagen (BD Rat Tail Type I Collagen, #354236), you may need either 4× or 5× DMEM. For this report, 4× DMEM was always used. The DMEM is prepared by combining Low Glucose powdered DMEM (Catalog #31600–034, Invitrogen, Corp., Carlsbad, CA) with milliQ $H_2O$. To determine the amount of stock collagen needed, use the following equation:

$$\left(ml\ of\ \ collagen\ stock\ needed\right) = \frac{\left(ml\ of\ \ gel\ needed\right) * \left(desired\ \ concentration\right)}{\left(stock\ \ concentration\ of\ \ collagen\right)},$$

where (*ml of collagen stock needed)* is the volume of collagen stock to put in the collagen solution that is being prepared, (*ml of gel needed)* is the total volume of collagen gel that is being made, (*desired concentration)* is the concentration (this is typically 3.0mg/ml) of

collagen gel that is be prepared, and (*stock concentration of collagen)* is the concentration of the stock of rat tail collagen that is being used to prepare the collagen gel. To determine the amount of concentrated DMEM that is needed to make the final concentration of the collagen gel be 1×, use one of the following equations:

$$(ml\ of\ 4X\ DMEM) = \frac{(ml\ of\ gel\ needed)}{4}$$

$$(ml\ of\ 5X\ DMEM) = \frac{(ml\ of\ gel\ needed)}{5}$$

If the total volume of DMEM and collagen stock do not add up to the volume of gel that is needed, then additional solution needs to be added to the collagen gel bring prepared. Typically, this solution was sterile milliQ water, however, when printing cells, this solution was media containing antibiotics.

To prepare the collagen gel, the necessary concentrations of stock collagen, DMEM, and media should be combined using sterile techniques with chilled utensils and containers. (Note: The collagen is viscous and tends to cling to the pipet tips used to dispense it. Thus, it is wise to be patient in extruding the material in order to get a majority of it. Also, in order to ensure that the proper volume of collagen is used, more collagen should be pulled up than is needed. A good rule of thumb is to pull up 1.2 times as much as is needed.) Once the first three ingredients are combined and vortexed to ensure proper mixing, the pH of the prepared collagen gel needs to be adjusted using sterile 1M NaOH. This is done by looking at the color of the collagen gel. The collagen gel should be a deep pink color. If it is yellow, it is too acidic; and if it is closer to purple, it is too basic.

The following is an example of preparing 1.0ml of collagen gel using a stock collagen with a concentration of 5.06mg/ml:

$$\left(ml\ of\ collagen\ stock\ needed\right) = 0.59ml = \frac{1.0ml * 3.0mg/ml}{5.06mg/ml}$$

$$\left(ml\ of\ 4X\ DMEM\ needed\right) = 0.25ml = \frac{1.0ml}{4}$$

$$\left(ml\ of\ sterile\ media\ needed\right) = 0.16ml = 1.0ml - \left(0.59ml + 0.25ml\right)$$

Counting Cells

Cells were counted using one of two methods: Beckman Coulter Counter (Beckman Coulter, Inc., Fullerton, CA) and SPotlite® Hemacytometer (Baxter Healthcare Corp., McGaw Park, IL). For either cell counting technique, the cells were first trypsinized from a culture flask. After the cells were no longer adherent to the flask, the trypsin was inactivated by adding an equal volume of media containing fetal bovine serum.

Suspending Cells in 3.0mg/ml Collagen Gel

After counting the cells in order to determine the number of cells/ml, the cells are suspended in collagen using the following steps:

1. Calculate the volume that is required to give the desired cell concentration. This is done using the following equation:

$$\left(ml\ of\ cell\ solution\ to\ spin\ down\right) = \frac{\left(desired\ number\ of\ cells\right)}{\left(concentration\ of\ cell\ solution\right)}$$

For example, if the desired concentration is $1 \times 0^6$ cells/ml of collagen and 2ml of collagen is being made, $2 \times 10^6$ cells are required. If the concentration of the cell

solution is $4.4 \times 10^5$ cells/ml, then the total volume of cell solution that should be spun down is $4.5\text{ml} = (2 * 10^6 \text{ cells})/(4.4 * 10^5 \text{ cells/ml})$.

2. Put the determined into a sterile tube and spin at 172 rcf for 5 minutes.
3. Aspirate off the supernatant and put the tube with the cell pellet on ice. (Note: As this sits on ice, some of the supernatant may slide down the edges of the tube such that it appears that there is still a substantial amount of liquid above the pellet. If this happens, aspirate off the supernatant again.)
4. Keep all of the material on ice, including the collagen, cell pellet, and print pen to be filled. Get pipets out of the freezer and pipet the desired volume of collagen gel into the cell pellet.
5. Pipet the material up and down to mix well. (Note: The collagen clings to the sides of the pipet tip. Thus, it may take a little time to get most of the collagen out of the tip.)
6. Again, using a cold pipet, or the same one, pipet the desired volume of cellular collagen material into the cold print pen. Do not transfer the solution to the print pen until it is time to begin printing.
7. Transfer the print pen to the BAT cabinet and place in a chilled pen holder.

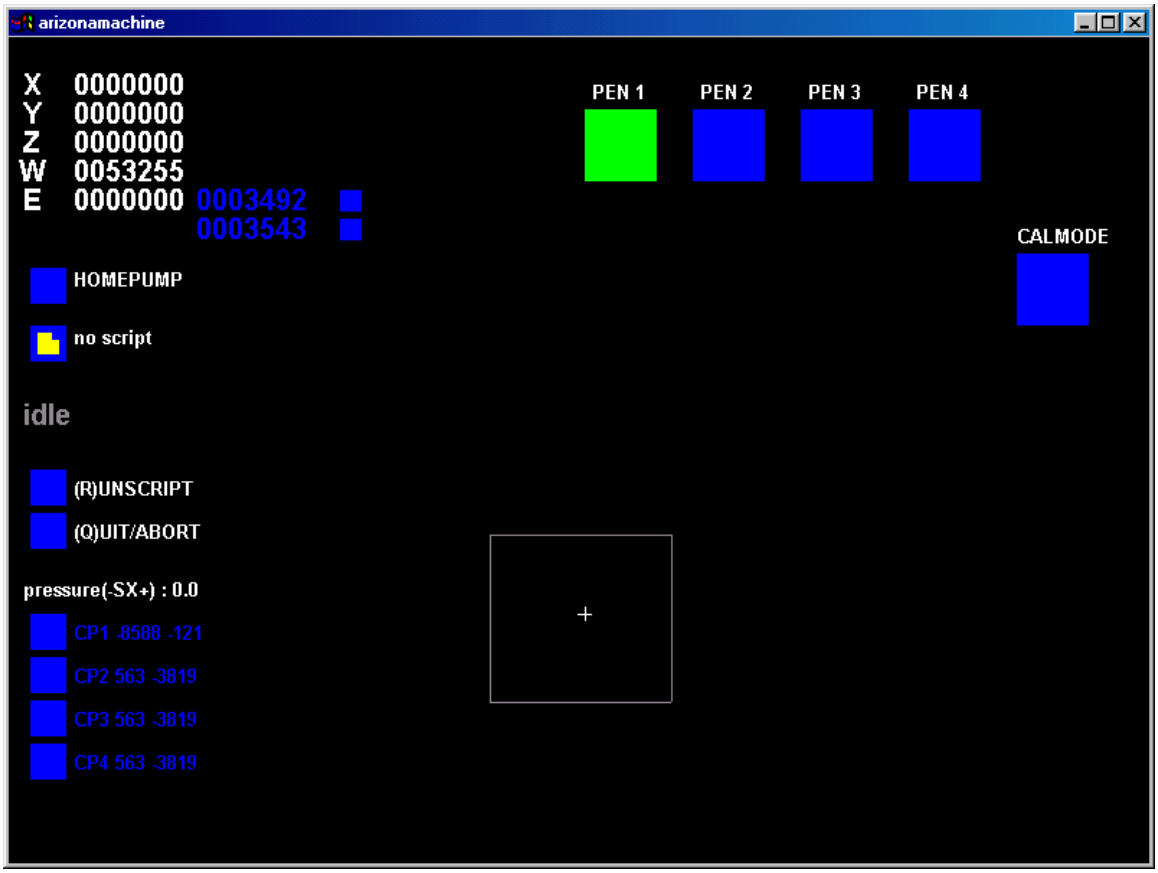


FIGURE B.1, BAT Computer Interface When It Is Initially Opened

Currently pen 1 is selected, which is denoted by the square below it being green. Also, no script has been entered into the interface, which is denoted by the words “no script” next to the Open Script button on the left side of the interface.

## INITIATING THE BAT FOR PRINTING

Before running the program for the BAT, the compressed air tank needs to be turned on. At first the tank was not turned off between sessions, but the air tank seemed to run out too quickly. After that was noticed, a slow leak was found in the tubing in the BAT's black box. This has since been repaired. However, in order to prevent more leaks from occurring, the tank is usually turned off after each printing session. The air tank is in the storage cabinet just outside of the BAT lab area. It is connected to the BAT through a pipe through the ceiling of the lab just above the BAT. The regulator should be set to a maximum of 20 psi to ensure that tubing connectors within the BAT's black box do not get blown off.

The BAT control unit should be turned on before the computer is turned on. (This is done by hitting the switch in the top left corner of the front of the BAT's black box. When it is toggled up to "ON", it will light up with a green light.) Next, the computer should be turned on. There is a vented area on the bottom right corner of the front of the box that has a key. Turn the key to open this area. Flip up the switch on the front left of the computer box. This switch has a 1 at the top and a 0 at the bottom. If the computer does not come on, ensure that all of the power strips are on and try hitting the "Reset" button next to the switch. When the computer comes on and asks for a password for "alstone", just hit <enter>. This will bring up the Windows 98 operating system.

To start the interface for the BAT, double click on the last icon on the desktop. It is titled "Shortcut to arizonamachineSLIDE1use as of 030507". When the program is opened, the stage and print pens inside the cabinet will begin to move. The BAT

interface, which is illustrated in Figure B.1, will also be displayed. In the top right corner of the interface, each pen is represented by a blue or green square. The green square represents the pen that is currently selected. Thus, in Figure B.1, pen 1 is selected. When the program is initiated, pen 1 is the default pen. The numbers on the left of the screen represent the locations of the stage axes (*x* and *y*), pen axis (*z*), print pen calibration axis (*W*), and pen 1 displacement axis (*E*).

Selecting a Script to Direct the BAT

On the left side of the screen are two squares denoted by the words "HOMEPUMP" and "no script". The "HOMEPUMP" button is used in conjunction with pen 1 which is a combined positive displacement and air pressure driven pen. The button beside the words "no script" is the open script button. When this button is clicked, a file dialog box is opened. This dialog allows the user to open a "pen script file" to be input into the system to direct the movements of the BAT. In this dialog, the user can scroll through various files in the computer and select the one to use as a script. Once a script is found, the user can select it by highlighting the file and double clicking on it or by hitting the Open button. If the script has no detectable errors, the name of the script will appear beside the open script button followed by "ok: " and a count of the total number of commands. If there is an error in the script, "BADSCRIPT" will appear next to the open script button, followed by a line number where the error was found as well as the text that triggered the error message.

Once a valid script has been selected, the interface is ready to be used to run the program. In the bottom middle of the interface, there is a white outline of a square.

Inside this square will be a green outline of a square on top of a white cross. The cross represents the current location of the pen and the green square represents the area that will be covered by the script. If this square is red, it means that the script is taking the pen outside of the printable region, i.e., the script will take the pen off of the stage. If this square is red, the pen should be repositioned or the script should be modified such that it will not take the print pen outside of the printable region. If a script is modified while it is being used by the printer, in order for the changes to be realized by the BAT, the script must be saved and opened once more within the BAT interface.

Running the Script

Once a script is opened and ready to be used to direct the movements of the BAT, the pen that will be used should be selected. This can be done using the BAT interface or the Wingman controller. To use the BAT interface, using the mouse, click on the square in the upper right corner that corresponds with the desired pen. To use the Wingman controller, use one of the buttons in the upper right corner of the controller, where "X" corresponds to pen 1, "Y" corresponds to pen 2, "A" corresponds to pen 3, and "B" corresponds to pen 4. Once the proper pen is selected, ensure that the scaffold to be printed upon is on the stage. This scaffold can be held down by taping it in place or by using a vacuum pump.

To turn on the vacuum pump, use the script titled "VacuumOn" in the arizonamachine directory. Open this script file, then click the blue button on the left side of the BAT interface that has the caption " (R)UN SCRIPT". This will turn on relay 1 using the command "relay1on". (This command could also be put as the first line in the

script that will be used to print the desired construct.) This will turn on the vacuum pump until the script "VacuumOff" is opened and run or until the command "relay1off" is executed by the BAT interface. If the "VacuumOn" script is used, the user will need to go back and open the script that will be used to direct the movements of the BAT.

Once the proper script is selected, the scaffold is secured on the stage, and the desired pen is selected, the pen must be lowered to the stage such that it is just touching the scaffold. This is done using the Wingman Controller. Note that the left knob moves the pens along the Z axis and the right knob moves the stage along the *x*- and *y*-axes. The location of the pen on the scaffold is considered the point of origin for the script, i.e., *(x, y, z) = (0, 0, 0)*. Once the pen is lowered onto the stage, clicking the run button on the left side of the BAT interface will start the script. Note that it generally takes a few seconds before actual movement is seen. If the script needs to be terminated while it is running, the user can click on the " (Q)UIT/ABORT" button using the mouse or hit the Q button on the keyboard.

### IMAGING THE PRINTING SESSION

There is a high-magnification camera inside the BAT cabinet. This has an output feed to a TV/VCR combo that is sitting next to the monitor associated with the BAT printer. To get a magnified image of what is happening during a printing session, turn the TV on. If the screen is blue and asksfor input information, the TV can be turned off and back on and this should bring up a display of the BAT cabinet. However, if the image on the screen is not of the BAT cabinet, ensure that the channel that is being displayed is "Line 1". The camera may need to be adjusted such that it focuses properly on the pen

tip. The end of the camera lens can be used to adjust the focus of the image. The camera can also be adjusted up/down and left/right. Figure B.2 displays an illustration of the camera lens within the BAT printer cabinet. In order to aim the camera at the print pen, the pen should be situated such that it is touching the stage. Next, using the coarse adjustment ball, the camera should be aimed at the tip of the print pen. Once it is tightened into place, fine adjustments can be made using the left/right or up/down fine adjustment knobs. This camera and TV/VCR combo can be used to video tape a printing session by inserting a VCR tape in the VCR and hitting "Record".

### PRINTING USING THE PNEUMATIC PRINT PENS

Initially, there were three pneumatic print pens. Currently, only pens 2 and 4 are installed on the printer. (Recall that pen 1 is a combined positive displacement and air pressure driven pen.) Pen 3 was removed when the pen cooling systems were installed, because there was not enough space for all three pens. The pneumatic pens consist of a 3ml syringe-style barrel with a modular tip and a piston based on the viscosity of the material being extruded. If a viscous solution such as collagen is being used, a white piston should be used. If a non-viscous solution such as water is being used, a blue high flow piston should be used. These pistons have a small hole in them.

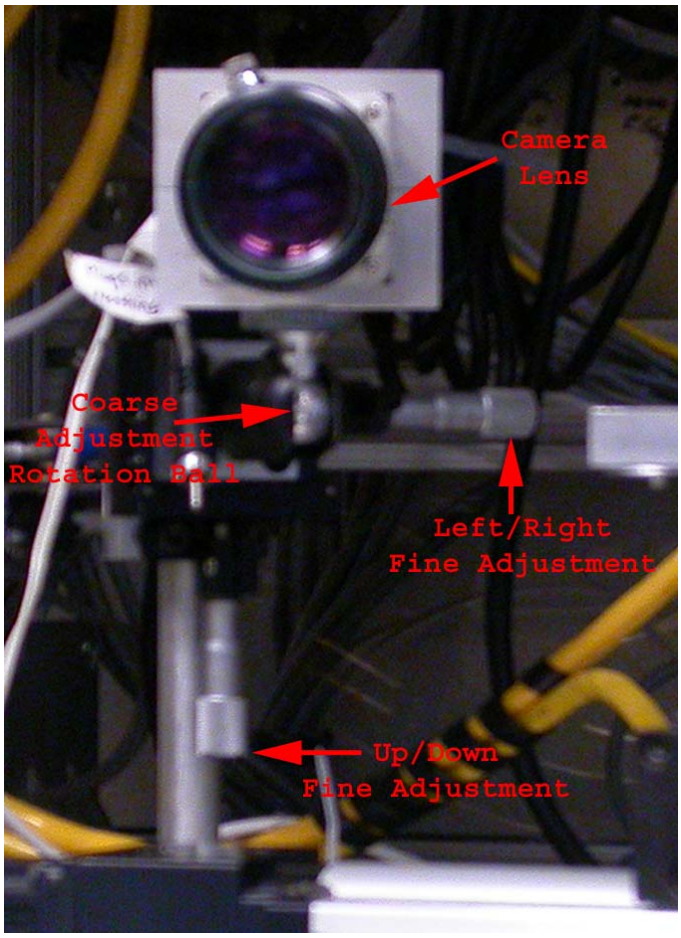


FIGURE B.2, High Magnification Camera Lens inside BAT Cabinet

This high magnification lens within the BAT cabinet provides a close up view of the actual extrusion of material from the BAT print pens.

A 3ml printer pen barrel should be connected to a modular pen tip, e.g., a 25 gauge or 33 gauge tip. After the desired printing solution has been pipetted into the pen, a piston should be placed inside the pen barrel. It is only necessary to slide the piston down far enough such that it is no longer sticking out. Once the pistron is in place, the air supply that corresponds to the desired pen number (either 2 or 4) should be connected to the end of the pen. Note that this will likely push the piston down a little further and some of the printing solution may ooze out of the pen tip. Once the air supply connector is twisted onto the end of the tip such that it is locked in place, the pen can be dropped into the BAT pen-holder that corresponds to the desired pen number (again, either 2 or 4). If the pen does not slide down easily, the screw in the side should be loosened until the pen falls all the way down. If the solution being extruded is temperature sensitive, i.e., the pen is being maintained at some specified temperature, the pen should only be dropped down into the pen-holder such that a small amount of the nozzle is seen. The pen should be secured in the pen-holder by tightening a small screw into the side of the barrel. There is no need to tighten this too much as the screw could puncture the barrel.

All pneumatic pens should be primed before they are used in a printing session. And, if between generating constructs, it is noticed that the printing solution is not flowing from the pen tip in the same manner that it was initially, the pen may need to be primed again. To ensure that the flow from the pen remains as consistent as possible, it is wise to prime the pen tip before starting to print a construct. Once the pen is inserted into the pen-holder and has the air supply connected to it, that pen can be primed. Pressing the "S" key on the keyboard will apply pressure to the selected pen. The longer the "S" key is

held down, the more pressure will be applied. On the left side of the BAT interface, there is an area that shows how much pressure is currently being applied to the selected print pen. Before any pressure is applied, it will read: "Pressure (-SX+): 0.0". Once pressure is applied by pressing the "S" key, the 0.0 value will increase. Slowly increase this number so as not to blow out all of the printing solution in the priming step! Once some material has been extruded through the pen's nozzle, release the pressure applied to the pen by pressing the "X" key on the keyboard. This key works similar to the "S" key in that the longer it is held down, the more the pressure will decrease.

Sometimes over-priming can occur. When this occurs, the printing solution continues to be extruded through the pen nozzle even when no pressure is being applied to that pen. To try to prevent over-priming of the pen, use the least amount of pressure required to get the printing solution to initially flow from the pen tip.

### CALIBRATING THE BAT FOR MULTIPLE PENS

When two pneumatic print pens will be used within a script, they must be calibrated with respect to each other before the printing session should begin. To begin the calibration session, click on the CalMode button on the BAT interface. Once this button is clicked, it will turn red. Figure B.3 illustrates the BAT interface when it is calibration mode. The high magnification lens will be needed for the calibration. Thus, it is imperative that it be set up such that it is properly focusing on the pen tip (See the previous section, "Imaging the Printing Session"). Generally, once the camera is focused on the pen tip touching the stage, it will need to be adjusted down a little for focusing on the pen tip during calibration. This can be done using the Up/Down fine adjustment knob.

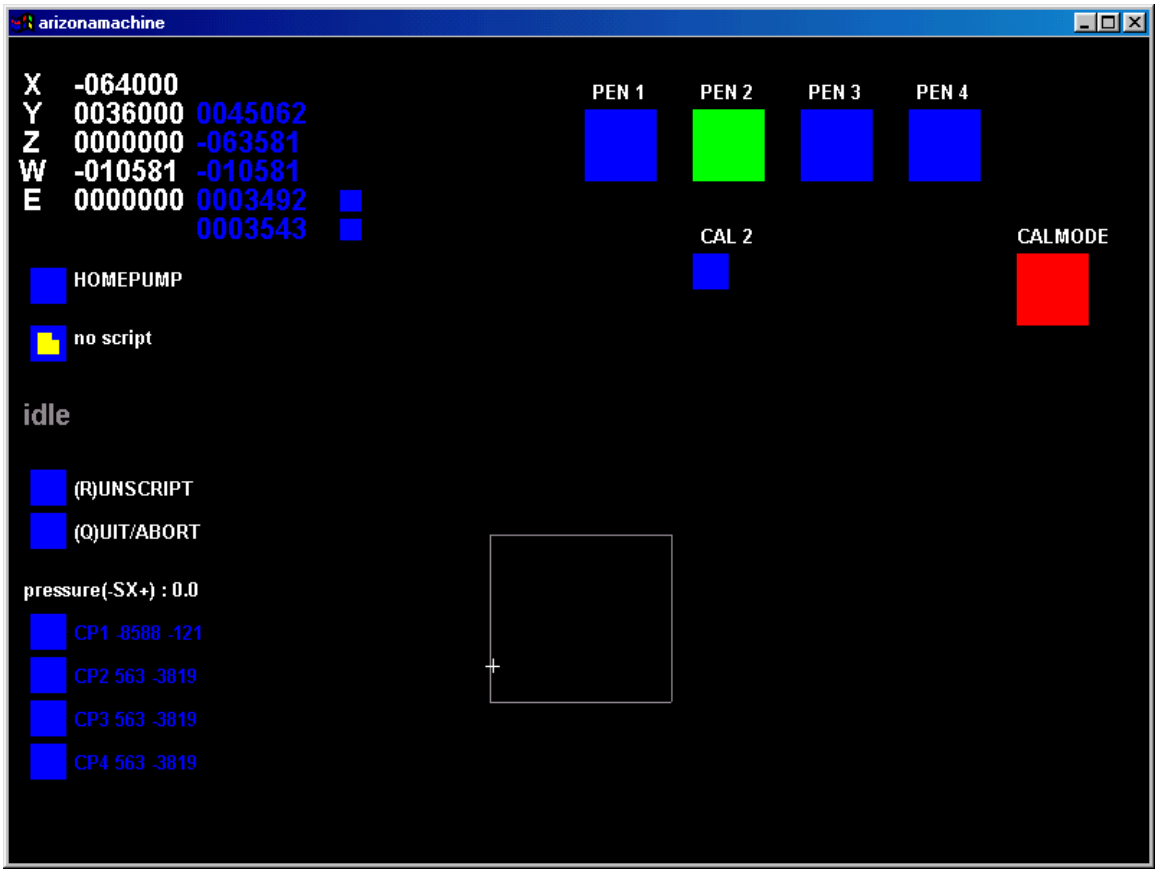


FIGURE B.3, BAT Computer Interface as Seen In Calibration Mode

It is easily seen that the interface is in calibration mode because the square below the phrase “CALMODE” is red. Pen 2 is currently selected, which is denoted by the square below pen 2 being green and the small blue box below that has “CAL 2” written below it.

Once the BAT interface is in calibration mode and the high magnification camera is focused properly, the pen and stage should be moved (using the WingMan Controller) such that the pen is lowered onto the stage touching a marked area. There are numerous marked areas on the small square block that is attached to the front left of the stage. Select a marking and use that to calibrate both pens. Once the pen is lowered onto the stage and is centered on a marking, click the small blue square below the selected pen. In Figure B.3, the square that would be clicked is the small blue square below the phrase "CAL 2". Once this is clicked the numbers on the left of the interface will change to reflect the calibration of that pen.

In order to calibrate another pen, click on the large blue box below the phrase that indicates that pen, i.e., if pen 4 is the next pen to be calibrated, click on the blue box below the phrase "PEN 4". When this button is clicked, the BAT will lower the selected pen and the blue box will change to green. The pen should then be lowered such that it is centered and touching the same mark that was used for the previous pen. Again, to actually calibrate the pen, the small blue square below the selected pen must be clicked. When all of the desired pens have been calibrated with respect to each other, the calibration session can be ended. Before terminating calibration mode, the selected pen *must* be lifted off the stage. To terminate calibration mode, click on the red button below the phrase "CALMODE". This will move the currently selected pen back over the printable area of the stage. If the pen has not been lifted such that it is not touching the stage, it will scratch across the stage and the calibration steps will need to be repeated. Thus, it is imperative that the pen be lifted off of the stage before Calibration Mode is

ended! Once all of the pens that are used in the script have been calibrated, the script can be used to generate a construct using separate printing solutions.

### Culturing Printed Constructs Containing Cells

After a construct has been generated using cells, it needs to be cultured to maintain the viability of those cells. Thus, warm culture media should be added to the constructs to feed the cells and to prevent the constructs from dehydrating. If that media is added to the constructs before they have polymerized, the constructs will either disintegrate or be washed off of the scaffold onto which they were printed. Thus, after being printed, the constructs need a little bit of time to polymerize. The amount of time required will depend on numerous factors such as the volume of the construct, the printing polymer used, and the BAT cabinet environment. When using Type I Collagen, the constructs are generally maintained at 37°C for 2 minutes before adding warm culture media.

While the supplies used in generating the constructs are sterilized before being used in a printing session with cells, the printing environment is not fully sterile. Thus, the culture media that is used to feed the printed cells always contains antibiotics. This has been a sufficient method to ensure that the printed constructs are not contaminated with bacteria.

When the type I collagen constructs were maintained in 6 well plates rather than individual 35ml or 50ml petri dishes, there were fewer problems with the collagen being washed off of the Mylar™. It is believed that the constructs were held more level and thus there was not as much movement of the media within the well plate when the constructs

were being moved. With less movement and turbulence of the media, there was a smaller chance that the collagen would be washed off of the Mylar™, resulting in constructs that were better able to stay intact. This has the added benefit of requiring less media to cover the printed constructs.

# APPENDIX C: CONFOCAL IMAGE PROCESSING PROGRAM

## STARTING THE IMAGE PROCESSING PROGRAM

To start the image processing program, double click on the executable named "confocalProject.exe". This will bring up the Main Image Processing Window, which can be seen in Figure C.1. Initially, this window is blank and contains default information that will be explained later in this section. To open a stack of images, click on the File menu and select Open. This will open an Open Image Stack Window, which can be seen in Figure C.2. To select the directory in which the pictures reside, use the Select Directory Box. When a directory is double-clicked, it will open to reveal any sub directories that it has and all image files with a ".bmp" extension will appear in the Select Image File Box. To select a stack of images, double click on one of the image files in the Select Image File Box. This will put the base file name of the selected image file in the Base File Name Box. The base file name contains the directory information and the file name up to the three digit image number, e.g., the base file name of "c:\confocal_image_005-G.bmp" is "c:\confocal_image _". Note that the file names have an extension after the three digit number that includes ".bmp". Table C.1 gives a list of the possible extensions and their meanings.

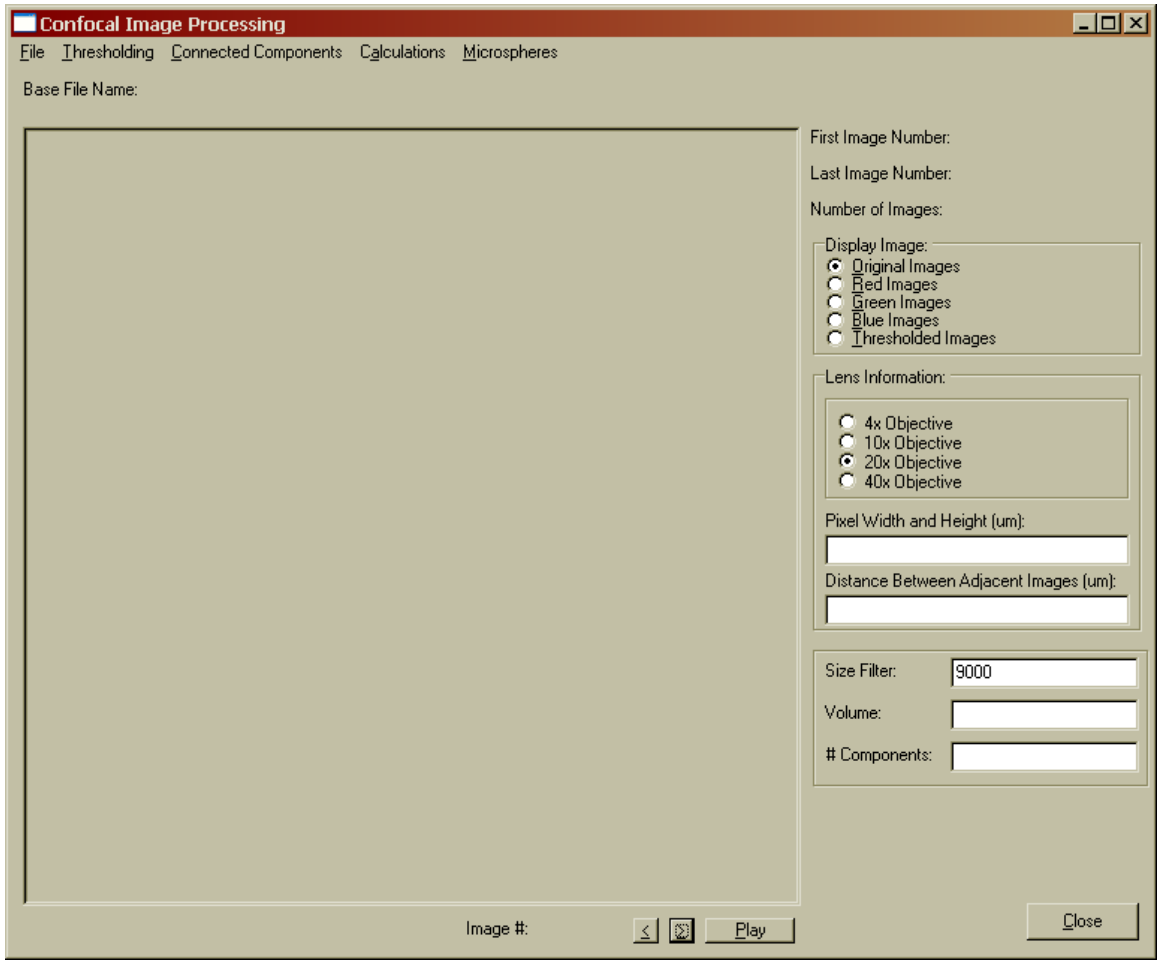


FIGURE C.1, Main Image Processing Window

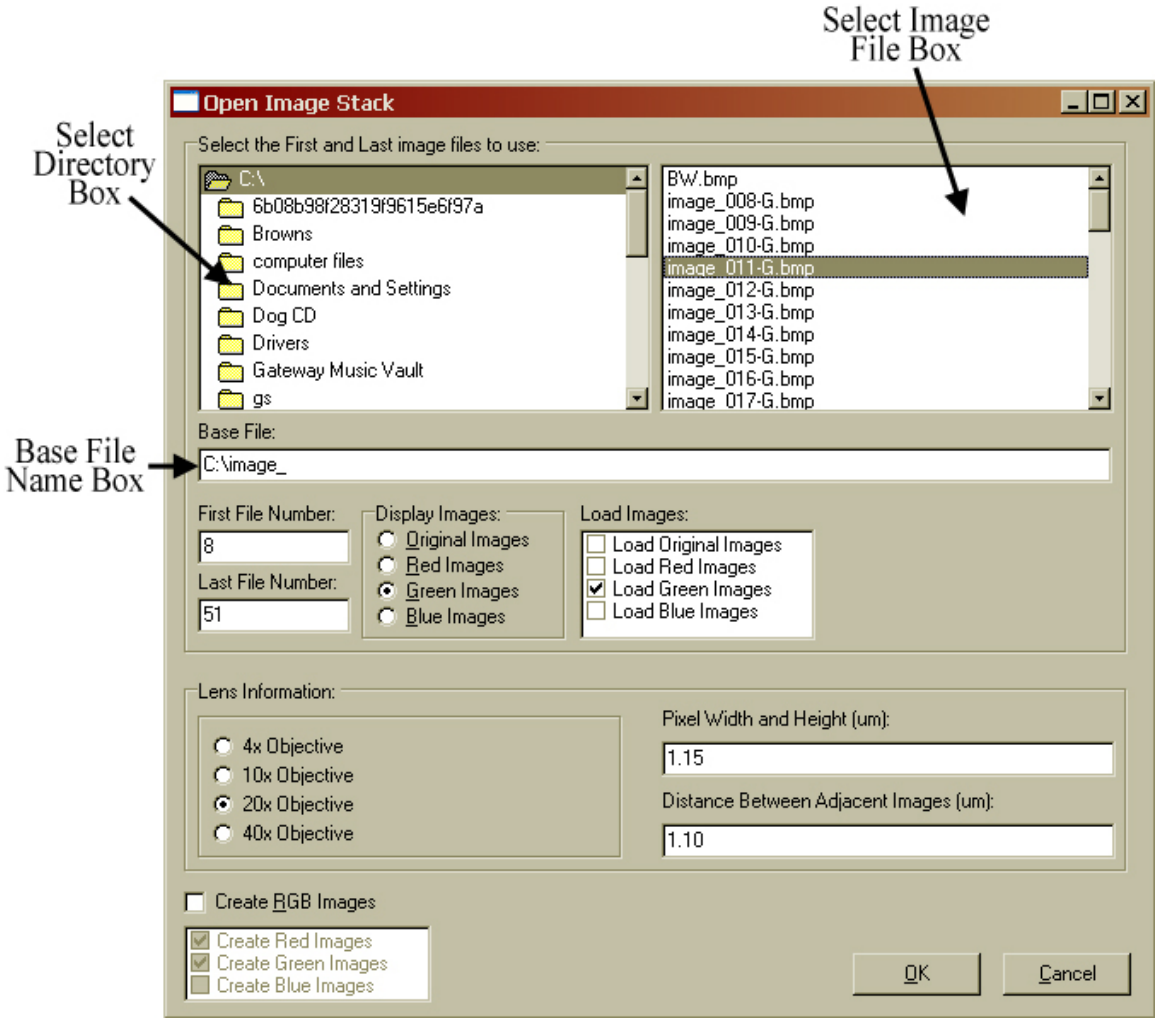


FIGURE C.2, Open Image Stack Window

With the current parameters input, a base file name of "C:\image_" will be opened. Image file numbers 8-51 will be used to open only green images, i.e., "c:\image_008-G.bmp" through "c:\image_051-G.bmp". The lens information was entered as an objective of 20× with a voxel size of 1.15µm × 1.15µm × 1.10µm.

| Extension | Example | File Type |
|---|---|---|
| .bmp | Image_001.bmp | Original image files that are gray scale or RGB. |
| -R.bmp | Image_001-R.bmp | Red scale image file |
| -G.bmp | Image_001-G.bmp | Green scale image file |
| -B.bmp | Image_001-B.bmp | Blue scale image file |

TABLE C.1, Image File Extensions

Once a base file name is selected, the user must enter the first and last image file numbers to use as well as what image types to open. As can be seen in Figure C.2, the user can elect to open only green scale image files, or he can open any combination of original, red scale, green scale, and blue scale image files. (Note that a red scale image file is similar to a gray scale image file in that it uses a range of black to red colors to shade the image.) Also, the user can select which image type (original, red, green, or blue) to display when the image stack is opened. Of course, this should correspond to one of the image types being opened. Next, the lens information should be entered. The objective that was used should be selected and the pixel dimensions and *z*-step should be entered. (Note that the available objectives are 4×, 10×, 20×, and 40×. In the studies presented in Chapter 2, a 20× objective was used.) Finally, the user can indicate whether or not red, green, and blue images should be generated. If the "Create RGB Images" check box is checked, the checkboxes below it become activated allowing the user to select which types of images to generate. If the Green box is checked, the input images will be used to generate images that contain only the green pixels. The new green images will automatically be saved using the base file name with an extension of "-G.bmp". At any point, if the user decides not to open the image stack, he may click on the Cancel button. This will close the Open Images Window and return to the Main Image Processing Window. Once all of the information is entered, the user can click on the OK button to open the image stack. Figure C.3 shows the Main Image Processing Window after a stack of microvascular images has been opened.

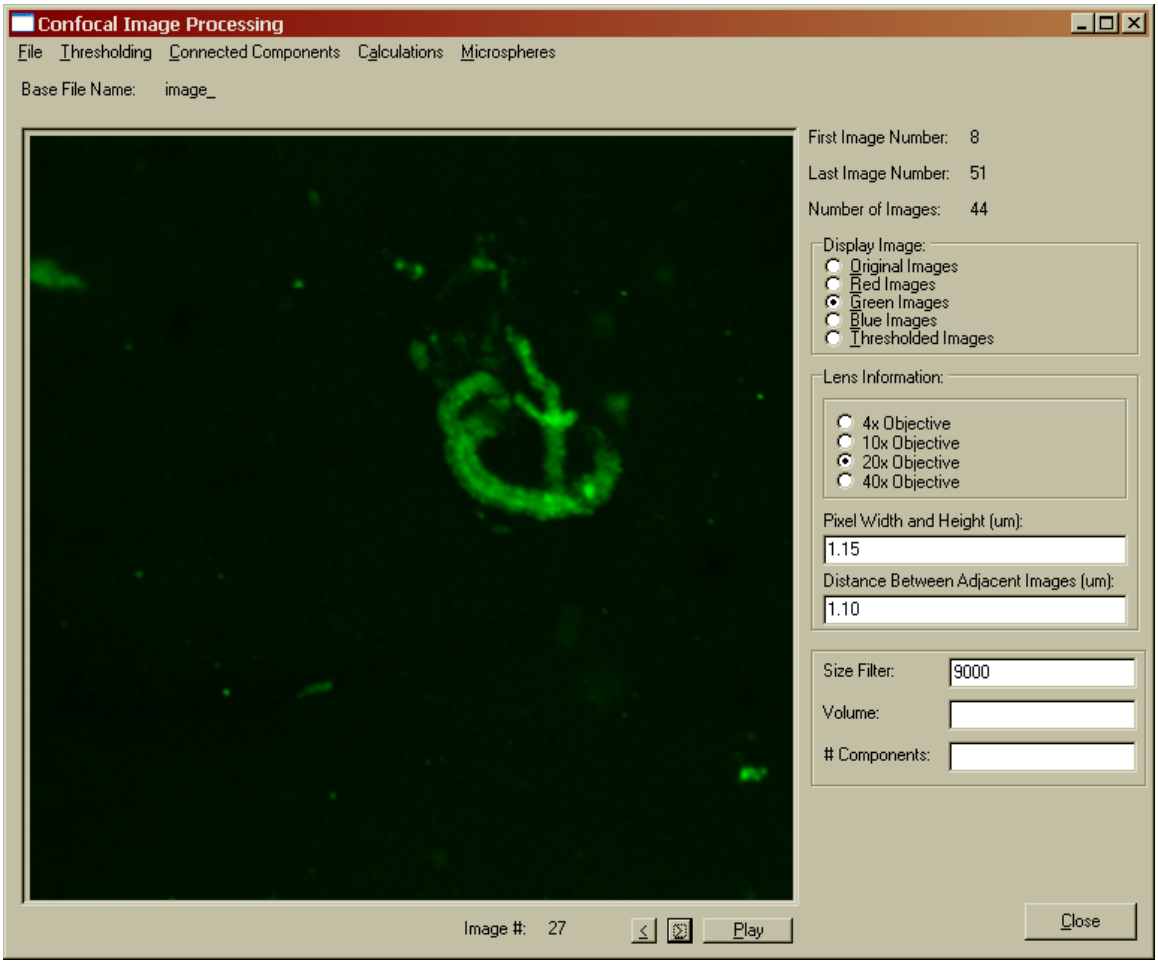


FIGURE C.3, Displaying Microvascular Image Stack

The Main Image Processing Window after opening a stack of images with the parameters detailed in Figure C.2. The indexed image, or the image currently being displayed, is image number 27, i.e., “c:\image_027-G.bmp”.

As can be seen in Figure C.3, the indexed image is displayed in the large screen that takes up most of the Main Image Processing Window. The indexed image number is displayed below this screen after the label “Image #”. The image number information is displayed in the upper right corner. This includes the first image number, the last image number, and the total number of images. The Display Images Radio Button group allows the user to select the type of images to display. If a radio button is selected, but there are no images opened of that type, then the screen on the left side of the window would be blank. For example, if the user selected Thresholded Images but the image stack has not yet been thresholded, the screen will be blank like it is in Figure C.1. Also on this screen, the objective and voxel dimensions entered when the image stack was opened are included in a read only box with the heading “Lens Information”. Information appears in the bottom right corner that corresponds to thresholding and connected components.

### THRESHOLDING THE IMAGE STACK

Once the image stack is opened, the user can threshold those images. To threshold the stack of images using the Dual Thresholding Rule described in Chapter 3, click on the Thresholding menu and select DTR. The green image stack will automatically be thresholded and the black-and-white images will be displayed on the screen. Note that the Thresholded Images radio button is now selected in the Display Images box. Note that while the user is allowed to open original, red, and blue images, the thresholding is performed on the green image stack. Thus, if no green images are opened, the thresholding algorithm will do nothing. (This code can be modified to threshold red and blue images.)

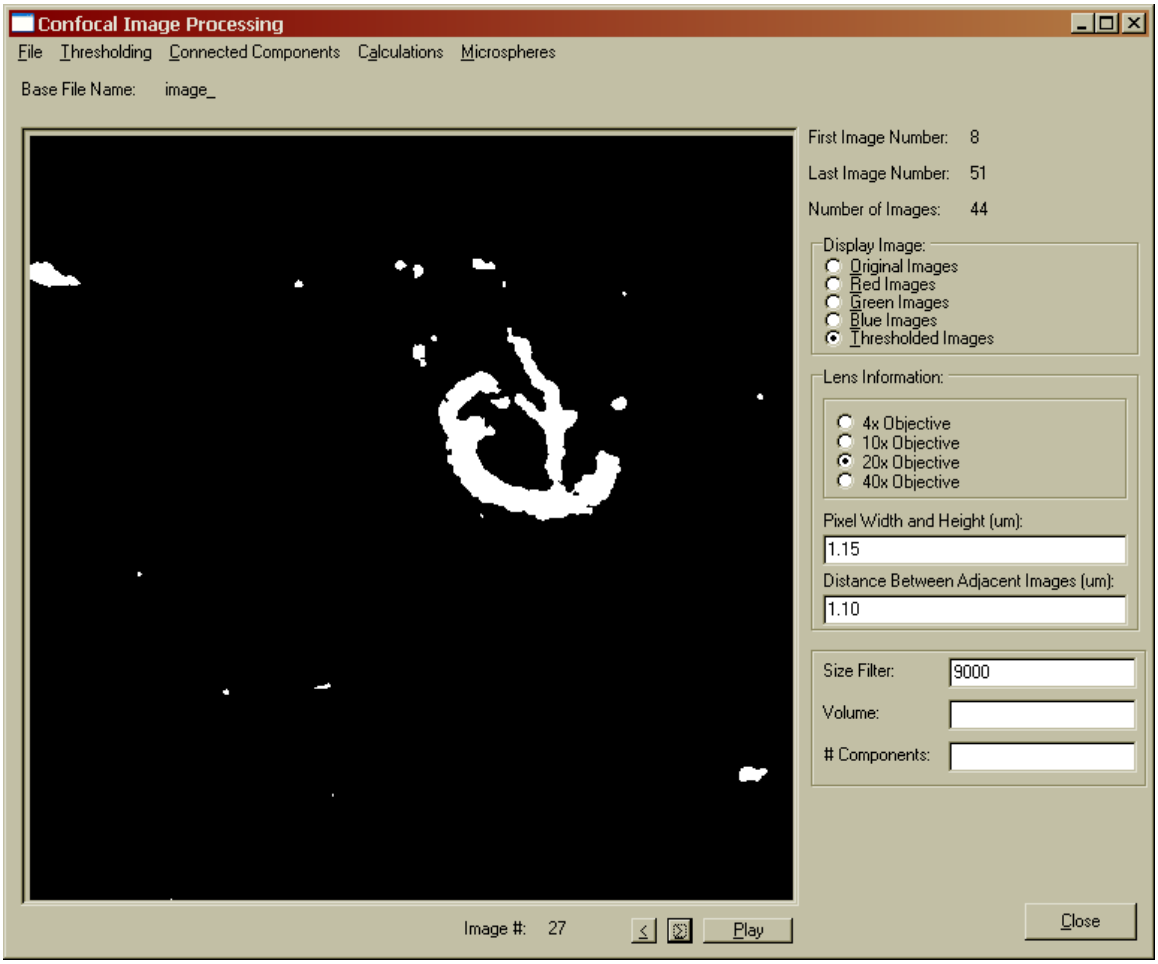


FIGURE C.4, Displaying Thresholded Image Stack

The Main Image Processing Window after thresholding the stack of images seen in Figure C.3 using the DTR thresholding algorithm. The indexed image is still number 27.

Figure C.4 illustrates an example of the window after the image stack has been thresholded. White voxels represent foreground and black voxels represent background. The thresholded images are not automatically saved. To save the thresholded images, click on the File menu and select Save Thresholded Images. As seen in Figure C.5, this will open a Save Image Stack Window. Here, the user can enter the directory to which the image stack should be saved as well as the base file name to use in saving the image stack. Also, the user should enter which types of files to save (original, red, green, blue, or thresholded). Once the user has entered all of the save information, he should click the OK button to save the files. If he decides not to save the images, he can click the Cancel button or close the window by clicking on the × in the upper right corner.

To determine the total volume of the foreground voxels in the thresholded image, the user should click on the Calculations menu and select either Calculate Volumes or Calculate Voxels. If Calculate Voxels is selected, the total number of white voxels will be counted and displayed on the Main Image Processing Window in the box labeled Voxel Count. In the displayed figures, this is the box labeled “Volume”; however, when the number of voxels is counted, the label is changed to “Voxel Count”. If Calculate Volume is selected, the total volume is calculated as the total number of voxels multiplied by the pixel width, pixel height, and distance between adjacent images.

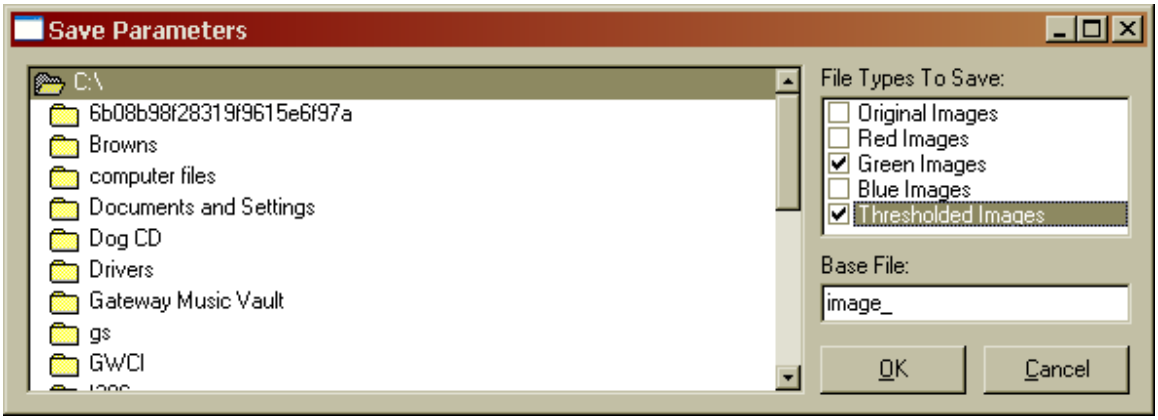


FIGURE C.5, Save Image Stack Window

With the current parameters input, a base file name of “image_” will be used to save the green and thresholded images into the directory “C:\”.

## CONNECTED COMPONENTS LABELING

A 3D connected components labeling algorithm was implemented to provide information about the total number of components in the image stack and about the volume of the components within the image stack. This feature can also be used to size filter the thresholded images, i.e., a filter volume limit can be entered such that any component with a volume less than that limit will be removed from the foreground. The Size Filter Volume box on the right side of the screen allows the user to enter the desired filter volume. This 3D connected components algorithm is an extension of the 2D connected components algorithm (Sonka, et al., 1998).

As can be seen in Figure C.6, after the 3D connected components algorithm has completed, the total volume of foreground voxels as well as the total number of components is displayed on the bottom right of the Main Image Proccessing Window. Also, the thresholded images are modified from black-and-white images to RGB images, such that the background is still black and each 3D component is assigned a different color (not black). This way, the user can easily follow a single component through the stack of images. When size filtering is used (Figure C.6b), there are considerably fewer components than when size filtering is not used (Figure C.6a). This feature is especially valuable when examining stacks of images containing microvasculature as compared with the tissue phantoms containing microspheres that were described in Chapter 3.

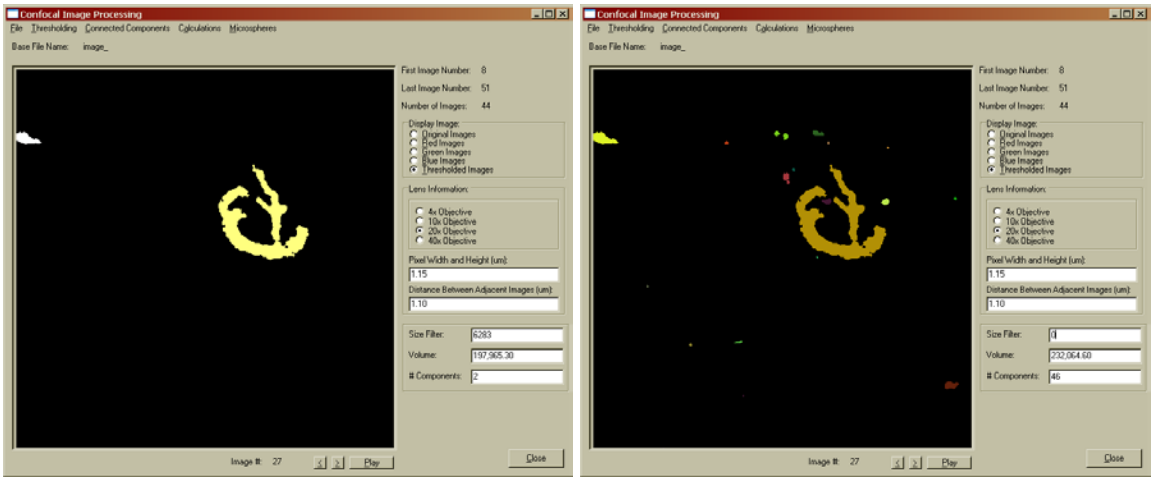


**a** **b**

FIGURE C.6, After Connected Components Labeling

The Main Image Processing Window after thresholding the stack of images seen in Figure C.4 (a) with and (b) without size filtering. The indexed image is still number 27.

### Closing and Exiting

Once the user has finished examining and thresholding a stack of images, he can close the open stack by selecting the File menu and clicking on Close. This will leave the program open, but close the open image files, making the main window look like Figure C.1. If the user wants to completely exit the program, he may click on the × in the upper right corner, or select the File menu and click on Exit.

### Menu Functions

There are multiple main menu items the user can select. These include the File, Thresholding, Connected Components, Calculations, and Spheres menus. These menus and the procedures that are followed when each menu item is selected are described in the following tables. Table C.2 gives a description of the File Menu commands. Table C.3 gives a description of the Thresholding Menu commands. Table C.4 gives a description of the Connected Components Menu commands. Table C.6 gives a description of the Calculations Menu commands. Table C.7 gives a description of the Spheres menu commands.

| Sub Menu | Function |
|---|---|
| Open | This menu item will open the window seen in Figure C.2, which allows the user to enter the pertinent information about the image stack that should be opened. This action is described in more detail above. |
| 3D Average Images | This menu item inputs the open stack of images and averages each voxel in the stack with respect to its 26-connected neighborhood of each voxel, i.e., it uses the 9-connects voxels above and below it as well as the 8-connected voxels in the same image. The averaged images are not automatically saved. Note that this menu item will only work if there is currently a stack of images open. |
| Save | This menu item will open the window seen in Figure C.5, which allows the user to enter the pertinent information for saving the image stack, including the directory, base file name, and types of image files to save. This action is described in more detail above. |
| Close | This menu item will close the opened image stack, leaving the program open as seen in Figure C.1. |
| Exit | This menu item will close the opened image stack as well as the program. This has the same functionality as clicking on the × in the upper right corner. |

TABLE C.2, File Menu Sub Menu Commands

| Sub Menu | Function |
|---|---|
| DTR | This menu item will threshold the stack of green images using the Dual Threshold Rule with an Exponential OR as described in Chapter 3. (Note: This is the same as selecting "Dual Threshold Rule" then clicking "Exponential OR".) |
| Thresholds From Literature | This menu item opens the window seen in Figure C.7, which allows the user to select the type of thresholding algorithm to use, including:<br>• Selecting a threshold based on a unimodal histogram (Umesh Adiga, 2002) (Algorithm: Umesh Adiga) for each image (Histogram: 2D) or to use for the entire stack (Histogram: 3D).<br>• Selecting thresholds based on edge and intensity information as seen in the Objective Threshold Selection method (Xavier, et al., 2001). (Algorithm: OTS)<br>• Selecting a threshold based on a bimodal histogram (Kittler & Illingworth, 1986) (Algorithm: Kittler) for each image (Histogram: 2D) or to use for the entire stack (Histogram: 3D).<br>• Manually entering a threshold to use on the entire stack of images (Algorithm: Manual). If this algorithm is used, the user should also enter threshold values for each image type that will be thresholded.<br>Note: These methods have been implemented to threshold any red, green, and blue images that are open. |
| Dual Threshold Rule | This menu item has several sub menus items which include:<br>• Exponential OR<br>• Exponential AND<br>• Linear OR<br>• Linear AND<br>• Exponential Intensity OR Linear Gradient<br>• Exponential Intensity AND Linear Gradient<br>• Linear Intensity OR Exponential Gradient<br>• Linear Intensity AND Exponential Gradient<br>These menus threshold the stack of green images as described in Chapter 3. The thresholded images can then be seen by selecting the Thresholded Images radio button on the right of the Main Image Processing window. |

TABLE C.3, Thresholding Menu Sub Menu Commands

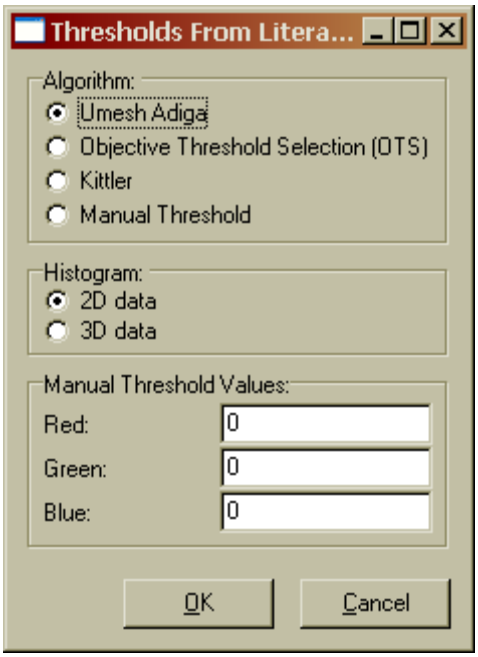


FIGURE C.7, Thresholds From Literature Window

| Sub Menu | Function |
|---|---|
| 3D Connected Components | This menu item examines the thresholded images and finds each 3D foreground (white) component within the stack, i.e., for each voxel it examines the 9-connected neighborhoods above and below the voxel as well as the 8-connected neighborhood within that image. If a size filter volume is entered in the Size Filter box on the Main window, any components with a total volume less than the entered filter volume are removed from the foreground, i.e., they are painted black. Also, all foreground components are labeled with a different color, enabling the user to easily follow a single component throughout the stack of images. |
| Save 3D Component Info | This menu item does the same thing as the 3D Connected Components menu item. It also saves component information to a file "componentStats.dat". An example of this file can be found in Table C.5. The recorded values are described in more detail in this table. |

TABLE C.4, Connected Components Sub Menu Commands

14

| Comp# | NumVox | Vol | xWid | minX | maxX | yWid | minY | maxY | zHei | minZ | maxZ |
|---|---|---|---|---|---|---|---|---|---|---|---|
| 1 | 2007 | 2323.35 | 13.7 | 335 | 347 | 13.65 | 402 | 414 | 19.95 | 3 | 21 |
| 2 | 1974 | 2285.15 | 13.7 | 217 | 229 | 13.65 | 126 | 138 | 19.95 | 5 | 23 |
| 3 | 2208 | 2556.04 | 13.7 | 381 | 393 | 15.75 | 11 | 25 | 21 | 11 | 30 |
| 4 | 1813 | 2098.77 | 13.7 | 303 | 315 | 13.65 | 344 | 356 | 19.95 | 14 | 32 |
| 5 | 1925 | 2228.43 | 13.7 | 203 | 215 | 14.7 | 235 | 248 | 21 | 18 | 37 |
| 6 | 1718 | 1988.8 | 13.7 | 165 | 177 | 14.7 | 425 | 438 | 18.9 | 19 | 36 |
| 7 | 1733 | 2006.16 | 12.6 | 276 | 287 | 13.65 | 190 | 202 | 19.95 | 21 | 39 |
| 8 | 1350 | 1562.79 | 13.7 | 425 | 437 | 13.65 | 194 | 206 | 16.8 | 21 | 36 |
| 9 | 1665 | 1927.45 | 12.6 | 78 | 89 | 13.65 | 151 | 163 | 19.95 | 22 | 40 |
| 10 | 1995 | 2309.46 | 13.7 | 19 | 31 | 14.7 | 259 | 272 | 22.05 | 25 | 45 |
| 11 | 1504 | 1741.07 | 13.7 | 299 | 311 | 12.6 | 240 | 251 | 18.9 | 27 | 44 |
| 12 | 243 | 281.3 | 2.1 | 0 | 1 | 12.6 | 260 | 271 | 17.85 | 27 | 43 |
| 13 | 2500 | 2894.06 | 16.8 | 495 | 510 | 14.7 | 136 | 149 | 22.05 | 30 | 50 |
| 14 | 1586 | 1835.99 | 13.7 | 281 | 293 | 13.65 | 131 | 143 | 18.9 | 31 | 48 |

| | Ave #Vox | Ave Vol | Ave X | Ave Y | AveZ |
|---|---|---|---|---|---|
| **Ave Vals** | 1730.07 | 2002.77 | 12.9 | 14 | 19.8 |
| **Std Dev** | 519.21 | 601.05 | 3.25 | 0.87 | 1.48 |

TABLE C.5, Example of Component Information Stored in "componentStats.dat"

When the user selects Save 3D Component Info in the Connected Components menu, a data file titled componentStats.dat is saved. This file contains the total number of components (in this case 14), the average number of voxels per component, the average volume per component, the average *x* dimension, the average *y* dimension, and the average *z* height for each component. Also, for each component, the total number of voxels, total volume, minimum dimensions (*x*, *y*, and *z*), total width (*x* and *y*), and total *z* height are recorded.

| Sub Menu | Function |
|---|---|
| Calculate Volumes | This menu item calculates the total volume of foreground voxels based on the total number of foreground voxels (i.e., white voxels) as well as the volume of a voxel (i.e., the pixel width × pixel height × distance between images in the stack). |
| Calculate Voxels | This menu item counts the total number of voxels that have been marked as foreground voxels, i.e. white voxels. |

TABLE C.6, Calculations Menu Sub Menu Commands

| Sub Menu | Function |
|---|---|
| Save Intensity Cubes | This menu item opens the Save Intensity Cubes window as seen in Figure C.8. This window will only pop up if a stack of images is currently open. This window allows the user to select the text file that contains the center information for each sphere in the image stack, in the format *x* dimension tab *y* dimension *z* dimension. This calculates the average intensity for the 17 × 17 × 17 voxel cube around each input center coordinate and saves it in a text file titled "intensities.txt". |
| Create Usphere Image Stack | This menu item opens the Create Sphere Images window as seen in Figure C.9. This window allows the user to input the text file that contains the center information (format described in the above row) as well as the first and last image number in the image stack. This function calculates the true thresholded sphere images for each image in the stack based on the template in Figure 3.1 and saves the images to files titled "sphere_001.bmp", "sphere_002.bmp", etc. |
| Calculate Specificity | This menu item opens the Calculate Specificity window as seen in Figure C.10. This window allows the user to enter the true thresholded images (sphere files), the original images (before thresholding), and the thresholded images. Using this information, the true positives, false positives, true negatives, and false negatives are recorded in the file "trueFalse.txt". Note that positive refers to foreground and negative refers to background. Also note that the last file type that is selected indicates what directory will contain the "trueFalse.txt" file. Thus, it is prudent to select the thresholded images last. |

TABLE C.7, Temp Menu Sub Menu Commands

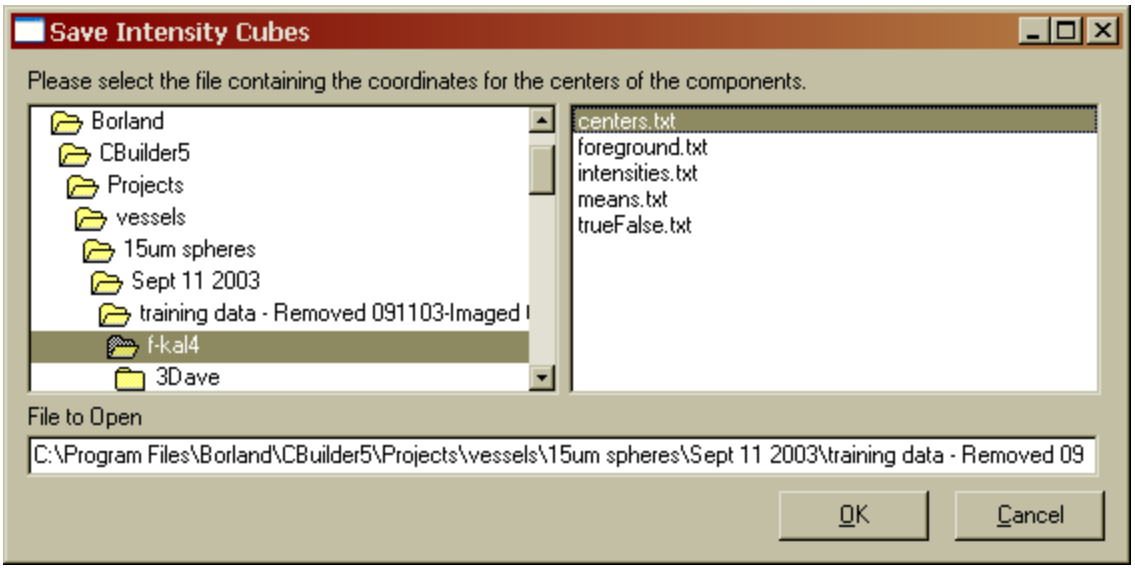


FIGURE C.8, Save Intensity Cube Window

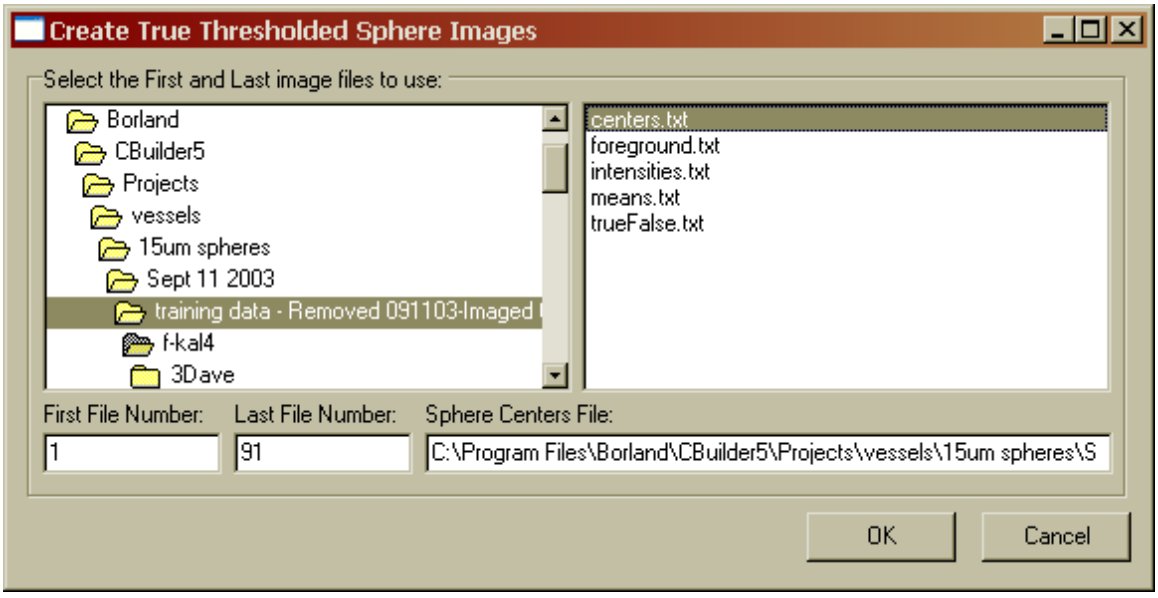


FIGURE C.9, Create Sphere Images Window

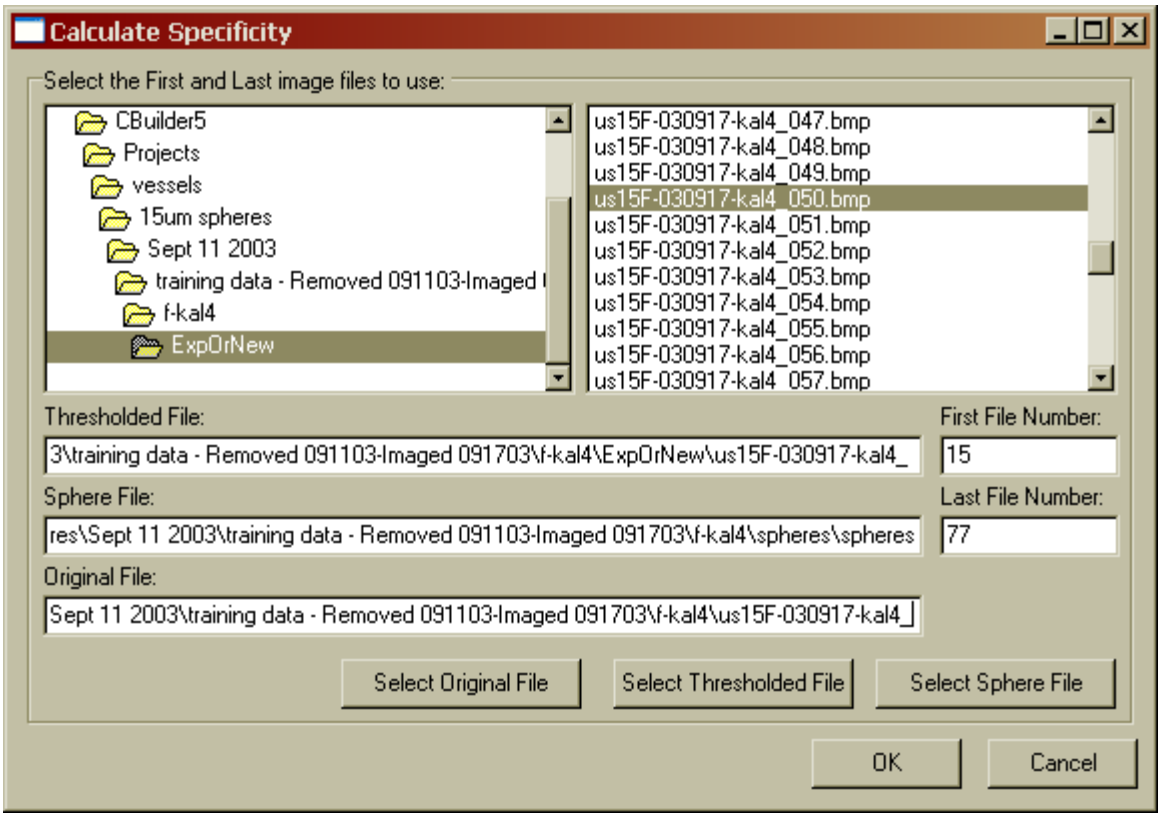


FIGURE C.10, Calculate Specificity Window

# APPENDIX D: LIST OF ABBREVIATIONS

2D – two-dimensional
3D – three-dimensional
3DP – three-dimensional printing
α-SMC actin – alpha smooth muscle cell actin
μCP – micro contact printing
BAEC – bovine aortic endothelial cell
BAPO – bis (2, 4, 6-triethylbenzoyl)phenylphosphine oxide
BAT – BioAssembly Tool
bFGF – basic fibroblast growth factor
BSA – bovine serum albumin
CAD – computer aided design
CAM – computer aided manufacturing
DTR – dual thresholding rule
EC – endothelial cell
ECM – extracellular matrix
ePTFE – expanded polytetrafluoroethylene
ESC – embryonic stem cell
FDA – Food and Drug Administration
FDM – fused deposition modeling
HUCBC – human umbilical cord blood mononuclear progenitor cell
ID – inner diameter
LAD – left anterior descending
MAPLE-DW – Matrix Assisted Pulsed Laser Evaporation Direct-Write
MHC – myosin heavy chain
Mylar™ – flat sheets of PET
OTS – objective threshold selection
PBS – phosphate buffered saline
PET – polyethylene terephthalate
PF-127 – polyoxyethylene / polyoxypropylene or pluronic F-127
PGA – polyglycolic acid
PLA – polylactic acid
PLGA – polylactic-co-glycolic acid
PPF – polypropylene fumarate
PPF-PEG – polypropylene fumarate-co-ethylene glycol
psi – pounds per square inch
PTFE – polytetrafluoroethylene or Teflon®
RFMF – rat fat microvascular fragments
RMC – rat microvascular cells
RMVEC – rat microvascular endothelial cells
RP – rapid prototyping

SCID – severe combined immunodeficient
SEM – scanning electron microscopy
SLA – stereolithography
TE – Tissue Engineering
TEM – transmission electron microscopy
TLS – tube like structure
VE-Cadherin – Vascular Endothelial cadherin
VEGF – vascular endothelial growth factor
vWF – von Willebrand Factor
ZO-1 – zonula occludens 1
ZO-2 – zonula occludens 2

# APPENDIX E: REPRINT PERMISSIONS

## PERMISSION TO USE RAPID PROTOTYPING SCHEMATICS (FIGURES 1.2-1.4)

From: EdGrenda@aol.com Add to Address Book
Date: Wed, 4 Feb 2004 16:05:22 EST
Subject: Re: Rapid Prototyping Web Site
To: cutiger1996@yahoo.com
Top of Form

Bottom of Form

In a message dated 04-02-04 15:34:38 EST, you write:
<< Subj: Rapid Prototyping Web Site
Date: 04-02-04 15:34:38 EST
From: cutiger1996@yahoo.com (Cindy Smith)
To: EdGrenda@aol.com

I am a graduate student in Biomedical Engineering at the University of Arizona. I am currently working with a three dimensional printer to create tissue engineered constructs.

In order to explain my research, it is good to also explain other types of rapid prototyping techniques that are out there. I did a search on the internet and your web site was by far the best at providing information and news about rapid prototyping. I would like to get permission to use some of the pictures on your web site for presentations at conferences and universities in order to provide background information on rapid prototyping techniques as well as the utility of rapid prototyping in biomedical engineering. The pictures in quest are the "cartoons" depicting some rapid prototyping techniques as well as some pictures in your "Picture of the Week" section on medicine and dentistry.

Thank you for taking the time to consider my request. I look forward to hearing from you.

Sincerely,
Cynthia Smith

>>
Dear Cynthia:

Thanks for your kind words.

Permission is hereby granted for you to use material from the Worldwide Guide to Rapid Prototyping web-site for your article or presentations, on the condition that you mark the materials:



It would be nice if you could also add our URL and a link for your readers in any published materials, but that isn't mandatory.

We are very happy that you find the site useful and send best regards.

Ed Grenda
Castle Island Co.
19 Pondview Road
Arlington, MA 02474 USA
781-646-6280 (voice or fax)
EdGrenda@aol.com (email)

The Worldwide Guide to Rapid Prototyping
http://home.att.net/~castleisland/

PERMISSION TO USE DWB™ SCHEMATIC (FIGURE 1.5)

Permission From Journal:

Dear Ms. Smith:

Permission is granted for you to use the below referenced figure providing you cite the source and contact the author directly. Please note that the correct paper number is Q5.2.

If you have any questions, feel free to contact me.

Sincerely,

Bonnie Darr

-----Original Message-----
From: Linda Baker
Sent: Tuesday, August 02, 2005 11:19 AM
To: MRS E-Proceedings
Subject: FW: Use of Image in Dissertation Introduction

-----Original Message-----
From: Cindy Smith [mailto:cindy.m.smith@gmail.com]
Sent: Tuesday, August 02, 2005 11:14 AM
To: Linda Baker
Subject: Use of Image in Dissertation Introduction

I am a Ph.D. student in Biomedical Engineering at the University of Arizona. I am working with a three-dimensional direct-write system to generate viable tissue engineered constructs.

In the introduction of my dissertation, I am including a description of other Rapid Prototyping systems for generating 3D tissue engineered constructs. I would like to include a figure of the aerosol based system that was published in your proceedings in 2002.

The reference for this article is as follows: Marquez, G.J., Renn, M.J., & Miller, W.D. (2002) Aerosol-based direct-write of biological materials for biomedical applications. Materials Research Society

Symposium Proceedings 698. 5.2.1-5.2.7.

I am attaching the picture that I have from this publication.

Thank you for considering this request.
Cynthia Smith

Permission From Author:

Hi Cynthia,

There is no problem with using the schematic as long as you give Optomec proper credit. I believe most people say "Courtesy of Optomec, Inc." or something along those lines. Good luck with your dissertation! And if you have any questions, please feel free to contact me.

Jennifer

Subject: Use of a Picture in Dissertation

I am a Ph.D. student in Biomedical Engineering at the University of Arizona. I am working with a three-dimensional direct-write system to generate viable tissue engineered constructs. In the introduction of my dissertation, I am including a description of other Rapid Prototyping systems for generating 3D tissue engineered constructs and I wanted to know if I could have your permission to include a schematic of the DWB system that was published in Materials Research Society Symposium Proceedings in 2001.

I am attaching the picture that I have from this publication.

Thank you for considering this request.

Cynthia Smith

Jennifer M. Hogans
Optomec Design Company
(505) 761-8250, ext. 1506
3911 Singer Blvd., NE
Albuquerque, NM 87109

PERMISSION TO USE MAPLE-DW SCHEMATIC (FIGURE 1.6)

Permission From Journal – permission request submitted. Waiting for response


13 August 2005 Our ref: HG/SS/Aug 05/J050

Cynthia Smith

University if Arizona

cindy.m.smith@gmail.com

Dear Ms Smith

**BIOMATERIALS, Vol 23, No 1, 2002, pp 161-166, Ringeisen et al, "Generation of mesoscopic…" 1 figure only**

**TRENDS IN BIOTECHNOLOGY, Vol 21, No 4, 2003, pp 157-161, Mironov & Boland, "Organ printing…" 1 figure only**

As per your letter dated 2 August 2005, we hereby grant you permission to reprint the aforementioned material at no charge **in your thesis** subject to the following conditions:

1. If any part of the material to be used (for example, figures) has appeared in our publication with credit or acknowledgement to another source, permission must also be sought from that source. If such permission is not obtained then that material may not be included in your publication/copies.

2. Suitable acknowledgment to the source must be made, either as a footnote or in a reference list at the end of your publication, as follows:

   "Reprinted from Publication title, Vol number, Author(s), Title of article, Pages No., Copyright (Year), with permission from Elsevier".

3. Reproduction of this material is confined to the purpose for which permission is hereby given.

4. This permission is granted for non-exclusive world **English** rights only. For other languages please reapply separately for each one required. Permission excludes use in an electronic form. Should you have a specific electronic project in mind please reapply for permission.

5. This includes permission for UMI to supply single copies, on demand, of the complete thesis. Should your thesis be published commercially, please reapply for permission.

Yours sincerely

Helen Gainford

RIGHTS MANAGER

**Your future requests will be handled more quickly if you complete the online form at www.elsevier.com/locate/permissions**

Permission From Author:

From: Brad Ringeisen <ringeisen@nrl.navy.mil>
Date: Aug 2, 2005 3:36 PM
Subject: Re: Use of a Picture in Dissertation
To: Cindy Smith <cindy.m.smith@gmail.com>

Yes feel free to use this picture, but it's pretty old. Take a look at these PDF's of more recent papers, it's an advancement on MAPLE-DW we now call BioLP for biological laser printing. Feel free to use any of these pictures as well, just reference the work.

What's your DW system look like? Thanks,

Brad

Brad R. Ringeisen, Ph.D.
Research Chemist
Biological Chemistry, Code 6113
Naval Research Laboratory
4555 Overlook Ave. SW
Washington, DC 20375

PH: 202-767-0719
FAX: 202-404-8119
ringeisn@ccs.nrl.navy.mil

----- Original Message -----
From: "Cindy Smith" <cindy.m.smith@gmail.com>
To: <ringeisn@ccs.nrl.navy.mil>
Sent: Monday, August 01, 2005 3:49 PM
Subject: Use of a Picture in Dissertation

I am a Ph.D. student in Biomedical Engineering at the University of Arizona. I am working with a three-dimensional direct-write system to generate viable tissue engineered constructs. In the introduction of my dissertation, I am including a description of other Rapid Prototyping systems for generating 3D tissue engineered constructs.

I wanted to know if I could have your permission to include a schematic of the MAPLE-DW system that was published in Biomaterials 2002.

I am attaching the picture that I have from this publication.

Thank you for considering this request.

Cynthia Smith

## PERMISSION TO USE MODIFIED INK JET SCHEMATICS (FIGURE 1.7)

Permission From Journal

See permission from previous section "Permission to Use MAPLE-DW Schematic (Figure 1.6)". The articles where these figures were found are both handled by Elsevier.

Permission From Author:

On 8/1/05, mironov <mironovv@musc.edu> wrote:
> Dear Cindy,
>
> Of course, you can include. I personally have no any problems with that.
> Technically speaking it is a property (copy rights) of Trends in
> Biotechnology.
> You can also contact with them if you wish.
> However, I am not sure that it is necessary for thesis.
> Good luck with your thesis.
> I would like to have copy of your thesis when it will be ready
> if it is possible.
>
>
> Sincerely,
>
> Vladimir
>
>
> Vladimir Mironov MD, PhD
> Research Associate Professor
> Director of Bioprinter Center
> Dept. of Cell Biology and Anatomy
> Medical University of South Carolina
> 173 Ashley Avenue. Suite 601
> PO 250508
> Charleston, SC 29425
> 843-792-7630 (office)
> 843-792-0664 (fax)
> mironovv@musc.edu
> --On Monday, August 1, 2005 3:54 PM -0400 Cindy Smith
> <cindy.m.smith@gmail.com> wrote:
>
> > I am a Ph.D. student in Biomedical Engineering at the University of

> > Arizona. We met a few years ago when my advisor, Stu Williams, invited
> > you out for a talk in our BME seminar series. I am just now trying to
> > finish up my dissertation working with the BAT, our 3D direct-write
> > system. In the introduction of my dissertation, I am including a
> > description of other Rapid Prototyping systems for generating 3D
> > tissue engineered constructs.
> >
> > I wanted to know if I could have your permission to include a
> > schematic of the modified ink-jet system that was published in Trends
> > in Biotechnology 2003.
> >
> > I am attaching the picture that I have from this publication.
> >
> > I hope all is well with you in Charleston! Thank you for considering
> > this request.
> >
> > Cynthia Smith

PERMISSION TO USE SCIPERIO BACTERIA IMAGES (FIGURE 1.9)

> Dear Ms. Smith:
>
> Permission is granted for you to use the below referenced figure,
> provided you cite the source and contact the author directly.
>
> If you need further assistance, feel free to contact me.
>
> Bonnie Darr
>
> -----Original Message-----
> From: Cindy Smith [mailto:cindy.m.smith@gmail.com]
> Sent: Monday, August 08, 2005 8:43 PM
> To: MRS E-Proceedings
> Subject: Another Request for Use of Image in Dissertation Introduction
>
> I apologize for not including this reference with my first request. I
> noticed that there is one more figure that I would like to use in my
> dissertation introduction. This is a picture of printed bacteria using
> the Biological Architecture Tool.
>
> The reference for this article is as follows: Kachurin, A.M., Stewart,
> R.L., Church, K.H., Warren, W.L., Fisher, J.P., Mikos, A.G., Kraeft,
> S.K., & Chen, L.B. (2002) Direct-write construction of
> tissue-engineered scaffolds. Materials Research Society Symposium
> Proceedings 698. Q5.5.1-Q5.5.6.
>
> I am attaching the picture that I have from this publication.
>
> Thank you for considering this request.
> Cynthia Smith
>
>

Permission To Use Figures from Tissue Engineering (Figures 2.1-2.6)
On 8/8/05, Ballen, Karen <KBallen@liebertpub.com> wrote:
Permission granted.
Karen Ballen
Manager, Reprint Dept.

> -----Original Message-----
> From: cindyms@u.arizona.edu [mailto:cindyms@u.arizona.edu]
> Sent: Monday, August 08, 2005 3:23 PM
> To: Ballen, Karen
> Subject: LiebertPub Website Customer Question
>
> 8/8/2005 3:23:23 PM
> Name - Cynthia M. Smith
> Position - Doctoral Candidate
> Department - Biomedical Engineering
> Institution/affiliation - University of Arizona
> Address Line1 - 1501 N. Campbell Ave
> City - Tucson
> State - Arizona
> Country - USA
> Zip - 85724
> Email - cindyms@u.arizona.edu
> Phone - 5209717763
> Fax -
> Quesions/Comments - I would like to reuse all of the figures that
> appeared in my paper (reference listed below) in my dissertation.
>
> Sincerely,
> Cynthia Smith
>
> Reference: Smith, CM, Stone, AL, et al. (2004) A Three-Dimensional
> BioAssembly Tool for Generating Viable Tissue Engineered Constructs.
> Tissue Eng 10.1566-1576.
> For Publication - Tissue Engineering
>

PERMISSION TO USE TEM IMAGE OF ENDOTHELIAL CELL LUMEN (FIGURE 6.3)

08/11/05 THU 10:06 FAX 212 327 8589 DIRECTOR R.U. PRESS 001

The Rockefeller
University Press
1114 First Avenue, 4th Floor
New York, New York 10021
(212) 327-8554
Fax (212) 327-8587

August 10, 2005

Ms. Cynthia Smith
Biomedical Engineering Program
University of Arizona
1501 N. Campbell Avenue
Tucson, AZ 85715

Dear Ms. Smith:

We will grant you permission for the print reproduction of JCB – vol: 97, pgs. 153-165, 1983 – fig. 8a as referred to in your letter dated August 8, 2005.

Permission is granted for one time use only. Please write to us each time for permission concerning future editions and translations, as we do not grant blanket permissions.

Since the article is over 10 years old, the author's permission is waived.

Please give suitable acknowledgment to the source in the following manner: Reproduced from **The Journal of Cell Biology, year, vol., pp.** by copyright permission of The Rockefeller University Press.

Sincerely yours,

THE JOURNAL OF
CELL BIOLOGY

JoAnn Greene
Permissions Coordinator

# REFERENCES

Abdul-Karim, M.A., Al Kofahi, K., Brown, E.B., Jain, R.K., & Roysam, B. (2003) Automated tracing and change analysis of angiogenic vasculature from in vivo multiphoton confocal image time series. Microvasc.Res. 66. 113-125.

Aebischer, P., Tresco, P.A., Winn, S.R., Greene, L.A., & Jaeger, C.B. (1991) Long-term cross-species brain transplantation of a polymer-encapsulated dopamine-secreting cell line. Exp.Neurol. 111. 269-275.

Ahlswede, K.M. & Williams, S.K. (1994) Microvascular endothelial cell sodding of 1-mm expanded polytetrafluoroethylene vascular grafts. Arterioscler.Thromb. 14. 25-31.

Al Kofahi, O., Can, A., Lasek, S., Szarowski, D.H., Turner, J.N., & Roysam, B (2003) Algorithms for accurate 3D registration of neuronal images acquired by confocal scanning laser microscopy. J.Microsc. 211. 8-18.

Alberts, B., Bray, D., Lewis, J., Raff, M., Roberts, K., & Watson, J.D. (1994) Molecular Biology of the Cell.3rd. 978-980.

Andersson, H. & van den Berg, A. (2004) Microfabrication and microfluidics for tissue engineering: state of the art and future opportunities. Lab Chip. 4. 98-103.

Anseth, K.S., Metters, A.T., Bryant, S.J., Martens, P.J., Elisseeff, J.H., & Bowman, C.N. (2002) In situ forming degradable networks and their application in tissue engineering and drug delivery. J.Control Release 78. 199-209.

Arthur, W.T., Vernon, R.B., Sage, E.H., & Reed, M.J. (1998) Growth factors reverse the impaired sprouting of microvessels from aged mice. Microvasc.Res. 55. 260-270.

Atala, A. (2000) New methods of bladder augmentation. BJU.Int. 85 Suppl 3. 24-34.

Barichello, J.M., Morishita, M., Takayama, K., & Nagai, T. (1999) Absorption of insulin from pluronic F-127 gels following subcutaneous administration in rats. Int.J.Pharm. 184. 189-198.

Bazaraa, M., Jarvis, J., & Sherali, H. (1990) Linear Programming and Network Flows.2n.

Ben Ze'ev, A., Robinson, G.S., Bucher, N.L., & Farmer, S.R. (1988) Cell-cell and cell-matrix interactions differentially regulate the expression of hepatic and cytoskeletal genes in primary cultures of rat hepatocytes. Proc.Natl.Acad.Sci.U.S.A 85. 2161-2165.

Becker,T.A., Kipke,D.R. , & Brandon,T. (2001) Calcium alginate gel: a biocompatible and mechanically stable polymer for endovascular embolization. J.Biomed.Mater.Res. 54. 76-86.

Becker, T.A. & Kipke, D.R. (2002) Flow properties of liquid calcium alginate polymer injected through medical microcatheters for endovascular embolization. J.Biomed.Mater.Res. 61. 533-540.

Berry, E., Marsden, A., Dalgarno, K.W., Kessel, D., & Scott, D.J. (2002) Flexible tubular replicas of abdominal aortic aneurysms. Proc.Inst.Mech.Eng [H.] 216. 211-214.

Bissell, M.J., Hall, H.G., & Parry, G. (1982) How does the extracellular matrix direct gene expression? J.Theor.Biol. 99. 31-68.

Boland, T., Mironov, V., Gutowska, A., Roth, E.A., & Markwald, R.R. (2003) Cell and organ printing 2: fusion of cell aggregates in three-dimensional gels. Anat.Rec. 272A. 497-502.

Boudreau, N., Myers, C., & Bissell, M.J. (1995) From laminin to lamin: regulation of tissue-specific gene expression by the ECM. Trends Cell Biol. 5. 1-4.

Breier, G., Breviario, F., Caveda, L., Berthier, R., Schnurch, H., Gotsch, U., Vestweber, D., Risau, W., & Dejana, E. (1996) Molecular cloning and expression of murine vascular endothelial-cadherin in early stage development of cardiovascular system. Blood 87. 630-641.

Brown, K.J., Maynes, S.F., Bezos, A., Maguire, D.J., Ford, M.D., & Parish, C.R. (1996) A novel in vitro assay for human angiogenesis. Lab Invest 75. 539-555.

Bucher, D., Scholz, M., Stetter, M., Obermayer, K., & Pfluger, H.J. (2000) Correction methods for three-dimensional reconstructions from confocal images: I. Tissue shrinking and axial scaling. J.Neurosci.Methods 100. 135-143.

Can, A., Al Kofahi, O., Lasek, S., Szarowski, D.H., Turner, J.N., & Roysam, B. (2003) Attenuation correction in confocal laser microscopes: a novel two-view approach. J.Microsc. 211. 67-79.

Can, A., Shen, H., Turner, J.N., Tanenbaum, H.L., & Roysam, B. (1999) Rapid automated tracing and feature extraction from retinal fundus images using direct exploratory algorithms. IEEE Trans.Inf.Technol.Biomed. 3. 125-138.

Cao, Y., Hong, A., Schulten, H., & Post, M.J. (2005) Update on therapeutic neovascularization. Cardiovasc.Res. 65. 639-648.

Carmeliet, P., Lampugnani, M.G., Moons, L., Breviario, F., Compernolle, V., Bono, F., Balconi, G., Spagnuolo, R., Oostuyse, B., Dewerchin, M., Zanetti, A., Angellilo, A., Mattot, V., Nuyens, D., Lutgens, E., Clotman, F., de Ruiter, M.C., Gittenberger-de Groot, A., Poelmann, R., Lupu, F., Herbert, J.M., Collen, D., & Dejana, E. (1999) Targeted deficiency or cytosolic truncation of the VE-cadherin gene in mice impairs VEGF-mediated endothelial survival and angiogenesis. Cell 98. 147-157.

Chawla, M.K., Lin, G., Olson, K., Vazdarjanova, A., Burke, S.N., McNaughton, B.L., Worley, P.F., Guzowski, J.F., Roysam, B., & Barnes, C.A. (2004) 3D-catFISH: a system for automated quantitative three-dimensional compartmental analysis of temporal gene transcription activity imaged by fluorescence in situ hybridization. J.Neurosci.Methods 139. 13-24.

Chen, C.S., Mrksich, M., Huang, S., Whitesides, G.M., & Ingber, D.E. (1997) Geometric control of cell life and death. Science 276. 1425-1428.

Chrisey, D.B., Pique, A., McGill, R.A., Horwitz, J.S., Ringeisen, B.R., Bubb, D.M., & Wu, P.K. (2003) Laser deposition of polymer and biomaterial films. Chem.Rev. 103. 553-576.

Chung, T.W., Yang, J., Akaike, T., Cho, K.Y., Nah, J.W., Kim, S.I., & Cho, C.S. (2002) Preparation of alginate/galactosylated chitosan scaffold for hepatocyte attachment. Biomaterials 23. 2827-2834.

Cohen, A.R., Roysam, B., & Turner, J.N. (1994) Automated tracing and volume measurements of neurons from 3-D confocal fluorescence microscopy data. J.Microsc. 173 ( Pt 2). 103-114.

Colton, C.K. (1995) Implantable biohybrid artificial organs. Cell Transplant. 4. 415-436.

Cooke, M.N., Fisher, J.P., Dean, D., Rimnac, C., & Mikos, A.G. (2003) Use of stereolithography to manufacture critical-sized 3D biodegradable scaffolds for bone ingrowth. J.Biomed.Mater.Res. 64B. 65-69.

Corbisier, P. (1997) Bacterial metal-lux biosensors for a rapid determination of the heavy metal bioavailability and toxicity in solid samples. Res.Microbiol. 148. 534-536.

Crouch, M.F. (2000) An automated fluorescence based assay of neurite formation. J.Neurosci.Methods 104. 87-91.

Curodeau, A., Sachs, E., & Caldarise, S. (2000) Design and fabrication of cast orthopedic implants with freeform surface textures from 3-D printed ceramic shell. J.Biomed.Mater.Res. 53. 525-535.

Dailey, S.W., Rose, D.G., Carabasi, R.A., Ahlswede, K., & Williams, S.K. (1991) Origin of Cells that Line Damaged Native Blood Vessels Following Endothelial Cell Transplantation. American Journal of Surgery. 162. 107-110.

Dang, W., Daviau, T., & Brem, H. (1996) Morphological characterization of polyanhydride biodegradable implant gliadel during in vitro and in vivo erosion using scanning electron microscopy. Pharm.Res. 13. 683-691.

Dar, A., Shachar, M., Leor, J., & Cohen, S. (2002) Optimization of cardiac cell seeding and distribution in 3D porous alginate scaffolds. Biotechnol.Bioeng. 80. 305-312.

DeFouw, D.O., Rizzo, V.J., Steinfeld, R., & Feinberg, R.N. (1989) Mapping of the microcirculation in the chick chorioallantoic membrane during normal angiogenesis. Microvasc.Res. 38. 136-147.

del Zoppo, G.J. (1994) Microvascular changes during cerebral ischemia and reperfusion. Cerebrovasc.Brain Metab Rev. 6. 47-96.

del Zoppo, G.J. & Mabuchi, T. (2003) Cerebral microvessel responses to focal ischemia. J.Cereb.Blood Flow Metab 23. 879-894.

Dellas, A., Moch, H., Schultheiss, E., Feichter, G., Almendral, A.C., Gudat, F., & Torhorst, J. (1997) Angiogenesis in cervical neoplasia: microvessel quantitation in precancerous lesions and invasive carcinomas with clinicopathological correlations. Gynecol.Oncol. 67. 27-33.

Dellian, M., Witwer, B.P., Salehi, H.A., Yuan, F., & Jain, R.K. (1996) Quantitation and physiological characterization of angiogenic vessels in mice: effect of basic fibroblast growth factor, vascular endothelial growth factor/vascular permeability factor, and host microenvironment. Am.J.Pathol. 149. 59-71.

Desai, S.D. & Blanchard, J. (1998) In vitro evaluation of pluronic F127-based controlled-release ocular delivery systems for pilocarpine. J.Pharm.Sci. 87. 226-230.

Desai, S.D. & Blanchard, J. (2000) Pluronic F127-based ocular delivery system containing biodegradable polyisobutylcyanoacrylate nanocapsules of pilocarpine. Drug Deliv. 7. 201-207.

Desai, T.A., West, T., Cohen, M., Boiarski, T., & Rampersaud, A. (2004) Nanoporous microsystems for islet cell replacement. Adv.Drug Deliv.Rev. 56. 1661-1673.

Edelman, G.M. & Crossin, K.L. (1991) Cell adhesion molecules: implications for a molecular histology. Annu.Rev.Biochem. 60. 155-190.

Edsman, K., Carlfors, J., & Petersson, R. (1998) Rheological evaluation of poloxamer as an in situ gel for ophthalmic use. Eur.J.Pharm.Sci. 6. 105-112.

Endrich, B., Reinhold, H.S., Gross, J.F., & Intaglietta, M. (1979) Tissue perfusion inhomogeneity during early tumor growth in rats. J.Natl.Cancer Inst. 62. 387-395.

Folkman, J. & Haudenschild, C. (1980) Angiogenesis in vitro. Nature 288. 551-556.

Folkman, J. & Hochberg, M. (1973) Self-regulation of growth in three dimensions. J.Exp.Med. 138. 745-753.

Fournier, E., Passirani, C., Montero-Menei, C.N., & Benoit, J.P. (2003) Biocompatibility of implantable synthetic polymeric drug carriers: focus on brain biocompatibility. Biomaterials 24. 3311-3331.

Frangi, A.F., Niessen, W.J., Hoogeveen, R.M., van Walsum, T., & Viergever, M.A. (1999) Model-based quantitation of 3-D magnetic resonance angiographic images. IEEE Trans.Med.Imaging 18. 946-956.

Freedman, S.B. & Isner, J.M. (2001) Therapeutic angiogenesis for ischemic cardiovascular disease. J.Mol.Cell Cardiol. 33. 379-393.

Freyman, T.M., Yannas, I.V., Yokoo, R., & Gibson, L.J. (2001) Fibroblast contraction of a collagen-GAG matrix. Biomaterials 22. 2883-2891.

Garellick, G., Malchau, H., Regner, H., & Herberts, P. (1999) The Charnley versus the Spectron hip prosthesis: radiographic evaluation of a randomized, prospective study of 2 different hip implants. J.Arthroplasty 14. 414-425.

Garey, M.R. & Johnson, D.S. (1979) Computers and Intractability: A Guide to the Theory of NP-Completeness.1st.

Geiger, B. & Ayalon, O. (1992) Cadherins. Annu.Rev.Cell Biol. 8. 307-332.

Glicklis, R., Shapiro, L., Agbaria, R., Merchuk, J.C., & Cohen, S. (2000) Hepatocyte behavior within three-dimensional porous alginate scaffolds. Biotechnol.Bioeng. 67. 344-353.

Gronet, P.M., Waskewicz, G.A., & Richardson, C. (2003) Preformed acrylic cranial implants using fused deposition modeling: A clinical report. J.Prosthet.Dent. 90. 429-433.

Guest, J.D., Rao, A., Olson, L., Bunge, M.B., & Bunge, R.P. (1997) The ability of human Schwann cell grafts to promote regeneration in the transected nude rat spinal cord. Exp.Neurol. 148. 502-522.

Guo, L., Burke, P., Lo, S.H., Gandour-Edwards, R., & Lau, D. (2001) Quantitative analysis of angiogenesis using confocal laser scanning microscopy. Angiogenesis. 4. 187-191.

Han, B., Huang, L.L.H., Cheung, D., Cordoba, F., & Nimni, M. (1999) Polypeptide growth factors with a collagen binding domain: Their potential for tissue repair and organ regeneration. 287-299.

Hauschka, S.D. & Konigsberg, I.R. (1966) The influence of collagen on the development of muscle clones. Proc.Natl.Acad.Sci.U.S.A 55. 119-126.

Hay, E.D. (1977) Interaction between the cell surface and extracellular matrix in corneal development. Soc.Gen.Physiol Ser. 32. 115-137.

He, W., Hamilton, T.A., Cohen, A.R., Holmes, T.J., Pace, C., Szarowski, D.H., Turner, J.N., & Roysam, B. (2003) Automated three-dimensional tracing of neurons in confocal and brightfield images. Microsc.Microanal. 9. 296-310.

Heath, C.A. (2000) Cells for tissue engineering. Trends Biotechnol. 18. 17-19.

Henning, R.J., Abu-Ali, H., Balis, J.U., Morgan, M.B., Willing, A.E., & Sanberg, P.R. (2004) Human umbilical cord blood mononuclear cells for the treatment of acute myocardial infarction. Cell Transplant. 13. 729-739.

Hirschi, K.K., Rohovsky, S.A., Beck, L.H., Smith, S.R., & D'Amore, P.A. (1999) Endothelial cells modulate the proliferation of mural cell precursors via platelet-derived growth factor-BB and heterotypic cell contact. Circ.Res. 84. 298-305.

Hirschi, K.K., Rohovsky, S.A., & D'Amore, P.A. (1998) PDGF, TGF-beta, and heterotypic cell-cell interactions mediate endothelial cell-induced recruitment of 10T1/2 cells and their differentiation to a smooth muscle fate. J.Cell Biol. 141. 805-814.

Hoch, J., Jarrell, B.E., Schneider, T., & Williams, S.K. (1989) Endothelial cell interactions with native surfaces. Ann.Vasc.Surg. 3. 153-159.

Hoerstrup, S.P., Sodian, R., Daebritz, S., Wang, J., Bacha, E.A., Martin, D.P., Moran, A.M., Guleserian, K.J., Sperling, J.S., Kaushal, S., Vacanti, J.P., Schoen, F.J., & Mayer, J.E., Jr. (2000) Functional living trileaflet heart valves grown in vitro. Circulation 102. III44-III49.

Hoying, J.B., Boswell, C.A., & Williams, S.K. (1996) Angiogenic potential of microvessel fragments established in three-dimensional collagen gels. In Vitro Cell Dev.Biol.Anim 32. 409-419.

Ingber, D. (1991) Extracellular matrix and cell shape: potential control points for inhibition of angiogenesis. J.Cell Biochem. 47. 236-241.

Iruela-Arispe, M.L., Hasselaar, P., & Sage, H. (1991) Differential expression of extracellular proteins is correlated with angiogenesis in vitro. Lab Invest 64. 174-186.

Itoh, M., Nagafuchi, A., Moroi, S., & Tsukita, S. (1997) Involvement of ZO-1 in cadherin-based cell adhesion through its direct binding to alpha catenin and actin filaments. J.Cell Biol. 138. 181- 192.

Jarrell, B.E. & Williams, S.K. (1991) Microvessel derived endothelial cell isolation, adherence, and monolayer formation for vascular grafts. J.Vasc.Surg. 13. 733-734.

Jarrell, B.E., Williams, S.K., Rose, D., Garibaldi, D., Talbot, C., & Kapelan, B. (1991) Optimization of human endothelial cell attachment to vascular graft polymers. J.Biomech.Eng 113. 120-122.

Jarrell, B.E., Williams, S.K., Solomon, L., Speicher, L., Koolpe, E., Radomski, J., Carabasi, R.A., Greener, D., & Rosato, F.E. (1986) Use of an endothelial monolayer on a vascular graft prior to implantation. Temporal dynamics and compatibility with the operating room. Ann.Surg. 203. 671-678.

Johnston, T.P., Punjabi, M.A., & Froelich, C.J. (1992) Sustained delivery of interleukin-2 from a poloxamer 407 gel matrix following intraperitoneal injection in mice. Pharm.Res. 9. 425-434.

Juliano, R.L. (2002) Signal transduction by cell adhesion receptors and the cytoskeleton: functions of integrins, cadherins, selectins, and immunoglobulin-superfamily members. Annu.Rev.Pharmacol.Toxicol. 42. 283-323.

Kachurin, A.M., Stewart, R.L., Church, K.H., Warren, W.L., Fisher, J.P., Mikos, A.G., Kraeft, S.K., & Chen, L.B. (2002) Direct-write construction of tissue-engineered scaffolds. Materials Research Society Symposium Proceedings 698. Q5.5.1-Q5.5.6.

Katstra, W.E., Palazzolo, R.D., Rowe, C.W., Giritlioglu, B., Teung, P., & Cima, M.J. (2000) Oral dosage forms fabricated by three dimensional printing. J.Control Release 66. 1-9.

Kellar, R.S., Kleinert, L.B., & Williams, S.K. (2002) Characterization of angiogenesis and inflammation surrounding ePTFE implanted on the epicardium. J.Biomed.Mater.Res. 61. 226-233.

Kellar, R.S., Landeen, L.K., Shepherd, B.R., Naughton, G.K., Ratcliffe, A., & Williams, S.K. (2001) Scaffold-based three-dimensional human fibroblast culture provides a

structural matrix that supports angiogenesis in infarcted heart tissue. Circulation 104. 2063-2068.

Kidd, K.R., Nagle, R.B., & Williams, S.K. (2002) Angiogenesis and neovascularization associated with extracellular matrix-modified porous implants. J.Biomed.Mater.Res. 59. 366-377.

Kirchner, L.M., Schmidt, S.P., & Gruber, B.S. (1996) Quantitation of angiogenesis in the chick chorioallantoic membrane model using fractal analysis. Microvasc.Res. 51. 2-14.

Kittler, J. & Illingworth, J. (1986) Minimum Error Thresholding. Pattern Recognition 19. 41-47.

Kleinman, H.K., McGarvey, M.L., Liotta, L.A., Robey, P.G., Tryggvason, K., & Martin, G.R. (1982) Isolation and characterization of type IV procollagen, laminin, and heparan sulfate proteoglycan from the EHS sarcoma. Biochemistry 21. 6188-6193.

Koike, N., Fukumura, D., Gralla, O., Au, P., Schechner, J.S., & Jain, R.K. (2004) Tissue engineering: Creation of long-lasting blood vessels. Nature 428. 138-139.

Kurzen, H., Manns, S., Dandekar, G., Schmidt, T., Pratzel, S., & Kraling, B.M. (2002) Tightening of endothelial cell contacts: a physiologic response to cocultures with smooth-muscle-like 10T1/2 cells. J.Invest Dermatol. 119. 143-153.

Lalan, S., Pomerantseva, I., & Vacanti, J.P. (2001) Tissue engineering and its potential impact on surgery. World J.Surg. 25. 1458-1466.

Langer, R. & Vacanti, J.P. (1993) Tissue engineering. Science 260. 920-926.

Langer, R.S. & Vacanti, J.P. (1999) Tissue engineering: the challenges ahead. Sci.Am. 280. 86-89.

Lanza, R.P., Langer, R., & Vacanti, J.P. (2000) Tissue Engineering. 2nd Edition.

Larue, L., Antos, C., Butz, S., Huber, O., Delmas, V., Dominis, M., & Kemler, R. (1996) A role for cadherins in tissue formation. Development 122. 3185-3194.

Lavik, E. & Langer, R. (2004) Tissue engineering: current state and perspectives. Appl.Microbiol.Biotechnol. 65. 1-8.

Lee, C.H., Singla, A., & Lee, Y. (2001) Biomedical applications of collagen. Int.J.Pharm. 221. 1-22.

Lenander, C. & Holmgren, L. (1999) A novel method of visualizing vessels in human tumor biopsies. Angiogenesis. 3. 291-293.

Leong, K.F., Phua, K.K., Chua, C.K., Du, Z.H., & Teo, K.O. (2001) Fabrication of porous polymeric matrix drug delivery devices using the selective laser sintering technique. Proc.Inst.Mech.Eng [H.] 215. 191-201.

Lermusiaux, P., Leroux, C., Tasse, J.C., Castellani, L., & Martinez, R. (2001) Aortic aneurysm: construction of a life-size model by rapid prototyping. Ann.Vasc.Surg. 15. 131-135.

Li, V.W., Folkerth, R.D., Watanabe, H., Yu, C., Rupnick, M., Barnes, P., Scott, R.M., Black, P.M., Sallan, S.E., & Folkman, J. (1994) Microvessel count and cerebrospinal fluid basic fibroblast growth factor in children with brain tumours. Lancet 344. 82-86.

Lin, G., Adiga, U., Olson, K., Guzowski, J.F., Barnes, C.A., & Roysam, B. (2003) A hybrid 3D watershed algorithm incorporating gradient cues and object models for automatic segmentation of nuclei in confocal image stacks. Cytometry A 56. 23 -36.

Lin, G., Bjornsson, C.S., Smith, K.L., Abdul-Karim, M.A., Turner, J.N., Shain, W., & Roysam, B. (2005a) Automated image analysis methods for 3-D quantification of the neurovascular unit from multichannel confocal microscope images. Cytometry A 66. 9-23.

Lin, G., Chawla, M.K., Olson, K., Guzowski, J.F., Barnes, C.A., & Roysam, B. (2005b) Hierarchical, model-based merging of multiple fragments for improved three-dimensional segmentation of nuclei. Cytometry A 63. 20-33.

Lindvall, O., Kokaia, Z., & Martinez-Serrano, A. (2004) Stem cell therapy for human neurodegenerative disorders-how to make it work. Nat.Med. 10 Suppl. S42-S50.

Lindvall, O., Rehncrona, S., Brundin, P., Gustavii, B., Astedt, B., Widner, H., Lindholm, T., Bjorklund, A., Leenders, K.L., Rothwell, J.C., &. (1990) Neural transplantation in Parkinson's disease: the Swedish experience. Prog.Brain Res. 82. 729-734.

Liu, S., Peulve, P., Jin, O., Boisset, N., Tiollier, J., Said, G., & Tadie, M. (1997) Axonal regrowth through collagen tubes bridging the spinal cord to nerve roots. J.Neurosci.Res. 49. 425-432.

Lysaght, M.J. & Aebischer, P. (1999) Encapsulated Cells as Therapy. Sci.Am. 280. 76-82.

Madri, J.A. & Pratt, B.M. (1986) Endothelial cell-matrix interactions: in vitro models of angiogenesis. J.Histochem.Cytochem. 34. 85-91.

Madri, J.A. & Williams, S.K. (1983) Capillary endothelial cell cultures: phenotypic modulation by matrix components. J.Cell Biol. 97. 153-165.

Marijnissen, A.C. & Lafeber, F.P. (2003) Re: E. B. Hunziker. Articular cartilage repair: basic science and clinical progress. A review of the current status and prospects. Osteoarthritis and Cartilage 2002; 10:432-63. Osteoarthritis.Cartilage. 11. 300 -301.

Marquez, G.J., Renn, M.J., & Miller, W.D. (2002) Aerosol-based direct-write of biological materials for biomedical applications. Materials Research Society Symposium Proceedings 698. Q5.2.1-Q5.2.7.

Matsumura, T., Wolff, K., & Petzelbauer, P. (1997) Endothelial cell tube formation depends on cadherin 5 and CD31 interactions with filamentous actin. J.Immunol. 158. 3408-3416.

McDevitt, T.C., Angello, J.C., Whitney, M.L., Reinecke, H., Hauschka, S.D., Murry, C.E., & Stayton, P.S. (2002) In vitro generation of differentiated cardiac myofibers on micropatterned laminin surfaces. J.Biomed.Mater.Res. 60. 472-479.

Melican, M.C., Zimmerman, M.C., Dhillon, M.S., Ponnambalam, A.R., Curodeau, A., & Parsons, J.R. (2001) Three-dimensional printing and porous metallic surfaces: a new orthopedic application. J.Biomed.Mater.Res. 55. 194-202.

Mironov, V., Boland, T., Trusk, T., Forgacs, G., & Markwald, R.R. (2003) Organ printing: computer-aided jet-based 3D tissue engineering. Trends Biotechnol. 21. 157-161.

Miyazaki, S., Tobiyama, T., Takada, M., & Attwood, D. (1995) Percutaneous absorption of indomethacin from pluronic F127 gels in rats. J.Pharm.Pharmacol. 47. 455-457.

Miyazaki, S., Yokouchi, C., Nakamura, T., Hashiguchi, N., Hou, W.M., & Takada, M. (1986) Pluronic F-127 gels as a novel vehicle for rectal administration of indomethacin. Chem.Pharm.Bull. (Tokyo) 34. 1801-1808.

Montesano, R., Orci, L., & Vassalli, P. (1983) In vitro rapid organization of endothelial cells into capillary-like networks is promoted by collagen matrices. J.Cell Biol. 97. 1648-1652.

Mooney, D.J., Organ, G., Vacanti, J.P., & Langer, R. (1994) Design and fabrication of biodegradable polymer devices to engineer tubular tissues. Cell Transplant. 3. 203-210.

Morikawa, K., Okada, F., Hosokawa, M., & Kobayashi, H. (1987) Enhancement of therapeutic effects of recombinant interleukin 2 on a transplantable rat fibrosarcoma by the use of a sustained release vehicle, pluronic gel. Cancer Res. 47. 37-41.

Mosahebi, A., Simon, M., Wiberg, M., & Terenghi, G. (2001) A novel use of alginate hydrogel as Schwann cell matrix. Tissue Eng 7. 525-534.

Mrksich, M., Chen, C.S., Xia, Y., Dike, L.E., Ingber, D.E., & Whitesides, G.M. (1996) Controlling cell attachment on contoured surfaces with self-assembled monolayers of alkanethiolates on gold. Proc.Natl.Acad.Sci.U.S.A 93. 10775-10778.

Mrksich, M. & Whitesides, G.M. (1996) Using self-assembled monolayers to understand the interactions of man-made surfaces with proteins and cells. Annu.Rev.Biophys.Biomol.Struct. 25. 55-78.

Murayama, A., Matsuzaki, Y., Kawaguchi, A., Shimazaki, T., & Okano, H. (2002) Flow cytometric analysis of neural stem cells in the developing and adult mouse brain. J.Neurosci.Res. 69. 837-847.

Nicosia, R.F. & Ottinetti, A. (1990a) Growth of microvessels in serum-free matrix culture of rat aorta. A quantitative assay of angiogenesis in vitro. Lab Invest 63. 115 - 122.

Nicosia, R.F. & Ottinetti, A. (1990b) Modulation of microvascular growth and morphogenesis by reconstituted basement membrane gel in three-dimensional cultures of rat aorta: a comparative study of angiogenesis in matrigel, collagen, fibrin, and plasma clot. In Vitro Cell Dev.Biol. 26. 119-128.

Nicosia, R.F., Tchao, R., & Leighton, J. (1982) Histotypic angiogenesis in vitro: light microscopic, ultrastructural, and radioautographic studies. In Vitro 18. 538-549.

Nör, J.E., Peters, M.C., Christensen, J.B., Sutorik, M.M., Linn, S., Khan, M.K., Addison, C.L., Mooney, D.J., & Polverini, P.J. (2001) Engineering and characterization of functional human microvessels in immunodeficient mice. Lab Invest 81. 453- 463.

Novikova, L.N., Novikov, L.N., & Kellerth, J.O. (2003) Biopolymers and biodegradable smart implants for tissue regeneration after spinal cord injury. Curr.Opin.Neurol. 16. 711-715.

Oliva, A.A., Jr., James, C.D., Kingman, C.E., Craighead, H.G., & Banker, G.A. (2003) Patterning axonal guidance molecules using a novel strategy for microcontact printing. Neurochem.Res. 28. 1639-1648.

Page-McCaw, A., Serano, J., Sante, J.M., & Rubin, G.M. (2003) Drosophila matrix metalloproteinases are required for tissue remodeling, but not embryonic development. Dev.Cell 4. 95-106.

Pan, W.J., Haut, P.R., Olszewski, M., & Kletzel, M. (1999) Two-day collection and pooling of peripheral blood stem cells with semiautomated density gradient cell separation. J.Hematother.Stem Cell Res. 8. 561-564.

Pancrazio, J.J., Whelan, J.P., Borkholder, D.A., Ma, W., & Stenger, D.A. (1999) Development and application of cell-based biosensors. Ann.Biomed.Eng 27. 697-711.

Pardanaud, L., Yassine, F., & Dieterlen-Lievre, F. (1989) Relationship between vasculogenesis, angiogenesis and haemopoiesis during avian ontogeny. Development 105. 473-485.

Park, A., Wu, B., & Griffith, L.G. (1998) Integration of surface modification and 3D fabrication techniques to prepare patterned poly (L-lactide) substrates allowing regionally selective cell adhesion. J.Biomater.Sci.Polym.Ed 9. 89-110.

Park, J.A., Choi, K.S., Kim, S.Y., & Kim, K.W. (2003) Coordinated interaction of the vascular and nervous systems: from molecule- to cell-based approaches. Biochem.Biophys.Res.Commun. 311. 247- 253.

Patel, N., Bhandari, R., Shakesheff, K.M., Cannizzaro, S.M., Davies, M.C., Langer, R., Roberts, C.J., Tendler, S.J., & Williams, P.M. (2000) Printing patterns of biospecifically-adsorbed protein. J.Biomater.Sci.Polym.Ed 11. 319-331.

Patel, N., Padera, R., Sanders, G.H., Cannizzaro, S.M., Davies, M.C., Langer, R., Roberts, C.J., Tendler, S.J., Williams, P.M., & Shakesheff, K.M. (1998) Spatially controlled cell engineering on biodegradable polymer surfaces. FASEB J. 12. 1447-1454.

Pec, E.A., Wout, Z.G., & Johnston, T.P. (1992) Biological activity of urease formulated in poloxamer 407 after intraperitoneal injection in the rat. J.Pharm.Sci. 81. 626-630.

Pentecost, J.O., Sahn, D.J., Thornburg, B.L., Gharib, M., Baptista, A., & Thornburg, K.L. (2001) Graphical and stereolithographic models of the developing human heart lumen. Comput.Med.Imaging Graph. 25. 459-463.

Post, M.J., Laham, R., Sellke, F.W., & Simons, M. (2001) Therapeutic angiogenesis in cardiology using protein formulations. Cardiovasc.Res. 49. 522-531.

Ptitsyn, L.R., Horneck, G., Komova, O., Kozubek, S., Krasavin, E.A., Bonev, M., & Rettberg, P. (1997) A biosensor for environmental genotoxin screening based on an SOS lux assay in recombinant Escherichia coli cells. Appl.Environ.Microbiol. 63. 4377-4384.

Ramanathan, S., Ensor, M., & Daunert, S. (1997) Bacterial biosensors for monitoring toxic metals. Trends Biotechnol. 15. 500-506.

Ringeisen, B.R., Chrisey, D.B., Pique, A., Young, H.D., Jones-Meehan, J., Modi, R., Bucaro, M., & Spargo, B.J. (2002a) Generation of mesoscopic patterns of viable Escherichia coli by ambient laser transfer. Biomaterials 23. 161-166.

Ringeisen, B.R., Heungsoo, K., Young, H.D., Spargo, B.J., Auyeung, R.C.Y., Pique, A., & Chrisey, D. (2002b) Cell-by-cell construction of living tissue. Materials Research Society Symposium Proceedings 698. Q5.1.1-Q5.1.13.

Ringeisen, B.R., Kim, H., Barron, J.A., Krizman, D.B., Chrisey, D.B., Jackman, S., Auyeung, R.Y., & Spargo, B.J. (2004) Laser printing of pluripotent embryonal carcinoma cells. Tissue Eng 10. 483-491.

Risau, W., Sariola, H., Zerwes, H.G., Sasse, J., Ekblom, P., Kemler, R., & Doetschman, T. (1988) Vasculogenesis and angiogenesis in embryonic-stem-cell-derived embryoid bodies. Development 102. 471-478.

Rowe, C.W., Katstra, W.E., Palazzolo, R.D., Giritlioglu, B., Teung, P., & Cima, M.J. (2000) Multimechanism oral dosage forms fabricated by three dimensional printing. J.Control Release 66. 11-17.

Rowley, J.A. & Mooney, D.J. (2002) Alginate type and RGD density control myoblast phenotype. J.Biomed.Mater.Res. 60. 217-223.

Sato, Y., Nakajima, S., Shiraga, N., Atsumi, H., Yoshida, S., Koller, T., Gerig, G., & Kikinis, R. (1998) Three-dimensional multi-scale line filter for segmentation and visualization of curvilinear structures in medical images. Med.Image Anal. 2. 143-168.

Sattar, S., Abbas, B., Jones, L., Saridogan, E., Mahmood, T., Mehta, J., & Djahanbakhch, O. (1999) Comparison of the growth patterns and morphological characteristics of mechanically and enzymatically isolated fallopian tube epithelial cells. Cell Biol.Int. 23. 379-383.

Saunders, R., Derby, B., Gough, J., & Reis, N. (2004) Ink-jet printing of human cells. Materials Research Society Symposium Proceedings EXS-1. F6.3.1-F6.3.3.

Sayers, R.D., Raptis, S., Berce, M., & Miller, J.H. (1998) Long-term results of femorotibial bypass with vein or polytetrafluoroethylene. Br.J.Surg. 85. 934-938.

Schechner, J.S., Nath, A.K., Zheng, L., Kluger, M.S., Hughes, C.C., Sierra-Honigmann, M.R., Lorber, M.I., Tellides, G., Kashgarian, M., Bothwell, A.L., & Pober, J.S. (2000) In vivo formation of complex microvessels lined by human endothelial cells in an immunodeficient mouse. Proc.Natl.Acad.Sci.U.S.A 97. 9191-9196.

Schmidt, C.E. & Baier, J.M. (2000) Acellular vascular tissues: natural biomaterials for tissue repair and tissue engineering. Biomaterials 21. 2215-2231.

Senger, D.R., Claffey, K.P., Benes, J.E., Perruzzi, C.A., Sergiou, A.P., & Detmar, M. (1997) Angiogenesis promoted by vascular endothelial growth factor: regulation through alpha1beta1 and alpha2beta1 integrins. Proc.Natl.Acad.Sci.U.S.A 94. 13612-13617.

Shepherd, B.R., Chen, H.Y., Smith, C.M., Gruionu, G., Williams, S.K., & Hoying, J.B. (2004) Rapid Perfusion and Network Remodeling in a Microvascular Construct After Implantation. Arterioscler.Thromb.Vasc.Biol. 24. 898-904.

Sherwood, J.K., Riley, S.L., Palazzolo, R., Brown, S.C., Monkhouse, D.C., Coates, M., Griffith, L.G., Landeen, L.K., & Ratcliffe, A. (2002) A three-dimensional osteochondral composite scaffold for articular cartilage repair. Biomaterials 23. 4739-4751.

Shibuya, Y., Mizoguchi, A., Takeichi, M., Shimada, K., & Ide, C. (1995) Localization of N-cadherin in the normal and regenerating nerve fibers of the chicken peripheral nervous system. Neuroscience 67. 253-261.

Shieh, S.J. & Vacanti, J.P. (2005) State-of-the-art tissue engineering: from tissue engineering to organ building. Surgery 137. 1-7.

Shotton, D. & White, N. (1989) Confocal scanning microscopy: three-dimensional biological imaging. Trends Biochem.Sci. 14. 435-439.

Smith, C.M., Stone, A.L., Parkhill, R.L., Stewart, R.L., Simpkins, M.W., Kachurin, A.M., Warren, W.L., & Williams, S.K. (2004) A Three-Dimensional BioAssembly Tool for Generating Viable Tissue Engineered Constructs. Tissue Eng 10.1566-1576.

Sodian, R., Hoerstrup, S.P., Sperling, J.S., Daebritz, S., Martin, D.P., Moran, A.M., Kim, B.S., Schoen, F.J., Vacanti, J.P., & Mayer, J.E., Jr. (2000a) Early in vivo experience with tissue-engineered trileaflet heart valves. Circulation 102. III22-III29.

Sodian, R., Hoerstrup, S.P., Sperling, J.S., Daebritz, S.H., Martin, D.P., Schoen, F.J., Vacanti, J.P., & Mayer, J.E., Jr. (2000b) Tissue engineering of heart valves: in vitro experiences. Ann.Thorac.Surg. 70. 140-144.

Sodian, R., Lemke, T., Fritsche, C., Hoerstrup, S.P., Fu, P., Potapov, E.V., Hausmann, H., & Hetzer, R. (2002a) Tissue-engineering bioreactors: a new combined cell-seeding and perfusion system for vascular tissue engineering. Tissue Eng 8. 863-870.

Sodian, R., Loebe, M., Hein, A., Martin, D.P., Hoerstrup, S.P., Potapov, E.V., Hausmann, H., Lueth, T., & Hetzer, R. (2002b) Application of stereolithography for scaffold fabrication for tissue engineered heart valves. ASAIO J. 48. 12-16.

Sodian, R., Sperling, J.S., Martin, D.P., Stock, U., Mayer, J.E., Jr., & Vacanti, J.P. (1999) Tissue engineering of a trileaflet heart valve-early in vitro experiences with a combined polymer. Tissue Eng 5. 489-494.

Sonka, M., Hlavac, V., & Boye, R. (1998) Image Processing, Analysis, and Machine Vision. 2nd Edition.

Stratton, L.P., Dong, A., Manning, M.C., & Carpenter, J.F. (1997) Drug delivery matrix containing native protein precipitates suspended in a poloxamer gel. J.Pharm.Sci. 86. 1006-1010.

Streekstra, G.J. & van Pelt, J. (2002) Analysis of tubular structures in three-dimensional confocal images. Network. 13. 381-395.

Takeichi, M. (1995) Morphogenetic roles of classic cadherins. Curr.Opin.Cell Biol. 7. 619-627.

Thomas, T.E., Miller, C.L., & Eaves, C.J. (1999) Purification of hematopoietic stem cells for further biological study. Methods 17. 202-218.

Umesh Adiga, P.S. (2002) An integrated system for feature evaluation of 3D images of a tissue specimen. Anal.Cell Pathol. 24. 47-58.

Umesh Adiga, P.S. & Chaudhuri, B.B. (1999) Deformable models for segmentation of CLSM tissue images and its application in FISH signal analysis. Anal.Cell Pathol. 18. 211-225.

Umesh Adiga, P.S. & Chaudhuri, B.B. (2001) Some efficient methods to correct confocal images for easy interpretation. Micron. 32. 363-370.

US Dept of Health and Human Services. (2003) Frequently Asked Questions about Organ Donation and Transplantation. http://www.4woman.gov/faq/organ_donation.htm.

Vacanti, J.P. & Langer, R. (1999) Tissue engineering: the design and fabrication of living replacement devices for surgical reconstruction and transplantation. Lancet 354 Suppl 1. SI32-SI34.

Vaissiere, G., Chevallay, B., Herbage, D., & Damour, O. (2000) Comparative analysis of different collagen-based biomaterials as scaffolds for long-term culture of human fibroblasts. Med.Biol.Eng Comput. 38. 205-210.

Vanezi, P., Vanezis, M., McCombe, G., & Niblett, T. (2000) Facial reconstruction using 3-D computer graphics. Forensic Sci.Int. 108. 81-95.

Vert, M., Schwach, G., Engel, R., & Coudane, J. (1998) Something new in the field of PLA/GA bioresorbable polymers? J.Control Release 53. 85-92.

Vittet, D., Buchou, T., Schweitzer, A., Dejana, E., & Huber, P. (1997) Targeted null-mutation in the vascular endothelial-cadherin gene impairs the organization of vascular-like structures in embryoid bodies. Proc.Natl.Acad.Sci.U.S.A 94. 6273-6278.

Vozzi, G., Previti, A., De Rossi, D., & Ahluwalia, A. (2002) Microsyringe-based deposition of two-dimensional and three-dimensional polymer scaffolds with a well-defined geometry for application to tissue engineering. Tissue Eng 8. 1089-1098.

Wagner, R.C. & Matthews, M.A. (1975) The isolation and culture of capillary endothelium from epididymal fat. Microvasc.Res. 10. 286-297.

Wessells, H. & Williams, S.K. (1999) Endothelial cell transplantation into the corpus cavernosum: moving towards cell-based gene therapy. J.Urol. 162. 2162-2164.

Wessells, N.K. & Cohen, J.H. (1968) Effects of collagenase on developing epithelia in vitro: lung, ureteric bud, and pancreas. Dev.Biol. 18. 294-309.

Whitesides, G.M., Ostuni, E., Takayama, S., Jiang, X., & Ingber, D.E. (2001) Soft lithography in biology and biochemistry. Annu.Rev.Biomed.Eng 3. 335-373.

Williams, S.K., Rose, D.G., & Jarrell, B.E. (1994) Microvascular endothelial cell sodding of ePTFE vascular grafts: improved patency and stability of the cellular lining. J.Biomed.Mater.Res. 28. 203-212.

Wilson, W.C., Jr. & Boland, T. (2003) Cell and organ printing 1: protein and cell printers. Anat.Rec. 272A. 491-496.

Witzenbichler, B., Asahara, T., Murohara, T., Silver, M., Spyridopoulos, I., Magner, M., Principe, N., Kearney, M., Hu, J.S., & Isner, J.M. (1998) Vascular endothelial growth factor-C (VEGF-C/VEGF-2) promotes angiogenesis in the setting of tissue ischemia. Am.J.Pathol. 153. 381-394.

Xavier, J.B., Schnell, A., Wuertz, S., Palmer, R., White, D.C., & Almeida, J.S. (2001) Objective threshold selection procedure (OTS) for segmentation of scanning laser confocal microscope images. J.Microbiol.Methods 47. 169-180.

Xia, Y., Rogers, J.A., Paul, K.E., & Whitesides, G.M. (1999) Unconventional Methods for Fabricating and Patterning Nanostructures. Chem.Rev. 99. 1823-1848.

Xu, X.M., Zhang, S.X., Li, H., Aebischer, P., & Bunge, M.B. (1999) Regrowth of axons into the distal spinal cord through a Schwann-cell-seeded mini-channel implanted into hemisected adult rat spinal cord. Eur.J.Neurosci. 11. 1723-1740.

Yeaman, C., Grindstaff, K.K., & Nelson, W.J. (1999) New perspectives on mechanisms involved in generating epithelial cell polarity. Physiol Rev. 79. 73-98.

Young, A.A., Legrice, I.J., Young, M.A., & Smaill, B.H. (1998) Extended confocal microscopy of myocardial laminae and collagen network. J.Microsc. 192 (Pt 2). 139-150.

Yourtee, D., Emery, J., Smith, R.E., & Hodgson, B. (2000) Stereolithographic models of biopolymers. J.Mol.Graph.Model. 18. 26-60.

Zahir, N. & Weaver, V.M. (2004) Death in the third dimension: apoptosis regulation and tissue architecture. Curr.Opin.Genet.Dev. 14. 71-80.

Zein, I., Hutmacher, D.W., Tan, K.C., & Teoh, S.H. (2002) Fused deposition modeling of novel scaffold architectures for tissue engineering applications. Biomaterials 23. 1169-1185.

Zhu, W.H., Guo, X., Villaschi, S., & Francesco, N.R. (2000) Regulation of vascular growth and regression by matrix metalloproteinases in the rat aorta model of angiogenesis. Lab Invest 80. 545-555.